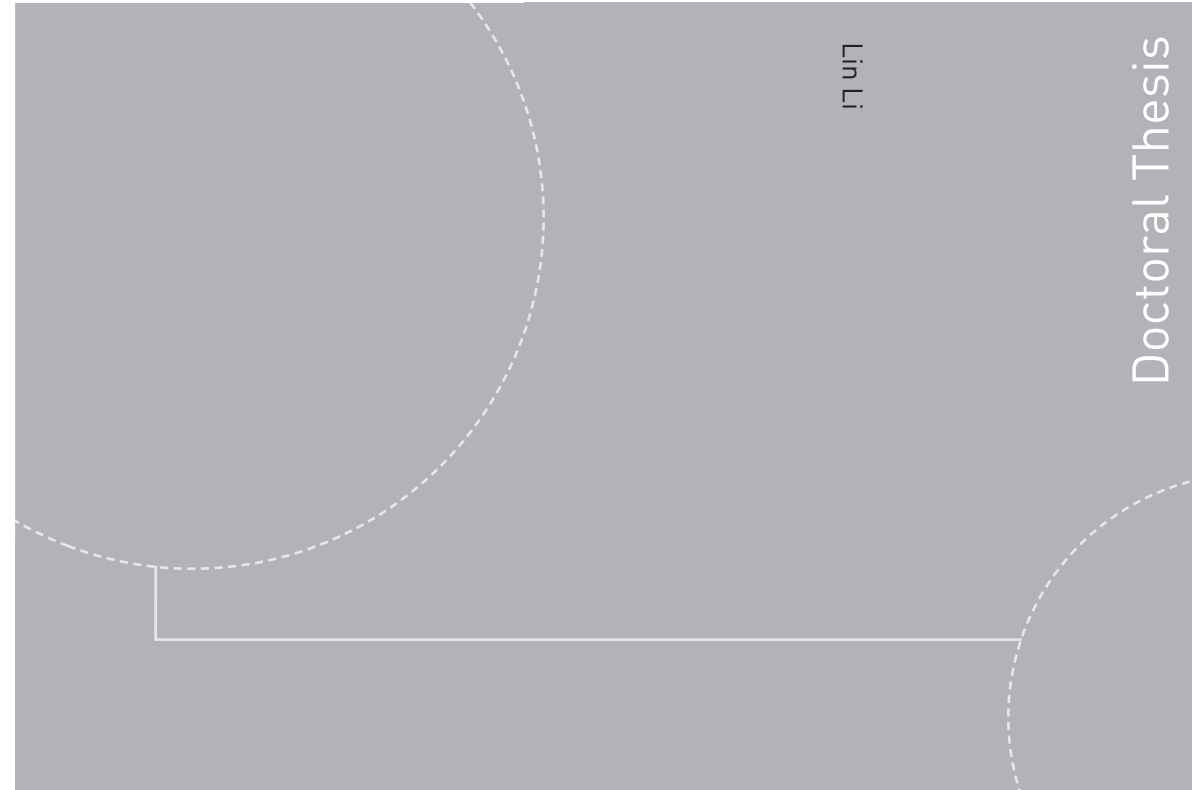


ISBN 978-82-326-1616-9 (printed version)
ISBN 978-82-326-1617-6 (electronic version)
ISSN 1503-8181



Lin Li

Dynamic Analysis of the Installation of Monopiles for Offshore Wind Turbines

Thesis for the degree of Philosophiae Doctor

Trondheim, May 2016

Norwegian University of Science and Technology
Faculty of Engineering Science and Technology
Department of Marine Technology



Norwegian University of
Science and Technology

NTNU

Norwegian University of Science and Technology

Thesis for the degree of Philosophiae Doctor

Faculty of Engineering Science and Technology

Department of Marine Technology

© Lin Li

ISBN 978-82-326-1616-9 (printed version)

ISBN 978-82-326-1617-6 (electronic version)

ISSN 1503-8181

Doctoral theses at NTNU, 2016:139



Printed by Skipnes Kommunikasjon as

Abstract

The installation of offshore wind farms presents great challenges as the industry move farther offshore and into deeper waters, and the turbines and foundations are getting larger and heavier. Current installation methods are all sensitive to weather conditions: lifting the foundations using floating crane vessels, deploying and retrieving jack-ups' legs, and lifting turbine nacelles and rotors at a large lift height. Careful numerical studies of these critical installation scenarios in the planning phase are therefore important to ensure safe executions. Monopiles (MP) are the most commonly used foundations for offshore wind turbines (OWT), but there is little work focusing on their installation phase. In order to predict the responses of the installation system, accurate numerical models and methods are needed.

This thesis addresses the modelling and dynamic analysis of two installation phases for monopiles: the lowering into the sea and the initial hammering phases. Due to nonstationarity, current numerical methods used for steady-state conditions are not applicable for simulating the lowering phase. In this thesis, new numerical methods were developed to account for the shielding effects from the floating installation vessel and the radiation damping of the monopile for analysing the nonstationary process. The shielding effects from the vessel are considerable especially in short waves, and the inclusion of the radiation damping of the MP may reduce the predicted responses. These methods also provide more accurate results than the commonly used simplified conservative methods, and they can be extended to apply for other structures. For the initial hammering process, the coupled vessel-monopile installation system with soil interaction was modelled. Dynamic analyses for various monopile penetration depths and soil conditions showed that the responses were sensitive to those factors.

These numerical models, methods and dynamic analysis form the basis for assessing the operational limits for different installation activities. The operational limits are essential during the planning phase of the operation, i.e. to size equipment, select installation vessel and optimize the installation method. The allowable sea states together with weather forecasts provide the basis for the decision making during the execution of the operation. Although many studies have focused on obtaining operational limits of specific installation activities, little work has been published on providing a general methodology to establish these limits.

Therefore, the thesis also addresses the development of a systematic methodology to assess the operational limits based on the installation procedure, numerical models and safety criteria. To demonstrate the methodol-

ogy, a detailed procedure for establishing the operational limits is presented for the monopile initial hammering process. First, the critical events and corresponding responses for this operation were identified. The allowable sea states were then obtained by comparing the characteristic responses with their allowable limits. For the monopile lowering process, the allowable sea states were also established using this methodology. An operability analysis at a selected offshore site using different numerical methods was carried out. It was showed that among different modelling parameters, the shielding effect is the most critical factor, followed by the nonstationary analysis approach, wave spreading and the radiation damping from the monopile. The methodology to assess the operational limits is general and can be extended to other marine operations.

The original contributions of this work include the development of new methods for simulating the nonstationary lowering operation, and development of a systematic methodology for assessment of the operational limits. These methods provide a basis for further studies on modelling and analysis of other marine operations.

Preface

This thesis is submitted to the Norwegian University of Science and Technology (NTNU) for partial fulfilment of the requirements for the degree of philosophiae doctor.

This doctoral work has been performed at the Centre for Ships and Ocean Structures (CeSOS), Department of Marine Technology, NTNU, Trondheim, with Professor Torgeir Moan as main supervisor and with Professor Zhen Gao as co-supervisor.

The thesis was financially supported by the Research Council of Norway through the Centre for Ships and Ocean Structures (CeSOS). This support is greatly appreciated.

Acknowledgement

My supervisors Prof. Torgeir Moan and Prof. Zhen Gao have provided me the opportunity to work at CeSOS and Department of Marine Technology at NTNU. I would like to express my deepest thanks for their guidance and supervision. I gained a lot from Torgeir's deep knowledge, experience and great enthusiasm and discipline in scientific research. I am grateful for Zhen's generous support and discussions on every detail in my work. It was a great pleasure and experience to work with them.

I would like to thank my colleague Wilson Guachamin Acero for the excellent cooperation during the last two years of my PhD and for being always supportive. I appreciate valuable discussions with Peter Sandvik of MARINTEK who often suggested me to think a bit more. The comments and positive feedback from Dr. Rune Yttervik of Statoil on my work are also appreciated. Many thanks to Prof. Gudmund Eiksund for valuable dissuasions on the monopile-soil interaction, to Dr. Harald Ormberg of MARINTEK for his support in using SIMO, to Dr. Erin Bachynski for her help on the coding and proof-reading this thesis, and to Dr. Amir Nejad for cooperation and discussions. I also benefited from conversations with Prof. Muk Chen Ong, Adjunct Prof. Jøgen Krokstad, Prof. Odd Faltinsen and Prof. Dag Myrhaug.

I also want to thank my great colleagues and friends who created a joyful and motivating atmosphere. I appreciate the sharing of knowledge between the PhD candidates and post-doctoral fellows at the department. The interactions with my lunch mates, officemates and friends around made each long working day less stressful. The Chinese community here was helpful and made me feel at home.

Finally, my warmest thank goes to my family in China for their support and endless love, and to my boyfriend Xiaopeng, for the encouragement and being the best companion - I am so happy we are both finishing our PhDs.

Lin Li
May 2016
Trondheim, Norway

List of Appended Papers

This thesis consists of an introductory part and six papers, which are appended.

Paper 1:

Analysis of Lifting Operation of a Monopile for an Offshore Wind Turbine Considering Vessel Shielding Effects.

Authors: Lin Li, Zhen Gao, Torgeir Moan, Harald Ormberg

Published in *Marine Structures*, 2014, Vol. 39, pp. 287-314.

Paper 2:

Comparative Study of Lifting Operations of Offshore Wind Turbine Monopile and Jacket Substructures Considering Vessel Shielding Effects.

Authors: Lin Li, Zhen Gao, Torgeir Moan

Published in *Proceedings of the Twenty-fifth (2015) International Ocean and Polar Engineering Conference, Kona, Big Island, Hawaii, USA, June 21-26, 2015.*

Paper 3:

Analysis of Lifting Operation of a Monopile Considering Vessel Shielding Effects in Short-crested Waves.

Authors: Lin Li, Zhen Gao, Torgeir Moan

Accepted for publication in *Proceedings of the Twenty-sixth (2016) International Ocean and Polar Engineering Conference, Rhodes, Greece, June 26-July 2, 2016.*

Paper 4:

Response Analysis of a Nonstationary Lowering Operation for an Offshore Wind Turbine Monopile Substructure.

Authors: Lin Li, Zhen Gao, Torgeir Moan

Published in *Journal of Offshore Mechanics and Arctic Engineering*, 2015, Vol. 137, DOI: 10.1115/1.4030871.

Paper 5:

Operability Analysis of Monopile Lowering Operation Using Different Numerical Approaches.

Authors: Lin Li, Zhen Gao, Torgeir Moan

Accepted for publication in *International Journal of Offshore and Polar Engineering*, June 2016

Paper 6:

Assessment of Allowable Sea States During Installation of OWT Monopiles with Shallow Penetration in the Seabed

Authors: Lin Li, Wilson Guachamin Acero, Zhen Gao, Torgeir Moan

Accepted for publication in *Journal of Offshore Mechanics and Arctic Engineering*, 2016

Declaration of Authorship

All the six papers that serve as the core content of this thesis are co-authored. In all these papers, I was the first author and responsible for initiating ideas, establishing numerical models, performing the analysis, providing the results and writing the papers. Professor Zhen Gao and Professor Torgeir Moan are co-authors of all the papers. They have contributed to the support, discussions and constructive comments to increase the scientific quality of the publications. Wilson Guachamin Acero is the second author of *paper 6*. He contributed in writing the operational procedure and assisted me to establish the methodology to assess the allowable sea states. Dr. Harald Ormberg is the fourth author of *paper 1*, and he supported me in developing the DLL in the SIMO program.

Additional Papers and Reports

The following papers and reports have been produced during the doctoral work but are not included in this thesis.

Additional Paper 1:

Numerical Simulations for Installation of Offshore Wind Turbine Monopiles Using Floating Vessels.

Authors: Lin Li, Zhen Gao, Torgeir Moan

Published in *Proceedings of the ASME 32th International Conference on Ocean, Offshore and Arctic Engineering, June 9-14, 2013, Nantes, France.*
(Not included because of scope)

Additional Paper 2:

Joint Distribution of Environmental Condition at Five European Offshore Sites for Design of Combined Wind and Wave Energy Devices.

Authors: Lin Li, Zhen Gao, Torgeir Moan

Published in *Journal of Offshore Mechanics and Arctic Engineering*, 2015, Vol. 137, DOI: 10.1115/1.4029842.

(This article is an extension of the conference paper titled *Joint Environmental Data at Five European Offshore Sites for Design of Combined Wind and Wave Energy Devices* which was published in *Proceedings of the ASME 32th International Conference on Ocean, Offshore and Arctic Engineering, June 9-14, 2013, Nantes, France*)

(Not included because of scope)

Additional Paper 3:

Methodology for Assessment of the Operational Limits and Operability of

Marine Operations.

Authors: Wilson Guachamin Acero, Lin Li, Zhen Gao, Torgeir Moan

To be submitted to *Journal of Offshore Mechanics and Arctic Engineering*, 2016

Additional Paper 4:

Correlation between Acceleration and Drivetrain Load Effects for Monopile Offshore Wind Turbines.

Authors: Amir R. Nejad, Erin E. Bachynski, Lin Li, Torgeir Moan

Accepted for publication in *Energy Procedia*, 2016

(Not included because of limited contributions)

Additional Report 1:

Environmental Data at Five Selected Sites for Concept Comparison.

Authors: Lin Li, Zhen Gao, Torgeir Moan

MARINA Platform Project WP3 Report, NTNU, August 2012.

Additional Report 2:

An Overview on Transportation and Installation of Offshore Wind Turbines.

Authors: Lin Li, Zhen Gao, Torgeir Moan

Report, Statoil Project on Installation Technology of Offshore Multi-use Platform, NTNU, September 2013.

Additional Report 3:

Analysis of Lifting Operation of a Jacket Foundation for a 10 MW Offshore Wind Turbine.

Authors: Lin Li, Oliver Stettner, Zhen Gao, Torgeir Moan

Report, Statoil Project on Installation Technology of Offshore Multi-use Platform, NTNU, July 2014.

Abbreviations

API	American Petroleum Institute
BWEA	British Wind Energy Association
COG	Centre of Gravity
DLL	Dynamic Library Link
DNV	Det Norske Veritas
DOF	Degree of Freedom
EWEA	The European Wind Energy Association
FEM	Finite Element Method
FFT	Fast Fourier Transform
GBS	Gravity-based Structure
HLV	Heavy Lift Vessel
IEA	International Energy Agency
ISO	International Organization for Standardization
JONSWAP	Joint North Sea Wave Project
ME	Morison's Equation
MP	Monopile
MW	Megawatt
NREL	National Renewable Energy Laboratory
OWT	Offshore Wind Turbine

RAO	Response Amplitude Operator
RNA	Rotor and Nacelle Assembly
RT	Retardation function
SEU	Self-elevating Unit
STD	Standard Deviation
WT	Wind Turbine

Contents

List of Tables	xvii
List of Figures	xix
1 Introduction	1
1.1 Background and motivation	1
1.2 State-of-the-art OWT installation methods	5
1.2.1 Installation methods for WT foundations	5
1.2.2 Installation methods for turbine components	8
1.2.3 Challenges in OWT installation	10
1.3 Modelling and analysis of marine operations	11
1.3.1 Modelling and analysis of marine operations, design of structures and planning of operations	11
1.3.2 Marine operations in the offshore wind and oil and gas industries	13
1.4 Aim and scope	15
1.5 Thesis outline	17
2 Installation systems and numerical models	19
2.1 General	19
2.2 Installation systems	20
2.2.1 Installation vessel, MP and jacket foundations	20
2.2.2 Monopile and jacket lowering systems	21
2.2.3 Monopile initial hammering system	23
2.3 Modelling of the couplings	24
2.3.1 Lift wire coupling	24
2.3.2 Modelling of the gripper device	25
2.3.3 MP-soil interactions	26
2.4 Numerical methods	28
2.4.1 Equations of motion	28

2.4.2	Eigenvalues of the system	29
2.4.3	Time-domain simulations	29
3	Dynamic analysis of monopile lowering and initial hammering processes	31
3.1	Overview	31
3.2	Shielding effects from the HLV	33
3.2.1	Morison's formula approximation for slender structures	33
3.2.2	Methodology to include shielding effects during non-stationary lowering process	34
3.2.3	Dynamic responses of the MP lowering system in disturbed waves	37
3.2.4	Comparative study of lowering a monopile and a jacket considering shielding effects	40
3.2.5	Shielding effects in short-crested waves	42
3.3	Radiation damping effects from the MP	45
3.3.1	Methodology to consider radiation damping on the MP for nonstationary lowering process	45
3.3.2	Effect from the radiation damping of the MP	48
3.4	Dynamic responses during the initial hammering process . . .	50
3.4.1	Dynamic responses with various MP penetrations . . .	50
3.4.2	Sensitivity study on the soil properties	53
4	Assessment of operational limits for monopile installation	55
4.1	Overview	55
4.2	Definition of terms	56
4.3	Methodology for assessing operational limits	57
4.4	Allowable sea states for the MP lowering process	58
4.4.1	Critical events and corresponding limiting parameters	58
4.4.2	Sensitivity of the allowable sea states to numerical methods	59
4.4.3	Sensitivity of the allowable sea states to vessel heading	62
4.4.4	Operability analysis on the MP lowering process . . .	63
4.5	Allowable sea states for MP initial hammering process . . .	64
4.5.1	Operational procedure for MP hammering	64
4.5.2	Critical events and limiting parameters	65
4.5.3	Methodology to assess the allowable sea states	66
4.5.4	Allowable sea states for initial hammering process . .	68

5	Conclusions and recommendations for future work	71
5.1	Conclusions	71
5.2	Original contributions	73
5.3	Recommendations for future work	74
	References	77
A	Appended papers	89
A.1	Paper 1	89
A.2	Paper 2	119
A.3	Paper 3	131
A.4	Paper 4	143
A.5	Paper 5	161
A.6	Paper 6	175
B	List of previous PhD theses at Dept. of Marine Tech.	215

List of Tables

1.1	Distribution of foundation types for offshore wind farms . . .	5
1.2	Transportation and installation methods for three types of bottom-fixed foundations	8
1.3	Main differences between operations in wind and in oil and gas industries	14
2.1	Main parameters of the floating installation vessel	21
2.2	Main parameters of the monopile and the hammer	21
2.3	Main parameters of the jacket foundation	22
4.1	Factors for case study in the time-domain simulations	60
4.2	Operability for MP lowering at North Sea Center in the pe- riod from April to September using different methods and heading angles	63

List of Figures

1.1	Cumulative and annual European offshore wind installations	2
1.2	Capital cost breakdown for land-based and offshore wind reference projects	2
1.3	Average water depth and distance to shore of online, under construction and consented wind farms	3
1.4	Capital costs of European offshore wind farms by year	3
1.5	Different foundation types for offshore wind turbines	4
1.6	Installation of bottom-fixed OWT foundations	7
1.7	Installation alternatives for turbine components	9
1.8	Link between modelling and analysis of marine operations, designing of structures and planning of operations	12
1.9	Scope of the thesis and interconnection between the appended papers	16
2.1	Lifting arrangement for monopile installation	22
2.2	Lifting arrangement for jacket installation	23
2.3	System set-up for the MP hammering process	23
2.4	Illustration of the physical and numerical models for gripper device during MP lowering process	25
2.5	Illustration of numerical model of the gripper device during MP hammering process	26
2.6	Numerical models for the soil-MP interactions during the initial hammering process	27
2.7	Natural periods for the coupled HLV-MP lowering system with varying MP positions	30
3.1	Interpolation of fluid kinematics in disturbed waves	35
3.2	Time-domain simulation approach considering vessel shielding effects	35

3.3	Comparison of the excitation force on the MP in incident wave and when accounting for shielding effects from the HLV	36
3.4	Spectral density of responses during lowering in incident and disturbed waves	37
3.5	Extreme rotation of the monopile in incident and disturbed waves at different wave directions	38
3.6	Extreme monopile rotations using a jack-up and the HLV at different wave conditions	39
3.7	RAOs of wave elevation at four wave frequencies in disturbed waves	40
3.8	<i>STDs</i> of MP and jacket motions in incident and disturbed waves	41
3.9	RAOs of fluid X-velocities at two wave frequencies in incident and disturbed waves with and without spreading	43
3.10	<i>STDs</i> of MP tip motions in incident and disturbed waves with and without wave spreading	44
3.11	Response spectra of MP in irregular waves	46
3.12	Comparison of the retardation functions at a draft of 7 m	48
3.13	Response spectra of the steady-state condition	49
3.14	<i>STDs</i> of the responses in the steady-state condition using the floating vessel	50
3.15	<i>STDs</i> of HLV motions at different MP penetration depths and wave conditions	51
3.16	<i>STDs</i> of MP inclinations and contact forces on one hydraulic cylinder	52
3.17	Extreme cylinder force versus MP maximum inclination for different sea states and soil properties at different penetrations	53
4.1	General methodology to establish the operational limits	57
4.2	Allowable sea states for MP lowering operation using different numerical approaches	61
4.3	Comparison on allowable sea states for case 1 with different heading angles	62
4.4	Flowchart of the MP hammering procedure	65
4.5	Methodology to find the allowable sea states for the initial hammering process	67
4.6	Allowable sea states for MP initial hammering operation for typical HLV headings	69

Chapter 1

Introduction

1.1 Background and motivation

The demands for renewable and reliable energy are becoming urgent due to global warming and the energy crisis. It is expected that 20 % of the world's electricity to be generated by renewable energies by 2040 (IEA, 2014). Wind energy is one of the most reliable and practical resources, due to its favourable combination of resource availability, energy cost and risk (BWEA, 2000).

Land-based wind turbines have been developed and used to generate clean energy for several decades (Burton et al., 2001; Hau, 2013). Compared with onshore wind turbines, offshore wind energy presents several advantages such as higher wind speeds, lower turbulence intensity, decreased visual and noise effects for humans and the possibility to transport larger turbines (Twidell, 2009). Because of this, the development of offshore wind has experienced a marked increase in the last two decades as shown in Figure 1.1, and it is expected to grow in the future. Assuming an average capacity of around 3 MW for each turbine, the number of turbines installed annually in Europe is more than 500 in recent years, which reflects that considerable offshore activities are involved in offshore wind.

However, offshore wind is facing great challenges. Studies show that the capital cost of offshore wind power is more than twice of onshore projects (Moné et al., 2015). The turbines, although based on onshore designs, need to be designed with additional protection against corrosion and the harsh marine environment (Ciang et al., 2008). The more significant increase of cost offshore is due to increased investments in constructing expensive foundations at sea, transportation and installation of foundations, equipment and turbines, and operation and maintenance (van Kuik et al., 2016).

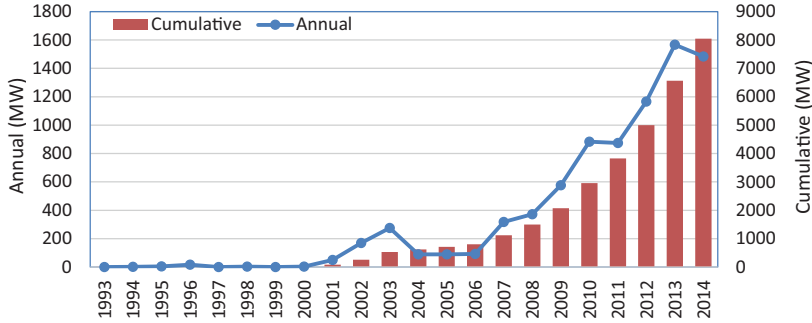


Figure 1.1: Cumulative and annual European offshore wind installations (MW) from 1993 to 2014 (EWEA, 2015)

Figure 1.2 compares the cost breakdown for a land-based and an offshore wind turbine. The installation and assembly of offshore wind turbines accounts for up to 20 % of the capital costs, compared to only 6% for land-based turbines (Moné et al., 2015). Compared with onshore work, offshore operations are much more risky and expensive, both from the financial and the engineering point of view. The variable and severe offshore environmental conditions are the primary concern, as they lead to larger loads on the structure and cause severe risks. Because of the low profit margin of the offshore wind industry, it is essential to reduce the installation costs by improving the methodology during the design and planning phase.

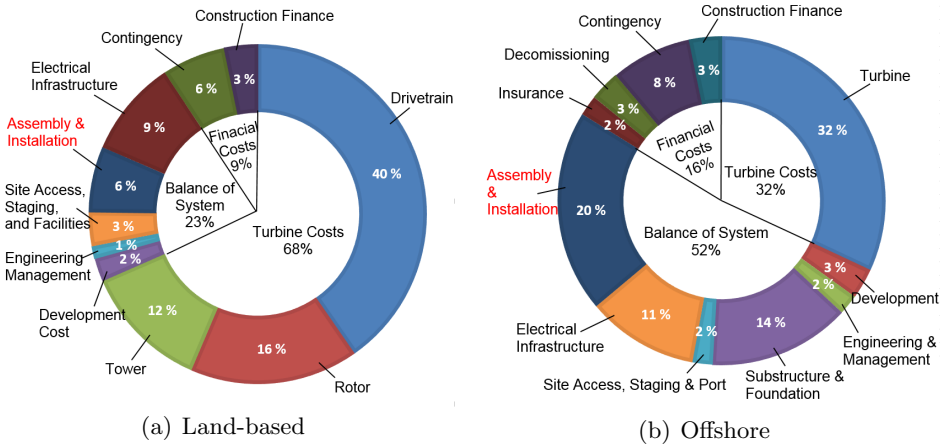


Figure 1.2: Capital cost breakdown for land-based and offshore wind reference projects (Moné et al., 2015)

Offshore wind farms are moving farther from shore and into deeper waters as shown in Figure 1.3, where the bubble size represents the capacity of the wind farm. At the end of 2014, the average water depth of online wind farms was 22.4 m and the average distance to shore was 32.9 km (EWEA, 2015). The projects under construction, consented, and planned confirm that average water depths and distances to shore are likely to increase, which brings more challenges to transportation, installation, operation and maintenance of the wind farm. Because of these aspects, the capital costs of European offshore wind farms have increased in recent years, see Figure 1.4. Better understanding of the key risks in offshore wind projects is needed in order to reduce the costs.

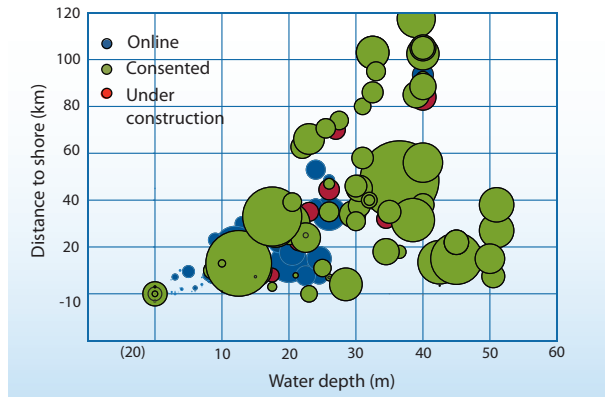


Figure 1.3: Average water depth and distance to shore of online, under construction and consented wind farms at the end of 2014 (EWEA, 2015)

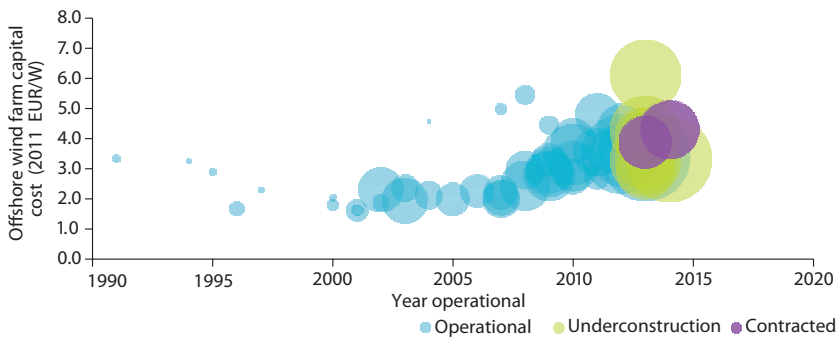


Figure 1.4: Capital costs of European offshore wind farms by year (EUR/W) (IEA, 2013)

An offshore wind turbine consists of a rotor and nacelle assembly (RNA), tower and support structure. Figure 1.5 shows various foundation types for offshore wind turbines. Monopiles are the most commonly used substructures in water depth up to 40 m due to the structural simplicity, and lower manufacturing and installation expenses (Thomsen, 2011). Gravity-based structures (GBS) are best suited to shallower water locations where pile driving is difficult. The deepest water depth for GBS is 28 m in Thornton Bank wind farm (Peire et al., 2009). Jackets and tripods might be able to fulfil the strength and stiffness requirements up to 60 m water depth (Musial et al., 2015). Floating concepts are likely to be more cost-efficient for locations deeper than 100 m, and three primary types are under consideration as shown in Figure 1.5. Up to now, there are only a few full scale floating wind turbines installed for testing purposes, i.e., Hywind in Norway and Windfloat off the coast of Portugal (StatOil, 2012; Principle Power, 2011).

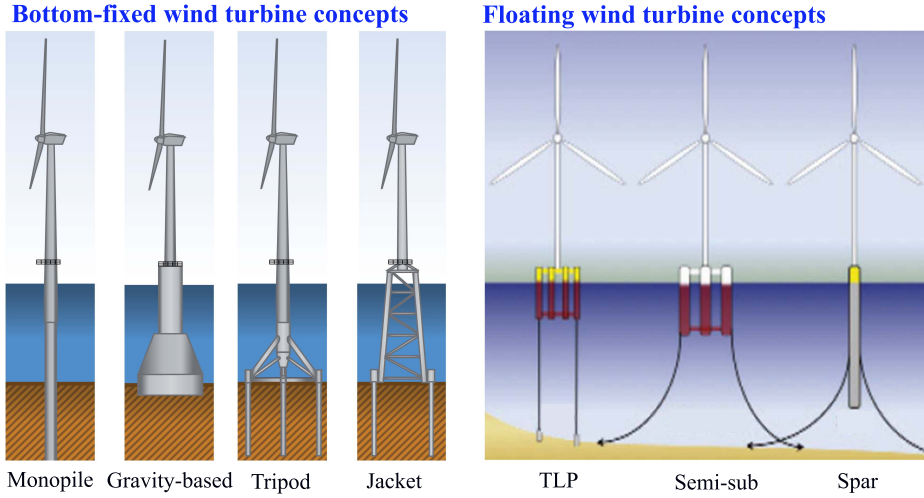


Figure 1.5: Different foundation types for offshore wind turbines (Wiser et al., 2011; Moan, 2014)

Table 1.1 shows the distribution of the installed bottom-fixed foundation types. The monopiles are the dominant foundations and are still installed at a dominant rate. No GBS have been installed in 2013 and 2014 because of the increasing water depth of the wind farms. The size and weight of the monopiles are increasing significantly to support heavier turbines in deeper water depth, and thus the installations are facing increasing challenges.

Table 1.1: Distribution of foundation types for offshore wind farms EWEA (2014, 2015)

Foundation type	Total installed by end of 2014	Annual installed in 2013	Annual installed in 2014
Monopile	78.8 %	79 %	91 %
Gravity-based	10.4 %	0.2 %	0
Jacket	4.70 %	14 %	8.10 %
Tripod	4.10 %	6 %	0.90 %
Tripiles	1.90 %	1.90 %	0

1.2 State-of-the-art OWT installation methods

The installation of an offshore wind farm includes the transportation and installation of foundations, turbine components (tower and RNA), substations and cables. The most commonly used method for foundation installation is heavy lifting operation using either floating cranes or jack-ups. For large substations, the float-over method is another alternative (OffshoreWind, 2014). Turbine components are normally lifted and installed using jack-up vessels. A large offshore wind farm consists of many units e.g., 88 wind turbines and 2 substations in the Sheringham Shoal wind farm (Statoil, 2009). The installation often requires many types of operations and lasts for a long duration. The time and cost saving for each type of activity will reduce the costs of the whole operation and hence the wind farm dramatically. Therefore, the choice of methods and equipment is essential for the planning of the installation.

A review of the current installation methods for bottom-fixed offshore wind turbine foundations and turbine components are presented in this section. Recently developed installation concepts are also discussed. The installation methods for floating wind turbines differ from those of bottom-fixed turbines and are not included in this thesis.

1.2.1 Installation methods for WT foundations

The methods for installing foundations depend on the foundation type, and the most commonly used methods are described below.

Monopiles

Monopiles are transported either on-board of a barge or an installation vessel or capped and wet towed (Herman, 2002). The size and weight of the monopiles are increasing, and it is expensive to use large installation vessels

to carry out the operations. As an alternative, the wet tow method can be used. The wet tow of a single floating monopile has already been applied during installation of two wind farms (Npower Renewable, 2006; Ballast Nedam, 2011). The transportation of more than one monopile per trip can be achieved using proper connection between the monopiles.

The installation of monopiles in general includes two main steps: upending and driving/drilling operations. A combined wet-tow and upending in water can be performed by lower capacity cranes than those required for transporting and upending on board. However, the upending of long monopiles in water is more weather sensitive than upending on board. The critical activities for monopile installation are the upending, lowering and driving operations. The verticality of the monopile during driving should also be carefully controlled.

Sarkar and Gudmestad (2012, 2011) suggested isolating the installation operation from the motion of the floating vessel by using a pre-installed submerged support structure. The monopiles are end-caped and wet towed. The new support structure is designed to support the monopile against the waves and the currents during the initial driving phase into the seabed.

Gravity-based foundations

Gravity-based structures for wind turbines weigh over 2500 tons. They can either be wet-towed or dry-transported on a barge or an installation vessel. Most of the existing GBS in very shallow waters are dry-transported to the offshore site. Wet-tow can reduce the installation costs by chartering lower capacity lifting vessels. Although the wet-tow method is widely used for transporting gravity based platforms, it has not been applied for installing GBS of OWTs because their weight is still within the crane capacity of available heavy lift vessels (HLVs). However, if larger GBS are applied for offshore farms in deeper waters, the wet-tow method may be more cost-efficient.

Recently a novel installation concept was proposed by Wåsijø et al. (2013) to transport and install a fully assembled gravity based foundation OWT using double-barge supports and standard tugboats. The concept aimed at reducing the costs by avoiding the use of heavy lift crane vessels. Model tests and numerical studies have been conducted to assess the feasibility of this concept (Bense, 2014).

Jackets and tripods

Jackets and tripods for OWTs can range from 400 to 1000 tons and with a height of 30 to 90 m in water depth of around 20 to 70 m. The jackets can be transported in either an upright or horizontal position depending



(a) Monopile lifting operation (source: <https://www.offshorewind.biz/>)



(b) GBS installation (Peire et al., 2009)



(c) Jacket upending operation (source: <http://www.4coffshore.com/>)



(d) Tripod lifting operation (source: <http://www.rechargenews.com>)

Figure 1.6: Installation of bottom-fixed OWT foundations

on the size of the foundations and the available transport barges. The installation of piles could be carried out either after positioning the jackets (*post-piling*) or before jackets installation (*pre-piling*) (LORC, 2013). Post-piling is traditionally used in the oil and gas industry and was applied for the two Beatrice jackets. Experience with pre-piling is limited, but it was first used for the six Alpha Ventus jackets (Østvik, 2010). Pre-piling is considered to be a faster method than post-piling. With pre-piling, smaller vessels can be employed for the piling operation and the HLVs are only required to lift the jackets into the pre-installed piles. With post-piling, the expensive HLVs are used to install both the jacket and the piles. In addition, a considerable amount of steel can be saved using pre-piling because the sleeves for the piles are unnecessary.

Table 1.2 summarizes the commonly used transportation and installation

methods for different types of bottom-fixed foundations discussed above, and Figure 1.6 displays the installation activities for different foundations.

Table 1.2: Transportation and installation methods for three types of bottom-fixed foundations

Type of foundation	Transportation method	Installation method
Monopile	Dry-transported	Upended and lowered
	Wet-tow (end-caps)	Upended and lowered (smaller crane)
Gravity-based	Dry-transported	Lifted and lowered (large crane)
	Wet-tow (large foundation)	Ballasted and lowered (smaller crane)
Jacket	Dry-transported in upright position	Lifted and lowered; pre- or post-piling
	Dry-transported in horizontal position	Upended and lowered; pre- or post-piling

1.2.2 Installation methods for turbine components

The transportation and installation methods for turbine components are very different from those for foundations. They must be dry-transported on-board an installation vessel or a feeder vessel. The turbine particularly the nacelle and the rotor has sensitive components which only tolerate very limited accelerations during transportation and installation. Moreover, lifting operations are weather sensitive especially at large lifting heights, and the mating between the components is challenging. Therefore, jack-up installation vessels are normally used for turbine installation.

There are many alternatives for turbine installation. Offshore lifts are risky and are susceptible to downtime due to wind, so some degree of onshore pre-assembly is generally preferred to minimize offshore assembly. Figure 1.7 shows the commonly used installation strategies. The weight of each component for the NREL 5MW reference turbine (Jonkman et al., 2009) is included in the figure.

By increasing the amount of onshore assembly, the offshore construction work can be reduced. However, the assembled components reduce the efficiency in using the deck space and increase the number of trips for transportation when installing a large wind farm. In addition, the weight of the fully assembled turbine with the large lift height requires very large and

expensive crane vessels (Ku and Roh, 2014). The weight for each lifting operation using different methods is also shown in Figure 1.7.







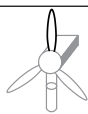





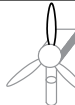




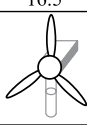



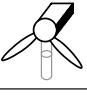
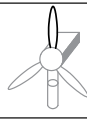
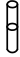

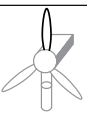
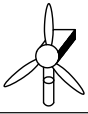
Components and weights	Installation method	Number of lifts					
		1	2	3	4	5	6
2 tower sections:  173.75 ton each	1						
	Lift weight	173.75	173.75	300.5	16.5	16.5	16.5
nacelle:  240 ton	2						
	Lift weight	347.5	300.5	16.5	16.5	16.5	
hub:  110 ton	3						
	Lift weight	173.75	173.75	240	110		
3 blades:  16.5 ton each	4						
	Lift weight	173.75	173.75	333.5	16.5		
	5						
	Lift weight	347.5	333.5	16.5			
	6						
	Lift weight	697.5					

Figure 1.7: Installation alternatives for turbine components including number of lifts and lift weights (Kaiser and Snyder, 2011)

The choice of method is related to the vessel size, distance from port to site, size of the WTs and the lifting capacity of the crane. For large WTs, the tower top mass limits the selection of installation method as well as installation vessel. Uraz (2011) compared the installation methods in terms of time estimations for transportation and installation. The approach can be extended with more practical information for optimization of the installation strategies.

Several innovative concepts to install fully-assembled tower and RNA have been proposed recently. Sarkar and Gudmestad (2013) designed a floating substructure to transport the fully assembled structure, but the concept was only applicable for telescopic tower. Guachamin Acero et al. (2016) proposed a new concept based on the principle of the inverted pendulum. The feasibility of this installation concept was assessed by numerical analyses.

1.2.3 Challenges in OWT installation

The main challenges for offshore wind farm installation can be summarized as follows.

- **Transportation.** Optimization of deck space is important to minimize the total number of transportation trips, especially when the distance from harbour to the site is large (Masabayashi, 2012). However, as mentioned, the maximum number of WT sets on-board depends on the installation methods, see Figure 1.7. Trade-off needs to be made by considering deck space and number of lifts offshore.
- **Lifting operation.** Heavy lifting is the means of load transfer, installation of foundations and WT components. For foundation installation, the hydrodynamic loads on the structure during lowering through the splash zone induce large loads to the system. If a floating installation vessel is employed, the lifting system is more sensitive to the waves and requires detailed response analysis in the planning phase. For turbine components, the large lifting height and pendulum motions due to wind are the main considerations. It is important to ensure that the lift at various heights is within the crane's capacity and the pendulum motions are below the operational limits.
- **Limited weather window.** Operational weather criteria determine the system downtime. The largest downtime is observed in the offshore lifting operations due to the waves when lifting foundations or wind when installing the RNA. Another significant downtime is found in the positioning of jack-ups. Thus, more floating installations are employed for foundation installations to increase the available weather window due to fast transit and relocation. However, for turbine installation jack-ups remain the preferred vessels. For installation of a wind farm consisting of many structures, increasing the weather window is imperative for cost reduction.

1.3 Modelling and analysis of marine operations

Marine operations represent intermediate phases for a structure (Nielsen, 2007). This is in contrast to the normal design condition where the permanent phase of the structure is considered. DNV-OS-C101 (DNV, 2011a) divided the design conditions for offshore structures into two: the operating condition wherein a unit is on location for purposes of production, drilling or other similar operations; and temporary conditions which are not covered by operating conditions, e.g., conditions during fabrication, mating and installation phases, transit phases, and accidental conditions. The installation phase is a temporary condition and the design focus and analysis methods are different from those in the operating phase.

The objective for studying marine operations is to ensure that the marine operations are performed within defined and recognised safety levels (DNV, 2011b). Acceptable safety shall normally be provided against loss of human lives or injury of human health, loss and damage to property, as well as pollution or other damage to the environment (DNV, 2012a).

In order to achieve the objective, extensive analyses are required, typically through numerical studies, model-scale experiments and full-scale sea trials. The present work focuses on numerical studies.

1.3.1 Modelling and analysis of marine operations, design of structures and planning of operations

Modelling and analysis of marine operations are essential for designing offshore structures, planning the operations. The flowchart in Figure 1.8 demonstrates the link between them.

Offshore structures should be designed for all conditions during the design life time. API (2007) states that temporary loading conditions (referred as “design situations” in ISO (1998) and “temporary design conditions” in DNV (2011a)) occurring during fabrication, transportation, installation or removal and re-installation of the structure should be considered.

The modelling and analysis of marine operations provide loads and responses which can be directly used in the design check of structures (e.g., monopiles) for the installation phase. Some structures or components experience the largest loads in their lifetime during the installation phase. A typical example is the design of the self-elevating units (SEUs) or jack-ups. Statistics show that most accidents occur during transit, installation and retrieval phases of a SEU (DNV, 2012c). Thus, the analysis of these marine operations directly governs the design of the SEU. Ringsberg et al. (2015) developed a numerical method to assess the weather window for the instal-

lation and retrieval phase of a SEU. Another example is that the pile wall thickness should be designed considering the stresses during pile driving operations. By modelling the driving operations, it is possible to predict the stresses during pile driving operation and use them in the design check of the piles (API, 2007).

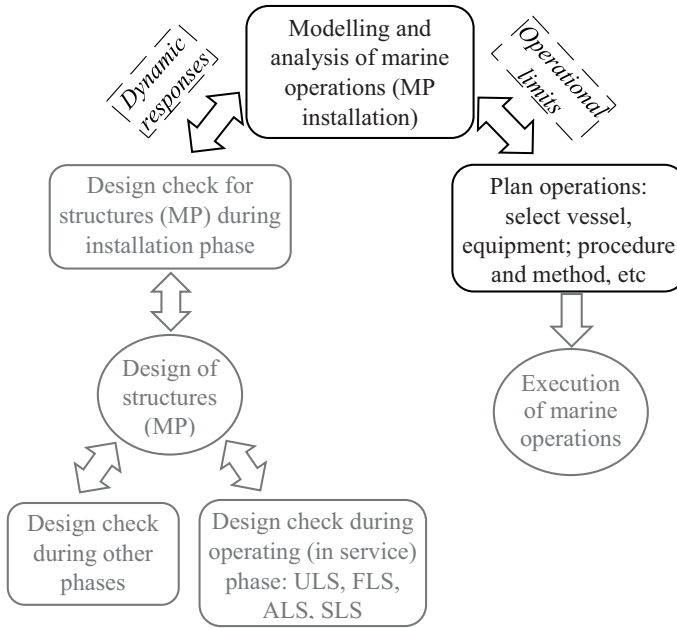


Figure 1.8: Link between modelling and analysis of marine operations, designing of structures and planning of operations

The analysis of operations is necessary for the planning phase, including selecting vessels, designing or selecting the installation equipment, and optimizing installation procedures and methods. The operational limits (e.g., allowable sea states) established during the planning phase need to be adhered to during the execution of the operations. Li et al. (2014a) compared the performance of the lifting system during MP lowering operations using a jack-up and a HLV. Advantages and disadvantages of the two vessels were pointed out. Mortola et al. (2012) proposed an operability calculation procedure to compare vessel operability in different conditions. Graczyk and Sandvik (2012) studied the landing and lift-off operation for wind turbine components during maintenance using a monohull and a catamaran. During the foundation installation of the Sheringham Shoal wind farm, the improper choice of the Svanen heavy lift barge delayed the project at an estimated cost of 600 million NOK (Sandelson, 2011). The lesson again

proved the importance of proper analysis of the operations in the planning phase.

The sizing and design of installation equipment depend greatly on the load and load effects obtained through the modelling of marine operations. Lifting pad-eyes, and spreader beams should be designed considering the loads during lift-off operations (API, 1993), and the selection of the slings should be done properly. If hydraulic cylinders are used in the gripper device during MP hammering operation, the capacity should be selected to sustain the extreme contact forces during the operation (Li et al., 2016c).

The analysis of marine operations also supports the development of improved installation procedures and methods. For example, the float-over method for deck installation has been developed as an alternative to lift operations using heavy lift crane vessels, and the development was to a large extent based on numerical and experimental studies (O'Neill et al., 2000; Tahar et al., 2006). A frequency domain analysis method was applied to assess two access concepts for docking operation between service vessels and offshore wind turbines in Wu (2014).

In addition, simulators which are built on the basis of numerical simulation tools are useful for training the operators, e.g., for crane and dynamic positioning operations. This can help to reduce human errors during execution of critical and complex installation activities and increase the safety margin (SMSC, 2015; OSC, 2015).

Therefore, modelling and analysis of marine operations, design of structures and planning of operations are closely connected. Robust and accurate modelling approaches will contribute to the structural design and increase the safety level of the operations. In order to find an optimum solution during the design phase, the three considerations in Figure 1.8 need to be repeatedly evaluated.

Chapters 2 to 4 of this thesis focus on modelling and analysis of the monopile installation activities. Numerical models and methods are developed, and followed by assessment of the operational limits.

1.3.2 Marine operations in the offshore wind and oil and gas industries

The main differences between marine operations in the offshore wind and oil and gas industries are summarized in Table 1.3 (Li et al., 2013b). Because of the low profit margin in the wind industry, reduction in installation costs seems to be urgent. Structures used in offshore wind farms are relatively small and light, but many. In contrast, oil and gas structures are one-of-a-

Table 1.3: Main differences between operations in wind and in oil and gas industries

Aspects	Oil and gas industry	Wind industry	Comments (for the wind industry)
Profit margin	high	low	Installation cost reduction is essential
Number of units to be installed	few	many	repetitive installation
Foundation size; weight	huge; heavy	smaller; lighter	need cost-effective installation method
Topside weight; lift height	heavy; low	lighter; very high	require large lift height and high installation accuracy
Installation vessels	many	few	need for tailor-made vessels is urgent
Experiences	much	very limited	Costs can be reduced by gaining experiences
Standards and guidelines	many	very few	Require further development

kind. The ability to install one wind turbine unit at a higher sea state is crucial for efficient installation of the wind farm. The large lift height of turbine components and requirement for high installation accuracy increase the challenges, especially as the size of offshore wind turbines increases. The vessels and equipment used in the oil and gas industry sometimes cannot fulfil the tasks for wind farm installation, so purpose-built vessels or equipment are required.

Besides, there is much less experience with marine operations for offshore wind farms and corresponding standards and guidelines as compared to those for oil and gas structures. For better design of marine operations and increased safety levels, reliable and accurate numerical models are therefore of great importance.

Despite the differences, many commonly used operation methods in the oil and gas industry can play important roles in wind farm installation. It is beneficial to utilize the experiences and methods in the oil and gas industry to wind farm installation in a reasonable way. From a practical point of view, the technologies developed for offshore construction vessels, dynamic positioning systems, heave compensated winches and cranes etc, can be incorporated into new vessels for wind turbine installation (Edwards and Dalry, 2011). Some of the guidelines developed for the oil and gas industry are also relevant for wind turbine installations, such as DNV rec-

ommended practices for modelling and analysis of different types of marine operations (DNV, 2011b, 2012a,b, 2013, 2014a,b), API recommended practice (API, 2007, 1993), Norsok standard for marine operations (NORSOK, 1997, 1995, 2007), ISO standard for marine operations (ISO, 2009), and GL Noble Denton guidelines (GL Noble Denton, 2010), etc.

1.4 Aim and scope

Based on the challenges described above, it is of great importance to improve operational procedures and numerical methods, and to develop methodologies for installation of offshore wind turbines. For analysis of monopile installations, a review of related work on numerical methods and on establishing operational limits is given in Sec. 3.1 and 4.1, respectively. Based on the literature review, the main research challenges for studying monopile installation can be summarized as follows:

- To develop accurate numerical methods to compute the dynamic responses for different installation activities.
- To establish a systematic methodology to assess the operational limits.

The aim of the thesis is therefore to contribute to the two goals given above for monopile installation. To achieve the goal, the following sub-objectives have been defined:

- To develop a numerical model and method to investigate the non-stationary lowering operation of the monopile considering shielding effects from the floating installation vessel and the radiation damping on the monopile.
- To develop a numerical model and method to study the initial hammering process of the monopile.
- To assess the characteristic responses of the system during various installation phases.
- To propose a methodology to establish the operational limits for monopile installation.
- To provide recommendations for modelling of lifting operations and for assessment of the operational limits.

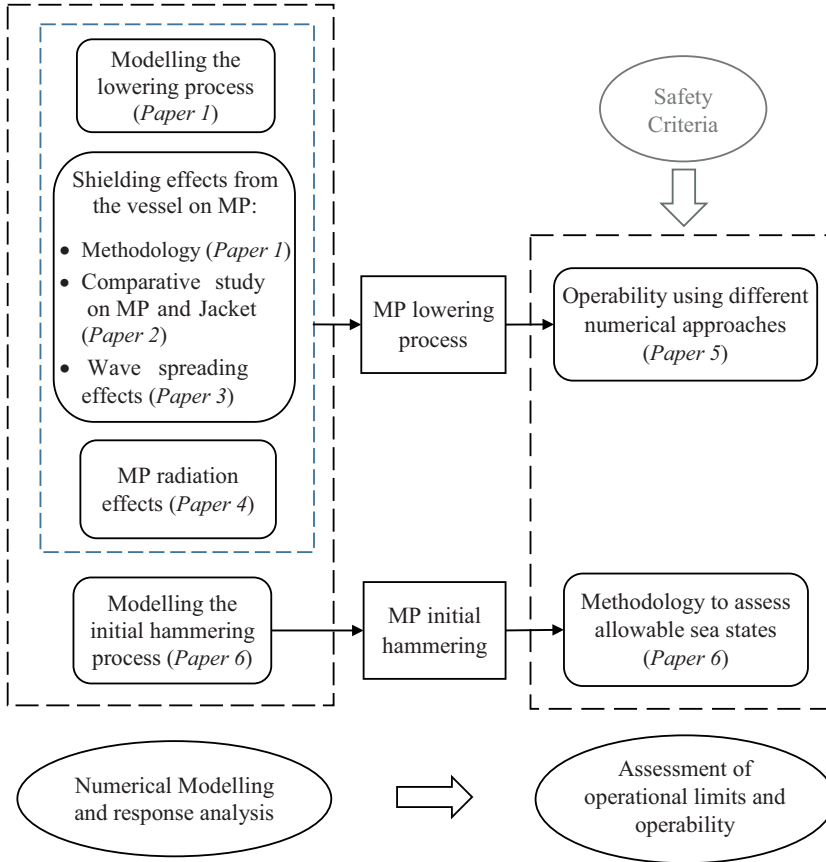


Figure 1.9: Scope of the thesis and interconnection between the appended papers

This thesis is written as a summary of published papers, including four journal articles and two conference papers as attached in the Appendix. The scope of the thesis is shown in Figure 1.9 where the main topics and the interconnection between the appended papers are illustrated.

This work started with the monopile lowering process. The numerical model for the coupled vessel-monopile system for this process was established in *Paper 1*. A methodology to model the shielding effects from the vessel during the nonstationary lowering process was developed. It was shown that the shielding effects influence the monopile responses greatly in short waves. Recommendations for choosing vessel headings and selecting vessel types (floating or jack-up vessels) were provided. This method was also applied on monopile and jacket lifting systems in *Paper 2*. Results

showed that the shielding effects are significant for monopiles while they can be ignored for lowering operation of jackets. Furthermore, the methodology to account for shielding effects was extended in *Paper 3* to consider wave spreading. The results showed that short-crestedness reduces the shielding effects from the vessel on the responses of the monopile.

The numerical methods in the previous papers neglected the radiation effects from the monopile. Thus, *Paper 4* deals with the development of a new method to include the radiation damping of the monopile during the nonstationary lowering process. The study showed that the radiation damping effects should be considered in short wave conditions for large diameter monopiles.

These developed numerical models and methods were applied to assess the operability for the monopile lowering process in *Paper 5*. The allowable sea states obtained using different numerical methods in *Papers 1, 3 & 4* were compared. The influence of each factor in the numerical method on the operability were assessed. Recommendations regarding numerical modelling were given to properly assess the operability.

The initial hammering operation of the monopile was investigated in *Paper 6*. The coupled vessel-monopile hammering system was firstly modelled, and the dynamic responses were studied quantitatively. Then, this study addressed a method for assessing the allowable sea states for this operation. The critical events and corresponding parameters to describe those events were identified. Based on the allowable limits and characteristic responses, the allowable sea states were established and followed by case studies. The systematic method established can be generalized to establish operational limits for other marine operations.

1.5 Thesis outline

The summary of the thesis consists of five chapters. A brief description of each chapter is provided as follow:

Chapter 1:

This chapter introduces the background, motivation, aim and scope and outline of the thesis. The state-of-art OWT installation methods, purpose for modelling and analysis of marine operations are also discussed.

Chapter 2:

This chapter presents the installation systems and the modelling methodologies for the monopile lowering and initial hammering operations using

a floating installation vessel. The modelling method for monopile lowering process was used in *Papers 1-5* and the modelling of the initial hammering process was used in *Paper 6*.

Chapter 3:

This chapter addresses the dynamic analysis of the coupled installation systems. Different numerical methods for the monopile lowering process are presented including the shielding effects from the vessel and the radiation damping effects from the monopile. The methodology and the dynamic responses from time-domain simulations are shown. This chapter covers the main results obtained in *Papers 1-4* for the monopile lowering process and the dynamic analysis part in *Paper 6* for the initial hammering process.

Chapter 4:

This chapter presents the methods and results for assessment of operational limits for the two monopile installation activities. The systematic methodology to obtain the operational limits based on the operational procedure, numerical analysis and safety criteria are discussed. Effects from different numerical approaches on the allowable sea states are studied for monopile lowering process in *Paper 5*. The proposed methodology is applied to establish the allowable sea states for the initial hammering process in *Paper 6*.

Chapter 5:

Conclusions, original contributions and the recommendations for future work are presented.

Chapter 2

Installation systems and numerical models

2.1 General

The fast growth in the offshore wind industry has lead to increasing demand for installation vessels. There are generally two types of vessels for installation of monopiles: the jack-ups and the floating crane vessels. A jack-up vessel provides a stable working platform for the lifting and piling operations. However, the installation and retrieval of the legs of the jack-ups are time-consuming and weather-sensitive (DNV, 2012c), and these operations have to be repeated for installation of each wind turbine unit. The weather window is thus very limited with long waiting times when installing a large offshore wind farm.

Compared to jack-ups, floating vessels have more flexibility for offshore operations and are effective in mass installations of a wind farm due to fast transit between foundations. Hence, the potential of reducing installation costs by using floating installation vessels is huge. On the other hand, the motions of the floating installation vessel and the lifted objects are fully coupled during the installation process and are sensitive to the environmental conditions (Li et al., 2014a). The vessel motions affect the dynamic response of the foundations, which may increase the operational risks. Therefore, it is of importance to examine the dynamic response of the coupled system during different phases of the installation to ensure safe offshore operations, and this is the focus of the thesis.

The installation of the monopile and transition piece is normally carried out by the same installation vessel. Assuming that the monopiles are transported on-board of the installation vessel, the installation process can

be summarized into the following four main steps:

- 1 Upending the monopile from a horizontal position on the vessel to a vertical position using the on-board crane and an upending frame.
- 2 Lowering the monopile through the wave zone down to the seabed. The hydrodynamic loads induce monopile motions when it passes through the wave zone.
- 3 Driving the monopile into the seabed with a hydraulic hammer. A gripper device is used to support the monopile during hammering which transfers the motions from the vessel to the monopile. The final inclination of the monopiles should satisfy the installation requirements.
- 4 Lifting the transition piece from the vessel and lowering it on top of the monopile. The transition piece is transported vertically on the vessel, lifted by the crane and installed onto the monopile.

The thesis deals with numerical studies on the lowering and the initial hammering processes of the monopile. The focus is on the dynamic response of the coupled installation system. This chapter presents the numerical models for the installation system.

2.2 Installation systems

2.2.1 Installation vessel, MP and jacket foundations

Two types of installation vessels were used in this thesis, i.e., the floating installation vessel and the jack-up vessel. The dynamic response of the installation system using the two vessels were compared in *Papers 1, 4, and 5*, and only the floating installation vessel was applied in *Papers 2, 3, and 6*. The jack-up vessel was assumed as a fixed platform during the installation of monopiles, and no wave-induced motions were considered. The floating installation vessel was a typical monohull heavy lift vessel (HLV), and the main parameters are presented in Table 2.1. The HLV can operate with different draughts according to the operational requirements. The operational draught was chosen as 12 m in *Papers 1 to 4* and was adjusted to 10.2 m in *Papers 5 to 6* for practical reasons.

The crane is capable of performing lifts of up to 5000 ton at an outreach radius of 32 m in fully revolving mode. The main hook featured a clear height to the main deck of the vessel of maximum 100 m. The vessel is positioned by an eight-line mooring system during operation. The positioning

system allows for vessel operations in shallow water and in close proximity to other structures.

Table 2.1: Main parameters of the floating installation vessel

Vessel		
Length overall	[m]	183
Breadth	[m]	47
Operational draught	[m]	10.2
Displacement	[ton]	5.12E4
Metacentric height	[m]	5.24
Vertical position of COG above keel	[m]	17.45

The monopile used in the numerical model was intended to support a 5 MW offshore wind turbine and it was a long slender hollow cylinder with main dimensions listed in Table 2.2. The weight of the hammer is also included which was used in the analysis of the initial hammering process in *Paper 6*.

Table 2.2: Main parameters of the monopile and the hammer

Monopile		
MP mass	[ton]	500
Length	[m]	60
Outer diameter	[m]	5.7
Thickness	[m]	0.06
Hammer Mass	[ton]	300

A 10 MW wind turbine jacket foundation was modelled in *Paper 2* for comparative studies. The geometry of the 10 MW jacket was interpolated between the existing jacket designs, i.e., the 5 MW and 20 MW UpWind turbines (De Vries, 2011). Common wind turbine and substructure scaling laws were applied (Hoving, 2013). The main parameters for the 10 MW jacket are shown in Table 2.3, and the detailed information of each member can be found in Li et al. (2014b).

2.2.2 Monopile and jacket lowering systems

The coupled lowering system for the monopile and jacket substructures are shown in Figures 2.1 and 2.2. The water depths for the installations were 25 m and 40 m, respectively.

Table 2.3: Main parameters of the jacket foundation

jacket		
Total height	[m]	64.75
Foot print	[m]	22 x 22
TP position *	[m]	(0 ,0, 65.25)
leg outer diameter	[m]	1.9
Brace outer diameter	[m]	1
Jacket mass	[ton]	1017
Transition piece mass	[ton]	250
Total mass	[ton]	1267

* refer to the center point of the jacket bottom

An internal lifting tool is often used for monopile and jacket lowering activities (IHC, 2014), and it is connected with the hook through slings. The slings were assumed to be very stiff in the current model, and the hook and the substructure were considered to be rigidly connected and were modelled as one body for simplicity. Therefore, both lowering systems included two rigid bodies which were coupled through the lift wire.

For the monopile lowering system, a gripper device is placed on the port side of the vessel to constrain the motions of the MP during the operation.

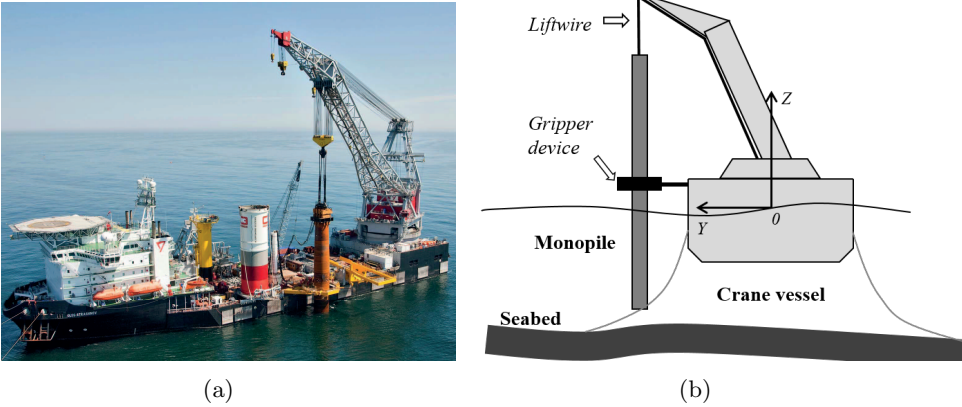


Figure 2.1: Lifting arrangement for monopile installation. (a) physical appearance (source: <http://www.seawayheavylifting.com.cy/>); (b) Schematic illustration.

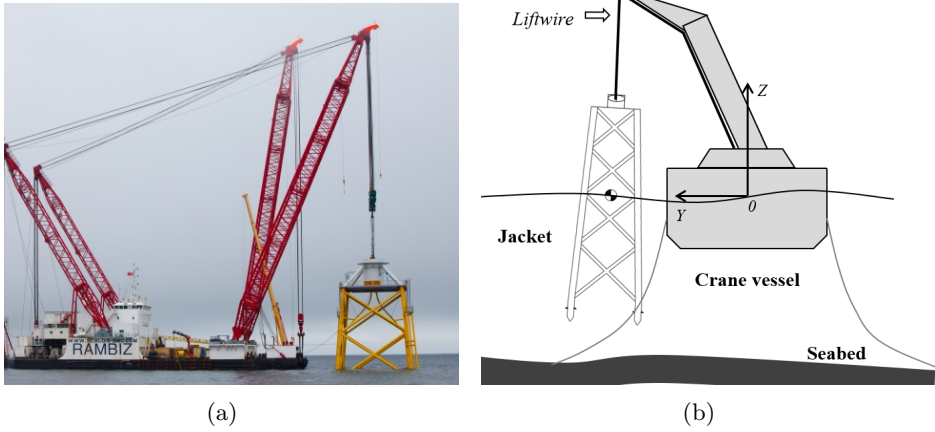


Figure 2.2: Lifting arrangement for jacket installation. (a) physical appearance (source: <http://www.marinetraffic.com/>); (b) Schematic illustration.

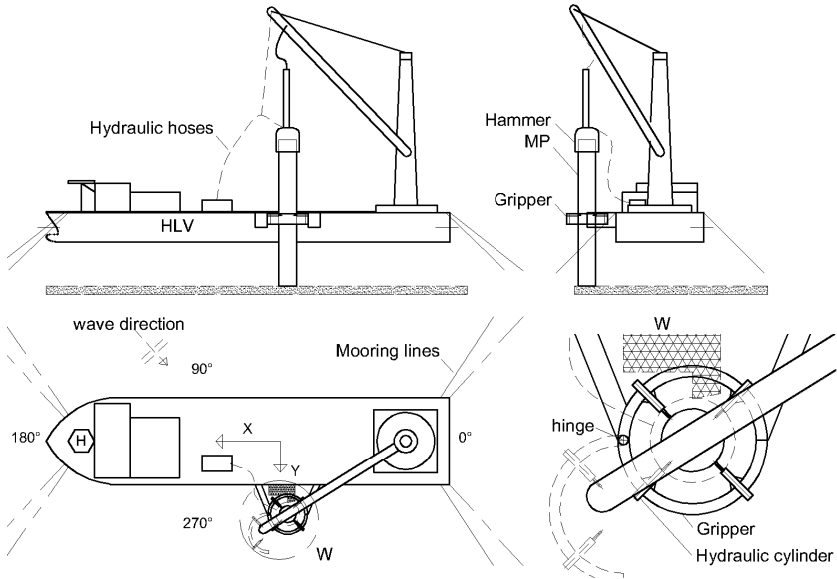


Figure 2.3: System set-up for the MP hammering process

2.2.3 Monopile initial hammering system

The system set-up for the MP initial hammering process is illustrated in Figure 2.3. The global coordinate system was a right-handed coordinate system with X axis pointed towards the bow, the Y axis pointed towards

the port side, and the Z axis pointed upwards. The origin was located at [mid-ship section, centre line, still-water line] when the vessel was at rest. The definition of global coordinate system and wave directions are shown in Figure 2.3 for the monopile system and the same global coordinate was applied for the jacket lowering system.

After being lowered down to the seabed, the MP is supported vertically by the soil and laterally by the gripper device. Then, the main lift wire is released. The hammer is then placed on top of the MP which increases its initial self-penetration. The gripper device is used to support the MP in the horizontal plane and correct its mean inclination during the initial hammering process.

2.3 Modelling of the couplings

The couplings between the vessel and the monopile include hydrodynamic interaction and mechanical couplings during the lowering process, and monopile-soil interaction during the initial hammering process. The hydrodynamic interaction will be discussed in detail in Sec. 3.2. In this section, the modelling methods for mechanical couplings including lift wire and gripper device, as well as monopile-soil interaction are given.

2.3.1 Lift wire coupling

The lift wire coupling force is modelled as a linear spring force according to the following equation:

$$T = k \cdot \Delta l \quad (2.1)$$

where T is the wire tension, Δl is the wire elongation and k is the effective axial stiffness assuming the crane and wire form a series connection, which is given by:

$$\frac{1}{k} = \frac{l}{EA} + \frac{1}{k_0} \quad (2.2)$$

where E is the modulus of elasticity, A is the cross-sectional area of the wire and l is the total length of the wire, which increases as the winch runs during the lowering operation. The effect of the elasticity of the crane boom is limited for the current two lifting systems because of low load mass compared to the crane capacity (Park et al., 2011). Thus, a low constant flexibility of the crane, $1/k_0$ was included. From the positions of the two ends of the wire, the elongation and thereby the tension can be determined. The material damping in the wire was included in the model.

2.3.2 Modelling of the gripper device

The gripper device normally consists of several hydraulic cylinders, see Figure 2.3, and it was modelled differently for the lowering and the initial hammering systems. For the lowering system, the gripper device was modelled as a contact point attached to the vessel in *Papers 1 to 3*. A cylinder fixed to the monopile with a vertical axis was modelled at the same time, and the contact point was placed inside the cylinder, see Figure 2.4 (b). This model was able to calculate the total contact force between the HLW and the MP during the nonstationary lowering process with changing position of the MP. Axisymmetric stiffness and damping were assumed and were defined by specifying restoring and damping forces F_i at several relative distances Δd_i between the contact point and the cylinder axis (see Figure 2.4 (b)).

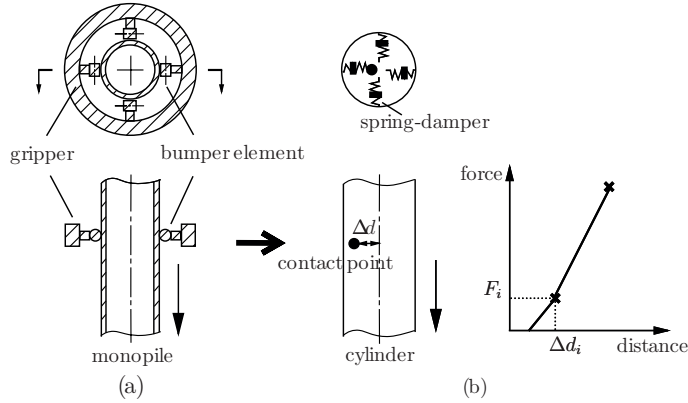


Figure 2.4: Illustration of (a) physical and (b) numerical models for the gripper device during MP lowering process

In the initial hammering phase, the dynamic system is in a steady-state condition when the penetration depth of the MP in soil is fixed. In addition, the contact force on each hydraulic cylinder needs to be analysed. The gripper device was thus modelled by four fender components with proper stiffness and damping coefficients. The elastic model for the gripper contact elements is illustrated in Figure 2.5.

During the lowering operation, the hydraulic cylinders are retracted and there is an initial gap between them and the wall of the MP. The initial gap depends on the stroke length of the cylinders, and is required during the lowering operation to avoid large contact forces, which may cause structural damage of the hydraulic cylinders. After the MP being lowered down to the seabed, the gripper is closed and the hydraulic cylinders provide pre-

compression forces on the MP before the hammering activity starts.

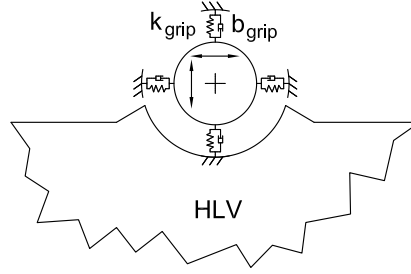


Figure 2.5: Illustration of numerical model of the gripper device during MP hammering process

The initial gap between the cylinder and the MP was chosen to be 10 cm in *Papers 1 to 3*, and huge impact force occurred (Li et al., 2014a) which was beyond the allowable limit of the hydraulic cylinders. It was found later that this initial gap was much smaller than the real value used in practice, and contact between the cylinders and the MP should always be avoided during the lowering process because of the high stiffness of the cylinders. In *Papers 4 and 5*, the gripper device in the numerical model was excluded, and the relative motion between the MP and the HLV was used as the limiting parameter to judge whether an impact would occur.

In the coupled model for the initial hammering process, the gripper was closed and a pre-compression force of 150 kN for each hydraulic cylinder was applied. The stiffness of the cylinder was chosen according to the common design of the hydraulic cylinders (IHC, 2015). The damping was taken to be 20% of critical damping according to empirical values (Albers, 2010). Sensitivity studies to quantify the effects of the gripper stiffness on the responses during the lowering of a MP were performed by Li et al. (2013a). The study showed that the contact force and the relative motion between the MP and the gripper device were very sensitive to the stiffness.

2.3.3 MP-soil interactions

The soil-pile interaction forces in the shallow soil penetration phases are three-dimensional (3D), and in principle a 3D finite element method (FEM) (Lesny and Wiemann, 2006) should be applied to predict the interaction forces. However, the FEM approach is time-consuming for the coupled global response analysis. Therefore, in this thesis the MP-soil interaction is modelled using the widely applied Winkler model by means of distributed

springs (Carswell et al., 2015; Bisoi and Haldar, 2014; Andersen et al., 2012; Gerolymos and Gazetas, 2006; Ong et al., 2013) and hysteretic material damping (Carswell et al., 2015; Hededal and Klinkvort, 2010). The proposed model included the traditional distributed $p - y$ curve for piles with large length-to-diameter ratio (DNV, 2014b; API, 2007), the distributed moment curve due to the vertical shear (skin friction) which was found to be important for short piles with large diameter (Byrne et al., 2015; Lesny and Wiemann, 2006) and the base shear curve.

Because of the large diameter of the monopile relative to the penetration depth, the commonly used 2D Winkler model is extended to 3D by using non-linear springs distributed in both axial and circumferential directions along the MP. The distributed springs include the lateral load-deflection $p - y$ curve, the friction $T - z$ curve, the base shear curve and the tip load-displacement $Q - z$ curve. The configuration of springs as shown in Figure 2.6 is summarized as follows: 4 vertical springs K_{q-z} to model $Q - z$ curves at the bottom of the MP; 4 springs T_z on the side of the MP to model the $T - z$ curve due to friction force from both inside and outside walls of the MP. For $p - y$ curves, the whole penetration was divided into several 2 m layers, and 4 circumferential springs K_{p-y} were applied for each layer. At the bottom of the MP, 4 springs K_{shear} were used to model the shear resistance force. The number of distributed springs was considered to be sufficient since the MP bottom tip experienced small displacement (less than 10 cm for typical sea states).

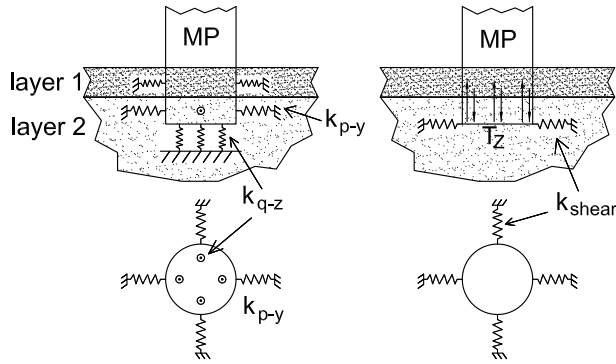


Figure 2.6: Numerical models for the soil-MP interactions during the initial hammering process

A sensitivity study on the soil properties concluded that the system behaviour and procedure to establish the allowable sea states for the initial hammering process did not depend on the soil properties (Li et al., 2016c)

(*Paper 6*). Therefore, representative values for the non-linear springs for the soil-MP interaction are considered to be sufficient for the case study, and the stiffness for all the non-linear distributed springs shown in Figure 2.6 was taken from the API guideline (API, 2007). Soil damping is included in this model in terms of dynamic friction force.

2.4 Numerical methods

Several numerical tools are available to carry out simulations for marine operations, e.g., MARINTEK SIMO program (MARINTEK, 2012a,b), ANSYS AQWA (ANSYS, 2011), MOSES (Ultramarine, 2009), OrcaFlex (Orcina, 2013) and LIFSIM (van Dijk and Friisk, 2005). These programs are capable of solving the non-linear equations of motion in the time domain for coupled marine systems exposed in wind, wave and current, e.g., lifting operations, launching and offshore mating operations.

The numerical models in the thesis were established using the SIMO program. For the initial hammering operation, the model in SIMO was verified with the one built in ANSYS AQWA, and consistent results were obtained.

2.4.1 Equations of motion

When using a floating installation vessel, the coupled system has 12 degrees of freedom (*DOFs*). The coupled equations of motion for the vessel-monopile system are as follows,

$$(\mathbf{M} + \mathbf{A})\ddot{\mathbf{x}} + \mathbf{D}_1\dot{\mathbf{x}} + \mathbf{D}_2f(\dot{\mathbf{x}}) + \mathbf{K}\mathbf{x} + \int_0^t \mathbf{h}(t - \tau)\dot{\mathbf{x}}(\tau)d\tau = \mathbf{F}_{ext}(\mathbf{x}, \dot{\mathbf{x}}, t) \quad (2.3)$$

where, \mathbf{M} is the total mass matrix; \mathbf{x} is the rigid-body motion vector with 12 *DOFs*; \mathbf{A} is the total added mass matrix; \mathbf{D}_1 and \mathbf{D}_2 are the linear and quadratic damping matrices. The viscous effects due to the vessel hull were simplified into linear damping terms in surge, sway and yaw. The roll damping of the vessel as well as the quadratic damping on the MP were also included. Additionally, \mathbf{K} is the total restoring matrix of the system, including the contributions from the hydrostatic restoring of the HLV and the MP, \mathbf{K}_{hydro} , the mooring lines of the vessel, \mathbf{K}_{moor} , the soil interaction on the monopile, \mathbf{K}_{soil} , and the coupling between the vessel and the load through lift wire or gripper device, \mathbf{K}_{cpl} . \mathbf{h} is the retardation function for the vessel calculated from the frequency-dependent added mass or potential

damping coefficients. \mathbf{F}_{ext} is the external force vector, including the first-order and second order wave excitation forces on the vessel, $\mathbf{q}^{(1)}_{WA}$ and $\mathbf{q}^{(2)}_{WA}$, and the wave excitation force on the monopile, \mathbf{F}_W .

The wave excitation forces on the MP, \mathbf{F}_W , were calculated using different methods for the lowering and the hammering processes. Because steady-state simulations were performed for the hammering process, the hydrodynamic interaction between the HLV and MP was directly solved in the multi-body panel method program WAMIT (Lee, 1995) in the frequency-domain and applied in the time-domain using the force transfer functions. The methodology to account for the hydrodynamic interaction during the MP nonstationary lowering process are discussed in Chapter 3.

In *Papers 1-4*, the wave forces on the HLV only included the first-order wave excitation force, and the mooring lines of the HLV were simplified as linear springs and included in the hydrostatic restoring matrix. In *Papers 5 and 6*, the second-order wave excitation forces were calculated based on the Newman's approximation and only the difference-frequency slowly varying forces were included (Newman, 1974). The eight catenary mooring lines for the HLV were also modelled. Both a quasi-static analysis and a simplified dynamic analysis accounting for the effect of drag loading on the lines were applied. Wind and current loads were not considered in the thesis work.

2.4.2 Eigenvalues of the system

The natural modes of the coupled HLV-MP lowering system include 12 DOFs. A detailed explanation of the modes and corresponding natural periods is given by Li et al. (2015c) (*Paper 4*). Figure 2.7 shows the natural periods of the system excluding the yaw mode of MP. The gripper was excluded, the draught of the HLV was 10.2 m and mooring lines were modelled when calculating the natural periods.

During the lowering process, the properties of the system vary with time due to the changing position of the MP. Thus, the natural modes and periods are dependent on the MP position as shown in Figure 2.7. It should be noted that all the modes are coupled, and only the dominant DOFs are mentioned in the figure. It can be expected that in short waves the MP rotational modes (modes 02 and 03) could be excited, and in longer waves the vessel motions in the vertical plane are more relevant.

2.4.3 Time-domain simulations

Time-domain simulations were performed to study the dynamic response of the non-linear systems. Step-by-step integration methods were applied using

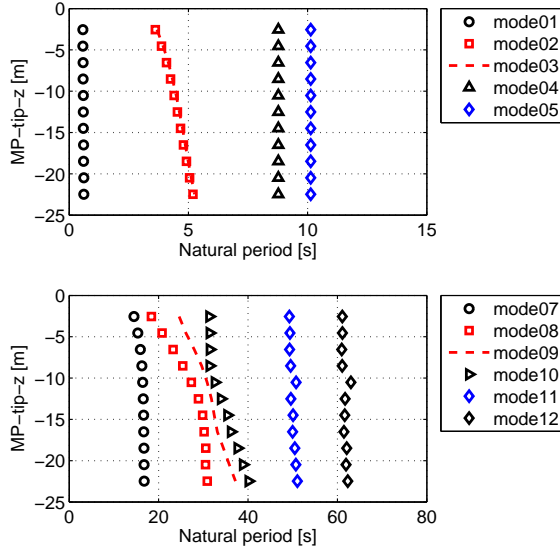


Figure 2.7: Natural periods for the coupled HLV-MP lowering system with varying MP positions. Dominant motion for each mode: mode01 (MP heave); mode02 and 03 (MP roll and pitch, MP rotational motions); mode04 (HLV pitch); mode05 (HLV heave); mode07 (HLV roll); mode08 and 09 (MP pendulum motions); mode10-12 (HLV yaw, sway and surge)

an iterative routine. The equations of motion were solved using Newmark-beta numerical integration with a time step of 0.01 sec in *Papers 1,4 and 6* and 0.02 sec in *Papers 2,3 and 5*. Stochastic irregular waves were used as environmental input. The time series of the wave kinematics were obtained using the Fast Fourier Transformation (FFT) algorithm from JONSWAP wave spectrum for selected significant wave height, H_s and spectral peak period, T_p . Long-crested waves were used in *Papers 1,2 and 4*, and short-crested waves were considered in *Papers 3, 5 and 6*. The first- and second-order wave forces were pre-generated using the FFT algorithm at the mean position of the HLV. The mechanical couplings, mooring line tensions as well as the soil-MP interaction forces were calculated in the time-domain.

The number and length of simulations were chosen in order to account for the variability of stochastic waves and to provide a reasonable statistical basis for comparison. For instance, 20 realisations of irregular waves were generated at each environmental condition using different seeds (400 sec for each seed) for monopile lowering process. 20 repetitions of the simulations corresponded to an operation with a duration of approximately two hours.

Chapter 3

Dynamic analysis of monopile lowering and initial hammering processes

3.1 Overview

Accurate and realistic modelling is required to quantify the dynamic responses of different installation systems, allowing for better planning of the operations. MP lowering process is a typical lifting operation activity. Many numerical studies have been performed to estimate the characteristic responses of offshore lifting operations, including the installation of sub-sea templates (Aarset et al., 2011), suction anchors (Gordon et al., 2013), foundations and topsides of platforms, and wind turbine components (Graczyk and Sandvik, 2012; Ku and Roh, 2014). A few experimental studies have also been conducted to obtain accurate hydrodynamic coefficients, e.g., the hydrodynamic mass and damping coefficients of ventilated piles (Perry and Sandvik, 2005), or to tune the critical parameters for numerical models, e.g., the damping or stiffness coefficients of important support structures in the lifting system (van der Wal et al., 2008).

One challenge when studying the MP lowering activity using a floating vessel is the hydrodynamic interaction between the vessel and the monopile during the nonstationary process with time-varying dynamic features of the system. In lifting operations using floating vessels, hydrodynamic interaction between the structures in waves is of great importance. Studies have been performed to investigate the heavy lift operations considering shielding effects, such as the lifting of a heavy payload from a transport barge using a

large capacity semi-submersible crane vessel (Mukerji, 1988; van den Boom et al., 1988; Baar et al., 1992). These studies found that the hydrodynamic interaction had little effect on the responses of the crane tip, but greatly affected the responses of the transport barge because of its small dimensions compared with the one of the crane vessel (Baar et al., 1992). Therefore, the hydrodynamic interaction between two floaters close to each other should be taken into consideration when estimating their responses.

Sandvik (2012) proposed two approaches that can be used to simulate nonstationary processes:

1. Find the most critical vertical position of the object and then make steady-state simulations in irregular waves at this position.
2. Simulate a repeated nonstationary lowering process with different irregular wave realizations, and study the extreme response observed in each simulation.

It was demonstrated that the second method provides more realistic results because an unrealistic build-up of the oscillation occurs in the first stationary approach. In principle, to provide more accurate estimates of the operations, analyses of the entire lowering process are required.

The properties of the nonstationary process are time-variant, i.e., the total mass, stiffness and damping of the system change with time. Therefore, the equations of motion, Equation (2.3) and the natural frequencies of the system (e.g., natural frequency of MP lowering system in Figure 2.7) are time-dependent. In addition, the use of traditional frequency-domain analysis to solve the hydrodynamic interaction problem is not applicable for the entire lowering process. The hydrodynamic properties in the frequency-domain analysis are expressed with the boundary condition given on the mean wet surface, while the lifted structure experiences a large change of position when it moves downward toward the seabed. Therefore, time-domain solutions that consider the nonstationarity of the process are required.

Li et al. (2014a) (*Paper 1*) proposed a method to account for the shielding effects from the installation vessel during the entire lowering process of a monopile. The approach applied Morison's formula to calculate the hydrodynamic forces on the monopile. The approach was further studied and extended to compare the performance during lifting a MP and a jacket OWT foundation, respectively in Li et al. (2015a) (*Paper 2*). Effects of short-crestedness on the shielding effects were also studied in Li et al. (2016a) (*Paper 3*). In addition, the importance of radiation damping of the MP during the nonstationary lowering process was examined by Li et al. (2015c) (*Paper 4*). An approach to account for the radiation damping of

the MP in the time-domain simulation of the nonstationary lowering process was also developed.

In addition to the wave loads on the vessel and on the MP, the soil reaction force plays an important role on the responses of the system during the MP initial hammering process. The soil reaction forces on the MP influence the vessel motions through the gripper device. Detailed global dynamic analysis on the initial hammering process was carried out by Li et al. (2016c) (*Paper 6*).

This chapter presents the dynamic responses of the MP lowering and initial hammering systems. Different numerical approaches are discussed and the results are obtained from time-domain simulations in stochastic waves.

3.2 Shielding effects from the HLV

3.2.1 Morison's formula approximation for slender structures

For slender bodies with diameter-to-wavelength ratio less than $1/5$, the empirical Morison's formula is often used to calculate hydrodynamic forces (Morison et al., 1950). The effects of diffraction and radiation are considered insignificant in the slender-body approximation. The Morison's formula is applied to calculate the wave forces on the MP with diameter of 5.7 m. The MP is divided into strips, and the wave force $f_{w,s}$ per unit length on each strip normal to the member is (Faltinsen, 1990):

$$f_{w,s} = \rho_w C_M \frac{\pi D^2}{4} \ddot{\zeta}_s - \rho_w C_A \frac{\pi D^2}{4} \ddot{x}_s + \frac{1}{2} \rho_w C_q D \left| \dot{\zeta}_s - \dot{x}_s \right| (\dot{\zeta}_s - \dot{x}_s) \quad (3.1)$$

where, $\ddot{\zeta}_s$ and $\dot{\zeta}_s$ are the fluid particle acceleration and velocity at the centre of the strip, respectively; \ddot{x}_s and \dot{x}_s are the acceleration and velocity at the centre of the strip due to the body motions; D is the outer diameter of the member; and C_M , C_A and C_q are the mass, added mass and quadratic drag force coefficients, respectively. The distributed wave forces $f_{w,s}$ are integrated along the MP to obtain the total wave forces and moments, F_W . The added mass coefficients for different strips along the MP are different. For the strips close to the bottom of the monopile, $C_A \approx 1$, whereas for strips located further away from the bottom, $C_A \approx 2$ because the wall thickness is small compared with the diameter, and the water trapped inside the monopile follows the motions of the structure (Li et al., 2015c). The excitation forces calculated using Morison's formula are later validated with those from panel method in Figure 3.3.

In addition, the nonlinear effects due to the instantaneous free surface and the instantaneous body positions can be also included in the time-domain. It can be done by evaluating at each time step and in each strip for instantaneous body positions and integrating up to the instantaneous free surface. The Morison's formula can be applied for both steady-state and nonstationary lowering analyses.

3.2.2 Methodology to include shielding effects during non-stationary lowering process

For the MP lowering operation, the hydrodynamic effects of the MP on the HLV are minor and can be neglected. However, the wave field near the HLV is altered from the original incident waves due to the diffraction and radiation from the vessel. Thus, the hydrodynamic interaction between HLV and MP can be simplified as "one-way" interaction by considering the shielding effects from the HLV on the MP while ignoring the effects from the MP on the HLV.

The waves affected by both radiation and diffraction of the vessel are defined as *disturbed waves*, which includes the vessel shielding effects, while the undisturbed waves are defined as *incident waves*. Li et al. (2014a) (*Paper 1*) studied the fluid kinematics around the HLV, and they concluded that the effects from the HLV were three-dimensional and would vary from vessel to vessel. Because the position of the monopile varied with time and with the increasing length of the lift wire, the fluid kinematics at each strip of the monopile were time- and position-dependent. Therefore, the following approach was used to account for the shielding effects from the HLV for the nonstationary lowering process.

1. First, generate time series of disturbed fluid kinematics at pre-defined *wave points* in space, i.e., wave elevation, velocities and accelerations.

Knowing incident wave elevation time history $x(t)$, the Fourier transform of the kinematics of the disturbed wave $Y(\omega)$ can be calculated based on the Fourier transform of $x(t)$, $\mathcal{F}\{x(t)\} = X(\omega)$, and the disturbed fluid kinematics transfer functions $H(\omega)$, see Equation (3.2). Thus, using inverse Fourier transform of $Y(\omega)$, the time series of wave kinematics in disturbed waves at each pre-defined wave point can be obtained.

$$Y(\omega) = H(\omega) \cdot X(\omega) \quad (3.2)$$

2. Then, at each time step, determine the instantaneous position of the MP based on the solutions from the previous time step. For each

strip on the MP, find the closest pre-defined eight wave points. By applying a 3D linear interpolation between these closest wave points, the kinematics at each strip in disturbed waves are calculated. The interpolation of the fluid kinematics is illustrated in Figure 3.1.

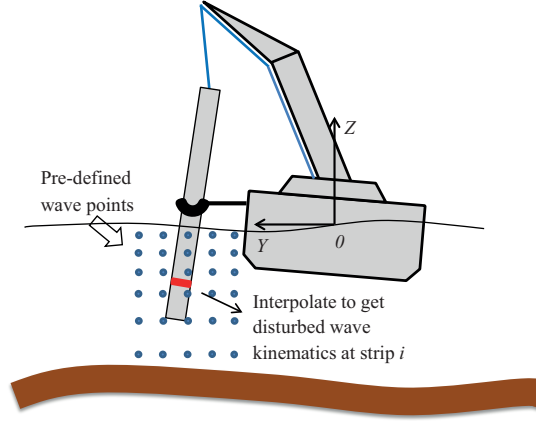


Figure 3.1: Interpolation of fluid kinematics in disturbed waves

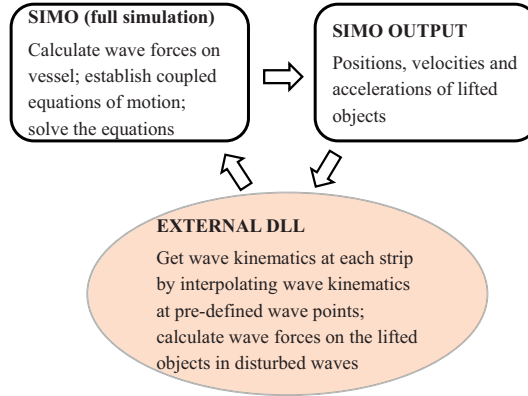


Figure 3.2: Time-domain simulation approach considering vessel shielding effects

3. Obtain the forces at each strip in disturbed waves using Morison's formula in Equation (3.1) and then integrate along the submerged part of the monopile to acquire the total wave forces and moments on the structure. It is necessary to integrate the forces up to the instantaneous wave elevation to account for non-linear force components.
4. Finally, perform time-domain simulations of the coupled HLV-MP sys-

tem using the multi-body code SIMO and an external DLL that interacts with SIMO at each time step. SIMO calculates the wave excitation forces on the vessel and the coupling forces between the vessel and the MP. The wave forces on the MP in disturbed waves are calculated in the DLL using the aforementioned interpolation method, and the total wave forces on the MP are returned to SIMO, so that the motions of the coupled system are solved. The time-domain approach is illustrated in Figure 3.2.

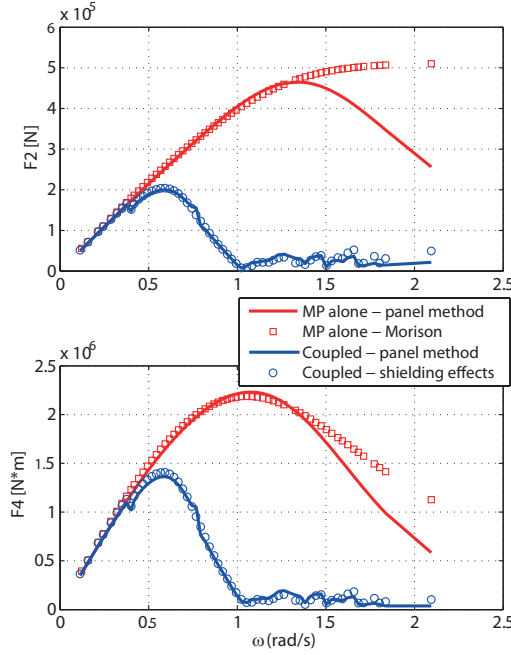


Figure 3.3: Comparison of the excitation force on the MP in incident wave and when accounting for shielding effects from the HLV (F_2 and F_4 denote the force in sway and moment in roll, $Dir = 90$ deg, draft = 15 m)

To demonstrate the accuracy of the slender body assumption, the wave excitation forces on the MP were calculated at a draft of 15 m and compared in Figure 3.3 for four cases: (1) MP alone using panel method; (2) MP alone using Morison's formula in incident wave; (3) HLV-MP coupled using panel method and (4) HLV-MP coupled using the proposed shielding effect method. It is evident that the shielding effects from the HLV (coupled HLV-MP case) reduce the excitation force on MP significantly from intermediate to short wave lengths. The results show good agreement between the slender body assumption and the multi-body panel method. Therefore,

the simplified approach to account for shielding effects is considered reasonable to calculate the excitation force on the MP for the HLV-MP coupled condition during the nonstationary lowering process.

Sensitivity studies on the resolution of the pre-defined *wave points* were performed in Li et al. (2014a) using different bin sizes between points in the horizontal plane and vertical direction. It was observed the responses in short waves were more sensitive to the resolution, and low resolution would result in large error in extreme responses. From the sensitivity study, for the MP lowering process, a resolution with gaps of 4 m in the horizontal plane and 2 m in the vertical direction was chosen.

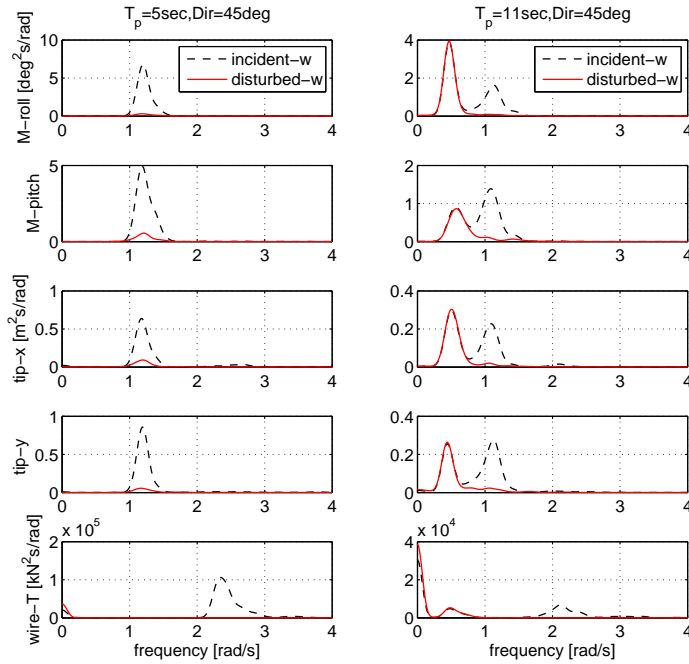


Figure 3.4: Spectral density of responses during lowering in incident and disturbed waves ($H_s = 2.5$ m)

3.2.3 Dynamic responses of the MP lowering system in disturbed waves

Li et al. (2014a) (*Paper 1*) studied the responses of the dynamic system for MP lowering in incident and disturbed waves comprehensively. Figure 3.4 compares the response spectra of the lowering phase at two wave conditions. The shielding effects from the HLV reduce the MP resonant motions (with

peaks at $\omega \approx 1.1$ rad/s) greatly for both wave conditions, while the vessel induced motions in long waves are not affected. These results indicate the significant influence of the shielding effects on the MP motions in short waves when the wave frequencies are close to the natural frequencies.

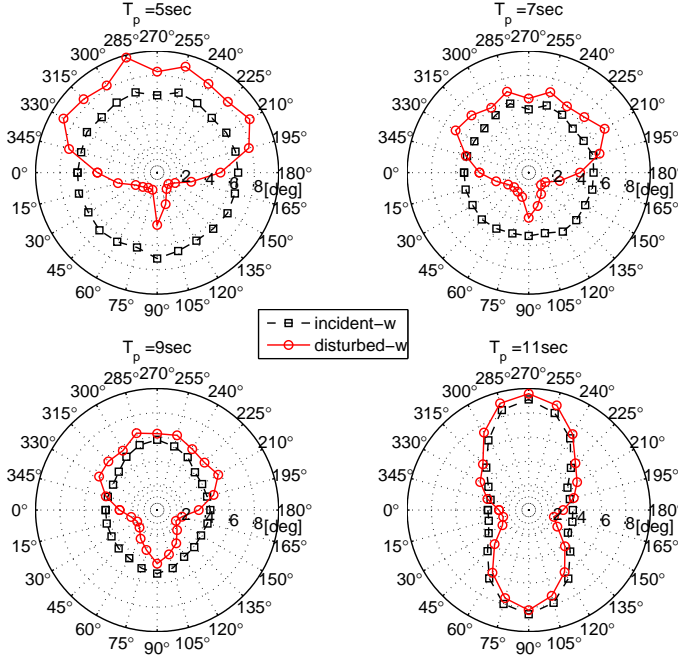


Figure 3.5: Extreme rotation of the monopile in incident and disturbed waves at different wave directions ($H_s = 2.5$ m)

Figure 3.5 compares the statistics of the extreme rotation of the MP (the maximum rotation angle during the entire lowering process) in disturbed waves with those in incident waves at different wave directions. In short waves ($T_p = 5$ and 7 sec), the responses are significantly reduced in disturbed waves when the MP is placed on the leeward side of the vessel. With increasing wave length, the differences between the responses in disturbed and incident waves are rapidly reduced. The results for long-crested waves show that the extreme responses reached minimum values for wave directions of approximately $Dir = 45$ to 60 deg in short waves when considering shielding effects. In long waves, the minimum extreme values were acquired at headings of about 15 deg. Therefore, it is possible to minimize the responses by selecting a proper heading of the vessel including shielding effects.

Figure 3.6 compares the extreme rotations of the MP in different wave directions when using a jack-up and the floating vessel. For the case with the floating vessel the shielding effects of the vessel were included, whereas only the incident waves were considered for the case with the jack-up vessel.

In short to intermediate waves, the resonant motions of the MP dominate (see the natural frequency in Figure 2.7); thus, the extreme rotations when using the floating vessel are lower than when using the jack-up vessel at $Dir = 0$ to 180 deg due to the shielding effects from the floating vessel. With increasing wave length, the motions of the floating vessel increase and dominate the responses of the system, and hence the responses when using the floating vessel exceed those using the jack-up vessel, particularly for headings close to beam seas.

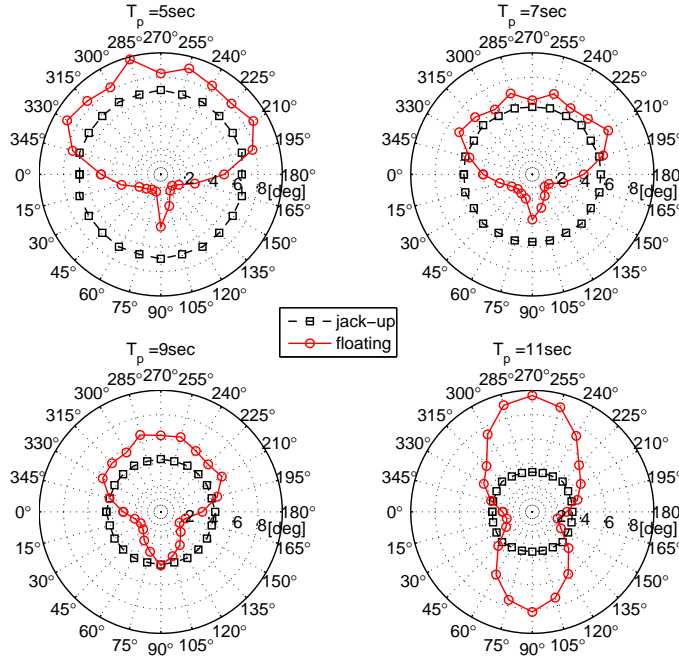


Figure 3.6: Extreme monopile rotations using a jack-up and the HLV at different wave conditions ($H_s = 2.5$ m)

Therefore, it is recommended to use the floating vessel in short to intermediate wave lengths with a proper heading of the vessel. Use of a jack-up vessel is recommended in long waves to prevent large crane tip motions that occur when using the floating vessels.

3.2.4 Comparative study of lowering a monopile and a jacket considering shielding effects

Li et al. (2015a) (*Paper 2*) compared the responses of lowering a monopile and a jacket considering shielding effects from the HLV. The lowering systems refer to Figures 2.1 and 2.2, respectively.

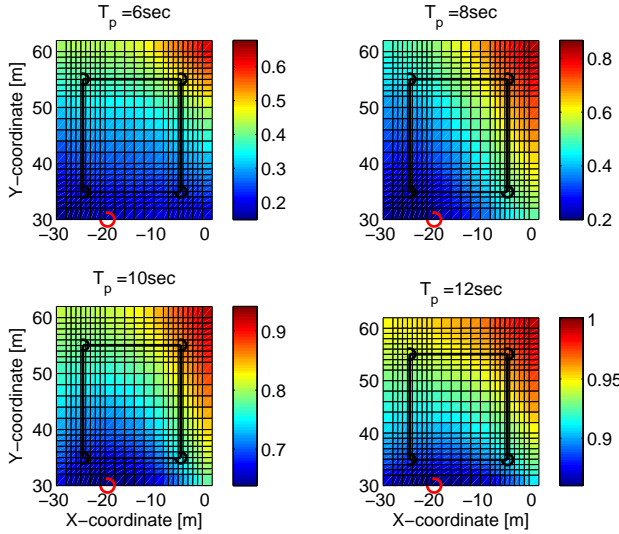


Figure 3.7: RAOs of wave elevation at four wave frequencies in disturbed waves in XY plane ($Dir = 150$ deg, $Z = 0$ m)

The wave kinematics near the positions of the structures in disturbed waves were studied in frequency domain. Figure 3.7 shows the variations of the wave elevation RAOs in disturbed waves. The coordinate system refers to Figure 2.3, and the initial positions of the four jacket legs (black circles) as well as the MP (red circles) are also shown. The RAOs depend greatly on the wave frequency and the positions relative to the vessel. Due to the large footprint of the jacket foundations, the wave kinematics are always smaller at the side close to the vessel (with small Y coordinate) compared to the side away from the vessel, especially in short waves. The RAOs at the MP positions are much less than all the four jacket legs.

The standard deviations ($STDs$) of the responses were obtained from the time-domain simulations of the two lifting system with a MP draft of 20 m and a jacket draft of 30 m and are compared in Figure 3.8.

For the MP lifting system, significant decrease of the MP tip motion in X direction can be observed in all wave conditions when considering shielding effects, but the effects are reduced with increasing wave length.

The motions in Y and Z directions are greatly affected by vessel roll motion which increases significantly when the wave direction moves to quartering seas in incident waves.

For the jacket system, however, the $STDs$ of the motions are much less influenced by the shielding effects compared to the MP system. Although a great decrease of jacket tip Y motion can be observed near quartering sea in short to medium waves when considering shielding effects, the responses in X and Z directions vary little.

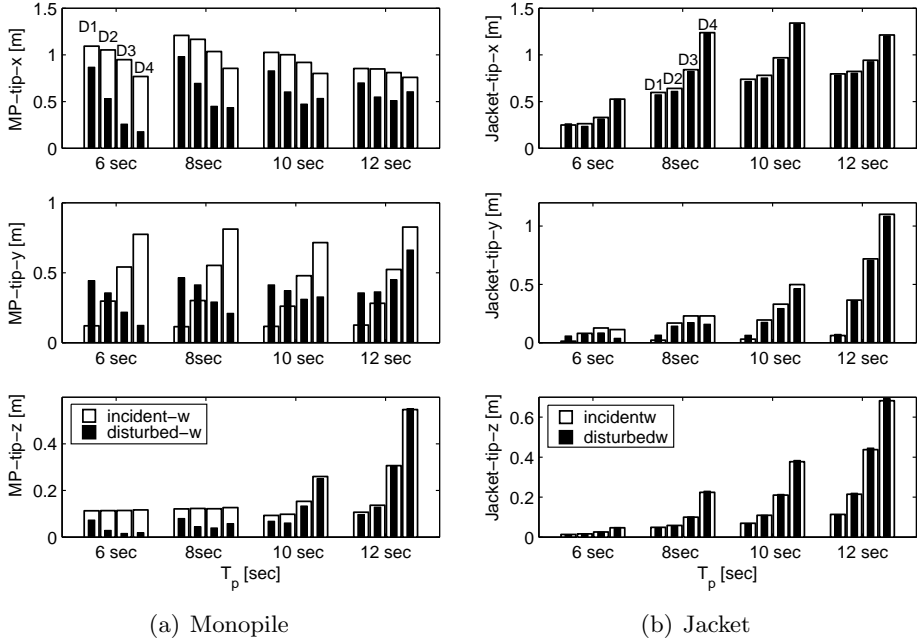


Figure 3.8: $STDs$ of MP and jacket motions in incident and disturbed waves ($H_s = 2$ m, for each T_p the directions from left to right are $D_1 = 180$ deg, $D_2 = 165$ deg, $D_3 = 150$ deg, $D_4 = 135$ deg)

The reasons for the differences between the two lifting systems are summarized as follows:

1. The response amplitudes at resonance are higher for the MP than for the jacket due to larger excitation force with larger dimension and lower quadratic damping of the MP.
2. The fluid kinematics in disturbed waves on the MP are much lower than the values on the jacket members because of the large footprint of the jacket structure.

3. The eigenvalues of the two systems are different for the rigging system selected in this study. For the MP system, the rotational natural periods are in the short wave ranges so that the resonant motions can be greatly reduced by the shielding effects. While for the jacket, all the natural periods are coupled with the vessel and in relatively long wave range, which makes the shielding effects less important.

3.2.5 Shielding effects in short-crested waves

Wind-generated seas in real sea conditions involve short-crested waves (Goda, 2010; Chakrabarti, 1987). The directional spreading of wave energy may give rise to forces and motions which are different from those corresponding to long-crested waves. DNV (2014c) recommends to check “whether long crested or short crested sea is conservative for the analysis concerned”. Li et al. (2016a) (*Paper 3*) evaluated the influence of the short-crestedness when including the shielding effects from the HLV on the responses of the MP lowering system.

The sea state is commonly represented by a wave spectrum as

$$S(\omega, \theta) = S(\omega)D(\omega, \theta) \quad (3.3)$$

$$\int_{-\pi}^{\pi} D(\omega, \theta) d\theta = 1 \quad (3.4)$$

The frequency dependence of the directional function is often neglected, that is, $D(\omega, \theta) = D(\theta)$. One of the most widely used $D(\theta)$ is the cosine power function given as (DNV, 2010)

$$D(\theta) = \begin{cases} C(n)\cos^n(\theta - \theta_0) & |\theta - \theta_0| \leq \pi/2 \\ 0 & |\theta - \theta_0| > \pi/2 \end{cases} \quad (3.5)$$

where θ_0 is the main wave direction about which the angular distribution is centred. The parameter n is a spreading index describing the degree of wave short-crestedness, with $n \rightarrow \infty$ representing a long-crested wave field. $C(n)$ is a normalizing constant ensuring that Equation (3.4) is satisfied. Typical values for the spreading index for wind generated sea are $n = 2$ to 4. Due to the fact that lifting operations are usually carried out in relatively low sea states, the spreading of the waves can be significant especially for floating structures.

For long-crested waves, the Fourier transform of the kinematics of the disturbed wave can be calculated based on Equation (3.2). For a wave direction θ_0 , it results:

$$Y(\omega, \theta_0) = H(\omega, \theta_0) \cdot X(\omega) \quad (3.6)$$

For short-crested waves, the incident wave realization includes different wave direction components and is generated from the two-dimensional wave spectrum from Equation (3.3). The Fourier transform of the incident wave at various directions $X(\omega, \theta)$ can be obtained. Thus, the disturbed fluid kinematics for direction θ_0 become

$$Y(\omega, \theta_0) = \left\{ \int_{\theta_1}^{\theta_2} H(\omega, \theta) \cdot X(\omega, \theta) d\theta \right\} \quad (3.7)$$

where θ_1 and θ_2 are the limits for the directions. Using Equation (3.1) and (3.7), the excitation forces on the MP account for both shielding effects and short-crestedness of the waves and can be applied for the nonstationary lowering process.

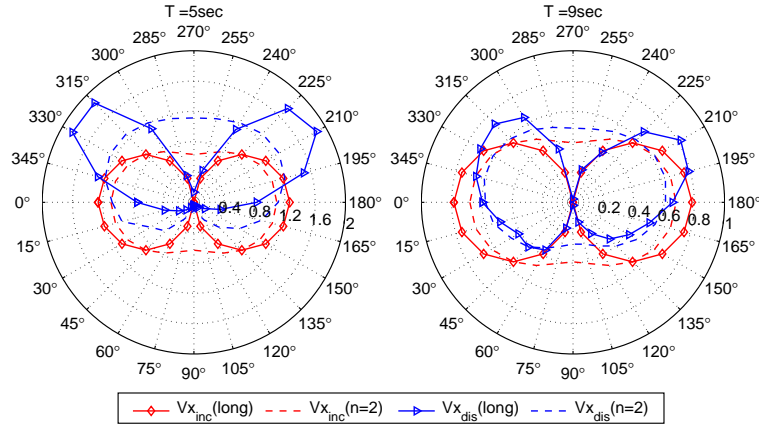


Figure 3.9: RAOs of fluid X-velocities at two wave frequencies in incident and disturbed waves with and without spreading

Figure 3.9 shows an example of the RAOs of fluid particle X-velocity near the MP in incident and disturbed waves. When only long-crested waves are considered, the differences between the RAOs in incident and disturbed waves are significant. However, these differences can be reduced considerably when including the wave spreading. For example, the RAOs of X-velocity at $T = 5$ sec near 180 deg direction in disturbed waves are close to those in incident waves with spreading index $n = 2$. This is because the spreading function averages the low RAOs in the leeward side of the vessel and the large RAO values in the windward side.

The approach proposed to consider shielding effects from the HLW in Sec. 3.2.2 was extended and applied in short-crested waves in Li et al. (2016a) and time-domain simulations were carried out. Figure 3.10 compares the *STDs*

of the MP tip motions in incident waves with those in disturbed waves with and without wave spreading, respectively. For both cases, it is observed the shielding effects reduce the responses significantly in short waves and the reduction decreases when increasing the wave length. The shielding effects are more pronounced in long-crested waves than in short-crested waves. Besides, the differences between responses at different headings are much smaller in short-crested waves than in long-crested waves as the spreading of the wave energy over neighbour directions averages the shielding effects.

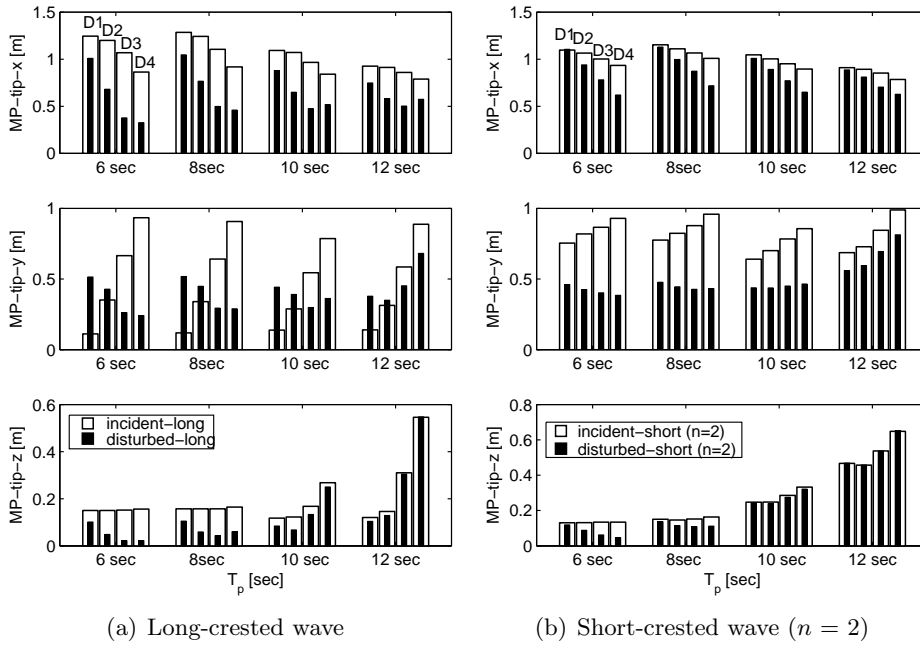


Figure 3.10: STDs of MP tip motions in incident and disturbed waves with and without wave spreading ($H_s = 2.0$ m, for each T_p the directions from left to right are $D_1 = 180$ deg, $D_2 = 165$ deg, $D_3 = 150$ deg, $D_4 = 135$ deg)

In both long and short-crested cases, the most suitable heading angle is observed close to quartering seas in short waves and it moves towards to heading seas with increasing wave length. However, the responses at the most suitable heading angles in long-crested waves are always lower than those in short-crested waves. Thus, the wave spreading should be considered to avoid non-conservative results. The influence from wave spreading is expected to be less when using higher spreading indexes.

3.3 Radiation damping effects from the MP

3.3.1 Methodology to consider radiation damping on the MP for nonstationary lowering process

As pointed out, Morison's formula is based on the slender body assumption when the effects of diffraction and radiation are insignificant. However, with the increased diameter of an offshore MP, the applicability of Morison's formula becomes questionable, especially in relatively short wave conditions. In such cases, the diffraction and radiation of the MP can be important. Li et al. (2015c) (*Paper 4*) studied the effects of radiation damping on the responses of the MP lowering system. First, a method was proposed to study the responses with a fixed draft by using Morison's equation and including the radiation damping. Because the goal is to calculate the non-stationary lowering process, time-domain simulations are required. Potential theory provides the frequency-dependent added mass and damping coefficients, and the retardation function is computed using a transform of the frequency-dependent added mass and damping to be used in the time domain, with reference to the following equation

$$h(\tau) = \frac{2}{\pi} \int_0^\infty c(\omega) \cos(\omega\tau) d\omega = -\frac{2}{\pi} \int_0^\infty \omega a(\omega) \sin(\omega\tau) d\omega \quad (3.8)$$

The frequency-dependent added mass $a(\omega)$ and damping $c(\omega)$ can also be derived from the retardation function:

$$\begin{aligned} a(\omega) &= -\frac{1}{\omega} \int_0^\infty h(\tau) \sin(\omega\tau) d\tau \\ c(\omega) &= \int_0^\infty h(\tau) \cos(\omega\tau) d\tau \end{aligned} \quad (3.9)$$

In the numerical program, frequency dependent damping is used for calculating the retardation functions. The radiation force in the time-domain is thus formulated as a convolution integral formulation representing the memory effects (Cummins, 1962).

The retardation forces on the MP corresponding to a given draft in the time-domain simulations are added to the equations of motion, i.e., Equation (2.3). If one discretises the retardation function into $(N + 1)$ values with a time interval $\Delta\tau$, the radiation force term, $\mathbf{F}_{RF}^S(t)$, in the steady-state (fixed draft) condition can be written as follows:

$$\mathbf{F}_{RF}^S(t) = \int_0^t \mathbf{h}(\tau) \dot{\mathbf{x}}_r(t - \tau) d\tau = \sum_{n=0}^N \mathbf{h}(n \cdot \Delta\tau) \cdot \dot{\mathbf{x}}_r(t - n \cdot \Delta\tau) \cdot \Delta\tau \quad (3.10)$$

The retardation function \mathbf{h} only depends on the time variable τ in the steady-state condition. $\dot{\mathbf{x}}_{\mathbf{r}}$ is the velocity of the structure at the reference point, which is located on the mean free surface. This radiation term needs to be calculated at each time step during the time-domain simulation.

The proposed method using Morison's equation and retardation function was abbreviated as $ME + RT$, and compared with the one only using Morison's equation, $ME - only$ and the one using potential theory plus viscous damping $PT + viscous$ in the steady-state condition. Figure 3.11 shows an example of the comparison with a fixed crane tip. It is observed $ME - only$ overestimates the responses at the resonant frequency greatly. By adding radiation damping using $ME + RT$, the responses are consistent with those from using potential theory. The results show the importance of radiation damping for the studied lifting system, and the method $ME + RT$ is validated with $PT + viscous$.

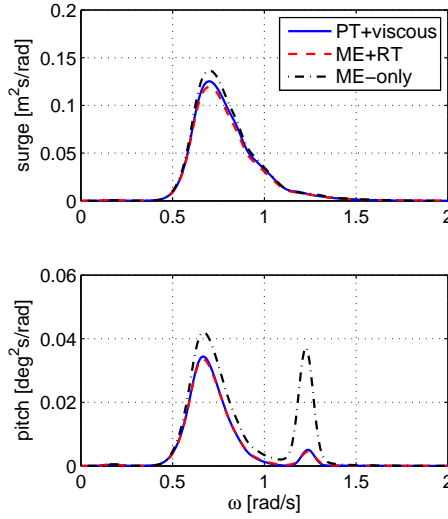


Figure 3.11: Response spectra of MP in irregular waves for $H_s = 2.0$ m, $T_p = 8$ sec, $Dir = 0$ deg (fixed crane tip, integrated up to $z = 0$ m)

Although the lowering operation is a non-stationary process, by assuming a small lowering speed, the entire lowering process can be divided into stepwise steady-state conditions. Thus, the parameters from each steady-state condition can be applied to the non-stationary process. The retardation function in this situation depends on both τ and the draft of the structure, d . The reference point of the retardation function is always located on the mean free surface in the global coordinate system, but changes

in the body-fixed coordinate due to the change of draft. Therefore, the retardation convolution term in the time-domain equation for the steady-state condition, Equation (3.10), must be modified to represent the memory effects in the non-stationary process as follows:

$$\begin{aligned} \mathbf{F}_{RF}^T(t) &= \int_0^t \mathbf{h}(d, \tau) \dot{\mathbf{x}}_r(d, t - \tau) d\tau \\ &= \sum_{n=0}^N \mathbf{h}_{d_{(t-n \cdot \Delta\tau)}}(n \cdot \Delta\tau) \cdot \dot{\mathbf{x}}_{r_{d_{(t-n \cdot \Delta\tau)}}}(t - n \cdot \Delta\tau) \cdot \Delta\tau \end{aligned} \quad (3.11)$$

where $d_{(t-n \cdot \Delta\tau)}$ is the draft at the time instant $(t - n \cdot \Delta\tau)$; $\mathbf{h}_{d_{(t-n \cdot \Delta\tau)}}$ is the retardation variable at draft $d_{(t-n \cdot \Delta\tau)}$; and $\dot{\mathbf{x}}_{r_{d_{(t-n \cdot \Delta\tau)}}}$ is the velocity of the reference point when the draft is equal to $d_{(t-n \cdot \Delta\tau)}$.

In the time-domain simulation, the retardation functions at several drafts along the MP were pre-calculated based on the panel method. Linear interpolations are subsequently applied between retardation functions at those pre-calculated drafts to obtain the retardation variable, $\mathbf{h}_{d_{(t-n \cdot \Delta\tau)}}$, in Equation (3.11) at any draft during the lowering process. The interpolation of the retardation functions in the time-domain is equivalent to the interpolation of the frequency-dependent coefficients between different drafts. The proposed method is based on the following assumptions:

- (1) The lowering speed of the MP needs to be small, and the stepwise steady-state conditions can be used to represent the continuous lowering process.
- (2) The retardation function for the structure should decay rapidly such that the system will only ‘remember’ the effects within a small change of the draft, in this manner the assumption is consistent with the assumption of the stepwise steady-state condition.
- (3) Linear interpolation of the retardation functions at pre-defined drafts can be applied to calculate the values at instantaneous drafts.

The winch speed for the lowering system was 0.05 m/s, and it takes 20 sec to increase the draft by 1 m, which is equivalent to approximately four cycles with a wave period of 5 sec. Thus, assumption (1) can be deemed reasonable because the change in the draft is sufficiently slow to represent the entire lowering process as stepwise steady-state conditions. It was observed that the retardation function approached zero after 10 sec. Thus, the system would only ‘remember’ the effects within 10 sec which corresponds to a draft change of 0.5 m. To validate assumption (3), the interpolated retardation

function at a draft of 7 m from drafts of 5 m and 10 m is for instance compared with the values directly obtained from panel method (see Figure 3.12). A good agreement between the two curves is observed.

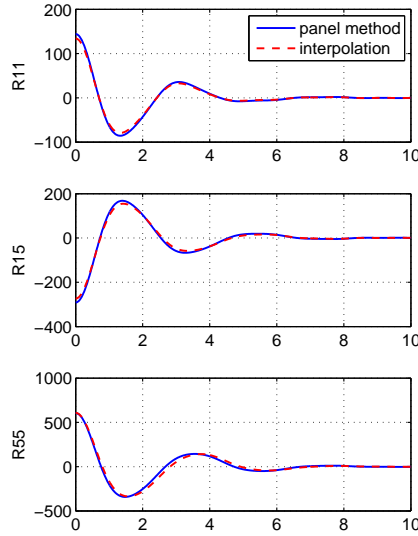


Figure 3.12: Comparison of the retardation functions at a draft of 7 m

The forces on the MP were calculated using the external DLL to account for the changing draft radiation forces. Second-order forces on the monopile were included by accounting for the effects associated with the instantaneous free surface and body positions.

3.3.2 Effect from the radiation damping of the MP

Detailed comparisons of responses from the lowering system with and without radiation damping of the monopile can be found in Li et al. (2015c). Figure 3.13 shows the response spectra in the steady-state condition after the lowering phase. The peaks of MP rotational motions are greatly reduced when accounting for the radiation damping, while the vessel-induced responses in long waves are minimally affected. Although little radiation damping exists at the pendulum natural frequency, the responses at the pendulum resonant frequency are still affected in short waves, see Figure 3.13 at $T_p = 5$ sec. Because the pendulum motions are excited by the second-order forces due to the effects from instantaneous free surface and body motions, they are reduced when the first-order motions decrease with the addition of the potential damping. In addition, the influences of po-

tential damping on the total motions of the monopile are smaller compared with the fixed crane condition because the vessel considerably affects the monopile motions in long waves.

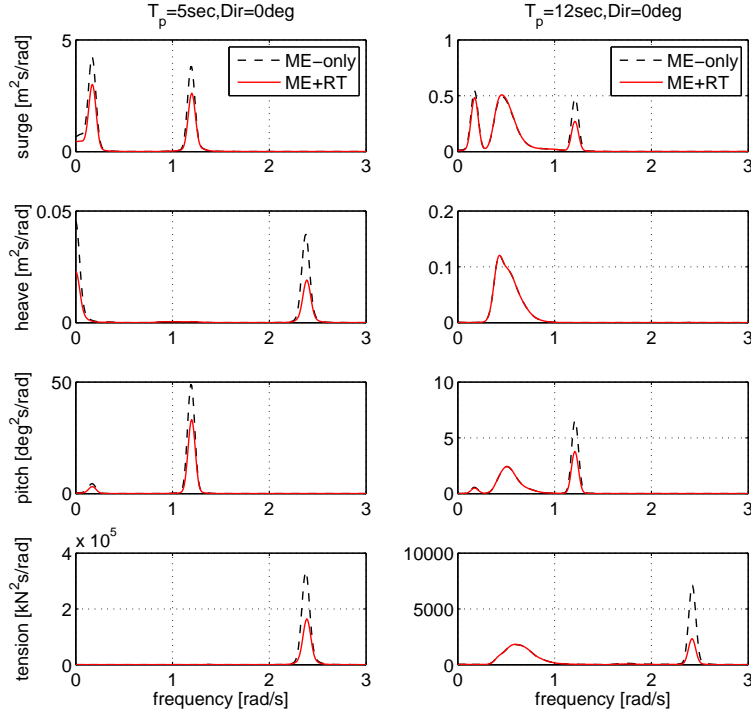


Figure 3.13: Response spectra of the steady-state condition (floating vessel, $H_s = 2.5$ m)

The *STDs* of the responses at various wave period conditions when using the floating vessel are shown in Figure 3.14 with varying irregular wave peak periods. The *STDs* are given at two resonant motions to compare the effects of radiation damping on them. The *STDs* at the rotational and pendulum resonant frequencies are compared individually by filtering the response signals close to the resonant frequencies.

The resonant motions at the rotational natural period decrease with T_p because the wave peak period moves away from the natural period. The pendulum motions also decrease with T_p due to lesser second-order forces. The differences between the methods *ME-only* and *ME+RT* are more significant for the rotational resonant motion. The pendulum motions are nearly the same in the two methods in long waves, whereas the rotational resonant motions can still be greatly reduced.

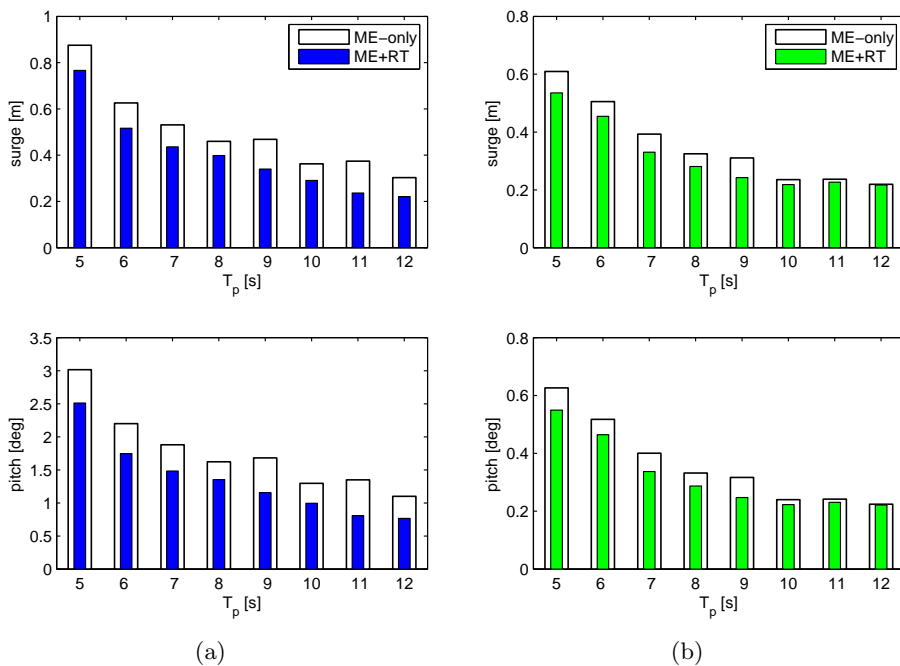


Figure 3.14: *STDs of the responses in the steady-state condition using the floating vessel ($H_s = 2.5$ m, $Dir = 0$ deg): (a) rotational resonant motion; (b) pendulum resonant motion*

3.4 Dynamic responses during the initial hammering process

3.4.1 Dynamic responses with various MP penetrations

Five penetration depths of the MP in seabed were considered, i.e., 2 m, 4 m, 6 m, 8 m, and 10 m, to study the responses of the MP in different stages during the initial hammering process in Li et al. (2016c) (*Paper 6*). The condition with HLV free floating was also included for comparison against the coupled HLV-MP dynamic responses at various loading conditions. The dynamic responses from the time-domain simulations include the motions of the HLV-MP system, and forces from the coupling in the gripper, the mooring lines of the HLV as well as the soil-MP interaction.

Figure 3.15 compares the responses of the HLV in free floating condition (*HLV – only*) and the HLV coupled with the MP at different penetration depths. This figure displays the standard deviations (*STD*) of the HLV

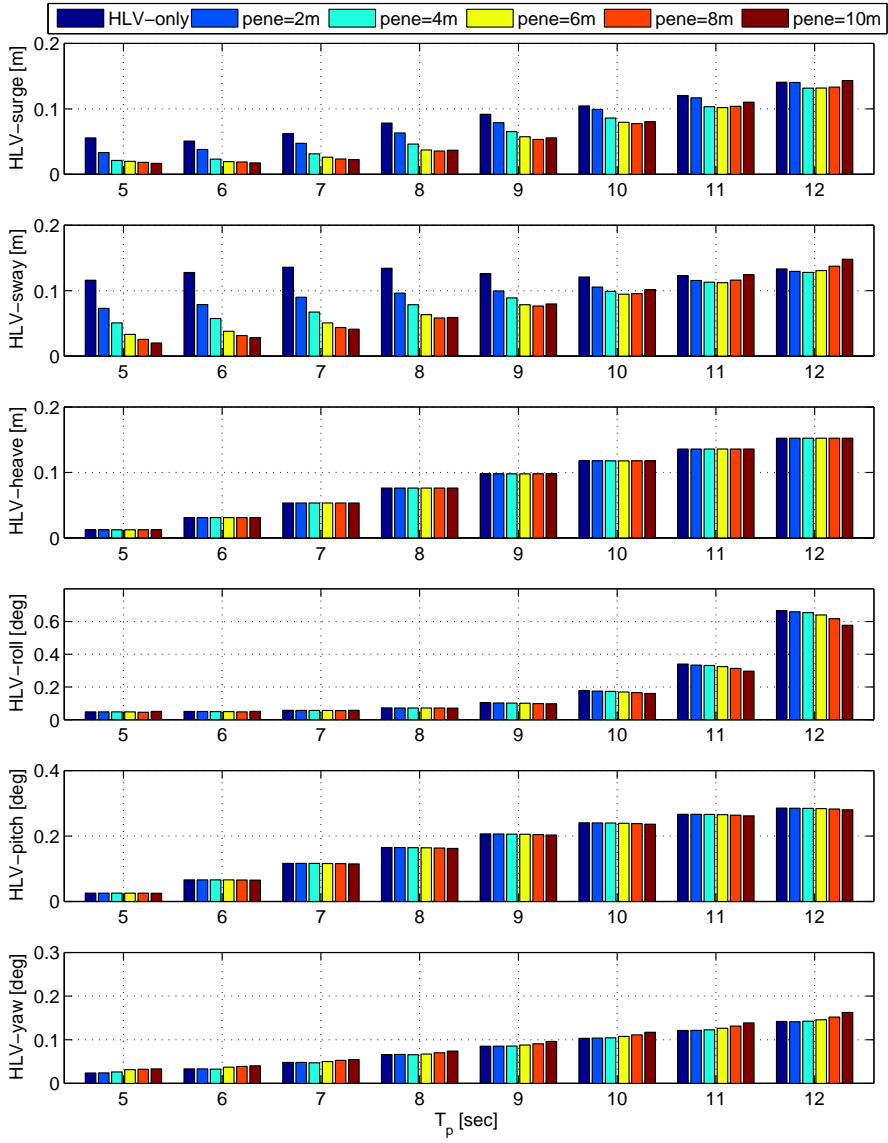


Figure 3.15: STDs of HLV motions at different MP penetration depths (pene) and wave conditions from 3-hour time-domain simulations ($H_s = 1.5$ m, $Dir = 150$ deg)

motions in 6 DOFs with respect to its COG. The responses at different wave peak periods show different trends when the penetration of the MP changes. In general, the motions of the HLV in the vertical plane (heave, roll and pitch) change little at different penetration depths. The roll motion decreases slightly with increasing MP penetrations because of the increase of restoring stiffness as contributed from the soil-MP interaction. On the other hand, the motions in the horizontal plane (surge, sway and yaw) show large variations for different loading conditions. In short waves, the surge and sway motions decrease rapidly with increasing penetrations. However, in long waves the motions first decrease and then increase for larger depths (8 m and 10 m). By studying the response spectra in Li et al. (2016c), it was observed the horizontal motions were dominated by the second-order motions in short waves and in long waves with shallow penetration depth, and the motions decreased with penetration depth due to large soil resistance. The first-order resonant motions began to dominate the responses in deeper penetrations. Because the natural periods decrease at large penetration depth and approach to the wave period in long waves, the responses increase in those conditions.

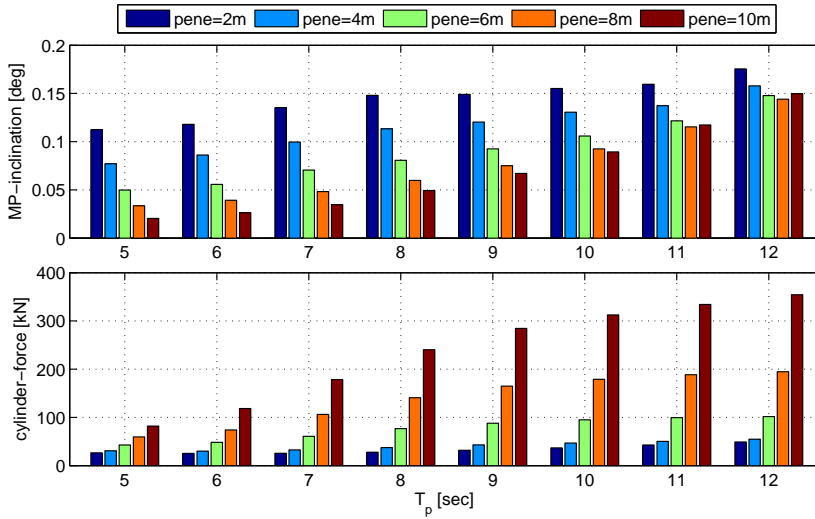


Figure 3.16: STDs of MP inclinations and contact forces on one hydraulic cylinder at different MP penetration depths (pene) and wave conditions from 3-hour time-domain simulations ($H_s = 1.5$ m, $Dir = 150$ deg)

Similarly, the responses of the MP inclination vary greatly with the MP penetration as observed in Figure 3.16. The first row in Figure 3.16 shows

the *STDs* of the MP inclination and the second row shows the *STDs* of the individual hydraulic cylinder contact force. Since the contact force between the hydraulic cylinders and the HLV is always dominated by first-order resonant motion, it increases with penetration depth in all wave period range.

3.4.2 Sensitivity study on the soil properties

Sensitivity studies were performed using three soil properties to compare the responses of the coupled MP hammering system. The chosen soil properties covered most of the sandy soils for shallow penetrations. The stiffness of the distributed springs K_{p-y} , T_z , K_{q-z} and K_{shear} as shown in Figure 2.6 increases from soft soil to hard soil. Dynamic analysis of the HLV-MP-soil system were performed in different sea states with MP at various penetrations.

Figure 3.17 displays the relation between the maximum individual cylinder contact force versus the maximum MP inclination, which were found to be the critical responses for the hammering operation. The results using different soil properties with MP at various penetrations are included in the same figure. The procedure followed for calculation of the maximum values is explained in Li et al. (2016c).

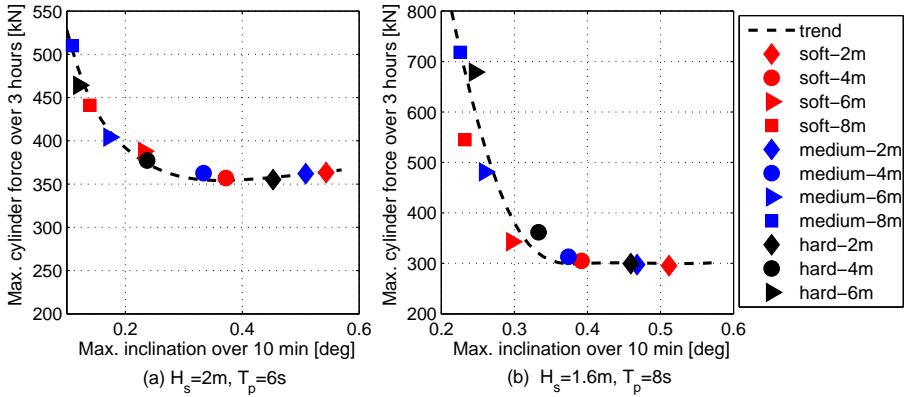


Figure 3.17: Extreme cylinder force in 3 hours versus MP maximum inclination in 10 min for different sea states and soil properties at different penetrations

For a given soil property, Figure 3.17 shows that the contact force and the MP inclination at different MP penetrations follow a trend. It can be observed that for both sea states, the contact force increases while the

MP inclination decreases in deeper seabed penetrations. For different soil types, the force-inclination relation follows the same trend. Although the maximum forces for $H_s = 1.6$ m, $T_p = 8$ sec scatter more at higher penetrations, the results show good consistency in the force-inclination trend and therefore in the dynamic system behaviour. Thus, it is evident that the force-inclination relation is not sensitive to the soil properties. For a given allowable limit of the contact force, the MP inclination for different soils are the same, but the penetration depths corresponding to this allowable limit are different - it is deeper in soft soil than in hard soil. Thus, it is sufficient to use representative soil properties to evaluate the operational limits.

Chapter 4

Assessment of operational limits for monopile installation

4.1 Overview

The operational limits are established from modelling and analysis of marine operations. The limits can be expressed in terms of environmental conditions (sea state, wind, current) or motions that could be monitored on-board the installation vessels before executing the operation.

The operational limits depend on the type of operation and the property of the dynamic system, and they are important for planning the operations as shown in Figure 1.8. The operational limits can be used to improve the system performance, i.e. to select vessels and equipment, to optimize the procedure and to propose contingency or mitigation actions. They can also be used together with the weather forecasts to help on-board decision making. Traditionally, operational limits have relied mostly on practical marine operation experiences (Nielsen, 2007). However, for operations with strict requirements and new kinds of operations there is a stronger need to quantify responses (forces, motions) and corresponding operational limits. A systematic method to establish the operational limits is thus required.

A few studies have been published on establishing operational limits. Clauss and Riekert (1990) presented a summary of operational limits in terms of H_s and floating vessel motion responses based on experience from projects in the North Sea. Cozijn et al. (2008) derived the operational limits for lifting operations of a module using a floating semi-submersible

crane onto a floating vessel based on numerical analysis, model tests and measurements from the actual offshore installation. Matter et al. (2005) derived the operational limits in terms of H_s and T_p for a drilling jack-up unit for the deployment and retrieval phase. The allowable limits corresponding to allowable stress in the spud cans, legs and pinions were derived from structural analysis. The allowable stresses were then transformed into the motions of the vessel and the sea state parameters. Ringsberg et al. (2015) obtained the allowable sea states for a jack-up deployment operation by directly comparing the allowable forces on the spud can and the characteristic responses of the impact forces from a coupled dynamic analysis.

The above studies showed the importance of obtaining operational limits in the planning phase. The approach to derive the limits for different operations has been improved from using past project experience to more comprehensive numerical studies or/and model tests. Besides, there has been a significant step forward from using H_s as the only parameter for operational limits towards using both H_s and T_p , and towards using the motions which can be monitored (Berg et al., 2015).

However, the previous studies mainly focused on a specific operation with known criteria and critical events that limit the operations. For many non-transitional operations, the critical events that may jeopardize the whole operation and the corresponding parameters to describe these events (limiting parameters) are unknown. Therefore, it is essential to develop a methodology to firstly identify the the critical events and corresponding limiting parameters and then establish the operational limits based on relevant safety criteria.

In this chapter, a systematic method to derive the operational limits combining the operational procedure, numerical analysis and safety criteria is proposed. The operational limits in terms of allowable sea states for the monopile lowering and initial hammering operations are then obtained using this method.

4.2 Definition of terms

In this section, the terms required for development of the methodology to assess the operational limits for marine operations are briefly defined as follows:

Critical events: the events which may jeopardize the operation (e.g., structural failure).

Limiting parameters: the parameters used to describe the critical events and limit the operation (e.g., wire tension can be used as a limiting param-

eter for wire breakage).

Allowable limits: the limits representing the threshold values for limiting parameters.

Operational limits: the limits used to support the decision-making for marine operations, these can be expressed in terms of allowable sea states or allowable motions.

4.3 Methodology for assessing operational limits

The methodology to identify critical events and corresponding limiting parameters as well as to establish the operational limits for a governing installation activity is described in the following steps and illustrated in Figure 4.1.

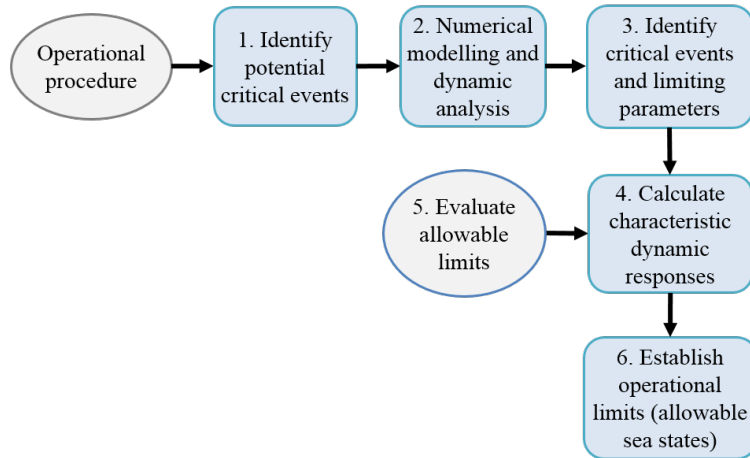


Figure 4.1: General methodology to establish the operational limits

1. Identification of potentially critical events. Based on the operational procedure, a preliminary selection of activities which could lead to critical events is required. The preliminary selection requires qualitative risk assessment of the operation and can be based on experience, guidelines and reviewing of relevant operations.

2. Numerical modelling of operational activities. Numerical models are required to simulate these activities and evaluate the dynamic responses. A quantitative assessment of the dynamic responses under reasonable environmental conditions will indicate which parameters may reach high levels and thus limit the operation. One activity may contain several critical events and corresponding dynamic responses.

3. Identification of critical events and limiting parameters.

Following the assessment of the dynamic responses, the ones governing each offshore activity and leading to failure events are identified. The governing dynamic responses are defined as limiting parameters.

4. Calculation of characteristic dynamic responses. Once the limiting parameter is identified, a characteristic value of its dynamic response needs to be calculated. For temporary design conditions, e.g. installation, the calculation of the characteristic loads should be based on practical requirements, e.g., the duration of the installation and the consequences associated with the failure events.

5. Evaluation of the allowable limits for the limiting parameters. The allowable limits need to be specified based on safety criteria. They are chosen to avoid failure during the marine operations due to large structural loads and the exceedance of specified installation requirements. Some allowable limits are given explicitly and are available for elements such as slings and wire ropes, crane capacity and mating gaps for float-over operations, etc. However, for events related to structural failure, the limits may not be available, and structural damage criteria are therefore required. Allowable limits can be provided in terms of impact velocities and contributing masses. Normally, structural analysis or finite element modelling is required to provide the allowable limits.

6. Assessment of the operational limits. By comparing the characteristic dynamic responses, S and their allowable limits, S_{allow} for all possible sea states, the ones complying with $S \leq S_{allow}$ correspond to the allowable sea states. These sea states can be transformed into allowable motion responses. In general both the allowable sea states and responses are known as operational limits.

4.4 Allowable sea states for the MP lowering process

By applying the methodology proposed above, the allowable sea states for MP lowering process are assessed.

4.4.1 Critical events and corresponding limiting parameters

The potentially critical events that can jeopardize the MP lowering process are as follows.

- **Lift wire breakage.** The tension in the lifting wires (limiting parameter) should never exceed the maximum working load of the wire.

Slack wires followed by snap forces should be avoided.

- **Large MP tip displacement before landing.** The motions of the monopile, particularly its rotations and the displacements of its end tip, affect the landing position. Large excursion of the MP tip may exceed the installation requirement. Moreover, the correction of the large inclination angle before hammering starts may exceed the capability of the hydraulic cylinders due to limited stroke length.
- **Failure of the hydraulic system in the gripper device.** The exceedance of the allowable forces on the system will result in a hydraulic system failure. The failure will not only stop the operation but may also pollute the environment if leakage of hydraulic fluid occurs.

For the selected installation set-up, the main lift wire tension is stable and no snap loads occur under reasonable environmental conditions from time-domain simulations. The installed position of the MP can vary from the target designed position in a relatively large range (around 2 m), which exceeds the motions of the MP in the operational sea states. In addition, the inclination angle after landing can be adjusted by moving the HLV using mooring lines and thus not considered as critical.

Thus, for the lowering phase of the MP, only the failure of the hydraulic system in the gripper device is considered as a critical event for determining the allowable sea states. The corresponding limiting parameter is taken as the relative motion between the MP and HLV at the gripper position and the allowable limit is the initial gap between them. Due to large stiffness of the hydraulic cylinders, impact forces occur when the relative motion exceeds the allowable gap. Based on the dimension of the MP and the most common designs for the hydraulic cylinders used in the industry, the allowable gap is chosen as 1 m. Therefore, the sea states which result in relative motions at the gripper position larger than this allowable limit are unacceptable. This criterion is used to find the allowable sea states for MP lowering operation.

4.4.2 Sensitivity of the allowable sea states to numerical methods

From time-domain simulations, the relative motions between the HLV and the MP at the gripper level are quantified. By comparing the relative motions with the allowable limit, the allowable sea states are established.

Case studies were performed in Li et al. (2016b) (*Paper 5*) to study the influence of different numerical approaches on the allowable sea states. The

factors include the wave spreading described in Sec. 3.2.5, shielding effects described in Sec. 3.2.2, MP radiation damping described in Sec. 3.3 and the nonstationarity of the process. Five cases are defined in Table 4.1 for the MP lowering analysis. Among those, case 1 accounts for all the factors that might affect the response of the system and represents the most accurate numerical method, while the other cases neglect one or two factors in order to study the influence of each factor.

Table 4.1: Factors for case study in the time-domain simulations

Factors	A	B	C	D
	wave spreading	shielding effects	MP radiation	Nonstationary
(1)	long-crested	incident wave	no radiation damping	steady-state simulation
(2)	short-crested	disturbed wave	radiation damping	lowering simulation
Simulation Cases		HLV - MP lowering system		
Case 1 ($A2B2C2D2$)	(2)	(2)	(2)	(2)
Case 2 ($A1B2C2D2$)	(1)	(2)	(2)	(2)
Case 3 ($A2B1C1D2$)	(2)	(1)	(1)	(2)
Case 4 ($A2B2C1D2$)	(2)	(2)	(1)	(2)
Case 5 ($A2B2C2D1$)	(2)	(2)	(2)	(1)

The spreading index $n = 3$ (see Equation (3.5)) was applied for the cases considering short-crested waves. For the steady-state analysis, the critical draft of the MP was found from the nonstationary lowering simulation, and twenty simulations were carried out for each sea state. The same simulation length as the nonstationary simulations was applied, and the maximum relative motions were used to determine the allowable sea states for the steady-state simulation.

Figure 4.2(a) compares the allowable sea states using different hydrodynamic modelling approaches. Case 3 neglects the hydrodynamic interactions between the HLV and MP (both shielding effects and radiation damping) and thus overestimates the responses in short waves significantly, see Figure 3.5. Case 4 only neglects the MP radiation damping and also overestimates the responses in short waves as shown in Figure 3.14. Thus, both cases underestimate the H_s values in short waves, and shielding effects are found to be more significant than the radiation damping effects. These effects can be ignored for wave period larger than 10 sec when assessing the allowable sea states.

Figure 4.2(b) displays the allowable sea states using long- and short-

created waves. For wave period less than 12 sec, the long-crested assumption greatly overestimates the allowable H_s values. As mentioned, the shielding effects are significant in short waves, however, the spreading of the waves averages the low wave kinematics in the leeward side of the vessel and the high values in the windward side, see Figure 3.9. Thus, the MP experiences less shielding effects from the HLV for the same heading angles in short-crested waves than in long-crested waves. In longer waves, the shielding effects are minor. However, the spreading of the waves increase the vessel motions in the transverse direction, and results in lower allowable sea states in short-crested waves.

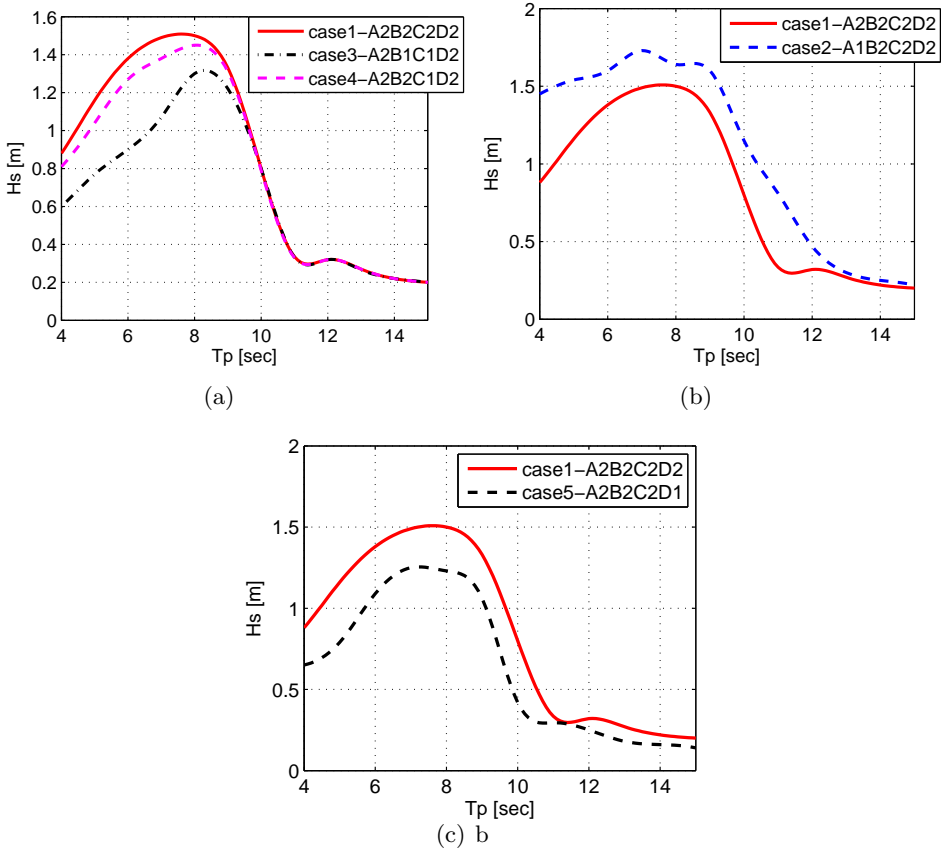


Figure 4.2: Allowable sea states for MP lowering operation using different numerical approaches

From nonstationary lowering simulations at various sea states, the most critical MP draft was found to be very shallow (around 2 to 3 m). Steady-

state simulations at the most critical drafts were performed and the corresponding allowable sea states are compared with those from the nonstationary lowering simulations in Figure 4.2(c). A considerable reduction of the allowable H_s value can be observed for almost all T_p conditions. The reduction appears to be more significant in shorter waves due to the resonance motions are excited in steady-state analysis. Although the steady-state analysis provide conservative results, it may greatly increase the waiting time, and consequently the cost during the operation.

4.4.3 Sensitivity of the allowable sea states to vessel heading

Because the shielding effects and the vessel motions are sensitive to the wave direction, three heading angles of the HLV are applied in the time-domain simulation, i.e., 150 deg, 165 deg and 180 deg. Figure 4.3 shows the allowable sea states for case 1 with different heading angles, and the maximum sea states for each T_p values are also shown in circles. One can observe that the system prefers 150 deg in short waves with T_p less than 7 sec. The most proper heading moves to 165 deg and then to heading seas in long waves. This is because the shielding effects from the HLV are stronger when the MP is close to quartering seas in short waves. In long waves, the shielding effects are minor, but the motions of the vessel increase greatly when the heading moves away from the heading seas because of the increasing transverse motions caused by short-crested waves.

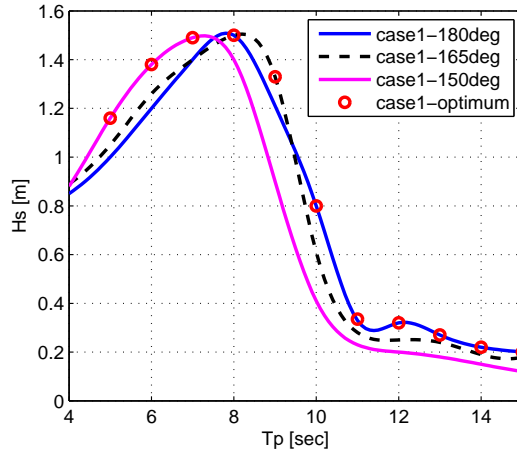


Figure 4.3: Comparison on allowable sea states for case 1 with different heading angles

Li et al. (2016b) also presented the most preferable heading angles which give the maximum allowable H_s values for cases 1 to 3. Cases 1 and 2 showed similar trends, but case 3 resulted in different angles in short waves. This is because case 3 excludes the shielding effects from the HLV and the most suitable headings are always close to the heading seas to avoid large transverse motions of the vessel. Thus, the most preferable headings are affected by the approach applied in the numerical analysis.

4.4.4 Operability analysis on the MP lowering process

Li et al. (2016b) (*Paper 5*) compared the influence of different factors in the numerical approach on the operability of the MP lowering process. The 10-year wave data from April to September at the North Sea Centre (Li et al., 2015b) was used for the operability analysis. Assuming the MP lowering operation lasts for one hour, the corresponding operability for different cases are calculated for this site using the derived allowable sea states in Figure 4.2. Table 4.2 presents the operability for different cases using the most preferable headings as well as the results from case 1 using various headings. The absolute errors of the operability for different cases are also shown with respect to case 1 which is considered to be the most accurate numerical model.

Table 4.2: Operability for MP lowering at North Sea Center in the period from April to September using different methods and heading angles

Method	Calculated Operability	absolute error w.r.t Case 1 (%)
Case 1 (A2B2C2D2)	57.5%	/
Case 2 (A1B2C2D2)	72.8%	15.3%
Case 3 (A2B1C1D2)	28.2%	-29.3%
Case 4 (A2B2C1D2)	50.3%	-7.2%
Case 5 (A2B2C2D1)	33.4%	-24.1%
Case 1 (best headings)	57.5%	/
Case 1 (180 deg)	49.2%	-8.3%
Case 1 (165 deg)	52.0%	-5.5%
Case 1 (150 deg)	55.1%	-2.4%

The results show that using long-crested waves overestimates the operability while the other three cases provide conservative results. The values in the table indicate the importance of each factor in the numerical method. For the studied scenario, the shielding effects are the most important factor, following by the nonstationary analysis approach and the wave spreading.

Although the MP radiation damping is less important than the other factors, the exclusion of the radiation damping underestimates the operability by around 7% for this site.

The comparison of the operability using three headings with the most preferable headings for case 1 shows that it is possible to increase the operability by varying the heading of the HLV in different sea states. Because the sea states in the North Sea Center from April to September are dominated by short waves with T_p less than 8 sec, 150 deg heading gives the largest operability compared with the other two headings due to the advantages of shielding effects from the HLV. However, the system may experience strong motions in long and short-crested waves with 150 deg heading.

4.5 Allowable sea states for MP initial hammering process

Li et al. (2016c) (*Paper 6*) proposed a methodology to assess the allowable sea states for the MP initial hammering process for use during the planning of the operation.

4.5.1 Operational procedure for MP hammering

The commonly applied hammering procedure is shown in Figure 4.4. The lowering process is assumed to have been completed and the hydraulic cylinders in the gripper have been connected to the MP.

After the lowering process, the initial mean inclination of the MP is measured and corrected by changing the stroke length of the hydraulic cylinders. Once the mean inclination is corrected, a pre-compression force is applied on the cylinder rod and the hammer blows initiate and drive the MP to deeper penetration. Due to the coupled HLV-MP motions in waves, the time interval elapsed between the previous inclination correction and the end of the hammer blows allows the gripper to move to another position. The hammer blows then create a new MP inclination which depends on the motions of the system and the length of the time interval after the correction. After each group of hammering blows, correction of the mean MP inclination is required to avoid cumulative inclination angle errors prior to the next hammering.

Due to the high resistance from the soil, the hydraulic cylinders can not correct the mean inclination of the MP themselves at a certain penetration depth. However, it is possible to apply the available thruster forces and change the mooring line length. These external forces can change the mean

position of the vessel and they are transferred to the hydraulic cylinders which correct the mean inclination of the MP. When the MP is driven deep enough into the soil, its inclination cannot be corrected due to high soil resistance. The hydraulic rods are retracted. The MP is then driven to its final penetration. The inclination of the MP before retracting the rods determines the final inclination of MP since no corrections can be applied afterwards.

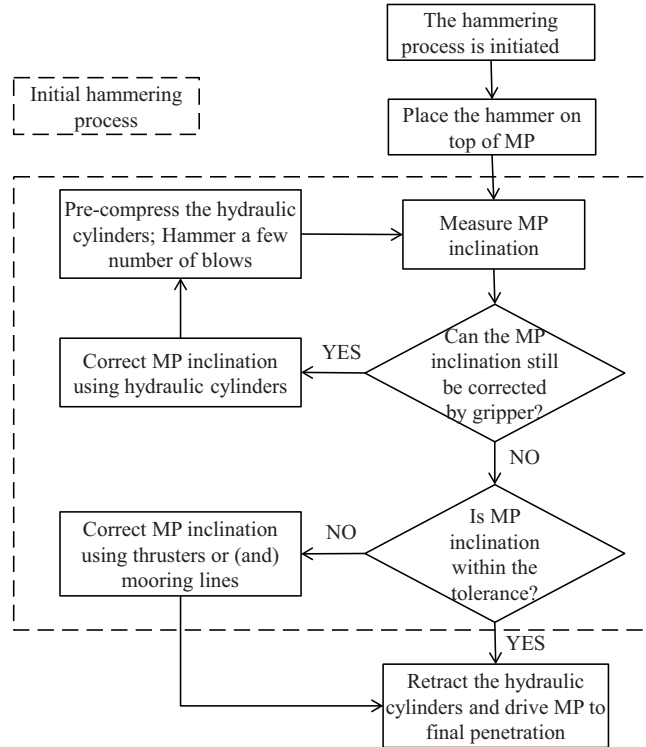


Figure 4.4: Flowchart of the MP hammering procedure

The initial hammering process is shown in Figure 4.4 which includes the hammering-measuring-correcting activities before retracting the rods of the hydraulic cylinders. This section focuses on the initial hammering process.

4.5.2 Critical events and limiting parameters

The possible critical events and limiting parameters from the initial hammering process that may lead to an unsuccessful operation are summarized as follows.

- **Failure of the hydraulic system.** The extreme force on the hydraulic system may exceed the allowable values. These forces include the dynamic component due to HLV-MP dynamic motions and the correction force which is required to correct the mean inclination of the MP. The exceedance of the allowable forces on the system will result in a hydraulic system failure and it is a critical event which will delay the entire operation and may also pollute the environment. The corresponding limiting parameter is the total force on individual hydraulic cylinder.
- **Insufficient thruster and mooring line forces available.** The thruster and mooring lines may not provide sufficient forces during the final correction of the MP's mean inclination. The limiting parameter is thus the available correction force.
- **Unacceptable MP inclination.** MP inclination may exceed the allowable limit and result in an unsuccessful installation, and the typical values are below 1° (Strandgaard and Vandenbulcke, 2002). The maximum inclination of the MP before retracting the hydraulic cylinders determines the final inclination of the MP. This event is not critical but restrictive for the installation requirement and its limiting parameter is the MP inclination due to the coupled HLV-MP motions.

In Li et al. (2016c) (*Paper 6*), the thruster and mooring line capacity was assumed to be sufficient during the hammering phase. From numerical studies on the dynamic responses of the coupled system, i.e., Sec. 3.4, it was found that the MP can reach unacceptable inclination angles during normal operational conditions, and the cylinder contact forces may exceed the allowable working limits. Thus, both MP inclination and cylinder contact force are considered to be limiting parameters for the initial hammering process.

4.5.3 Methodology to assess the allowable sea states

The initial hammering process is completed when the thrusters and the hydraulic cylinders cannot correct the inclination of the MP. The allowable sea states must ensure that the hydraulic system is intact and MP inclination is acceptable at this installation stage. Li et al. (2016c) (*Paper 6*) defined two “critical penetration depths”: d_{c1} , the penetration depth at which the MP can stand alone in the soil without any support from the vessel; d_{c2} , the penetration depth at which the hydraulic cylinders and thrusters are not able to correct the MP inclination.

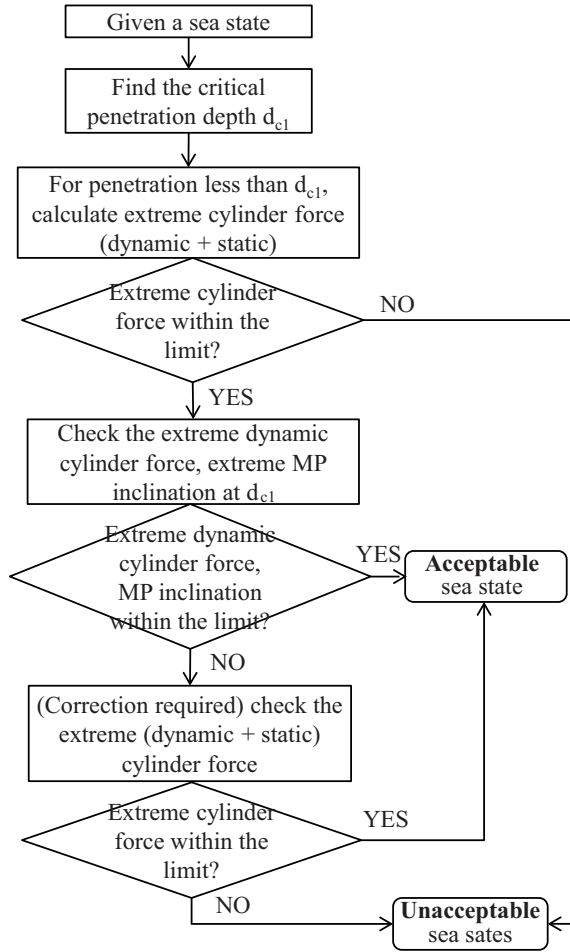


Figure 4.5: Methodology to find the allowable sea states for the initial hammering process

To ensure a safe hammering operation, it is necessary to satisfy:

$$d_{c2} \geq d_{c1} \quad (4.1)$$

which requires the hydraulic cylinders to be able to support the MP until it can stand alone in the soil. As observed from the dynamic responses in Figure 3.16, the forces on the hydraulic cylinders increase significantly with increasing penetration depth, so it is beneficial to retract the cylinder rods once reaching d_{c1} . Thus, the completion of the initial hammering process is achieved when the MP penetration depth reaches d_{c1} . The procedure shown in Figure 4.5 is then proposed to find the allowable sea states for the initial

hammering process.

- For a given sea state, calculate the “critical penetration depth” d_{c1} for which the MP (and the hammer on top) can stand in the soil without any external supports from the HLV.
- The limiting criterion in the first several hammering actions is the force on individual hydraulic cylinders. The extreme force should include both the dynamic force due to the relative HLV-MP motions and the one required to correct the MP from a certain mean inclination to a zero mean value. The limiting force criterion should be checked for each penetration depth less than d_{c1} to make sure the operation is acceptable for the following activities. If the requirement fails at any penetration, the input sea state is considered “unacceptable”, and a lower sea state should be selected and evaluated.
- When reaching d_{c1} , the hydraulic cylinder rods are about to be retracted. If both the dynamic cylinder forces and MP’s inclination at d_{c1} are within the limits, the given sea state is acceptable without any further correction of the MP inclination. On the other hand, if the MP inclination exceeds the allowable value, a last correction is required. Thus, the total correction and dynamic force on the hydraulic rods are calculated and it is acceptable if the total force is below the allowable value.

4.5.4 Allowable sea states for initial hammering process

Based on the proposed procedure, the allowable sea states for a given installation site can be derived in the planning phase of the operation. The characteristic values of the limiting parameters, i.e., the cylinder contact force and the MP inclination were obtained based on numerical simulations in Li et al. (2016c). The extreme forces on the hydraulic cylinders included the extreme dynamic force and the correction force. The extreme dynamic force was calculated as the maximum value in three hours, corresponding to a probability of exceedance of around 10^{-4} (DNV, 2011b) and was obtained from the steady-state time domain simulations using the empirical mean upcrossing rates (Naess, 1984a,b; Naess et al., 2007).

The correction force was calculated from quasi-static analysis by modelling this process without waves, and the detailed analysis can be found in Li et al. (2016c) (*Paper 6*). The mean inclination to be corrected after each hammering activity was taken as the maximum inclination over

10 min corresponding to the duration for the measurement and correction activities.

The allowable limits for the extreme hydraulic cylinder forces were selected based on common designs used in the industry. The allowable MP inclination was chosen as 0.5° . Based on the proposed procedure in Figure 4.5, case studies were performed from which different unacceptable conditions can be identified. The reasons for those cases to happen were given and can be useful for future improvement of the installation procedure, components design and contingency actions. It is recommended to reduce the second order motions in short waves and to migrate the first order resonant motions in long waves.

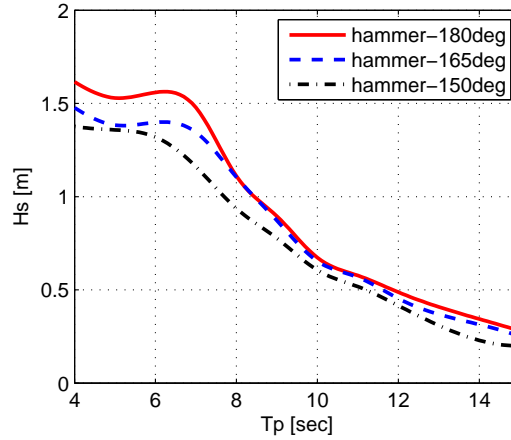


Figure 4.6: Allowable sea states for MP initial hammering operation for typical HLV headings

By assessing different wave conditions, the allowable sea states for the initial hammering process can be obtained and are shown in Figure 4.6 corresponding to three typical installation heading angles of the HLV. As shown here, the allowable sea states for MP hammering operation can be predicted by applying a systematic methodology to all possible environmental conditions during the planning phase. The allowable sea states can be used to support the on board decision-making together with the weather forecast.

Chapter 5

Conclusions and recommendations for future work

This thesis examined the installation of monopiles in particular the lowering and the initial hammering processes. First, methods for modelling and dynamic analysis of each phase were studied. Based on the dynamic analysis, the operational limits in terms of allowable sea states were assessed. The main conclusions, original contributions, and recommendations for future work are presented in this final chapter.

5.1 Conclusions

The main conclusions of the thesis are summarized as follows:

- A new numerical approach was developed to account for shielding effects from the floating installation vessel for nonstationary lowering operation of monopiles. The shielding effects reduce the responses of the monopile lifting system significantly in short waves while the influence decreases with wave length. The best heading angles when considering shielding effects ranged from close to quartering seas in short waves to heading seas in long waves. The performance using a jack-up vessel was compared with that using the floating vessel. In short waves, the floating vessel gives lower responses because of the shielding effects, while jack-up vessels are recommended in long waves to prevent the large crane motions induced by floating vessels.

- Shielding effects are insignificant and can be ignored for the jacket system because the vessel motions dominate the responses of the jacket in both short and long waves. Short-crested waves affect the responses in both incident and disturbed waves significantly. The spreading of wave energy narrows down the differences between the responses in incident and disturbed waves.
- A new approach was developed to account for the monopile's radiation damping during the nonstationary lowering process. The inclusion of radiation damping greatly reduced the responses at the monopile rotational natural frequency. The motions induced by the crane dominate the responses of the system in long waves and are not affected by the radiation damping of the monopile. The radiation damping should be considered in short waves and can be neglected in long waves when the vessel motion dominates.
- The allowable sea states for monopile lowering operations were assessed. Shielding effects from the vessel are more considerable than the radiation damping from the monopile. Assuming long-crested waves results in dramatic overestimation of the allowable sea states in both short and long wave conditions. Using steady-state analysis at the most critical draft of monopile underestimates the allowable sea states greatly compared with the nonstationary approach. Operability analysis was performed for one selected site. The exclusion of shielding effects, wave spreading and the nonstationarity of the process result in more than 15 % absolute error in the operability analysis. The radiation damping of the monopile gives around 7 % absolute error.
- The results for the coupled vessel-monopile system during the initial hammering process showed that the penetration depth of the MP and wave condition greatly influence the dynamic responses. The slowly varying second-order motions dominate the system in short waves and shallow penetration depths and first-order resonance motions dominate in deep penetration depths. The trend of the system dynamic behaviour is not sensitive to the soil properties, and the critical depths for allowable cylinder contact forces depend on the soil properties.
- A systematic methodology to obtain the operational limits was proposed and the allowable sea states for the initial hammering process were assessed using this methodology. The critical event for the initial hammering process was identified to be the structural failure of the hydraulic cylinders on the gripper, while the restrictive event was the

unacceptable monopile inclination at the end of the initial process. The limiting parameters are the cylinder contact force and the inclination of the monopile, respectively. The proposed methodologies can be generalized for planning of other marine operations.

5.2 Original contributions

Many issues related to monopile installation have been studied in the thesis. The main contributions of the thesis can be summarized as follow:

- *Development of a new approach to consider shielding effects from the vessel for nonstationary processes*

The approach is able to account for shielding effects from the installation vessel during nonstationary lowering or lifting operations of objects close to the splash zone. It can be used for more complicated structures such as jacket foundations, spools, and sub-sea templates, which can be modelled as a collection of slender structures. The approach was developed in an external Dynamic Library Link (DLL) which interacted with MARINTEK SIMO program in the time-domain simulations. The DLL can be adapted in other programs with an external interface (e.g., ANSYS AWQA).

- *Development of a new approach to account for radiation damping of structures during nonstationary lowering operation*

The approach applies for slender structures with low lowering/lifting speeds. It interpolates the retardation functions at different drafts of the structure to include the radiation damping for nonstationary processes. This approach was also developed in DLL interacting with SIMO program, and can be adapted for other programs.

- *Evaluation of influences from different numerical approaches on the operability of the monopile lowering operation*

The influences of different approaches were compared and quantified when assessing the operability. The comparisons provides a basis to improve numerical analysis for nonstationary lowering operation of slender structures.

- *Development of a systematic methodology for assessing operational limits of marine operations*

The methodology combines the operational procedure, numerical simulations and safety criteria. The methodology was developed based on the

monopile initial hammering operation, and can be generalized to other marine operations.

- *Establishment of operational limits for monopile lowering and initial hammering processes*

Using the proposed methodology, the operational limits in terms of allowable sea states for monopile lowering and initial hammering processes were assessed. The results are useful for planning of the operations.

5.3 Recommendations for future work

- *Further development and validation of the approach to consider shielding effects and radiation damping for nonstationary process*

The approaches developed in the thesis are based on Morison's formula and apply for low winch speeds. The applicability for larger diameter structures with increasing winch speeds should be studied. The validation of the approach can be performed by comparing the results from simulations using a numerical wave tank or from model tests.

- *Further development of the numerical models and method for monopile installation*

The environmental conditions in the current numerical method only include waves, wind and currents are not considered. The wind and currents may change the mean inclination of the monopile during the initial hammering process. In addition, the soil models were simplified by distributed non-linear springs. Thus, the numerical models and methods can be improved to be more realistic and robust.

- *Extension of the methodology for assessment of operational limits*

The thesis only deals with the monopile lowering and hammering activities. It is necessary to assess the allowable sea states of other individual activities and combine them to establish the operational limits of the complete operation. The methodology should hence be extended to consider different activities, sequence, and continuity.

- *Design of the installation equipment based on the numerical analysis*

The dynamic responses and operational limits obtained in the thesis can be used for the local analysis and design of the equipment for MP installation, such as the gripper device. Better design of the equipment can reduce

the risks for the equipment during installation.

- *Reliability-based methodology for assessment of operational limits*

When assessing the operational limits, a probabilistic approach should be applied to take into account the uncertainties in numerical models, environmental conditions, etc. Future work can be devoted to evaluate the uncertainties and propose reliability-based methodology to assess the operational limits.

- *Optimization of the operational limits*

The operational limits were established based on the identified critical events. It is therefore important to focus on improving the procedure and the system components related to those events to optimize the operational limits and so as to maximize the weather window.

- *Analysis of installation of turbine components*

The installation of turbine components including tower, nacelle and rotor assembly (RNA) are also critical and challenging operations. Analysis of both foundation and turbine installation are helpful for planning the installation of the whole wind farm.

- *Development of alternative cost-efficient installation methods*

Traditional installation methods for monopiles and turbine components require large crane vessels. More cost-efficient and safe installation methods are urgently needed to reduce the overall costs of offshore wind farms.

References

- Aarset, K., Sarkar, A., Karunakaran, D., 2011. Lessons learnt from lifting operations and towing of heavy structures in North Sea. In: Offshore Technology Conference, May 2-5, Houston, Texas, USA.
- Albers, P., 2010. Motion control in offshore and dredging. Springer Science & Business Media.
- Andersen, L. V., Vahdatirad, M., Sichani, M. T., Sørensen, J. D., 2012. Natural frequencies of wind turbines on monopile foundations in clayey soils a probabilistic approach. *Computers and Geotechnics* 43, 1–11.
- ANSYS, 2011. The AQWA Reference Manual - Version 14.0.
- API, 1993. API Recommended Practice for planning, designing and constructing fixed offshore platforms: Load and Resistance Factor Design (RP 2A-LRFD). American Petroleum Institute.
- API, 2007. API Recommended Practice for planning, designing and constructing fixed offshore platforms: Working Stress Design (RP 2A-WSD). American Petroleum Institute.
- Baar, J., Pijfers, J., Santen, J., 1992. Hydromechanically coupled motions of a crane vessel and a transport barge. In: 24th Offshore Technology Conference, May 4-7, Houston, Texas, USA.
- Ballast Nedam, 2011. Supporting offshore wind - alternative foundation installation. Tech. rep., Ballast Nedam Offshore B.V., Available from <http://flow-offshore.nl/images/flow-openbaar/alternative-foundation-installation.pdf>.
- Bense, M. P., 2014. Comparison of numerical simulation and model test for integrated installation of GBS wind turbine. Master's thesis, Department of Marine Technology, Norwegian University of Science and Technology, Trondheim, Norway.

- Berg, T. E., Selvik, Ø., Berge, B. O., 2015. Defining operational criteria for offshore vessels. In: *Maritime-Port Technology and Development - Ehlers et al. (Eds)*. Talor & Francis Group, London.
- Bisoi, S., Haldar, S., 2014. Dynamic analysis of offshore wind turbine in clay considering soilmonopiletower interaction. *Soil Dynamics and Earthquake Engineering* 63, 19–35.
- Burton, T., Jenkins, N., Sharpe, D., Bossanyi, E., 2001. *Wind energy handbook (Second Edition)*. John Wiley & Sons Ltd.
- BWEA, 2000. Prospects for offshore wind energy. Tech. rep., The British Wind Energy Association (www.bwea.com).
- Byrne, B. W., McAdam, R., Burd, H. J., Houlsby, G. T., Martin, C. M., Zdravkovi, L., Taborda, D., Potts, D., Jardine, R., Sideri, M., 2015. New design methods for large diameter piles under lateral loading for offshore wind applications. In: *Proc 3rd International Symposium on Frontiers in Offshore Geotechnics (ISFOG 2015)*.
- Carswell, W., Johansson, J., Løvholt, F., Arwade, S., Madshus, C., De-Groot, D., Myers, A., 2015. Foundation damping and the dynamics of offshore wind turbine monopiles. *Renewable Energy* 80, 724–736.
- Chakrabarti, S. K., 1987. *Hydrodynamics of offshore structures*. WIT press, Southampton, UK.
- Ciang, C. C., Lee, J.-R., Bang, H.-J., 2008. Structural health monitoring for a wind turbine system: a review of damage detection methods. *Measurement Science and Technology* 19 (12).
- Clauss, G. F., Riekert, T., 1990. Operational limitations of offshore crane vessels. In: *22nd Offshore Technology Conference*, May 7-10, Houston, Texas, USA.
- Cozijn, J. L., van der Wal, R. J., Dunlop, C., 2008. Model testing and complex numerical simulations for offshore installation. In: *Proceedings of the 18th International Offshore and Polar Engineering Conference*, July 6-11, Vancouver, BC, Canada.
- Cummins, W. E., 1962. The impulse response function and ship motions. *Schiffstechnik* 9 (47), 101–109.
- De Vries, W., 2011. Final Report WP 4.2 - support structure concepts for deep water sites (Deliverable D4.2.8). Tech. rep., Project Upwind.

- DNV, 2010. Recommended Practice DNV-RP-C205, Environmental conditions and environmental loads. Det Norske Veritas, Oslo, Norway.
- DNV, 2011a. Offshore Standard DNV-OS-C101, Design of offshore steel structures, General (LRFD method). Det Norske Veritas, Oslo, Norway.
- DNV, 2011b. Offshore Standard DNV-OS-H101, Marine Operations, General. Det Norske Veritas, Oslo, Norway.
- DNV, 2012a. Offshore Standard DNV-OS-H102, Marine operations, design and fabrication. Det Norske Veritas, Oslo, Norway.
- DNV, 2012b. Offshore Standard DNV-OS-H201, Load transfer operations. Det Norske Veritas, Oslo, Norway.
- DNV, 2012c. Recommended Practice DNV-RP-C104, Self-elevating units. Det Norske Veritas, Oslo, Norway.
- DNV, 2013. Offshore Standard DNV-OS-H204, Offshore installation operations (VMO Standard Part 2-4). Det Norske Veritas, Oslo, Norway.
- DNV, 2014a. Offshore Standard DNV-OS-H206, Loadout, transport and installation of subsea objects (VMO Standard Part 2-6). Det Norske Veritas, Oslo, Norway.
- DNV, 2014b. Offshore Standard DNV-OS-J101, Design of offshore wind turbine structures. Det Norske Veritas, Oslo, Norway.
- DNV, 2014c. Recommended Practice DNV-RP-H103, Modelling and analysis of marine operations. Det Norske Veritas, Oslo, Norway.
- Edwards, I., Dalry, C. D., 2011. Overcoming challenges for the offshore wind industry and learning from the oil and gas industry. Tech. rep., The Green House, Forrest Estate Dalry, Scotland, UK.
- EWEA, 2014. The European offshore wind industry - key trends and statistics 2013. Report, The European Wind Energy Association (<http://www.ewea.org/>).
- EWEA, 2015. The European offshore wind industry - key trends and statistics 2014. Report, The European Wind Energy Association (<http://www.ewea.org/>).
- Faltinsen, O. M., 1990. Sea Loads on Ships and Ocean Structures. Cambridge University Press.

- Gerolymos, N., Gazetas, G., 2006. Development of winkler model for static and dynamic response of caisson foundations with soil and interface nonlinearities. *Soil Dynamics and Earthquake Engineering* 26 (5), 363–376.
- GL Noble Denton, 2010. Guidelines for marine lifting operations (0027/ND). Noble Denton Group Limited, London, UK.
- Goda, Y., 2010. Random seas and design of maritime structures. World Scientific.
- Gordon, R. B., Grytoyr, G., Dhaigude, M., 2013. Modelling suction pile lowering through the splash zone. In: *Proceedings of the 32nd International Conference on Ocean, Offshore and Arctic Engineering*, June 9-14, Nantes, France.
- Graczyk, M., Sandvik, P. C., 2012. Study of landing and lift-off operation for wind turbine components on a ship deck. In: *Proceedings of the 31st International Conference on Ocean, Offshore and Arctic Engineering*, July 1-6, Rio de Janeiro, Brazil. pp. 677–686.
- Guachamin Acero, W., Moan, T., Gao, Z., 2016. Feasibility study of a novel concept for the installation of the tower and rotor nacelle assembly of offshore wind turbines based on the inverted pendulum principle. Under review in *Ocean Engineering*.
- Hau, E., 2013. *Wind Turbines - Fundamentals, Technologies, Application* (Third, translated edition). Springer.
- Hededal, O., Klinkvort, R. T., 2010. A new elasto-plastic spring element for cyclic loading of piles using the py curve concept. *Numerical Methods in Geotechnical Engineering*, 883–888.
- Herman, S. A., 2002. Offshore wind farms - analysis of transport and installation costs, report no. ECN-I-02-002. Tech. rep., Energy research Centre of the Netherlands.
- Hoving, J., 2013. *Bottom Founded Structures - Lecture Notes*. Delft University of Technology, The Netherlands.
- IEA, 2013. Technology roadmap - wind energy. Tech. rep., International Energy Agency (www.iea.org).
- IEA, 2014. Key world energy statistics. Tech. rep., International Energy Agency (www.iea.org).

- IHC, 2014. IHC Internal lifting tool (ILT). Available at <http://www.ihchs.com/oil-gas/structures/internal-lifting-tool/>, accessed: 2014-01-17.
- IHC, 2015. IHC Vremac Cylinders - Cylinder Catalogue 210 bar / 300 bar. Available at <http://www.ihcvremaccylinders.com/>, accessed: 2015-05-05.
- ISO, 1998. International Standard ISO 2394: General principles on reliability for structures.
- ISO, 2009. Petroleum and natural gas industries - Specific requirements for offshore structures - Part 6: Marine operations (ISO/FDIS 19901-6).
- Jonkman, J., Butterfield, S., Musial, W., Scott, G., 2009. Definition of a 5-MW reference wind turbine for offshore system development. Tech. rep., NREL/TP-500-38060, National Renewable Energy Laboratory (NREL), CO, USA.
- Kaiser, M. J., Snyder, B., 2011. Offshore wind energy installation and decommissioning cost estimation in the US outer continental shelf. Tech. rep., U.S. Dept. of the Interior, Bureau of Ocean Energy Management, Regulation and Enforcement, Herndon, VA. TA & R study 648. 340 pp.
- Ku, N., Roh, M.-I., 2014. Dynamic response simulation of an offshore wind turbine suspended by a floating crane. *Ships and Offshore Structures* 10 (6), 1–14.
- Lee, C. H., 1995. WAMIT theory manual. Department of Ocean Engineering, Massachusetts Institute of Technology, USA.
- Lesny, K., Wiemann, J., 2006. Finite-element-modelling of large diameter monopiles for offshore wind energy converters. In: *Geo Congress*.
- Li, L., Gao, Z., Moan, T., 2013a. Numerical simulations for installation of offshore wind turbine monopiles using floating vessels. In: *Proceedings of the 32nd International Conference on Ocean, Offshore and Arctic Engineering*, June 9-14, Nantes, France.
- Li, L., Gao, Z., Moan, T., 2013b. An overview on transportation and installation of offshore wind turbines. Tech. rep., Report, Statoil Project on Installation Technology of Offshore Multi-use Platform, NTNU.

- Li, L., Gao, Z., Moan, T., 2015a. Comparative study of lifting operations of offshore wind turbine monopile and jacket substructures considering shielding effects. In: The 25th International Offshore and Polar Engineering Conference, Hawaii, USA, June 21-26.
- Li, L., Gao, Z., Moan, T., 2015b. Joint distribution of environmental condition at five European offshore sites for design of combined wind and wave energy devices. *Journal of Offshore Mechanics and Arctic Engineering* 137 (3).
- Li, L., Gao, Z., Moan, T., 2015c. Response analysis of a nonstationary lowering operation for an offshore wind turbine monopile substructure. *Journal of Offshore Mechanics and Arctic Engineering* 137 (5).
- Li, L., Gao, Z., Moan, T., 2016a. Analysis of lifting operation of a monopile considering vessel shielding effects in short-crested waves. In: The 26th International Offshore and Polar Engineering Conference, Rhodes, Greece, June 26-July 2.
- Li, L., Gao, Z., Moan, T., 2016b. Operability analysis of monopile lowering operation using different numerical approaches, accepted for publication in *International Journal of Offshore and Polar Engineering*.
- Li, L., Gao, Z., Moan, T., Ormberg, H., 2014a. Analysis of lifting operation of a monopile for an offshore wind turbine considering vessel shielding effects. *Marine Structures* 39, 287–314.
- Li, L., Guachamin Acero, W., Gao, Z., Moan, T., 2016c. Assessment of allowable sea states during installation of OWT monopiles with shallow penetration in the seabed, accepted for publication in *Journal of Offshore Mechanics and Arctic Engineering*.
- Li, L., Stettner, O., Gao, Z., Moan, T., 2014b. Analysis of lifting operation of a jacket foundation for 10 MW offshore wind turbine. Tech. rep., Report, Statoil Project on Installation Technology of Offshore Multi-use Platform, NTNU.
- LORC, 2013. The jacket - a path to deeper waters. Available at <http://www.lorc.dk/offshore-wind/foundations/jackets>, accessed: 2013-05-11.
- MARINTEK, 2012a. SIMO - Theory Manual Version 4.0.
- MARINTEK, 2012b. SIMO - Users Manual Version 4.0.

- Masabayashi, K., 2012. Technical challenges in offshore wind turbine generator installation. In: Marine Renewable and Offshore Wind Energy Conference, RINA, London, UK.
- Matter, G. B., da Silva, R. R. M., Tan, P., 2005. Touchdown analysis of jack-up units for the definition of the installation and retrieval operational limits. In: Proceedings of the 24th International Conference on Offshore Mechanics and Arctic Engineering, June 12-17, Halkidiki, Greece.
- Moan, T., 2014. Stochastic dynamic response analysis of offshore wind turbines in a reliability perspective. In: Cunha A., Caetano E., Ribeiro P., and Muller G., editors, Proceedings of the 9th International Conference on Structural Dynamics, EUROODYN2014. pp. 21–36.
- Moné, C., Simith, A., Maples, B., Hand, M., 2015. 2013 cost of wind energy review. Tech. rep., NREL/TP-5000-63267, National Renewable Energy Laboratory (NREL), CO, USA.
- Morison, J. R., Johnson, J. W., Schaaf, S. A., 1950. The force exerted by surface waves on piles. *Journal of Petroleum Technology* 2 (05), 149–154.
- Mortola, G., Khalid, H., Judah, S., Incecik, A., Turan, O., 2012. A methodology for rapid selection of a seaworthy vessel for offshore wind turbine construction, operation and maintenance. In: Proceedings of the 2nd Marine Operations Specialty Symposium (MOSS), National University of Singapore, Singapore.
- Mukerji, P. K., 1988. Hydrodynamic responses of derrick vessels in waves during heavy lift operation. In: 20th Offshore Technology Conference, May 2-5, Houston, Texas, USA.
- Musial, W., Butterfield, S., McNiff, B., 2015. Energy from offshore wind. Tech. rep., NREL/CP-500-39450, National Renewable Energy Laboratory (NREL), CO, USA.
- Naess, A., 1984a. On the long-term statistics of extremes. *Applied Ocean Research* 6 (4), 227–228.
- Naess, A., 1984b. Technical note: On a rational approach to extreme value analysis. *Applied Ocean Research* 6 (3), 173–174.
- Naess, A., Gaidai, O., Teigen, P. S., 2007. Extreme response prediction for nonlinear floating offshore structures by Monte Carlo simulation. *Applied Ocean Research* 29 (4), 221–230.

- Newman, J. N., 1974. Second-order, slowly-varying forces on vessels in irregular waves. In: International Symposium on the Dynamics of Marine Vehicles and Structures in Waves, University College, London.
- Nielsen, F. G., 2007. Lecture Notes in Marine Operation. Department of Marine Technology, Norwegian University of Science and Technology, Trondheim, Norway.
- NORSOK, 1995. NORSOK Standard Common Requirements J-CR-003 Marine operations, (Rev. 1). Standards Norway, Oslo, Norway.
- NORSOK, 1997. NORSOK Standard J-003 - Marine operations (Rev. 2). Standards Norway, Oslo, Norway.
- NORSOK, 2007. NORSOK Standard N-003 Actions and action effects, (Edition 2). Standards Norway, Oslo, Norway.
- Npower Renewable, 2006. Capital grant scheme for the North Hoyle offshore wind farm annual report: July 2005-june 2006. Tech. rep., Npower Renewables Limited, Essen, Germany.
- OffshoreWind, 2014. Seaway installs Sylwin Alpha converter platform. Available at www.offshorewind.biz/2014/07/14/seaway-installs-sylwin-alpha-converter-platform/, accessed: 2016-01-07.
- O'Neill, L. A., Fakas, E., Ronalds, B. F., Christiansen, P. E., 2000. History, trends and evolution of float-over deck installation in open waters. In: SPE Annual Technical Conference and Exhibition, 1-4 October, Dallas, Texas, USA. Society of Petroleum Engineers.
- Ong, M. C., Li, H., Leira, B. J., Myrhaug, D., 2013. Dynamic analysis of offshore monopile wind turbine including the effects of wind-wave loading and soil properties. In: Proceedings of the 32nd International Conference on Ocean, Offshore and Arctic Engineering, June 9-14, Nantes, France.
- Orcina, 2013. OrcaFlex Manual, version 9.7a. Orcina Ltd., Ulverston, UK.
- OSC, 2015. Offshore Simulator Centre AS, Aalesund, Norway. Available at <http://osc.no/>, accessed: 2015-10-11.
- Østvik, I., 2010. Lessons learned from the first German offshore wind farm Alpha Ventus. Presented in SPE Conference, 14 April, Bergen, Norway.

- Park, K. P., Cha, J. H., Lee, K. Y., 2011. Dynamic factor analysis considering elastic boom effects in heavy lifting operations. *Ocean Engineering* 38 (10), 1100–1113.
- Peire, K., Nonneman, H., Bosschem, E., 2009. Gravity base foundations for the thornton bank offshore wind farm. *Terra et Aqua* 115, 19–29.
- Perry, M. J., Sandvik, P. C., 2005. Identification of hydrodynamic coefficients for foundation piles. In: *Proceedings of the 15th International Offshore and Polar Engineering Conference*, June 19-24, Seoul, Korea.
- Principle Power, 2011. WindFloat. <http://www.principlepowerinc.com/>, accessed: 2013-06-03.
- Ringsberg, J. W., Daun, V., Olsson, F., 2015. Analysis of impact loads on a self-elevating unit during jacking operation. In: *Proceedings of the 34th International Conference on Ocean, Offshore and Arctic Engineering*, May 31-June 5, St. John's, Newfoundland, Canada.
- Sandelson, M., 2011. Unsuitable boat raises Sheringham Shoal costs. Available at <http://theforeigner.no/pages/news/unsuitable-boat-raises-sheringham-shoal-costs/>, accessed: 2013-04-14.
- Sandvik, P. C., 2012. Estimation of extreme response from operations involving transients. In: *Proceedings of the 2nd Marine Operations Specialty Symposium (MOSS)*, National University of Singapore, Singapore.
- Sarkar, A., Gudmestad, O. T., 2011. Installation of monopiles for offshore wind turbine - by using end-caps and a subsea holding structure. In: *Proceedings of the 30th International Conference on Ocean, Offshore and Arctic Engineering*, June 19-24, Rotterdam, The Netherlands.
- Sarkar, A., Gudmestad, O. T., 2012. Study on a new methodology proposed to install a monopile. In: *Proceedings of the 22nd International Offshore and Polar Engineering Conference*, June 17-22, Rhodes, Greece.
- Sarkar, A., Gudmestad, O. T., 2013. Study on a new method for installing a monopile and a fully integrated offshore wind turbine structure. *Marine Structures* 33, 160–187.
- SMSC, 2015. Ship Modelling and Simulation Centre AS, Trondheim, Norway. Available at <http://www.smsc.no/>, accessed: 2015-10-11.

- Statoil, 2009. Off the UK coast, lies the wind farm, Sheringham Shoal. Available at <http://www.statoil.com/>, accessed: 2012-08-24.
- Statoil, 2012. Hywind brochure. Available at <http://www.statoil.com/>.
- Strandgaard, T., Vandenbulcke, L., 2002. Driving mono-piles into glacial till. IBCs Wind Power Europe.
- Tahar, A., Halkyard, J., Steen, A., Finn, L., 2006. Float over installation methodcomprehensive comparison between numerical and model test results. *Journal of offshore mechanics and Arctic Engineering* 128 (3), 256–262.
- Thomsen, K., 2011. Offshore wind: A comprehensive guide to successful offshore wind farm installation. Academic Press.
- Twidell, J., 2009. Offshore Wind Power. Multi-Science Publishing Company.
- Ultramarine, 2009. Reference Manual for MOSES. American Bureau of Shipping, Houston, Texas, USA.
- Uraz, E., 2011. Offshore wind turbine transportation and installation analyses - planning optimal marine operations for offshore wind projects. Master's thesis, Gotland University, Sweden.
- van den Boom, H. J., Dekker, J. N., Dallinga, R. P., 1988. Computer analysis of heavy lift operations. In: 20th Offshore Technology Conference, May 2-5, Houston, Texas, USA.
- van der Wal, R., Cozijn, H., Dunlop, C., 2008. Model tests and computer simulations for Njord FPU gas module installation. In: Marine Operations Specialty Symposium (MOSS), National University of Singapore, Singapore.
- van Dijk, R. R. T., H. A., Friisk, L., 2005. A dynamic model for lifting heavy modules between two floating offshore structures. EuroDyn Conference, 4-7 September, Paris, France.
- van Kuik, G. A. M., Peinke, J., Nijssen, R., Lekou, D. J., Mann, J., Sørensen, J. N., Ferreira, C., van Wingerden, J., Schlipf, D., Gebraad, P., P. H., Abrahamsen, A., van Bussel, G., S.J., D., Tavner, P., Bottasso, C. L., Muskulus, M., Matha, D., Lindeboom, H. J., Degraer, S., Kramer, O., Lehnhoff, S., Sonnenschein, M., Sørensen, P., Knneke, R. W. and Morthorst, P. E., Skytte, K., 2016. Long-term research challenges

- in wind energy research agenda by the European academy of wind energy. *Wind Energy Science* 1, 1–39.
- Wåsijø, K., Bermúdez, J. and Bjerks, M., Søreide, T., 2013. A novel concept for self installing offshore wind turbines. In: *Proceedings of the 32nd International Conference on Ocean, Offshore and Arctic Engineering*, June 9-14, Nantes, France.
- Wiser, R., Yang, Z., Hand, M., Hohmeyer, O., Infield, D., Jensen, P. H., Nikolaev, V., O'Malley, M., Sinden, G., Zervos, A., 2011. *Wind Energy in O. Edenhofer et al. (eds), IPCC Special report on renewable energy sources and climate change mitigation. Report*, Cambridge University Press, Cambridge and New York.
- Wu, M. K., 2014. Numerical analysis of docking operation between service vessels and offshore wind turbines. *Ocean Engineering* 91, 379–388.

Appendix A

Appended papers

A.1 Paper 1

Paper 1:

*Analysis of Lifting Operation of a Monopile for an Offshore Wind Turbine
Considering Vessel Shielding Effects.*

Authors: Lin Li, Zhen Gao, Torgeir Moan, Harald Ormberg

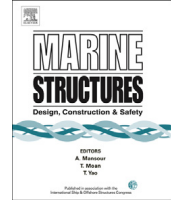
Published in *Marine Structures*, 2014, Vol. 39, pp. 287-314.



Contents lists available at ScienceDirect

Marine Structures

journal homepage: www.elsevier.com/locate/marstruc



Analysis of lifting operation of a monopile for an offshore wind turbine considering vessel shielding effects[☆]



Lin Li^{a, b, *}, Zhen Gao^{a, b}, Torgeir Moan^{a, b}, Harald Ormberg^c

^a Centre for Ships and Ocean Structures (CeSOS), NTNU, Trondheim, Norway

^b Centre for Autonomous Marine Operations and Systems (AMOS), NTNU, Trondheim, Norway

^c Norwegian Marine Technology Research Institute (MARINTEK), Trondheim, Norway

ARTICLE INFO

Article history:

Received 7 March 2014

Received in revised form 7 July 2014

Accepted 15 July 2014

Available online 16 September 2014

Keywords:

Lifting operation

Shielding effect

Monopile

Time-domain simulation

ABSTRACT

This study addresses numerical simulations of the lifting operation of a monopile for an offshore wind turbine with a focus on the lowering process. A numerical model of the coupled system of the monopile and vessel is established. The disturbed wave field near the vessel is investigated and observed to be affected by the diffraction and radiation of the vessel. The shielding effects of the vessel during the continuous lowering operation are accounted for in this study by developing an external Dynamic Link Library (DLL) that interacts with SIMO program in the time-domain simulations. The DLL is implemented by interpolating fluid kinematics between pre-defined wave points near the vessel. Based on the time-domain simulations, the critical responses, such as the motions of the monopile, the tensions in the lift wire and the contact forces in the gripper device in the disturbed wave fields, are compared with those in incident wave conditions. The results indicate that a great reduction in these extreme responses can be achieved when the shielding effects are considered. The sensitivity study of the responses in different wave directions is performed. The results indicate different behaviours with different wave directions and with short or long

[☆] Prof. Jørgen Juncher Jensen serves as editor for this article.

* Corresponding author. Centre for Ships and Ocean Structures (CeSOS), NTNU, Trondheim, Norway. Tel.: +47 73 55 11 12; fax: +47 73 59 55 28.

E-mail address: lin.li@ntnu.no (L. Li).

waves. A comparison of the responses when using a floating vessel and a jack-up vessel is also studied and can be used to support the choice of installation vessel type.

© 2014 Elsevier Ltd. All rights reserved.

1. Introduction

Various support structures have been proposed for offshore wind turbines (OWTs) at different water depths and soil conditions. With bottom-fixed OWTs, the industry prefers working with four types of foundations: gravity-based, monopile, jacket and tripod [1]. Of these foundations, monopiles are the most commonly used foundations in water depths up to 40 m, and it is estimated that more than 75% of all installations are founded on monopiles [2]. A typical monopile is a long tube with a diameter of 4–6 m. It is driven into the sea bed using a large hydraulic hammer if the soil condition is suitable. The pile diameter is limited by the size of the available driving equipment.

The installation of a monopile generally includes the following steps:

1. Upending the monopile from a horizontal position on the vessel to a vertical position.
2. Lowering the monopile down through the wave zone to the sea bed. The hydrodynamic wave loads induce the motions of the monopile when it passes through the wave zone. The monopile should be precisely landed at the designated point on the sea bed.
3. Driving the monopile into the sea bed with a hydraulic hammer.

This study focuses on the second step, i.e. the process of lowering the monopile.

Lifting operations are the most common means of installing monopiles and of many other offshore structures. Numerical studies have been commonly used to estimate the response characteristics of offshore lifting operations, including the installation of sub-sea templates [3], suction anchors [4], foundations and topsides of platforms, wind turbine components [5] and so on. A few experimental studies have also been conducted to obtain accurate hydrodynamic coefficients, e.g., the hydrodynamic mass and damping of ventilated piles [6], or to tune the critical parameters for numerical models, e.g., the damping or stiffness level of important support structures in the lifting system [7].

In lifting operations with objects (e.g., monopiles) lowered from air into the splash zone and towards the sea bed, the dynamic features of the system change continuously. A process dominated by transient or highly non-linear responses must be analysed differently from a stationary case. There are generally two approaches to simulate such cases [8]:

1. Find the most critical vertical position of the object by simulating a lowering in harmonic waves, and then make steady state simulations in irregular waves at this position.
2. Simulate a repeated lowering with different irregular wave realizations, and study the extreme response observed in each simulation.

It was demonstrated that the second method provides more realistic results [8]. The reason is that an unrealistic build-up of the oscillations that are observed in stationary cases is avoided. Therefore, to provide more accurate estimates of the operations, analyses of the entire lowering process are required.

In lifting operations conducted by floating vessels, hydrodynamic interactions between the structures in waves are of great importance. Studies have been performed to investigate the heavy lifting operations in the oil and gas industry considering shielding effects, such as the lifting of a heavy load from a transport barge using a large capacity semi-submersible crane vessel [9–11]. The studies found that the hydrodynamic interaction had little effect on the responses of the crane tip, but affected the responses of the transport barge and thus greatly affected the lifting operations because of the small dimension of the barge compared with that of the crane vessel [11]. Therefore, the hydrodynamic interaction between two floaters close to each other should be taken into consideration when estimating responses.

In the case of lifting a monopile using a floating vessel, due to the small dimension of the monopile compared with the vessel, the hydrodynamic effects of the monopile on the vessel are minor and can be ignored. However, the shielding effects of the vessel are expected to have a large influence on the responses of the monopile. The wave fields near the floating vessel are altered from the original incident waves, and three-dimensional effects would occur due to the diffraction and radiation from the vessel even if the incident wave is long-crested. If the lifting system and the vessel are placed in proper positions relative to the incident waves, the responses of the lifting system in waves can be less than those if the lifting system is exposed in the incident waves because of the wave shadow effects. Thus, it is crucial to study the vessel shielding effects when conducting lowering operations through waves in the vicinity of the vessel.

According to DNV-RP-C205 [12], with small structures close to a floater of large volume, the radiation and diffraction effects on fluid kinematics should be considered when calculating the forces on the structure. To account for those effects, the typical approach is to obtain the transfer functions of the fluid kinematics at the position of the operation near the floating vessel in the frequency domain and then to calculate the forces on the lifted object using the fluid kinematics obtained from the transfer functions. This approach is only valid when the lifting system is in a stationary position, i.e., when it has a stationary mean position. However, as discussed above, due to transients and the non-linearity of the system, the entire lowering process should be conducted with time-varying positions of the lifted objects. Therefore, time-domain methods to estimate the entire lowering process while considering the shielding effects by the vessel are required.

The current work focuses on the lowering phase of the installation of a monopile foundation with consideration of the shielding effects of the vessel. The fluid kinematics near the installation vessel were studied first. Time-domain simulations were performed using multi-body code SIMO [13]. The wave forces on the monopile during lowering were calculated using an external Dynamic Link Library (DLL) that included the shielding effects from the installation vessel. The responses of the lifting system in disturbed wave fields were quantified and compared with the responses in undisturbed incident waves. The simulation model and the methodology are presented first, followed by discussions of the results. Finally, conclusions and recommendations are given to guide future lifting operations with regards to issues of shielding effects.

2. Modelling of the lifting system

2.1. Model description

A floating installation vessel was chosen for the monopile installation. The main dimensions of the vessel are presented in Table 1. The vessel was a monohull heavy lift vessel. The crane was capable of performing lifts of up to 5000 tons at an outreach of 32 m in fully revolving mode. The main hook featured a clear height to the main deck of the vessel of maximum 100 m. The vessel had been designed with a combination dynamic positioning system and eight-line mooring system. The positioning system allowed the operations of the vessel in shallow water and in close proximity to other structures. Therefore, the lifting capacity and the positioning system of the floating vessel made it capable of performing the installation of monopiles in shallow-water sites. The monopile used in the model was a long slender hollow cylinder with main dimensions listed in Table 1.

Fig. 1 shows a schematic layout of the arrangement of the operation. The system included two rigid bodies, i.e., the floating installation vessel and the monopile. A hook is generally used to connect the lift wire and the sling that attached the monopile. In the current model, the sling was assumed to be very

Table 1
Main parameters of the floating installation vessel and the monopile.

Vessel			Monopile		
Length overall	[m]	183	Total mass	[tons]	500
Breadth	[m]	47	Length	[m]	60
Operational draught	[m]	12	Outer diameter	[m]	5.7
Displacement	[tons]	52,000	Thickness	[m]	0.06

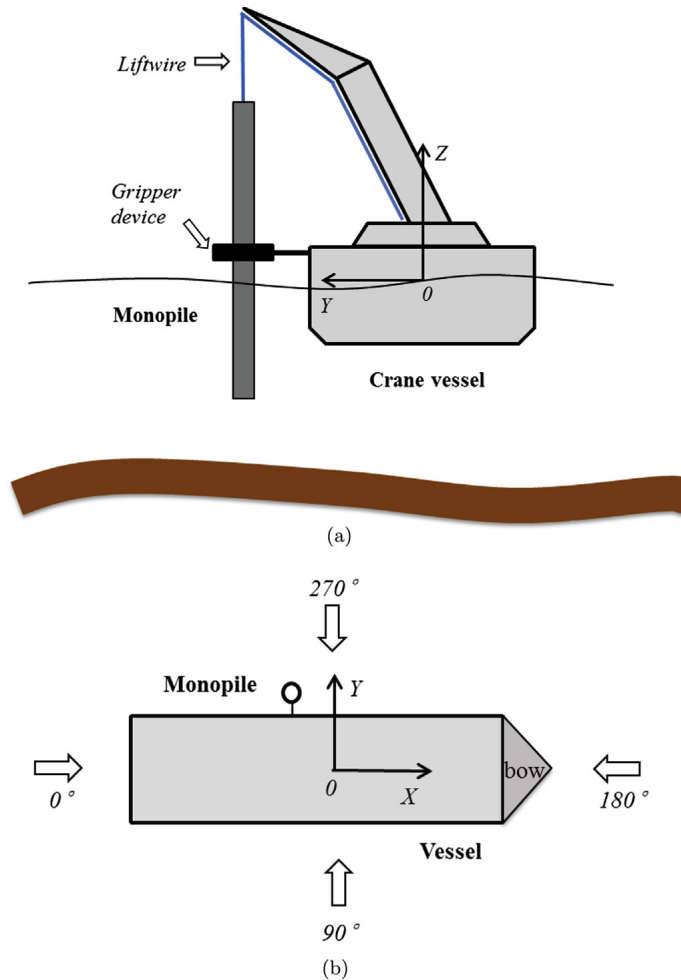


Fig. 1. Monopile lifting arrangement (a) and definitions of global coordinate system (b).

stiff. Hence, the hook and the monopile were considered to be rigidly connected and were modelled as one body for simplicity.

The dynamic responses of a floating crane and a heavy load with a flexible boom were studied in Ref. [14] by modelling the crane boom using finite element method (FEM). The dynamic factor analysis showed a difference of less than 5% between the elastic boom and the rigid boom in their study. It was also shown that the influence of the elastic boom decreased significantly with the decrease of the load mass. In their study, the maximum lifting capacity of the crane was 3600 tons and the load considered was above 1300 tons, more than 30% of the crane capacity. By comparison, the monopile mass is around 10% of the crane capacity in the current study. Thus, the effect of the elasticity of the crane boom is negligible. The crane was rigidly connected to the vessel in the numerical model, and a low constant flexibility of the crane was included.

The global coordinate system was a right-handed coordinate system with the following orientation: the X axis pointed towards the bow, the Y axis pointed towards the port side, and the Z axis pointed upwards. The origin was located at [mid-ship section, centre line, still-water line] when the vessel was at rest. The positions of the crane tip and the monopile were chosen based on practical operations.

Two types of couplings between the vessel and the monopile were included in the numerical model: the wire coupling through the main lift wire and the coupling via the gripper device. The lift

wire started at the bottom of the crane where a winch was located; thus, the lift wire could be extended through the winch to lower the monopile. The function of the gripper device was to control the horizontal motions of the monopile during lowering and landing as well as to support the monopile during driving operations. The gripper device was also rigidly fixed to the vessel.

2.2. Coupled equations of motion

The two-body coupled lifting system included 12 degrees of freedom (DOFs) of rigid body motions. The 12 equations of motion are given in Eqn. (1).

$$(M + A(\infty)) \cdot \ddot{x} + D_1 \dot{x} + D_2 f(\dot{x}) + Kx + \int_0^t h(t - \tau) \dot{x}(\tau) d\tau = q(t, x, \dot{x}) \quad (1)$$

where,

M the total mass matrix of the vessel and the monopile;

x the rigid body motion vector with 12 DOFs;

A the frequency-dependent added mass matrix;

D_1 the linear damping matrix;

D_2 the quadratic damping matrix;

K the coupled hydrostatic stiffness matrix;

h the retardation function of the vessel, which is calculated from the frequency-dependent added mass or potential damping;

q the external force vector that includes the wind force q_{WI} , the 1st and 2nd order wave excitation forces $q_{WA}^{(1)}$ and $q_{WA}^{(2)}$, the current force q_{CU} and any other external forces q_{EXT} .

The coupled stiffness matrix K includes the hydrostatic stiffness of the vessel, the stiffness from the mooring line, and the coupling between the vessel and the monopile via the lift wire and gripper device.

2.3. Modelling of the vessel and the monopile

The potential added mass and damping coefficients, the hydrostatic stiffness and the first order wave excitation force transfer functions were calculated in WADAM based on the panel method [15], and then the retardation functions in Eqn. (1) and the 1st order excitation force were obtained. In the current vessel model, the following simplifications were applied:

1. Waves were considered as main factor, and wind and current forces were not included.
2. The exciting forces on the floating vessel in the model consisted of only the 1st order wave excitation force vector $q_{WA}^{(1)}$, and no 2nd order wave forces were included as shielding effects are only relevant in the wave frequency range.
3. The mooring line system was simplified into linear stiffness terms in surge, sway and yaw. The viscous effects from the vessel hull and the mooring system were simplified into linear damping terms in surge, sway and yaw. The roll damping of the vessel was also included.

The external forces on the monopile included the gravity force, the buoyancy force, as well as the hydrodynamic wave forces. Because the structure was a hollow steel cylinder of low thickness, the wave forces acting on the bottom of the monopile were negligible. The main contributions, therefore, were the wave forces normal to the monopile's central axis.

In an operational sea state, the diameter of the monopile is relatively small compared with the wave length, and the ratio of wave height to structure diameter is low. According to the wave force regimes in Refs. [12], the inertial force is the governing force on the monopile. Furthermore, the motion of the monopile is large and the submergence increases during the lowering phase; thus, the linear theory from the panel method based on a mean position is not applicable. The instantaneous position of the monopile must be considered at each time step. Thus, Morison's formula should be used, and the monopile should be simulated as a slender body using strip theory. The horizontal wave force $f_{w,s}$ per

unit length on each strip of a vertical moving circular cylinder can be determined using Morison's equation [16].

$$f_{w,s} = \rho_w C_M \frac{\pi D^2}{4} \ddot{\zeta}_s - \rho_w C_A \frac{\pi D^2}{4} \ddot{x}_s + \frac{1}{2} \rho_w C_q D \left| \dot{\zeta}_s - \dot{x}_s \right| \cdot (\dot{\zeta}_s - \dot{x}_s) \quad (2)$$

In this equation, the positive force direction is the wave propagation direction. $\ddot{\zeta}_s$ and $\dot{\zeta}_s$ are fluid particle acceleration and velocity at the centre of the strip, respectively; \ddot{x}_s and \dot{x}_s are the acceleration and velocity at the centre of the strip due to the body motions; D is the outer diameter of the cylinder; and C_M , C_A and C_q are the mass, added mass and quadratic drag force coefficients, respectively.

The first term in the equation is the wave excitation force, including diffraction and Froude–Krylov force (FK term). The second term is the inertial term and the third term is the quadratic drag term. C_M and C_q are dependent on many parameters, such as the Reynolds number (Re), the Kaulegan–Carpenter number (KC) and the surface roughness ratio [16]. The outer surface of the monopile was assumed to be smooth, and Re number had a magnitude of 10^6 to 10^7 . The KC number in the operational sea states was in the range of 1–3. According to [12], the quadratic drag coefficient can be chosen as $C_q = 0.7$, which takes into account the flow separation of the water outside of the monopile.

The monopile was a bottomless cylinder that partly filled with water as it was lowered. This water influenced the hydrodynamic coefficients of the cylinder. Moreover, the submerged length of the cylinder increased with time. Several numerical studies have been conducted to estimate the hydrodynamic coefficients and excitation forces on bottomless cylinders with finite wall thickness, and the results showed a great dependency of these parameters on the wall thickness and the submergence of the cylinder [17–19]. Therefore, it is necessary to investigate the hydrodynamic coefficients of the bottomless monopile considering different submergences. The added mass coefficients of the monopile at different submergences were calculated using WADAM [15]. The results were three-dimensional (3D) hydrodynamic added mass of the whole body. However, in order to use strip theory to simulate the hydrodynamic forces in SIMO, 2D coefficients are required. Hence, the 2D added mass coefficients were obtained by dividing the 3D coefficients by the submerged length.

Fig. 2 shows the non-dimensional 2D added mass coefficients in transverse directions at different submergence. The figure shows that the 2D added mass coefficients increase with submerged length. However, at submergences of greater than 5 m, the non-dimensional 2D added mass coefficients approach to a constant of approximately 1.8 at the wave frequencies considered. Furthermore, the total

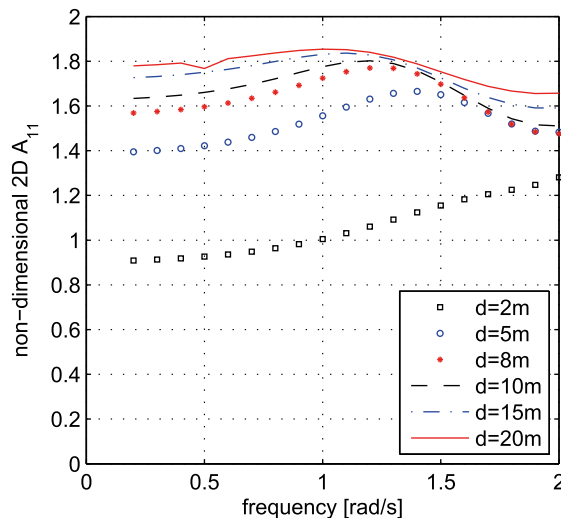


Fig. 2. Non-dimensional 2D added mass coefficient.

excitation forces calculated using Morison's equation and strip theory with the 2D added mass coefficients were compared with the 3D excitation forces calculated directly using WADAM. Good agreement was obtained at submergences larger than 5 m. Because the response at submergence of less than 5 m is not as critical as at greater submergences, an asymptotic value of $C_M = C_A = 1.8$ was chosen as the 2D added mass coefficient in Eqn. (2). Thus, forces at each strip can be obtained and then integrated along the submerged part to obtain the total force and moment. It was also confirmed that the resonant flow motions (sloshing) inside the monopile did not occur at the wave frequencies of interest. Moreover, in the simplified 2D model the effects of water exchange and flow separation at the end of the monopile were not considered.

The water depth at the installation site is 25 m, and the significant wave height for performing such lifting operations is normally below 2.5 m. According to the ranges of validity for various wave theories [12], the wave conditions considered in the numerical study are near the boundary of the 1st order linear waves and the 2nd order waves. The non-linearities in waves and the fluctuating wave elevation in shallow-water depth will induce the high-frequency components in wave load and result in larger responses of the structure [20]. These are relevant in predicting extreme loads on the monopile in severe conditions during its operational phase. However, as the installation phase is very transient and the sea states are low, the effects of the non-linearities in waves on the lifting system are expected to be very small and the linear wave theory is used for calculating the wave forces in the current model.

2.4. Mechanical couplings

The coupling between the on-board crane and the monopile was achieved using a lift wire. The wire coupling force was modelled as a linear spring force according to the following equation [13]:

$$T = k \cdot \Delta l \quad (3)$$

where T is the wire tension, Δl is the wire elongation and k is the effective axial stiffness, which is given by:

$$\frac{1}{k} = \frac{l}{EA} + \frac{1}{k_0} \quad (4)$$

where E is the modulus of elasticity, A is the cross-sectional area of the wire, $1/k_0$ is the crane flexibility and l is the total length of the wire, which increases as the winch runs during the lowering operation.

From the positions of the two ends of the wire, the elongation and thereby the tension can be determined. The material damping in the wire was included in the model.

The physical model of the gripper device is normally a ring-shaped structure with several contact elements in the inner circumference which behave like bumpers during installation (see section view Fig. 3(a)). Thus, the gripper force in the numerical model was simplified by a spring-damper system. The gripper device was modelled as a contact point attached to the vessel. A cylinder fixed to the monopile with a vertical axis was modelled at the same time, and the contact point was placed inside the cylinder (see Fig. 3(b)). When the monopile tends to move away from the gripper, the contacts between the cylinder and the contact point will provide restoring and damping forces for the monopile and control its horizontal motions. With the lowering of the monopile, the contact force always occurs at the gripper position which corresponds to the contact point in the numerical model. Rotation symmetric stiffness and damping around the axis were assumed and were defined by specifying restoring and damping forces F_i at several relative distances Δd_i between the contact point and the cylinder axis. An interpolation was used for all the other relative distances and the gripper forces at each time instance can be obtained. The physical and numerical models for the gripper coupling are illustrated in Fig. 3. Sensitivity studies to quantify the effects of the gripper stiffness on the responses during the lowering of a monopile were performed in Ref. [21]. The study showed that the gripper contact force and the relative motion between the monopile and the gripper device were very sensitive to the gripper stiffness, while the influence on the monopile rotational motion and lift wire tension were minor. In the current study, a representative gripper device stiffness was used for all the simulations.

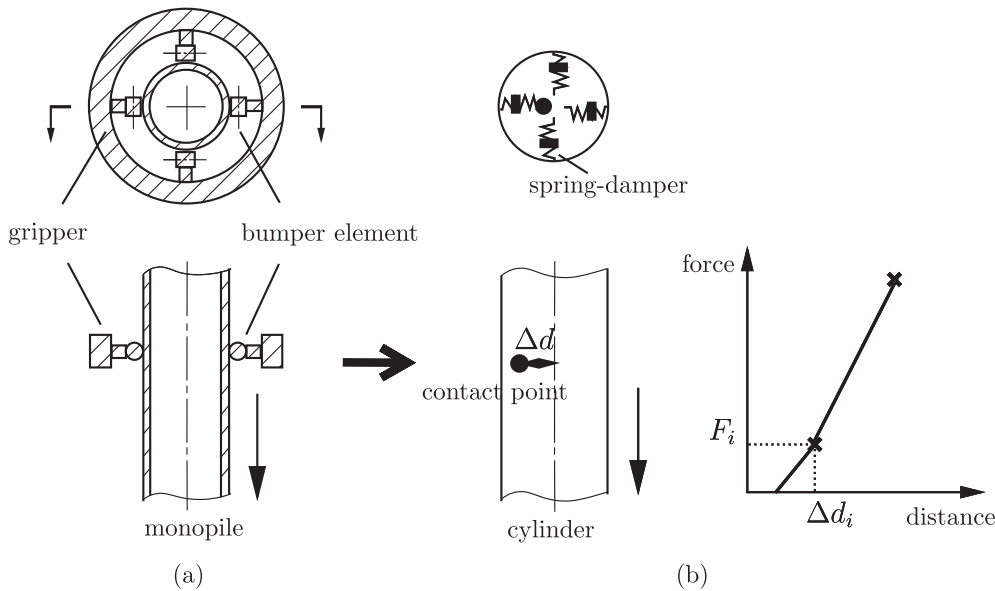


Fig. 3. Illustration of (a) physical and (b) numerical models for gripper device coupling.

The properties of the lift wire and the gripper device are presented in Table 2.

2.5. Eigen value analysis

The eigen value analysis was conducted in the frequency domain to investigate the eigen periods of the rigid body motions of the lifting system. The natural modes and natural periods were obtained by solving Eqn. (5).

$$[-\omega^2(M + A) + K] \cdot x = 0 \tag{5}$$

where M is the mass matrix of the vessel and the monopile. A is the added mass matrix; for the vessel the added mass with infinite frequency was used. K is the total restoring stiffness matrix, which is split into three contributions: hydrostatic restoring, mooring restoring and coupling between the vessel and the monopile. The coupling restoring includes the wire coupling and the gripper device coupling. x is the eigen vector that represents rigid body motions with 12 DOFs in the two-body coupled system and 6 DOFs if a single body is considered. The eigen values of the vessel alone and of the monopile alone were studied as well as the eigen values of the coupled system.

The natural periods and natural modes of the vessel and of the monopile are listed in Table 3 and Table 4, in which the dominated rigid motions are emphasised. The natural periods of the heave, pitch and roll motions of the vessel indicate small motions in short waves and larger motions when the wave period is close to the natural periods. In lifting operations, the motions of the vessel affect the motions of the monopile through the lift wire and the gripper device, the motions of which in three directions are formulated in Eqn. (6):

Table 2
Main parameters of the mechanical couplings.

Lift wire			Gripper device		
EA/l_0	[kN/m]	7.00E + 04	Stiffness	[kN/m]	4.00E + 03
k_0	[kN/m]	5.00E + 05	Damping	[kNs/m]	8.00E + 02
Damping	[kNs/m]	1.40E + 03			

Table 3

Eigenperiods and eigenvectors of vessel rigid body motions.

Mode		1	2	3	4	5	6
Surge	[m]	−0.15	−0.06	0.00	0.00	1.00	0.00
Sway	[m]	0.00	0.00	0.06	0.86	0.00	− 0.79
Heave	[m]	−0.29	1.00	0.00	0.00	0.00	0.00
Roll	[deg]	0.00	0.00	1.00	0.02	0.00	0.03
Pitch	[deg]	1.00	0.19	0.00	0.00	0.00	0.00
Yaw	[deg]	0.00	0.00	−0.01	1.00	0.00	1.00
Natural period	[s]	9.44	10.65	13.54	93.89	99.98	105.36

$$s = (\eta_1 + z\eta_5 - y\eta_6)\hat{i} + (\eta_2 - z\eta_4 + x\eta_6)\hat{j} + (\eta_3 + y\eta_4 - x\eta_5)\hat{k} \quad (6)$$

where η_1 to η_6 are the rigid body motions of the vessel and (x,y,z) is the position of the crane tip or gripper relative to the fixed coordinates of the vessel body. It is expected that the vessel motions will play an important role in the response of the monopile when the wave periods are approximately $T_p = 9$ s to 14 s.

In the case of the monopile by itself, the vessel was assumed to be a fixed structure and the lift wire and the gripper provided the restoring force for the monopile; the natural periods of the monopile in Table 4 correspond to the initial position of the monopile in air before being lowered and the eigenvectors refer to the monopile body-fixed coordinate with the origin at the center of the monopile (see Fig. 4). The 1st mode is dominated by the heave motion of the monopile, and the stiffness in heave is mainly from the lift wire axial stiffness. Modes 2 to 5 are dominated by a combination of the rotational motion in vertical plane and the translational motion in the horizontal plane, and the last mode is pure yaw motion. The eigenvectors in Table 4 show that modes 2 and 3 are symmetric and correspond to the same eigenperiods, but occur in different planes. It is the same for mode 4 and 5. The mode shapes are illustrated in Fig. 4, where the eigenvectors from Table 4 are magnified by a factor of 10. The eigenmodes are shown in different planes in order to observe the differences. The eigenperiods for modes 4 and 5 are much longer than modes 2 and 3. This can be explained as follows: both the translations and the rotations in mode 2 and 3 tend to increase the relative displacement between the monopile and the gripper. In this case, the gripper should provide enough restoring force to force the monopile move back to its initial position. On the other hand, the rotations and translations in modes 4 and 5 counteract each other and result in less displacement of the monopile relative to the gripper. The restoring provided by the gripper is then reduced compared with the previous case and results in longer eigenperiods. This can also be observed from the eigenmodes in Fig. 4.

In the coupled system of the vessel and the monopile, it is difficult to interpret the twelve eigenmodes because of the coupling effects. However, it was observed that in general the motions of the vessel slightly decreased the natural periods of the rotational modes of the monopile, and the natural period of the vessel roll motion was also reduced due to the effect from the lifting system.

During the installation, the position of the monopile changes with the running winch. This results in changes in the total restoring force due to changes in the length of the lift wire and in the gripper

Table 4

Eigenperiods and eigenvectors of monopile rigid body motions.

Mode		1	2	3	4	5	6
Surge	[m]	0.03	−0.23	−0.23	0.39	−0.32	0.00
Sway	[m]	−0.03	−0.22	0.24	0.32	0.39	0.00
Heave	[m]	1.00	0.00	0.06	0.00	−0.03	0.00
Roll	[deg]	−0.28	− 0.96	1.00	− 0.82	− 1.00	0.00
Pitch	[deg]	−0.29	1.00	0.96	1.00	− 0.82	0.00
Yaw	[deg]	0.00	0.00	0.00	0.00	0.00	1.00
Natural period	[sec]	0.72	1.01	1.02	3.58	3.67	40.04

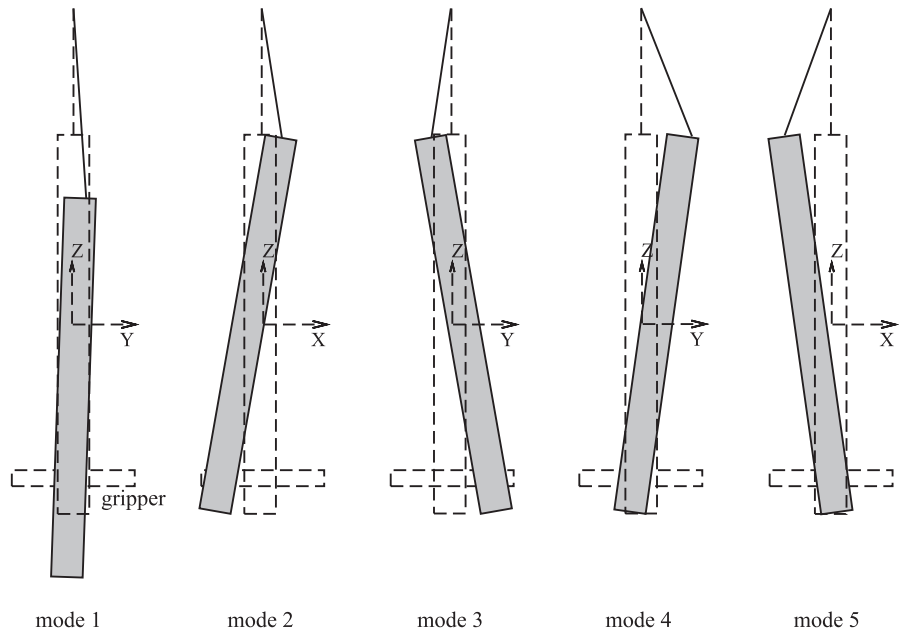


Fig. 4. Illustration of eigenmodes of monopile rigid body motions (eigenvectors are magnified by a factor of 10).

position relative to the centre of the pile. Additionally, the added mass matrix increases due to the increasing submergence. Fig. 5 shows how the eigen periods of modes 1 to 5 varied depending on the vertical position of the lower end of the monopile. The wave spectra are also included to show the modes that dominated the response at different sea states. The natural periods of mode 1 (which is

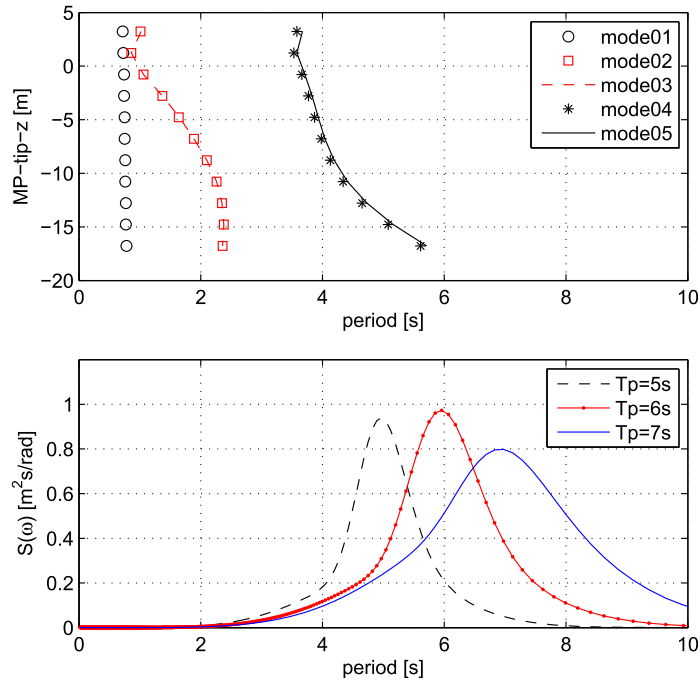


Fig. 5. Eigen frequency of monopile rigid body motion vs. position and representative wave spectra.

heave dominated) decreased slightly with increasing submergence due to the increase in the length of the lift wire. The other four modes all increased greatly due to significant contributions from the added mass.

For wave spectra with a peak period T_p greater than 5 s, there is little wave power near the natural period of the first three modes. However, modes 4 and 5 could be excited and dominate the responses at $T_p = 5$ s and $T_p = 6$ s, especially at a large submergence. With increasing T_p , the power of the wave spectra moves away from the natural periods of the monopile, and thus the resonance motions of the monopile would be reduced. Note that all the natural periods shown here are undamped periods and hence would increase slightly if damping were included.

3. Modelling of the shielding effects

The wave field around the floating vessel is different from incident wave field due to the presence and the motions of the vessel. The linear wave potential theory splits the total velocity potential into the radiation and diffraction components given by Ref. [22]:

$$\phi = \phi_D + \phi_R = \phi_I + \phi_S + \phi_R \quad (7)$$

where ϕ_D is the diffraction potential and ϕ_R is the radiation potential. ϕ_D can be further broken down into the sum of the incident velocity potential ϕ_I and the scattering velocity potential ϕ_S , which represents the disturbance to the incident wave caused by the presence of the body in its fixed position. By applying boundary conditions, i.e., the free surface condition, the seabed condition, the body surface condition and the far field condition, the boundary value problem can be solved by numerical methods such as the panel method in the frequency domain. Thus, the hydrodynamic coefficients of the vessel and the fluid kinematics at any point in the wave field in the frequency domain can be acquired. The waves affected by both radiation and diffraction of the vessel are defined as *disturbed waves* in this paper which account for the vessel shielding effects, and the undisturbed waves are defined as *incident waves*.

To calculate the wave forces on the monopile in the disturbed wave field during lowering, the fluid kinematics ζ_s and $\dot{\zeta}_s$ in Eqn. (2) should be based on the disturbed fluid kinematics. Because the position of the monopile varies with time and with the increasing length of the lift wire, the fluid kinematics at each strip of the monopile are time- and position-dependent. Therefore, the following approach was chosen to simulate the lowering process of the multi-body system in the time domain while considering the shielding effects:

1. First, generate time series of disturbed fluid kinematics at pre-defined *wave points* in space. The boundary of the wave points should cover all possible positions of the wet part of the monopile during the entire lowering process.

Calculate the disturbed fluid kinematics time series, i.e., wave elevation, velocities and accelerations at pre-defined wave points, using the fluid kinematics transfer functions in the frequency domain that are obtained using WADAM. The transfer function expresses the amplitude ratio and the phase angle between the disturbed fluid kinematics and regular incident wave amplitude. Knowing incident wave realisation $x(t)$, the Fourier transform of the kinematics of the disturbed wave $Y(\omega)$ can be calculated in the frequency domain based on $X(\omega)$, the Fourier transform of $x(t)$, and the disturbed fluid kinematics transfer functions $H(\omega)$, i.e., Eqn. (8). Thus, using inverse Fourier transform of $Y(\omega)$, the time series of wave elevations, fluid particle velocities and accelerations in disturbed waves at each pre-defined wave point can be obtained before the time-domain simulations.

$$Y(\omega) = H(\omega) \cdot X(\omega) \quad (8)$$

2. Then, at each time step of the simulation, determine the instantaneous position of the monopile based on the solutions from the previous time step. For each strip on the monopile, find the closest pre-defined wave points by comparing the coordinates of each strip on the monopile and the pre-defined wave points. By applying a 3D linear interpolation between these closest wave points, the

- kinematics (elevations, fluid velocities and accelerations) at the centre of each strip in disturbed waves are achieved. The interpolation of the fluid kinematics is illustrated in Fig. 6.
3. Obtain the forces at each strip in disturbed waves using Eqn. (2) and then integrate along the submerged part of the monopile to acquire the total wave forces and moments on the structure. Note that due to the running winch and the motions of the monopile itself, the wet length of the monopile changes with time. The wave elevation also affects the submergence of the monopile. Therefore, it is necessary to integrate the forces up to the instantaneous wave elevation to account for non-linear force components. The instantaneous wave elevation can also be determined by an interpolation of the wave elevations at pre-defined points given the instantaneous position of the monopile.
 4. Finally, perform the time-domain simulations of the coupled vessel-monopile system in irregular waves using the multi-body code SIMO and an external DLL that interacts with SIMO at each time step. SIMO calculates the wave excitation forces on the vessel and the coupling forces between the vessel and the monopile. The wave forces on the monopile in disturbed waves are calculated in DLL using the interpolation method described above, and the total wave forces on the monopile are returned to SIMO, with which the motions of the coupled system are solved. The time-domain simulation approach is illustrated in Fig. 7.

4. Fluid kinematics in the disturbed wave field

Fig. 8 shows the response amplitude operator (RAO) of wave elevation, fluid particle velocities and accelerations as a function of frequency with wave directions of 0 deg and 45 deg.

The RAOs that are given refer to the pre-defined wave points at the mean free surface when the monopile was at rest with coordinates of (−20 m, 30 m, 0 m) in the global coordinate system. The RAOs of fluid kinematics in incident waves are shown for comparison.

In long waves (with $\omega < 0.4$ rad/s), the RAOs in disturbed waves are nearly identical to those in incident waves, which indicates that the diffraction and radiation of the vessel are negligible in long-wave conditions. However, as the frequency increases, the RAOs in disturbed waves deviate from those in incident waves, and the difference increases with frequency. When the wave length is shorter than the dimension of the vessel (approximately $\omega > 1.0$ rad/s), the RAOs in disturbed waves are much lower than those in incident waves (with the exception of the Y-velocity at Dir = 0 deg), mainly due to the diffraction of the vessel while the radiation is minor in short waves. At a frequency near $\omega = 0.5$ rad/s,

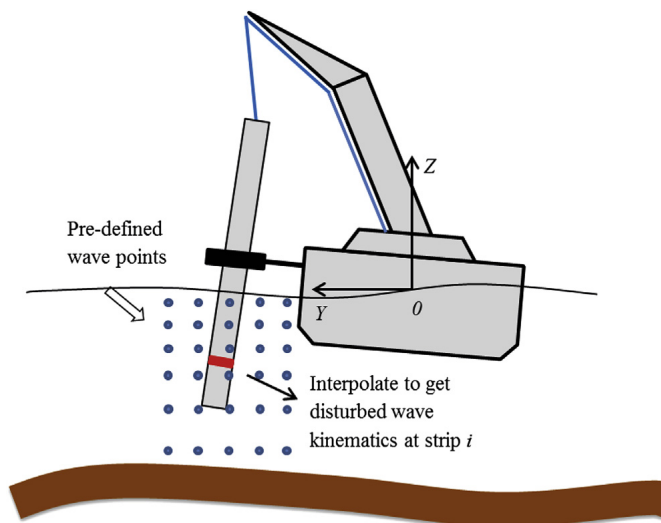


Fig. 6. Interpolation of fluid kinematics in disturbed waves.

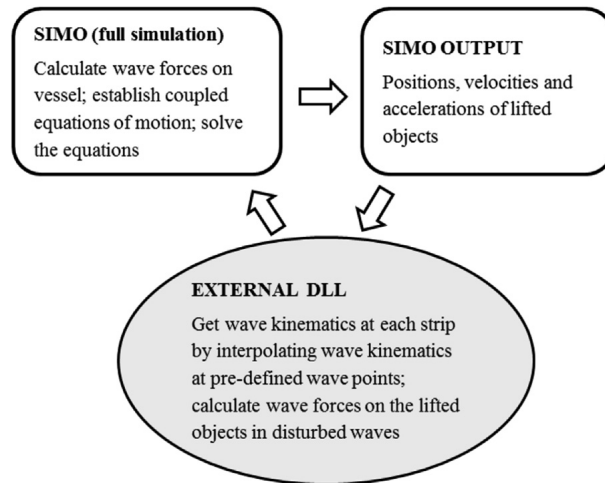


Fig. 7. Time-domain simulation approach considering vessel shielding effects.

the RAOs shift away from the main trend of the curve due to the large resonance motions of the vessel, which occur close to the natural frequencies of the vessel motions. With an increase in the frequency, the effects of the diffraction of the vessel dominate the RAOs.

The RAOs also depend greatly on the wave directions. Comparing the RAOs in Fig. 8 at 0 deg and 45 deg shows that larger discrepancies in the fluid kinematics of the two wave fields occur at 45 deg. Additionally, when $\text{Dir} = 0$ deg, the fluid particle velocity in Y direction is not zero as it is in incident waves, which indicates the presence of 3D effects from the diffraction and radiation that could induce extra wave forces on the monopile in the direction perpendicular to that of long-crested incident waves.

Fig. 9 shows the variations in the fluid kinematics in all wave directions. The results in the figures, which also refer to point $(-20 \text{ m}, 30 \text{ m}, 0 \text{ m})$, include four representative wave frequencies that cover long and short waves. Although the RAOs in disturbed waves are very close to those in incident waves in all wave directions in long waves, in short waves the results change considerably with direction. In general, the RAOs are reduced when the waves come from the leeward side relative to the vessel and may greatly increase when the waves come from the windward side. It is noticed that the RAOs of wave elevation and kinematics in X direction are amplified at wave directions that are larger than 180 deg in short waves, whereas the kinematics in Y direction decrease at $T_p = 7 \text{ s}$. In fact, the fluid kinematics in the disturbed wave field are also sensitive to the position of the monopile relative to the vessel and the wave length, and cancellations may occur if this position is close to the nodes of the disturbed fluid kinematics profile. When the waves come from the leeward side, a great reduction in the RAOs occurs due to the vessel shielding effects, which results in a reduction of wave forces on the monopile during installation. Therefore, operations should be performed on the leeward side of the vessel in order to minimise the responses.

The variations in the fluid kinematics at the heading angle of 45 deg with respect to depth and to the horizontal position near the monopile installation region are shown in Figs. 10 and 11. The results in Fig. 10 correspond to points at $(x = -20 \text{ m}, y = 30 \text{ m})$ with varying depth, and the results in Fig. 11 correspond to points at the mean free surface $(z = 0 \text{ m})$ with varying X and Y positions.

As previously observed, in long waves the RAOs in disturbed waves are close to those in incident waves. Moreover, in long waves the RAOs of the fluid kinematics decay very slowly and vary little in the horizontal plane compared with those in short waves. 3D effects are observed in short waves along the horizontal plane as shown in Fig. 11, in which the contours of the elevation RAOs do not follow the incident wave direction of 45 deg. The 3D effects are also present in Fig. 10, e.g., at $T_p = 7$ and 9 s, at which the fluid particle velocities do not follow the decay rate as those in incident waves at depth of less than -10 m . The 3D effects come from the diffraction and radiation of the vessel; thus, the effects

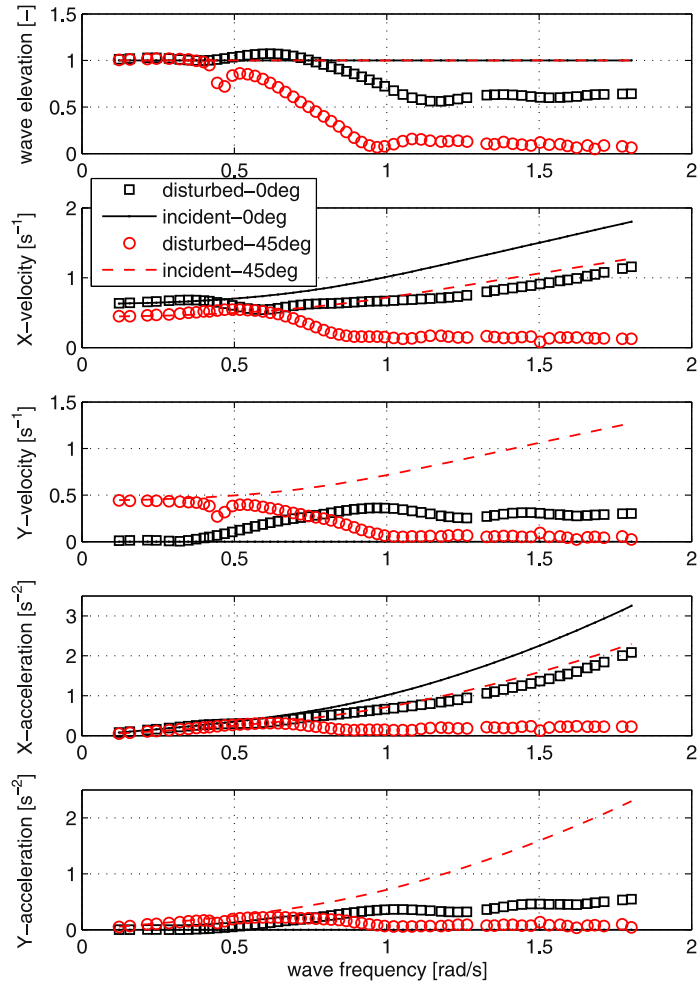


Fig. 8. RAOs of fluid kinematics vs. wave frequency ($x = -20$ m, $y = 30$ m, $z = 0$ m).

would vary from vessel to vessel. To account for the 3D effects when calculating the wave forces on the monopile, a 3D interpolation of the fluid kinematics is required.

5. Time-domain simulations

5.1. Time-domain simulation method

Step-by-step integration methods were applied to calculate the responses of the lifting system using an iterative routine. The equations of motion were solved by Newmark-beta numerical integration ($\beta = 0.1667$, $\alpha = 0.50$) with a time step of 0.01 s. The 1st order wave forces of the vessel were pre-generated using Fast Fourier Transformation (FFT) at the mean position. The fluid particle motions used to calculate the hydrodynamic forces on the monopile were calculated in the time domain using the interpolation of the pre-generated fluid kinematics at pre-defined wave points in disturbed waves. The winch started at 300 s to avoid initial transient effects with a constant speed of 0.05 m/s, and stopped at 700 s. Thus, the total lowering length was 20 m. During the lowering process, the gripper device provided horizontal forces to the monopile.

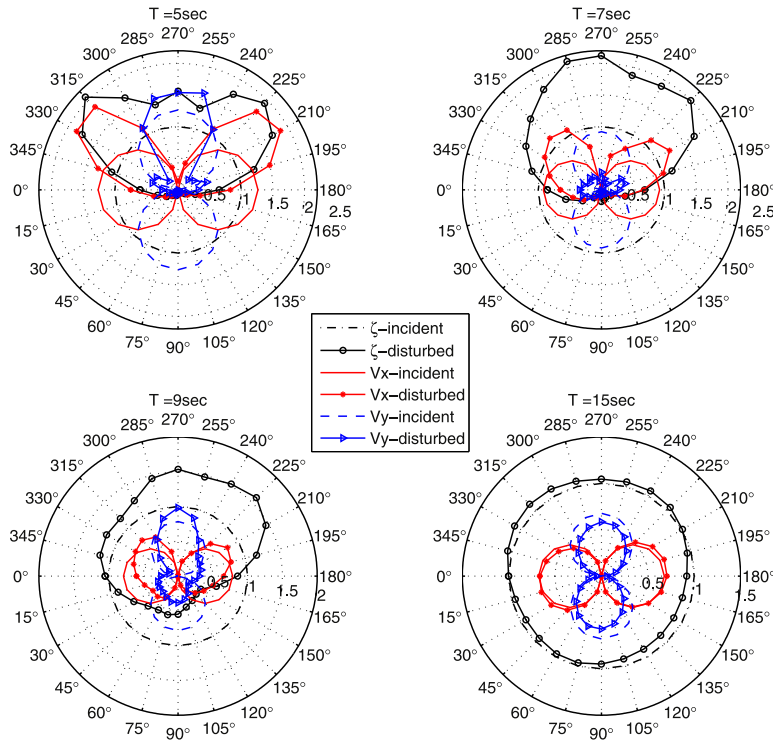


Fig. 9. RAOs of wave elevation and fluid particle velocities at varying directions ($x = -20$ m, $y = 30$ m, $z = 0$ m).

The environmental condition of the time-domain simulations was $H_s = 2.5$ m. The wave spectral peak period (T_p) varied from 5 s to 12 s, thus covering a realistic range. At each combination of H_s and T_p the irregular waves were modelled by JONSWAP spectrum [12]. In order to account for the variability of stochastic waves, 20 realisations of irregular waves were generated at each of the environmental conditions using different seeds. Thus, 20 repetitions of the lowering simulations (400 s for each seed) corresponded to an operation with a duration of approximately two hours.

5.2. Sensitivity study on the resolution of the pre-defined wave points

The response of the lifting system with varying resolutions of the pre-generated wave points was studied. As mentioned, the fluid kinematics at pre-defined wave points were generated based on linear wave theory, whereas those at other locations in space were obtained using a 3D linear interpolation. Theoretically, when a higher resolution is used, more accurate responses can be estimated. If a low resolution is chosen, the number of wave points might not be sufficient to represent the variation of the fluid kinematics in space, which would result in a large uncertainty in the simulation results. However, a high resolution of wave points results in a large number of points at which the fluid kinematics must be pre-generated, and therefore the efficiency of the interpolation is reduced; a high resolution increases the simulation time significantly. Therefore, a reasonable resolution of wave points should be determined to provide results with an acceptable level of accuracy while at the same time shortening the simulation time.

The wave points spread in all three directions in space. The sensitivity studies in the horizontal (XY) plane and in the vertical (Z) direction were performed separately. The gaps between points in the three directions were chosen as the parameters in the sensitivity study (see Fig. 12). The parameters of the different cases are listed in Table 5. The gaps in Z direction were fixed, and all points were evenly spaced when studying the different horizontal resolutions. In the sensitivity study in the vertical direction, all the wave points were chosen at a fixed (x_0 y_0) position, and only one-dimensional interpolation in Z

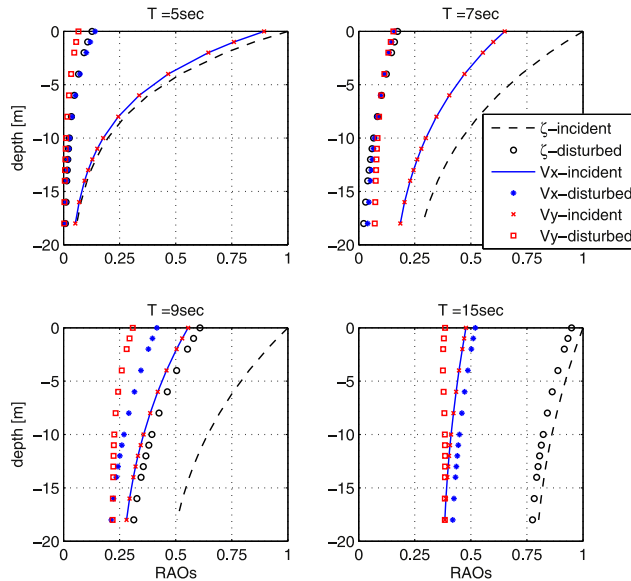


Fig. 10. RAOs of wave elevation and fluid particle velocities vs. water depth ($x = -20$ m, $y = 30$ m).

direction was used when calculating the wave forces on the monopile. A hybrid case (case 6) was included that had gaps of 0.5 m when the depth larger than -2 m and gaps of 2 m when the depth was less than -2 m. This case was selected because that the fluid kinematics decay with decreasing water depth, and it is interesting to study the effects of the resolutions of wave points near the free surface. In the other cases the wave points were all evenly spaced.

As shown in the eigen value analysis, only in relatively short waves were the resonance motions excited, and in short waves the responses are more sensitive to the interpolation resolution due to the shorter wave lengths compared with long waves. Hence, the environmental conditions for the sensitivity study focused on relatively short waves with two wave directions, as shown in Table 5. Note that the ratio between the gap and the wave length can be used to characterise the convergence. Thus, the regular wave lengths λ with periods equal to the irregular wave peak periods were also included in Table 5 for reference.

Fig. 13 compares the extreme response statistics with different wave point resolutions in the XY plane and in the Z direction. The extreme values presented are the mean values of the maximum responses from 20 irregular wave seeds during the lowering phase. The results in the horizontal plane show that the results from the first three cases are close to each other with errors of the responses in case 2 and case 3 being less than 5% compared with case 1. However, the results from case 4, which had gaps of 8 m, deviate from those with higher resolutions. For some responses, e.g., the monopile tip motions and rotations, the errors are approximately 10%–20% compared with case 1. Therefore, a resolution with gaps of 4 m in the XY plane was chosen in the time-domain simulations.

Similarly, the results in the vertical direction show increasing errors with decreasing resolutions, and the errors of the motions and rotations of the monopile in case 8 are approximately 5%–10% in most of the environmental conditions. The differences in the results from cases 6 and 7 are minor, which indicates that the responses were not very sensitive to resolution near the free surface. This is due to the extreme responses occurred at a large draft in which the wave forces on the monopile are the summation of the forces from all the strips instead of dominated by the forces at strips near the free surface. However, for structures with a smaller draft and large dimension in horizontal plane the extreme responses occur when the structures are near the free surface. The resolution of wave points near the free surface might be critical, and therefore higher resolutions should be used. In this study, a resolution of 2 m in the vertical direction was used.

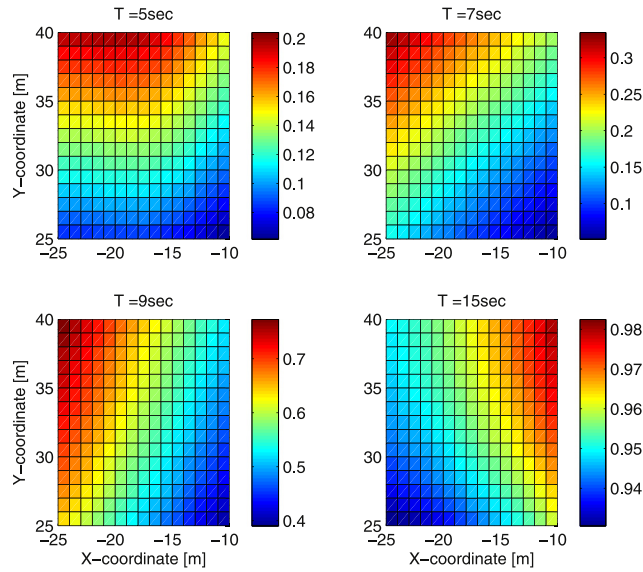


Fig. 11. RAOs of wave elevation of disturbed waves in XY plane ($z = 0$ m).

6. Results and discussion

6.1. Operational criteria

The operational criteria of the lifting operation of a monopile should be established by assessing the whole installation phase, including the upending, lowering and landing operations. Because this study is limited to the lowering phase, the critical responses of this phase are given.

1. Lift wire tension. The tension in the lift wire should never exceed the maximum working load of the wire, which depends on the property of the wire. According to DNV-RP-H103 [23], a slack wire and snap forces should be both avoided. In addition, extreme dynamic loads on the wire should be limited by checking the dynamic amplification factor (DAF) [23].

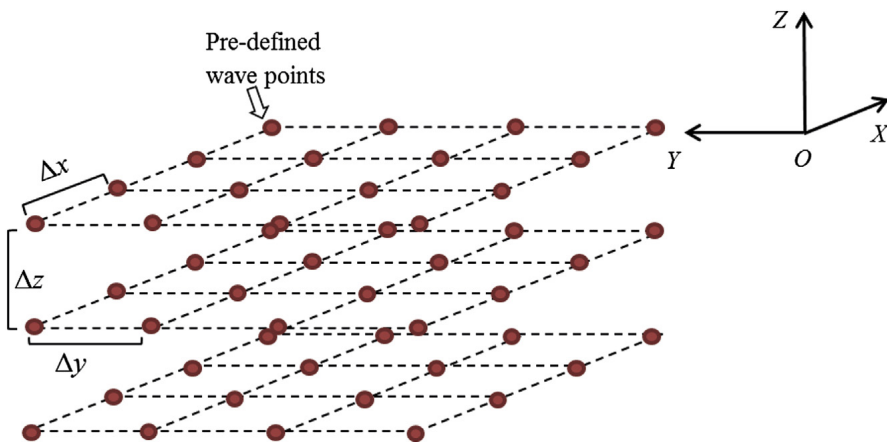


Fig. 12. Parameters in sensitivity study of wave point resolution.

Table 5
Parameters for sensitivity study of wave point resolutions and environmental conditions.

Sensitivity study case no.		1	2	3	4	5	6	7	8
Δx	[m]	0.5	2	4	8	—	—	—	—
Δy	[m]	0.5	2	4	8	—	—	—	—
Δz	[m]	2	2	2	2	0.5	0.5/2	2	4
Environmental condition no.		1		2		3		4	
T_p	[s]	5		7		5		7	
Dir	[deg]	0		0		45		45	
λ	[m]	39		75		39		75	

2. Gripper contact force. The gripper device was the main support structure that controlled the horizontal motions of the monopile. The relative motion between the monopile and the gripper induced huge impulse forces. The extreme contact loads should be estimated in order to perform the structural analysis of both the gripper device and the monopile to ensure their structural integrity at different environmental conditions.
3. Monopile motions. The motions of the monopile, particularly its rotations and the displacements of its end tip, affect the landing process that follows the lowering process examined in this study. Extreme motions should be estimated to ensure a successful landing at the designated position.

This study focuses on predicting the extreme responses during the lowering phase in various environmental conditions. Operational criteria should be established by further analysis, e.g., a

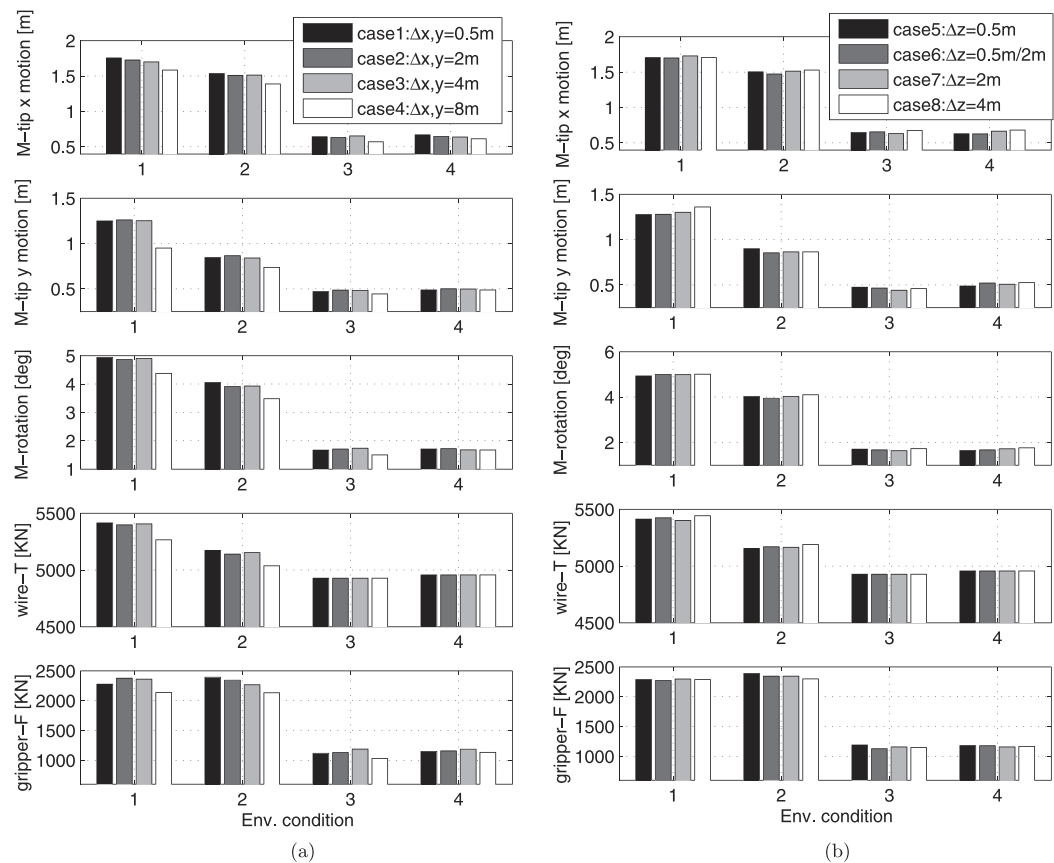


Fig. 13. Extreme response statistics with different resolutions in XY plane (a) and in Z direction (b).

structural analysis based on the predicted extreme responses. By applying these criteria, safe operational environmental conditions could be predicted. The results of the time-domain simulations presented below will focus on the critical responses given above.

6.2. Response time series and spectra

Fig. 14 and Fig. 15 show the time history of the responses of the lifting system during lowering at two wave conditions. The responses in the figures include the motions of the monopile end tip, the contact forces of the gripper and the tensions in the lift wire. The lowering phase started when the winch was activated at 300 s. The monopile was lowered through the splash zone until the winch stopped at 700 s. During the process, the length of the lift wire increased with a fixed speed, and the added mass of the structure increased with its submergence. Both increases contributed to a continuous decrease in the natural frequencies of the lifting system. While the increasing wave forces acting on the monopile induced motions, the gripper device was placed to control its horizontal motions.

Comparing the responses in incident and disturbed waves shows that in short waves with $T_p = 5$ s and $\text{Dir} = 45$ deg, the rotations of the monopile, lift wire tensions and contact forces of the gripper device are significantly reduced when shielding effects are considered, whereas in long waves with $T_p = 11$ s the influence of shielding effects is much less. These results again indicate that the shielding effects of the vessel have more influence on the fluid kinematics in short waves, which is consistent with the RAOs of the fluid kinematics shown in Fig. 8.

The response spectra of the lowering phase were obtained using Fourier transformation of the time series. Fig. 16 shows the response spectra at $T_p = 5$ s and 11 s with direction $\text{Dir} = 45$ deg. In short waves, the resonant motions of the monopile are excited near the wave period, which corresponds to the peak frequency of the spectrum. The hydrodynamic wave loads on the monopile dominate the response of the system in this case. In long waves, however, there are two peaks in the motion spectrum. The frequencies of the secondary peak with $\omega \approx 1.1$ rad/s match the natural frequencies of the monopile rotational motion, while the frequencies of the main peak with $\omega \approx 0.5$ rad/s are the wave spectrum peak frequencies. Due to the couplings of the monopile and the vessel, the increasing response of the vessel in long waves dominates the motions of the monopile. The peak frequency of the wire tension is consistently twice of the rotational peak frequency, which means that one cycle of rotational motion induces two cycles of variations in the wire tension.

For both wave conditions, the peaks at $\omega \approx 1.1$ rad/s in the response spectra, which is close to the natural frequency of the rotational motions of the monopile, are significantly reduced when the shielding effects of the vessel are considered. However, in long waves with $T_p = 11$ s the response peaks corresponding to the long wave peak period do not decrease in disturbed waves. These results indicate the significant influence of the shielding effects on the monopile motions, particularly in short waves when the wave frequencies are close to the natural frequencies of the monopile.

6.3. Response statistics

Fig. 17 compares the extreme values of the critical responses during the lowering process in incident and disturbed waves with a wave direction of 45 deg. These extreme values presented are the mean values of the maximum responses from 20 irregular wave seeds used in the lowering phase. The extreme monopile tip distance in the figures refers to the maximum offset of the monopile tip from the designated landing position in the XY plane during lowering. The rotational motions of the monopile in the figure are the maximum rotations relative to the horizontal plane and were calculated by combining the pitch and roll motions. The responses of the lifting system were sensitive to the shielding effects of the vessel as shown.

In incident waves, the extreme responses of the lifting system first decrease and then increase as the wave length increases. The maximum rotations and tip distances occur at $T_p = 6$ s, which is close to the natural periods of the rotations. The rapid increase in the motions and rotations in long waves is due to the increasing crane tip motions that are induced by the vessel motion (see Eqn. (6)). The extreme motions of the crane tip in X and Y directions at varying wave periods are shown in Fig. 18. The main contribution to the rapid increase in the crane tip motions comes from the vessel roll motion at a large

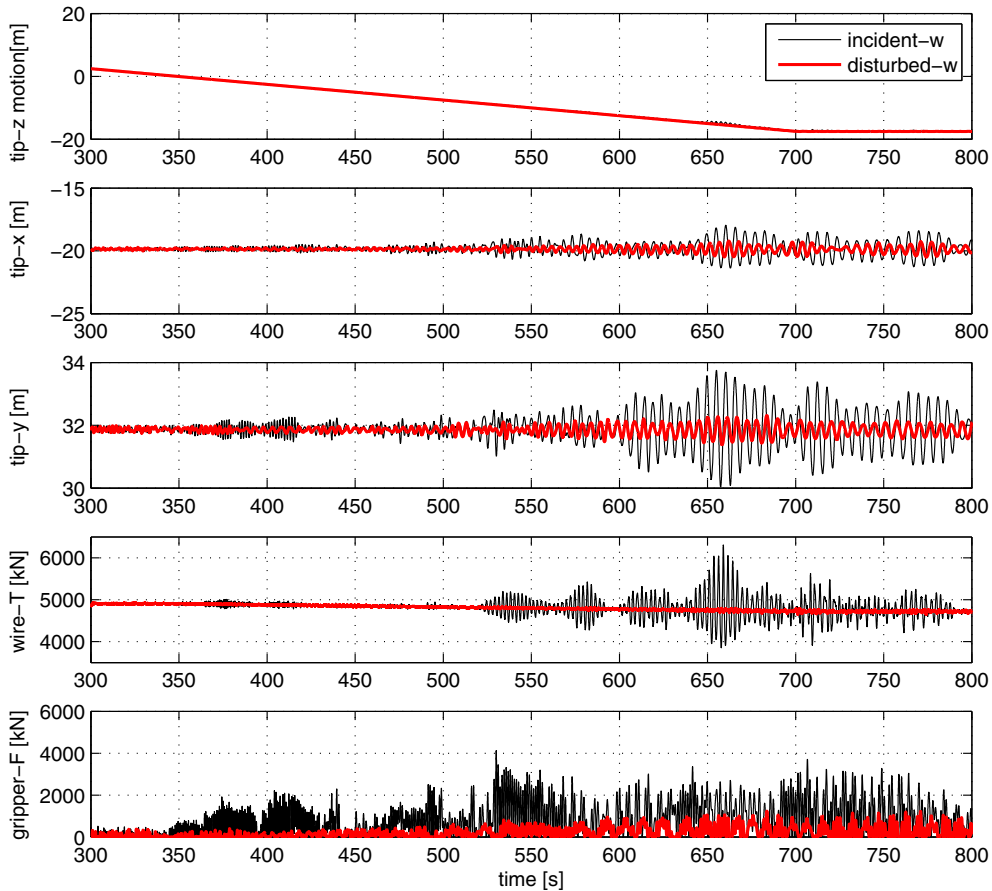


Fig. 14. Time series of responses in incident and disturbed waves ($H_s = 2.5$ m, $T_p = 5$ s, $\text{Dir} = 45$ deg).

lifting height. It should be mentioned that the increasing distance from the monopile tip to the designated position would result in difficulty during the landing operations and huge landing forces if the landing devices were used at the designated position as discussed in Ref. [21]. Fig. 18 also indicates that the effects of the monopile motions on the vessel motions are negligible. Because the gripper contact forces and lift wire tensions are more dependent on monopile motions at its own natural periods, these extreme responses do not increase as much as the monopile motions in long waves as shown in Fig. 17.

In the disturbed wave field, the extreme responses are greatly reduced in short waves compared with long waves with $\text{Dir} = 45$ deg. As shown above, the fluid kinematics in disturbed wave field depend greatly on the wave directions; the shielding effects of the vessel on the responses of the lifting system are expected to vary with wave direction. The comparison of the RAOs at $\text{Dir} = 0$ deg and $\text{Dir} = 45$ deg in Fig. 8 suggests that at smaller wave directions the shielding effects would be reduced, particularly in short waves. Therefore, the current results at $\text{Dir} = 45$ deg do not represent the shielding effects at different wave directions. Results at various wave directions are required.

6.4. Responses at different wave directions

The sensitivity of the extreme responses at different wave directions was studied. Fig. 19 compares the statistics of the extreme rotations of the monopile in disturbed waves with those in incident waves at four irregular wave conditions.

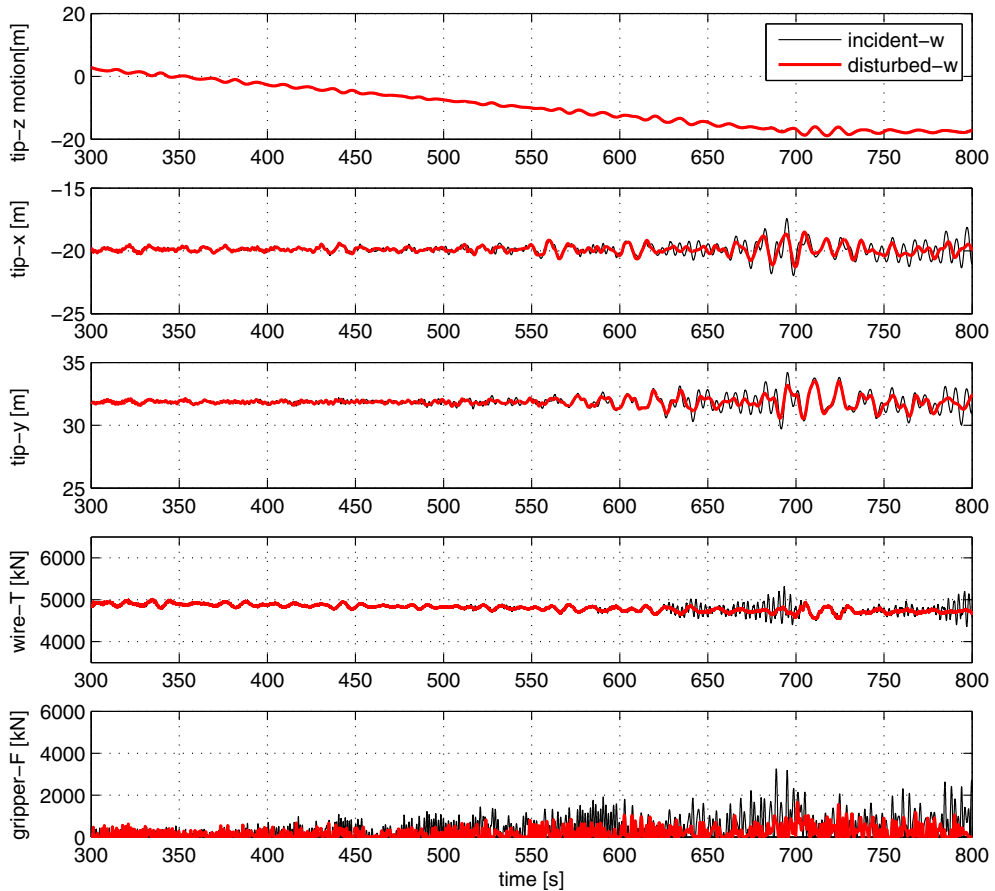


Fig. 15. Time series of responses in incident and disturbed waves ($H_s = 2.5$ m, $T_p = 11$ s, $Dir = 45$ deg).

In incident waves, the responses with waves coming from the port side are similar to the responses with waves coming from the starboard side due to the symmetry of the vessel about its X axis. This means the responses are independent of whether the monopile is in the windward side ($Dir = 180$ to 360 deg) or the leeward side ($Dir = 0$ to 180 deg) of the vessel. However, when shielding effects are taken into account, the responses are greatly affected.

In relatively short waves ($T_p = 5$ and 7 s), the responses are significantly reduced when the monopile is placed on the leeward side of the vessel when shielding effects are considered, and the rotational motions of the monopile and wire tension greatly increase when the monopile is on the windward side of the vessel. Therefore, the lifting operation should be performed on the leeward side of the vessel to utilise the shielding effects of the vessel. With increasing wave length, the differences between the extreme responses in disturbed and incident waves are rapidly reduced. The directional plots show that the responses in both incident and disturbed waves are almost symmetric about the beam sea direction because the installation of the monopile was carried out close to mid-ship in the longitudinal direction.

When only the extreme responses of monopile rotations from $Dir = 0$ to 90 deg are considered, the extreme responses reach their minimum values at approximately $Dir = 45$ to 60 deg in short waves, whereas in long waves the minimum values occur at approximately $Dir = 15$ to 30 deg. Both the resonance motions of the monopile and the vessel motions affect the responses of the lifting system, and the factor that dominates the responses depends on both the wave direction and the wave length.

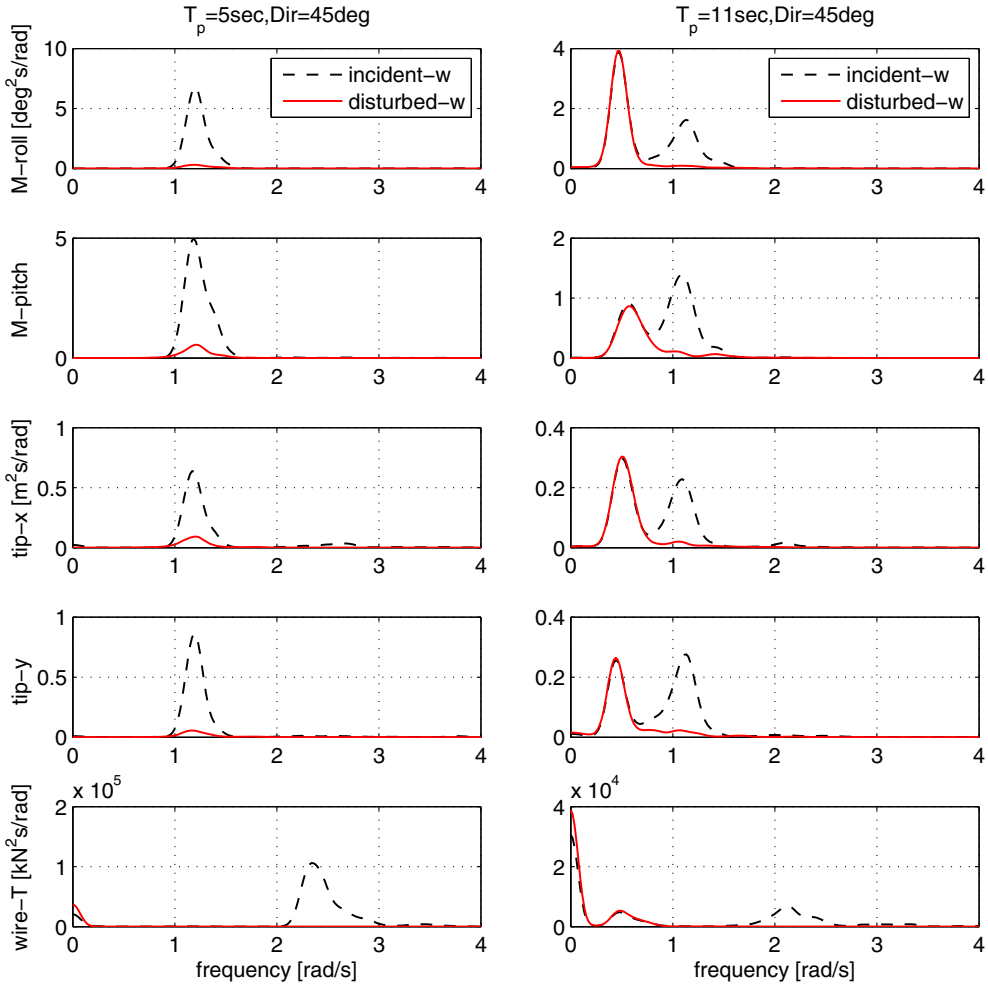


Fig. 16. Spectrum density of responses during lowering in incident and disturbed waves ($H_s = 2.5$ m).

As shown in the eigen value analysis, in short waves, the resonance motions of the monopile were excited and affected the responses of the lifting system. The RAOs of the fluid kinematics near the monopile position varied with the wave direction and in general reached a minimum near the beam sea condition ($\text{Dir} = 90^\circ$), and they increased gradually when the direction moved towards following sea or heading sea conditions. Hence, the resonance motions of the monopile decreased from $\text{Dir} = 0^\circ$ to 90° . On the other hand, although the vessel motions were minor in short waves, the crane tip motions always increased as the wave direction moves from heading sea to beam sea conditions due to the roll motion of the vessel and the large lift height. Thus, near heading sea conditions, the resonance motion dominated and the extreme responses decreased as the wave direction moved to quartering sea conditions. However, when the direction increased further, due to the increase in the vessel roll motion and the decrease in the resonance motion, the crane tip motions began to dominate the response of the system. Hence, the extreme responses increased again until $\text{Dir} = 90^\circ$. The minimum values were approximately $\text{Dir} = 45$ to 60° .

However, in long waves, the resonance motion of the monopile was secondary because the wave peak periods were away from the eigen periods of the monopile. At the same time the vessel motions increased significantly so that the crane tip motions dominated the responses of the system even at a

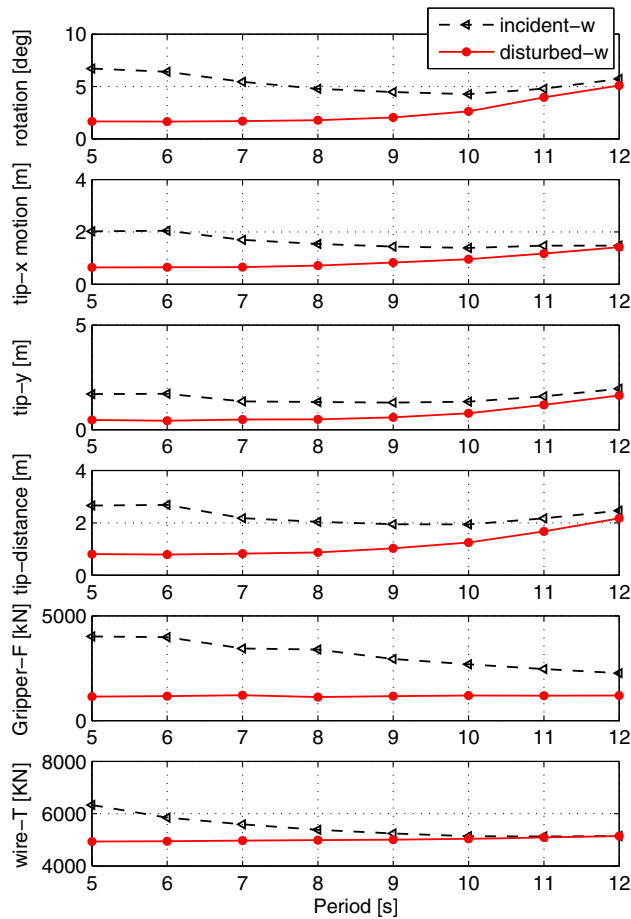


Fig. 17. Extreme responses of lifting system in incident and disturbed waves ($H_s = 2.5$ m, $Dir = 45$ deg).

relatively small wave direction of approximately 15–30 deg. Thus, the responses continued to increase when the wave direction increased towards beam sea conditions.

Therefore, the minimum extreme responses at different sea states occurred at different wave directions. In order to utilise the shielding effects to increase the weather window as much as possible, the most suitable wave directions at different wave lengths should be applied.

Because the motions of the monopile are dominated by the vessel motion in long waves, the lift wire and the gripper control the motions of the monopile in a way that follows the motions of the vessel. At $T_p = 11$ s, the rotational motions of the monopile decreased slightly at $Dir = 0$ to 180 deg; thus, the extreme tensions in the lift wire in disturbed waves were very close to those in incident waves in all wave directions. In spite of this, the extreme gripper contact forces were greatly decreased at $Dir = 0$ to 180 deg. This is due to the high stiffness of the gripper device and the sensitivity of the contact force to the monopile rotational motions. Therefore, to reduce the contact forces, the lifting operation should be conducted in the leeward side of the vessel even in very long waves.

The differences in the extreme responses in disturbed and incident waves, including the extreme rotations of the monopile, the extreme tensions in the lift wire and the extreme contact forces of the gripper are quantified in Table 6 at directions from 0 deg to 90 deg at four wave period conditions. The ratios in the table are given as percentages and were calculated as the difference of the responses in disturbed and incident waves divided by the response in incident waves. The bold figures show the

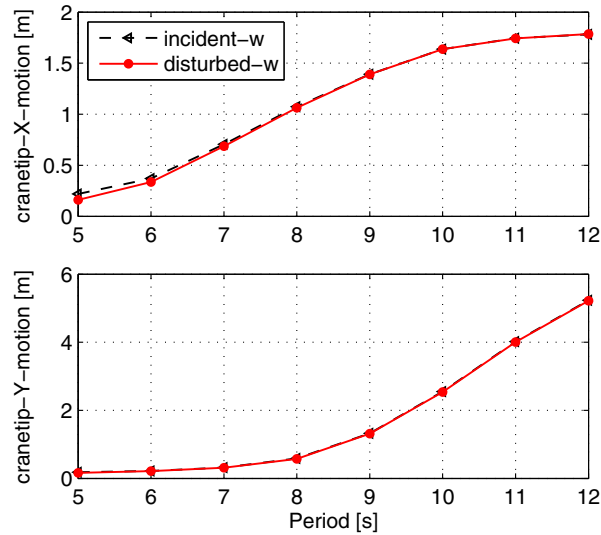


Fig. 18. Extreme crane tip motions in incident and disturbed waves ($H_s = 2.5$ m, Dir = 45 deg).

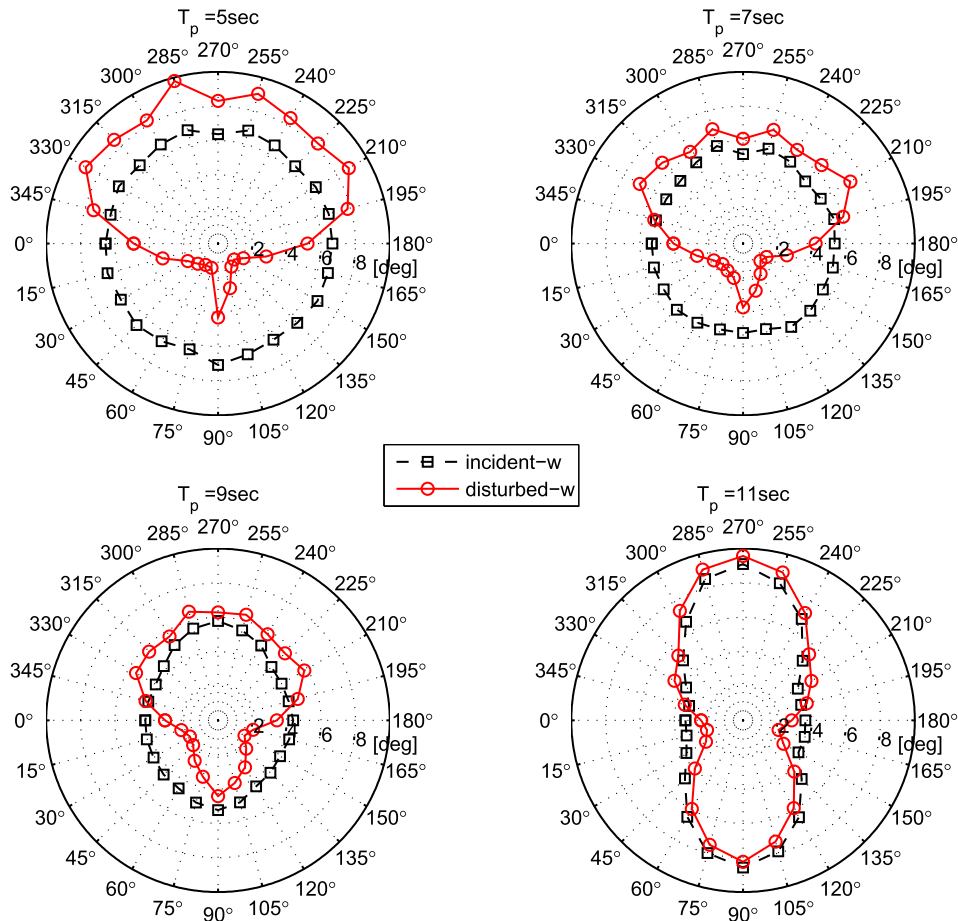


Fig. 19. Extreme rotations of monopile in incident and disturbed waves at different wave directions ($H_s = 2.5$ m).

maximum reduction of the responses in different wave periods. The corresponding wave directions are shown to decrease with increasing wave period.

The maximum decrease in the responses in short waves is approximately 70% for both monopile rotational motion and gripper contact force. In long waves ($T_p = 11$ s), the ratios become approximately 35% and 50%, respectively, which shows the decrease in shielding effects with increasing wave period. The reduction in the tensions in the lift wire is somewhat less compared with the other two responses.

6.5. Comparison of responses using floating and jack-up vessels

The jack-up installation vessel is another choice in the installation of a monopile. The hull of the jack-up vessel is raised above the sea surface on legs, and the vessel is fixed to the sea bed during lifting operations. The greatest advantage of a jack-up vessel is that it provides a stable working platform for lifting operations so that only the wave forces on the monopile itself matter during the lowering phase. However, because only the legs of the jack-up vessel are in the water during the operation, the shielding effects from the jack-up vessel are very small and can be ignored. Thus, the waves on the monopile are incident waves in all wave directions, and may induce larger motions compared with the disturbed waves that occur when the floating vessel is used. It is interesting to compare the responses of these two types of vessel to select the most suitable vessel in different environmental conditions.

Fig. 20 compares the extreme monopile rotations in different wave directions when using the jack-up vessel and the floating vessel. The responses when using the floating vessel were calculated to include the shielding effects of the vessel, whereas only the incident waves were considered in the case of the jack-up vessel.

In short to intermediate waves, the resonance motions of the monopile dominated; thus, the extreme rotations when using the floating vessel were lower than using jack-up vessel at $\text{Dir} = 0$ to 180° due to the shielding effects of the floating vessel. With increasing wave length, the motions of the floating vessel increased and began to dominate the responses, and hence the responses when using the floating vessel exceeded those when using the jack-up vessel, particularly in large wave directions. The responses were even larger when using the floating vessel if the installation was performed in the windward side of the vessel.

Therefore, to reduce the extreme responses, it is better to use the floating vessel in short to intermediate waves and to use the shielding effects of the vessel, whereas in long waves (in the current model $T_p > 11$ s), the jack-up vessel is better. If the floating vessel is used in long waves, the operations should be carried out close to heading seas or following seas to avoid large roll motions of the vessel.

7. Conclusions

In this study, a numerical coupled model of lowering an offshore wind turbine monopile was established. A continuous lowering process was analysed. The effects of vessel shielding on the responses of the lifting system were calculated by establishing an external DLL and implementing it in SIMO. The wave forces on the monopile were calculated during lowering by interpolating fluid kinematics between pre-defined wave points near the floating vessel. It is concluded that the shielding effects from the vessel

Table 6

Differences in percentage between extreme responses in disturbed and incident waves.

Dir [deg]	Monopile rotation				Lift wire tension				Gripper force			
	5 s	7 s	9 s	11 s	5 s	7 s	9 s	11 s	5 s	7 s	9 s	11 s
0	–25.0	–23.7	–27.1	–27.2	–13.2	–8.0	–3.8	–0.9	–43.9	–35.4	–27.5	–27.2
15	–49.9	–48.4	–48.5	–36.3	–19.9	–11.1	–5.0	–0.7	–56.7	–50.2	–45.9	–40.9
30	–68.8	–63.2	–56.4	–34.5	–21.5	–11.2	–4.8	–1.1	–69.7	–62.0	–59.2	–48.6
45	–75.3	–68.9	–54.4	–17.1	–22.1	–11.2	–4.4	0.1	–71.5	–64.9	–60.4	–51.6
60	–78.1	–65.9	–40.6	–8.1	–21.2	–10.4	–3.6	0.7	–73.6	–67.7	–55.0	–47.0
75	–77.1	–60.0	–31.4	–6.3	–19.6	–8.5	–3.3	0.9	–74.7	–65.5	–56.3	–45.9
90	–39.1	–28.7	–15.6	–3.8	–10.1	–2.3	–0.7	1.0	–56.0	–51.1	–46.2	–35.7

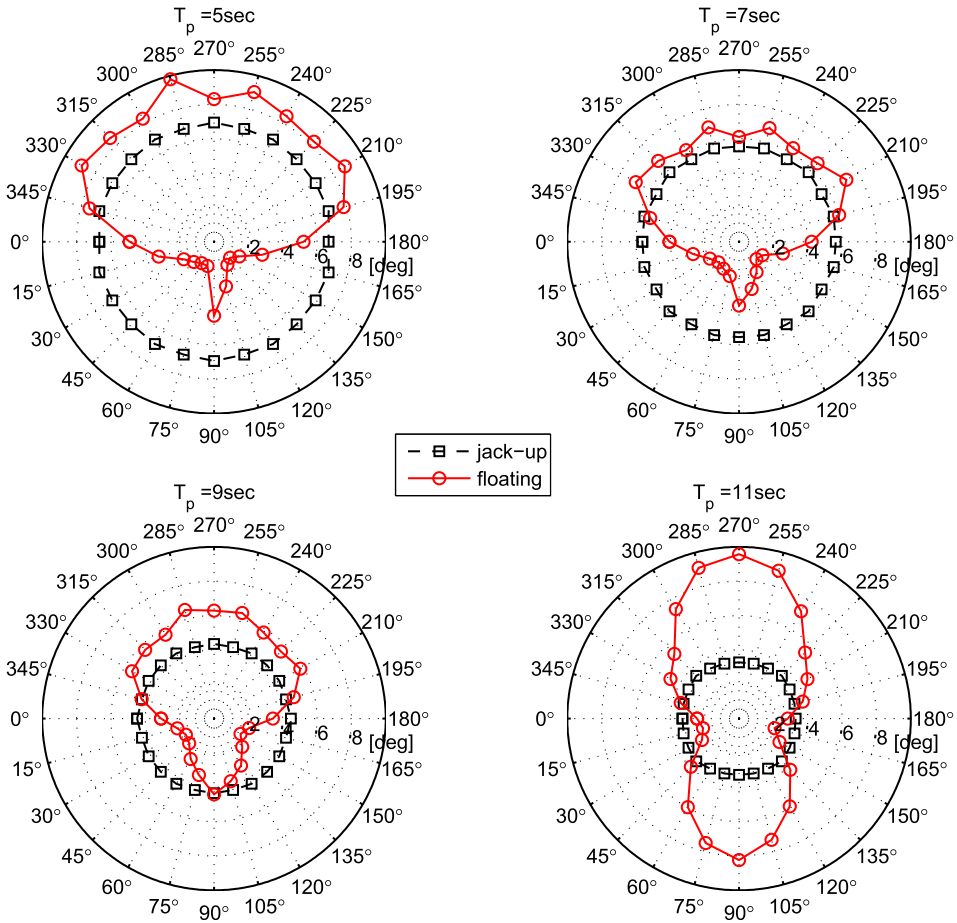


Fig. 20. Extreme monopile rotations by using jack-up and floating installation vessels at different wave directions ($H_s = 2.5$ m).

reduce the extreme responses of lifting operations conducted in the vicinity of the vessel at proper vessel heading angles. The shielding is more significant in short waves than in long waves.

The fluid kinematics in disturbed waves show a great dependence on the wave direction; the RAOs are reduced when the wave comes from the leeward side of the vessel and may increase greatly when the wave comes from the windward side. In addition, the shielding effects of the vessel depend greatly on the position of the lifted object relative to the vessel. The reduction in the extreme responses that results from shielding effects is expected to decrease when the lifted object is located further away from the vessel.

The numerical simulations show that the extreme responses, i.e., the rotations of the monopile, the tension in the lift wire and the contact force of the gripper, reached minimum values at wave directions of approximately $\text{Dir} = 45$ to 60 deg in short waves, and the extreme motions of the monopile in disturbed waves could be reduced by more than 50% compared with those in incident waves. In long waves, the minimum extreme values were acquired at directions approximately $\text{Dir} = 15$ to 30 deg, and the reduction of the extreme rotation and gripper contact force is greater than 30% due to shielding effects. Therefore, the responses can be greatly overestimated in the design of marine operations if shielding effects are not considered. This fact implies an underestimation of the weather window in such operations.

Although the shielding effects of the vessel cause a great reduction in the extreme responses at many sea conditions, the vessel heading angle should be adjusted carefully in very long waves that

have peak periods close to the natural periods of the vessel, conditions in which the vessel motions can induce severe motions in the lifted object through the crane tip. Use of a jack-up vessel is recommended in cases of very long waves to prevent these large crane tip motions that are induced by floating vessels.

The approach proposed in this study to consider the shielding effects of the vessel is also applicable to simulating operations of more complicated structures, such as jacket foundations and sub-sea templates, which can be modelled as a collection of separate slender elements [24]. For continuous lowering simulations of large volume structures such as gravity-based structures (GBS), the hydrodynamic coupling between the vessel and the GBS must be calculated continuously with an increasing draft of the GBS using numerical method such as panel method to consider the shielding effects of the vessel, which is beyond the capability of the current approach. Another limitation of the current approach is that only long-crested waves are considered. The vessel crane tip motions as well as the shielding effects from the vessel will be influenced by the spreading of the waves. The shielding effects are expected to be less in short-crested waves than in long-crested waves, especially in short waves with vessel heading close to beam seas. Moreover, the most suitable directions that have the minimum extreme responses might also shift if short-crested waves are considered. The influence of the short-crested waves on the shielding effects will be studied in the future.

Acknowledgements

The authors gratefully acknowledge the financial support from the Research Council of Norway granted through the Department of Marine Technology, Centre for Ships and Ocean Structures (CeSOS) and Centre for Autonomous Marine Operations and Systems (AMOS), NTNU. Thanks are extended to Wilson Guachamin Acero and Erin Bachynski from CeSOS for valuable discussions.

References

- [1] Thomsen K. Offshore wind: a comprehensive guide to successful offshore wind farm installation. Academic Press; 2011.
- [2] Moller A. Efficient offshore wind turbine foundations. In: POWER EXPO 2008-International Exhibition on Efficient and Sustainable Energy; 2008.
- [3] Aarset K, Sarkar A, Karunakaran D. Lessons learnt from lifting operations and towing of heavy structures in North Sea. In: Offshore Technology Conference, May 2–5, Houston, Texas, USA; 2011.
- [4] Gordon R, Grytoyr G, Dhaigude M. Modelling suction pile lowering through the splash zone. In: Proceedings of the 32nd International Conference on Ocean, Offshore and Arctic Engineering, June 9–14, Nantes, France; 2013.
- [5] Graczyk M, Sandvik P. Study of landing and lift-off operation for wind turbine components on a ship deck. In: Proceedings of the 31st International Conference on Ocean, Offshore and Arctic Engineering, July 1–6, Rio de Janeiro, Brazil; 2012.
- [6] Perry M, Sandvik P. Identification of hydrodynamic coefficients for foundation piles. In: Proceedings of the 15th international Offshore and Polar Engineering Conference, June 19–24, Seoul, Korea; 2005.
- [7] van der Wal R, Cozijn H, Dunlop C. Model tests and computer simulations for Njord FPU gas module installation. In: Marine Operations Specialty Symposium. Singapore: Research Publishing Services; 2008.
- [8] Sandvik P. Estimation of extreme response from operations involving transients. In: Proceedings of the 2nd Marine Operations Specialty Symposium, Singapore; 2012.
- [9] Mukerji P. Hydrodynamic responses of derrick vessels in waves during heavy lift operation. In: 20th Offshore Technology Conference, Houston; 1988.
- [10] van den Boom H, Dekker J, Dallinga R. Computer analysis of heavy lift operations. In: 22nd Offshore Technology Conference, Houston; 1990.
- [11] Baar J, Pijfers J, Santen J. Hydromechanically coupled motions of a crane vessel and a transport barge. In: 24th Offshore Technology Conference, Houston; 1992.
- [12] DNV, Recommended practice DNV-RP-C205, environmental conditions and environmental loads; October 2010.
- [13] MARINTEK. SIMO – theory manual version 4.0; 2012.
- [14] Park K, Cha J, Lee K. Dynamic factor analysis considering elastic boom effects in heavy lifting operations. *Ocean Eng* 2011; 38(10):1100–13.
- [15] DNV. Wadam theory manual. Det Norske Veritas; 2008.
- [16] Faltinsen O. Sea loads on ships and ocean structures. Cambridge University Press; 1990.
- [17] Mavrakos S. Wave loads on a stationary floating bottomless cylindrical body with finite wall thickness. *Appl Ocean Res* 1985;7(4):213–24.
- [18] Mavrakos S. Hydrodynamic coefficients for a thick-walled bottomless cylindrical body floating in water of finite depth. *Ocean Eng* 1988;15(3):213–29.
- [19] Garrett C. Bottomless harbours. *J Fluid Mech* 1970;43(03):433–49.
- [20] Zheng X. Random wave forces on monopile wind turbine foundations: a comparison of wave models. In: Proceedings of the 32nd International Conference on Ocean, Offshore and Arctic Engineering, June 9–14, Nantes, France; 2013.

- [21] Li L, Gao Z, Moan T. Numerical simulations for installation of offshore wind turbine monopiles using floating vessels. In: *Proceedings of the 32nd International Conference on Ocean, Offshore and Arctic Engineering*, June 9–14, Nantes, France; 2013.
- [22] Lee C. WAMIT theory manual. Massachusetts Institute of Technology, Department of Ocean Engineering; 1995.
- [23] DNV. Recommended practice DNV-RP-H103, modelling and analysis of marine operations; April 2011.
- [24] Jacobsen T, Leira B. Numerical and experimental studies of submerged towing of a subsea template. *Ocean Eng* 2012;42: 147–54.

A.2 Paper 2

Paper 2:

Comparative Study of Lifting Operations of Offshore Wind Turbine Monopile and Jacket Substructures Considering Vessel Shielding Effects.

Authors: Lin Li, Zhen Gao, Torgeir Moan

Published in *Proceedings of the Twenty-fifth (2015) International Ocean and Polar Engineering Conference, Kona, Big Island, Hawaii, USA, June 21-26, 2015.*

Comparative Study of Lifting Operations of Offshore Wind Turbine Monopile and Jacket Substructures Considering Vessel Shielding Effects

Lin Li¹, Zhen Gao^{1,2,3}, and Torgeir Moan^{1,2,3}

¹Centre for Ships and Ocean Structures (CeSOS), NTNU, Trondheim, Norway

²Department of Marine Technology, NTNU, Trondheim, Norway

³Centre for Autonomous Marine Operations and Systems (AMOS), NTNU, Trondheim, Norway

ABSTRACT

In this paper, the shielding effects from an installation vessel during lifting operations are investigated. The study compared the lifting operations of two commonly used offshore wind turbine substructures: the monopile and the jacket substructure. The fluid characteristics near the vessel are firstly studied in the frequency-domain. The numerical model of the coupled lifting system is established and eigenvalue analysis is carried out. The shielding effects from the floating installation vessel during the lifting operation are accounted for by interpolating wave kinematics between pre-defined wave points near the vessel in the time-domain simulations. The responses of the monopile and the jacket considering shielding effects are compared with those assuming wave kinematics due to incident waves only. The results indicate that a great reduction in the responses can be achieved when the shielding effects are considered during lowering the monopile, while the effects are very limited when installing the jacket foundation. The effects on the monopile and the jacket are compared and discussed in detail.

KEY WORDS: Lifting operation; shielding effect; monopile; jacket; time-domain simulation.

INTRODUCTION

Among offshore wind turbine (OWT) cost challenges, offshore installation is a critical issue and is getting more and more important when larger machines need to be installed further from the coast. Compared with onshore work, offshore operations are much more risky and expensive, both from the financial and the engineering point of view. Due to the great environmental loads, larger support structures are called for, which will in turn raise challenges for the offshore operations. Besides, the components of OWTs should be installed to very precise tolerances, so the weather window for the installation will be very limited Twidell and Gaudiosi (2009). Therefore, it is of great importance to study new methods and optimize current methods for offshore installation.

Monopiles are the most commonly used WT foundations due to the

structural simplicity, manufacturing and installation expenses (Moller, 2008). However, monopiles are limited by water depth and the data showed a decline in recent years as the technology moves to deeper water (Kaiser and Snyder, 2010). Hence, projects using jackets are increasing, which are more cost-effective in deeper waters. The present work focuses on the lifting operation of OWT monopiles and jackets.

Offshore lifting operation is one of the most important operations for offshore installation and has been investigated for years by many researchers (Mukerji, 1988; Van den Boom et al., 1990; Baar et al., 1992; Witz, 1995; Cha et al., 2010). The previous studies focused on establishing numerical models for the coupled system and to predict the extreme responses in complex environmental conditions. Compare with lifting operations in the oil and gas industry, the structures in wind farms are relatively smaller and lighter. However, instead of one large structure at a single position, several tens or even hundreds of structures have to be installed over an area of often several square kilometers (Junginger and Faaij, 2003). In order to complete the installation of one unit, only a limited time window is available before significant wave heights or wind speeds become too high. Thus, the ability to both install a wind turbine unit at a higher sea state and to move quickly between units and the site are crucial for efficient installation. One of the challenges is to choose a proper vessel to perform the lifting operations.

The installation of substructures can be carried out either by a jack-up vessel or by a floating vessel. A jack-up vessel provides a stable working platform for the operations. However, the operability of a jack-up vessel is limited by the water depth and the positioning process is time consuming and requires a low sea state. On the other hand, floating vessels have more flexibility for offshore operations and will be effective in mass installations of a wind farm due to fast transportations between units. However, jack-up vessels are more commonly used for installation of wind turbine tower and rotor and nacelle assembly, and floating vessels can hardly fulfil the installation criteria due to the motions induced by wind, waves and currents.

For lifting operations conducted by floating vessels, hydrodynamic interaction between the structures in waves is of great importance. Studies have been performed to investigate the heavy lifting operations in the oil and gas industry considering the interactions, such as the

lifting of a heavy load from a transport barge using a large capacity semi-submersible crane vessel (Mukerji, 1988; Van den Boom et al., 1990; Baar et al., 1992). The studies found that the hydrodynamic interaction had little effect on the responses of the crane tip, but affected the responses of the transport barge due to its small dimension compared to the crane vessel, and thus greatly affected the lift-off operations (Baar et al., 1992). The sheltering effects from columns and caissons of a gravity based substructure (GBS) on the barge during a float-over installation were studied by Sun et al. (2012). It has been shown that the motions of the barge and the contact forces between the barge the GBS can be amplified due to the hydrodynamic interaction.

The shielding effects in those studies were considered by calculating the coupled hydrodynamic coefficients in frequency-domain when all the bodies were at their mean position. This implies that the motions of all bodies in the system are assumed to be small. However, it is not always the case when considering a continuous lowering operation that the positions of the lifted objects change continuously with time. Li et al. (2014a) introduced a method to account for the shielding effects from the installation vessel on a monopile during the entire lowering process. The wave forces on the monopile were calculated using Morison's equation by interpolating the disturbed wave kinematics at pre-defined wave points at each time step. It was concluded that the responses can be greatly reduced in short waves considering shielding effects. The study also showed the possibility to place the vessel and lifting system in a good position to minimize the responses using the shielding effects. Thus, it is essential to study the shielding effects of the vessel when performing lifting operations for various structures.

In this paper, the approach used for modelling shielding effects by Li et al. (2014a) will be further studied. Two lifting systems will be included in the study, i.e., the lifting of a monopile and a jacket. The shielding effects on the two systems will be compared by performing time-domain simulations. Conclusions and recommendations will be given based on this study.

DESCRIPTION OF THE LIFTING SYSTEMS

Installation Vessel and Crane

A floating installation vessel was chosen for the installation Li et al. (2014a). The main dimensions of the vessel are presented in Table 1. The vessel was a monohull heavy lift vessel. The positioning system allowed the operations of the vessel in shallow water and in close proximity to other structures. The water depths for the monopile and the jacket installation are 25 m and 40 m, respectively. The crane was capable of performing lifts of up to 5000 tons at an outreach of 32 m. The main hook featured a clear height to the main deck of the vessel of maximum 100 l. Therefore, the lifting capacity and the positioning system of the floating vessel made it capable of performing the installation of monopiles and jackets in shallow-water sites.

Table 1: Main parameters of the floating installation vessel

Vessel		
Length overall	[m]	183
Breadth	[m]	47
Operational draft	[m]	12
Displacement	[tons]	52000

The Monopile and the Jacket

The monopile used in the model is to support a 5 MW offshore wind turbine and it is a long slender hollow cylinder with main dimensions listed in Table 2. A 10 MW wind turbine jacket foundation is applied in the current study. The jacket has a height of 64.75 m and a footprint of 22 m times 22 m. The total mass of the jacket and the transition piece

(TP) is over 1200 tons. The geometry of the 10 MW jacket was interpolated from existing jacket designs, i.e., the 5 and 20 MW UpWind turbines (Vries, 2011). Common wind turbine and substructure scaling laws are applied (Hoving, 2013). The main parameters for the 10 MW jacket are shown in Table 3, and the detailed information of each member can be found in Li et al. (2014b). The significant difference in mass and geometry will lead to different dynamic behaviors of the monopile and the jacket systems.

Table 2: Main parameters of the monopile

Monopile		
Total mass	[tons]	500
Length	[m]	60
Outer diameter	[m]	5.7
Thickness	[m]	0.06

Table 3: Main parameters of the jacket

Jacket		
Total height	[m]	64.75
Foot print	[m]	22x22
TP position*	[m]	(0,0,65.25)
leg outer diameter	[m]	1.9
Brace outer diameter	[m]	1
Jacket mass	[tons]	1017
Transition piece mass	[tons]	250
Total mass	[tons]	1267
* refer to the center point of the jacket bottom		

Lifting Arrangement

The lifting system of the monopile and the jacket are shown in Fig. 1 and 2, respectively. For both systems, only two rigid bodies are included, i.e., the floating vessel and the substructure. The hook is replaced by a lifting device which can be inserted into the monopile and TP so to perform the lifting operations. Hence, only the main lift wire is necessary to connect the crane and the substructure. For the monopile system, a gripper device rigidly connected to the vessel is applied to control the motions of the monopile during the lifting operations, while there is no such device used for the jacket installation.

It was demonstrated that the elasticity of the crane boom mattered for heavy lifting operations of a load with more than 30% of the crane capacity (Park et al., 2011). For the current cases, the effect of the elasticity of the crane boom can be neglected. The crane was rigidly connected to the vessel in the numerical model, and a low constant flexibility was included.

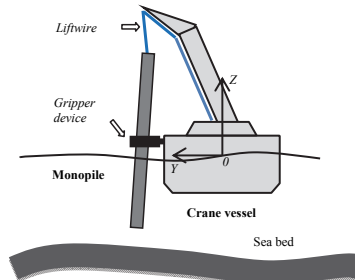


Figure 1: Lifting arrangement of the monopile

The global coordinate system (GCS) was a right-handed coordinate system, with the following orientation used: X axis pointed towards the

bow, Y axis towards the port side, and Z axis upwards. The origin was located at [mid-ship section, center line, still water line] when the vessel was at rest. Fig.3 shows the definition of global coordinate system and wave directions for the jacket system and the same global coordinate was applied for the monopile system.

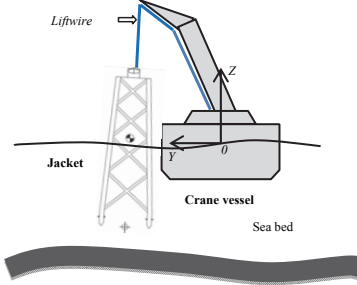


Figure 2: Lifting arrangement of the jacket

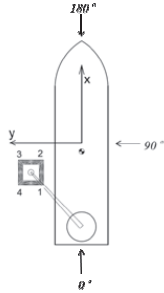


Figure 3: Definitions of the global coordinate and wave direction

Table 4: Coordinates of COG and coupling points for two lifting systems

Point	X [m]	Y [m]	Z [m]	coordinate syst.
COG of vessel	-7.25	0	2.17	VCS
COG of MP	0	0	0	MCS
crane tip (MP)	-20	30	80	MCS
hook point on MP	0	0	34	MCS
gripper position	-20	30	4.5	MCS
COG of jacket	0	0	39.7	JCS
crane tip (Jacket)	-15	45	80	JCS
hook point on jacket	0	0	66	JCS

Beside the global coordinate system, the body fixed coordinate of each of the body is also defined. The body fixed coordinate moves with the body and is used to define the coupling points between bodies. Three body fixed coordinates were defined as follows:

- 1) the vessel-fixed coordinate system (VCS) is overlapped with the global coordinate when the vessel was at rest;
- 2) the monopile-fixed coordinate system (MCS) originated at the middle of the monopile with axis parallel to the global coordinate system in the initial condition.
- 3) the jacket-fixed coordinate system (JCS) originated at the bottom center of the structure with axis parallel to the global coordinate system in the initial condition.

The COG for each body as well as the coupling points are then summarized in Table 4 referring to different coordinate systems.

NUMERICAL MODELS

Coupled Equations of Motion

The two-body coupled lifting system included 12 degrees of freedom (DOF s) of rigid body motions. The 12 equations of motion are given in Eqn. 1.

$$\begin{aligned} & (\mathbf{M} + \mathbf{A}(\infty)) \cdot \ddot{\mathbf{x}} + \mathbf{D}_1 \dot{\mathbf{x}} + \mathbf{D}_2 f(\dot{\mathbf{x}}) + \mathbf{Kx} \\ & + \int_0^t \mathbf{h}(t-\tau) \ddot{\mathbf{x}}(\tau) d\tau = \mathbf{q}(t, \mathbf{x}, \dot{\mathbf{x}}) \end{aligned} \quad (1)$$

where,

\mathbf{M} the total mass matrix of the vessel and the substructures;

\mathbf{x} the rigid-body motion vector with 12 DOF s;

$\mathbf{A}(\infty)$ the frequency-dependent added mass matrix at infinite wave frequency;

\mathbf{D}_1 the linear damping matrix;

\mathbf{D}_2 the quadratic damping matrix;

\mathbf{K} the coupled hydrostatic stiffness matrix;

\mathbf{h} the retardation function of the vessel, which is calculated from the frequency-dependent added mass or potential damping;

\mathbf{q} the external force vector that includes the wind force \mathbf{q}_{WI} , the 1st and 2nd order wave excitation forces $\mathbf{q}_{WA}^{(1)}$ and $\mathbf{q}_{WA}^{(2)}$, the current force \mathbf{q}_{CU} and any other external forces \mathbf{q}_{CU} .

The coupled stiffness matrix \mathbf{K} includes the hydrostatic stiffness of the vessel, the stiffness from the mooring line, and the coupling between the vessel and the substructure via the lift wire and gripper device

Wave Forces on the Structures

The potential added mass and damping coefficients, the hydrostatic stiffness and the first order wave excitation force transfer functions of the vessel were calculated in WADAM based on the panel method (DNV, 2008), and then the retardation functions in Eqn. 1 and the 1st order excitation force were obtained. In the current vessel model, waves were considered as main factor, and wind and current forces were not included. The exciting forces on the floating vessel in the model consisted of only the 1st order wave excitation force vector $\mathbf{q}_{WA}^{(1)}$.

The external forces on the monopile and the jacket include the gravity force, the buoyancy force, as well as the hydrodynamic wave forces. The monopile and the jacket members are seen as slender elements. For each member, the wave forces normal to the member's central axis were calculated by applying Morison's formula. Each member was divided into strips and the forces on the whole slender elements were calculated by strip theory. The wave forces $f_{W,s}$ per unit length on each strip of a moving circular cylinder normal to the member can be determined using Morison's equation (Faltinsen, 1990).

$$\begin{aligned} f_{W,s} = & \rho_w C_M \frac{\pi D^2}{4} \cdot \ddot{\zeta}_s - \rho_w C_A \frac{\pi D^2}{4} \cdot \ddot{x}_s \\ & + \frac{1}{2} \rho_w C_D D \cdot |\dot{\zeta}_s - \dot{x}_s| \cdot (\dot{\zeta}_s - \dot{x}_s) \end{aligned} \quad (2)$$

In this equation, the positive force direction is the wave propagation direction. $\ddot{\zeta}_s$ and $\dot{\zeta}_s$ are fluid particle acceleration and velocity at the center of the strip, respectively; \ddot{x}_s and \dot{x}_s are the acceleration and

velocity at the center of the strip due to the body motions; D is the outer diameter of the member; and C_M , C_A and C_q are the mass, added mass and quadratic drag force coefficients, respectively. The first term in the equation is the wave excitation force, including diffraction and Froude-Krylov force (FK term). The second term is the inertial term and the third term is the quadratic drag term. C_M and C_q are dependent on many parameters, such as the Reynolds number (Re), the Kaulegan-Carpenter number (KC) and the surface roughness ratio (Faltinsen, 1990). The quadratic drag coefficient for the monopile was chosen as $C_q = 0.7$, and $C_q = 1.0$ was used for all the jacket members

Both the monopile and the jacket four legs are flooded and filled with water during installation, while all the other braces of the jacket are hollow. Therefore, different mass coefficients should be applied. The added mass coefficient of the monopile at different submergences was studied by Li et al. (2014a). In the current model, the following coefficients were used: monopile $C_M = C_A = 1.8$; jacket legs $C_M = C_A = 1.9$; jacket braces $C_M = 2.0$ and $C_A = 1.0$.

The forces on each strip was calculated first and integrated to obtain the forces on the whole member. The monopile was a single member, while the jacket included 40 members in the numerical model. The forces on each member were then summed up to get the forces on the whole jacket structure. It should be mentioned that there was no vertical wave force on the monopile since it was bottomless. The slamming forces on the jacket were observed to be little in the operational sea states and were neglected in the time-domain simulations.

Mechanical Couplings

The couplings in the numerical model include the lift wire couplings and the gripper device coupling. The wire coupling force was modelled as a linear spring force according to the following equation (MARINTEK, 2012):

$$T = k \cdot \Delta l \quad (3)$$

where T is the wire tension, Δl is the wire elongation and k is the effective axial stiffness, which is given by:

$$\frac{1}{k} = \frac{l}{EA} + \frac{1}{k_0} \quad (4)$$

where E is the modulus of elasticity, A is the cross-sectional area of the wire, l/k_0 is the crane flexibility and l is the total length of the wire, which increases when the winch runs during the lowering operation. From the positions of the two ends of the wire, the elongation and thereby the tension can be determined. The material damping in the wire was included in the model.

The gripper device is normally a ring-shaped structure with several contact elements in the inner circumference which behave like bumpers during installation. Thus, the gripper force in the numerical model was simplified by a spring-damper system (Li et al., 2014a). Rotation symmetric stiffness and damping around the axis were assumed to calculate the coupling forces. Sensitivity studies to quantify the effects of the gripper stiffness on the responses during the lowering of a monopile were performed by Li et al. (2013). In the current study, a representative gripper device stiffness was used for all the simulations.

Shielding Effects Modelling

Due to the small dimension of the monopile and the jacket members compared to the vessel, the hydrodynamic effects on the vessel from the substructure are minor and can be ignored. However, the shielding effects from the installation vessel may be relevant for the wave forces

on the monopile as well as the jacket in the wave zone. The waves affected by both radiation and diffraction of the vessel are defined as *disturbed waves* in this paper which account for the vessel shielding effects, and the undisturbed waves are defined as *incident waves*.

To calculate the wave forces on the monopile and jacket in the disturbed wave field during lowering, the fluid kinematics $\ddot{\zeta}_s$ and $\dot{\zeta}_s$ in Eqn. 2 should be based on the disturbed fluid kinematics. Because the position of the structure varies with time and with the increasing length of the lift wire, the fluid kinematics at each strip are time- and position-dependent. Therefore, the approach proposed by Li et al. (2014a) was applied to simulate the lowering process of the multi-body system in the time domain while considering the shielding effects. The approach in Li et al. (2014a) was only for one slender element and it was further developed in this paper to be used for jacket structure which is modelled as a collection of slender elements. The approach is briefly discussed below:

1. First, generate time series of disturbed fluid kinematics at pre-defined wave points in space. The boundary of the wave points should cover all possible positions of the wet part of the substructures.
2. Then, at each time step find the closest pre-defined wave points for each strip on the element. Apply a 3D linear interpolation to obtain the kinematics at the centre of each strip in disturbed waves.
3. Calculate the forces at each strip in disturbed waves using Eqn. 2 and then integrate along the submerged part of the slender element to acquire the total wave forces and moments on the element. The forces on each element are integrated up to the instantaneous wave elevation.
4. Finally, perform the time-domain simulations of the coupled vessel-monopile system. The wave forces on the substructures in disturbed waves are calculated in DLL using the interpolation method described above, and the total wave forces on the substructure are returned to SIMO, with which the motions of the coupled system are solved.

EIGENVALUE ANALYSIS

The eigenvalue analysis was conducted in the frequency domain to investigate the eigenperiods of the rigid body motions of the lifting system. The natural modes and natural periods were obtained by solving Eqn. 5 in the frequency domain.

$$[-\omega^2(\mathbf{M} + \mathbf{A}) + \mathbf{K}] \cdot \mathbf{x} = 0 \quad (5)$$

where \mathbf{M} is the mass matrix of the vessel and the monopile. \mathbf{A} is the added mass matrix; the added mass with infinite frequency was used for the vessel. \mathbf{K} is the total restoring stiffness matrix, which is split into three contributions: hydrostatic restoring, mooring restoring and coupling between the vessel and the monopile. The coupling restoring includes all the mechanical couplings. \mathbf{x} is the eigenvector that represents rigid-body motions with 12 DOFs in the two-body coupled system and 6 DOFs if a single body is considered.

Table 5: Eigenperiods and eigenvectors of vessel rigid body motions (water depth = 25 m)

Mode	1	2	3	4	5	6
Surge [m]	-0.15	-0.06	0.00	0.00	1.00	0.00
Sway [m]	0.00	0.00	0.06	0.86	0.00	-0.79
Heave [m]	-0.29	1.00	0.00	0.00	0.00	0.00
Roll [deg]	0.00	0.00	1.00	0.02	0.00	0.03
Pitch [deg]	1.00	0.19	0.00	0.00	0.00	0.00
Yaw [deg]	0.00	0.00	-0.01	1.00	0.00	1.00
Period [sec]	9.44	10.65	13.54	93.89	99.98	105.36

The natural periods and natural modes of the vessel and of the monopile are listed in Table 5 and Table 6, in which the dominated rigid motions are emphasized. The natural periods of the heave, pitch and roll motions of the vessel indicate small motions in short waves and resonance motions when the wave period is close to the natural periods. It is expected that the vessel motions will play an important role in the response of the substructure when the wave periods are approximately $T_p = 9 \text{ sec}$ to 14 sec .

Table 6: Eigenperiods and eigenvectors of monopile rigid body motions lifted by a fixed vessel (draft of MP = 20 m)

Mode		1	2	3	4	5	6
Surge	[m]	-0.01	-0.60	-0.55	0.05	0.05	0.00
Sway	[m]	-0.01	0.54	0.60	0.05	-0.05	0.00
Heave	[m]	1.00	0.00	-0.02	0.00	0.02	0.00
Roll	[deg]	-0.04	-0.91	-1.00	-0.93	1.00	0.00
Pitch	[deg]	-0.05	1.00	-0.91	1.00	0.93	0.00
Yaw	[deg]	0.00	0.00	0.00	0.00	0.00	1.00
Period	[sec]	0.79	2.28	2.28	6.63	6.75	40.04

In the case of the monopile by itself, the vessel was assumed to be a fixed structure and the lift wire and the gripper provided the restoring force for the monopile; the natural periods of the monopile in Table 6 correspond to MP submergence of 20 m and the eigenvectors refer to the monopile body-fixed coordinate with the origin at the center of the monopile. The 1st mode is dominated by the heave motion, and the stiffness in heave is from the lift wire axial stiffness. Modes 2 to 3 are dominated by a combination of the rotational motion in vertical plane and the translational motion in the horizontal plane. Modes 4 and 5 are dominated by pitch and roll motions and the last mode is pure yaw motion. The eigenvectors in Table 6 show that modes 2 and 3 are symmetric and correspond to the same eigenperiods, but occur in different planes. It is the same for mode 4 and 5. The eigenperiods for modes 4 and 5 are much longer than modes 2 and 3 due to different contributions of the restoring from the gripper device and the lift wire.

In the coupled system of the monopile and the floating vessel, in general the natural periods of the rotational modes of the monopile slightly decreased, and the natural period of the vessel roll motion was also reduced. As the changes are small, the coupled eigenperiods are not shown here.

Compared to the eigenperiods of the monopile with those of the free floating vessel, it can be seen the relevant eigenperiods of the monopile (mode 4 and 5) are shorter than those from the vessel. Hence, it can be expected in short waves the wave excitation forces on the monopile will dominate the responses of the lifting system, while in long waves the motions of the vessel will play a more important role.

Table 7: Eigenperiods and eigenvectors of jacket rigid body motions lifted by a fixed vessel (draft of jacket = 30 m)

Mode		1	2	3	4	5	6
Surge	[m]	-0.15	-0.06	0.00	0.00	1.00	0.00
Sway	[m]	0.00	0.00	0.06	0.86	0.00	-0.79
Heave	[m]	-0.29	1.00	0.00	0.00	0.00	0.00
Roll	[deg]	0.00	0.00	1.00	0.02	0.00	0.03
Pitch	[deg]	1.00	0.19	0.00	0.00	0.00	0.00
Yaw	[deg]	0.00	0.00	-0.01	1.00	0.00	1.00
Period	[sec]	9.44	10.65	13.54	93.89	99.98	105.36

Table 7 shows the eigenvalues of the jacket when the vessel is assumed to be fixed. Only the lift wire provides restoring force for the jacket. Similar to the monopile case, the 1st eigenmode is dominated by heave motion with very low natural period due to the high axial stiffness of

the lift wire. Eigenmode 2 and 3 are symmetric modes and dominated by pitch and roll motions with contributions from surge and sway. Modes 4 and 5 are also symmetric and corresponding to the pendulum modes, so they are dominated by combined translations and rotations. Mode 6 is the uncoupled mode of the jacket's yaw motion with very long eigenperiod.

Table 8: Eigenmodes of the coupled jacket-vessel system (draft of the jacket = 30 m)

Body	Mode	2	3	4	5	6
Vessel	Surge [m]	0.00	0.00	-0.03	-0.05	0.00
Vessel	Sway [m]	0.00	0.00	0.00	-0.02	0.03
Vessel	Heave [m]	0.00	0.01	-0.06	0.95	0.00
Vessel	Roll [deg]	-0.06	0.00	0.00	-0.03	0.47
Vessel	Pitch [deg]	0.00	-0.02	0.17	0.23	0.00
Vessel	Yaw [deg]	0.00	0.00	0.00	0.00	0.00
Jacket	Surge [m]	-0.01	-0.37	-0.40	-0.29	0.02
Jacket	Sway [m]	0.37	-0.01	-0.01	0.00	0.56
Jacket	Heave [m]	-0.05	0.00	-0.01	1.00	0.38
Jacket	Roll [deg]	1.00	-0.01	-0.03	-0.09	1.00
Jacket	Pitch [deg]	0.02	1.00	1.00	0.78	-0.01
Jacket	Yaw [deg]	-0.02	-0.02	-0.02	-0.01	-0.02
Natural period [sec]		7.94	8.10	9.15	9.93	14.54
Body	Mode	7	8	9	10	11
Vessel	Surge [m]	-0.02	0.00	-0.14	0.89	0.13
Vessel	Sway [m]	0.00	-0.02	-0.87	-0.12	0.64
Vessel	Heave [m]	0.00	0.00	-0.01	0.00	0.00
Vessel	Roll [deg]	0.00	-0.05	0.01	0.00	-0.02
Vessel	Pitch [deg]	0.00	0.00	0.00	0.00	0.00
Vessel	Yaw [deg]	0.02	0.00	-1.00	0.02	-0.84
Jacket	Surge [m]	1.00	-0.05	0.76	1.00	0.90
Jacket	Sway [m]	0.05	1.00	-0.74	-0.15	1.00
Jacket	Heave [m]	0.00	-0.04	0.01	0.00	-0.01
Jacket	Roll [deg]	0.03	0.64	-0.07	-0.01	0.07
Jacket	Pitch [deg]	-0.70	0.03	-0.07	-0.08	-0.07
Jacket	Yaw [deg]	0.00	-0.01	-0.03	-0.05	-0.06
Natural period [sec]		31.26	33.33	94.15	100.84	106.31

From the eigenperiods in the table, it can be seen that at this draft Mode 2 and 3 are of high importance for wave conditions with peak periods from 8sec to 10sec, which are also close to the natural periods of the vessel. The coupled eigenmodes of jacket and the floating vessel are shown in Table 8, where mode 1 (dominated by jacket heave) and mode 12 (dominated by vessel yaw) are exclusive. It can be seen that the eigenperiods of modes 2 to 6 are in the range of 8 to 15 sec, which are critical for the wave conditions concerned. The other modes are less critical during lifting.

Compared to Table 5 and the eigenvalues of the jacket connected to a fixed crane in Table 7, the eigenvalues of the jacket modes 2 to 3 and the vessel eigenmodes in vertical plane are fully coupled. Hence, the eigenvalues are shifted compared to the individual cases. Moreover, the symmetries of the eigenmodes for the jacket disappear in the coupled system due to the influence by the crane tip position. On the other hand, the eigenvalues of jacket pendulum modes change little after coupling with the floating vessel. The coupled eigenmodes provide a good understanding of when and how the system will be excited in different wave conditions.

Compare to the monopile case, the eigenperiods of the jacket and vessel are more coupled, which indicate that the motions of the jacket will be more influenced by the vessel motions. Moreover, unlike the monopile system, the jacket motions will not be excited in short waves due to the all the coupled natural periods are relatively high. The low natural periods in the monopile system are due to the gripper device, which

provides large restoring stiffness for the monopile in horizontal plane compared to the lift wire.

WAVE KINEMATICS IN DISTURBED WAVES

Before carrying time domain simulations, the kinematics near the position of the structures in disturbed waves are studied in frequency domain and compared with those in incident waves. Fig. 4 shows the variations of the wave elevation RAOs (Response Amplitude Operator) in disturbed waves. The results correspond to points at the mean free surface with varying X Y positions. The initial position of the four jacket legs (black circles) as well as the MP (red circles) are also shown in the figure. The RAOs for incident wave elevation are always 1 at any position.

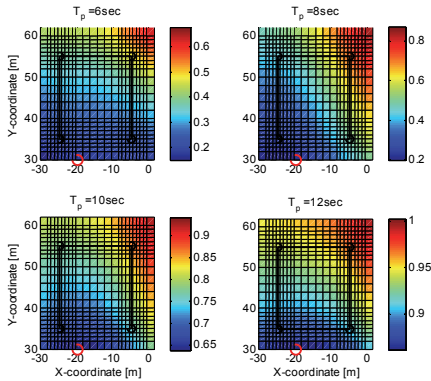


Figure 4: RAOs of wave elevation in disturbed waves in XY plane ($Dir = 150\text{ deg}$, $Z = 0\text{ m}$)

It can be observed that the RAOs depend greatly on the wave frequency and the positions relative to the vessel. In long waves, the RAOs are close to those in incident waves, which indicate the diffraction and radiation of the vessel are minor. However, as the wave period decreases the RAOs in disturbed waves decrease significantly. Due to the large footprint of the jacket foundations, the wave kinematics are always smaller at the side close to the vessel (with small Y coordinate) compared to the side away from the vessel, especially in short waves. The RAOs at the MP positions are much less than all the four jacket legs.

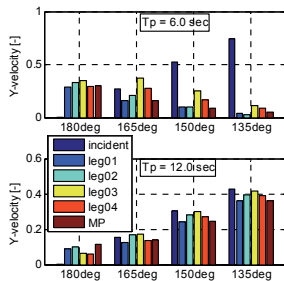


Figure 5: Comparisons of RAOs of fluid Y -velocities in different wave directions and frequencies ($Z = 0\text{ m}$)

The RAOs also depend on wave direction. Fig. 5 compared the RAOs of Y component of the fluid particle velocity at four jacket legs and MP position in disturbed and incident waves, respectively. The results correspond to the positions at the mean free surface, and the index of the legs refers to Fig. 3. The RAOs at different positions vary little with wave directions with $T_p = 12\text{ sec}$, while in short waves, the RAOs changed rapidly with both direction and position. The Y -velocities at leg 3 are higher than the other three legs in most conditions and the kinematics at MP are close to those at leg 1 and smaller than other three legs except in heading seas.

In heading sea condition, the Y -velocities in incident waves are always zero, while it is not the case in disturbed waves due to the 3D shielding effects from the vessel. The velocities in disturbed waves are reduced greatly compared to those in incident waves with wave direction moves to quartering seas.

From the wave kinematics discussed above, it can be expected the shielding effects will be more significant in short waves than in long waves, in quartering seas than in heading seas and the effects on the monopile are expected to be larger compared to the jackets.

TIME DOMAIN SIMULATIONS

Time-domain Simulation Method

Step-by-step integration methods were applied to calculate the responses of the lifting system using an iterative routine. The equations of motion were solved by Newmark-beta numerical integration ($\beta = 0.1667$, $\alpha = 0.50$) with a time step of 0.02 sec . The 1st order wave forces of the vessel were pre-generated using Fast Fourier Transformation (FFT) at the mean position. The hydrodynamic forces on the substructure were calculated in the time domain using the interpolation of the pre-generated fluid kinematics at pre-defined wave points in disturbed waves. The resolution of the pre-generated wave points has been studied by Li et al. (2014a). In this study, a resolution of 4 m in XY plane and 2 m in Z direction was used.

The environmental conditions of the time-domain simulations were $H_s = 2.0\text{ m}$ with T_p varied from 6 sec to 12 sec , thus covering a realistic range. For each combination of H_s and T_p , the irregular waves were modelled by JONSWAP spectrum (DNV, 2010). For the each wave condition, the same incident waves were applied for the monopile and jacket systems. Linear wave theory and long-crested wave approximation were applied for all conditions. In order to account for the variability of stochastic waves, 10 realizations of irregular waves were generated at each of the environmental conditions using different seeds, and each realization lasted 20 minutes. Thus, 10 seeds corresponded to an operation with duration of approximately three hours.

In order to compare the behavior of the two lifting system easily, the winch was fixed in the time-domain simulations and steady-state responses were analyzed. The draft of the monopile and the jacket was chosen as 20 m and 30 m , respectively.

Response Time Series and Spectra

Response of the monopile lifting system

Fig. 6 and Fig. 7 show the time history of the responses of the MP lifting system at two wave conditions with wave direction $Dir = 150\text{ deg}$. The responses in the figures include the motions of the MP end tip, the contact forces on the gripper and the tensions in the lift wire. Comparing the responses in incident and disturbed waves shows that in short waves with $T_p = 6\text{ sec}$, the responses are significantly reduced

when shielding effects are considered, whereas in long waves with $T_p = 12 \text{ sec}$ the influence of shielding effects is much less.

These results again indicate that the shielding effects of the vessel have more influence on the fluid kinematics in short waves, which is consistent with the RAOs of the fluid kinematics shown in Fig. 4.

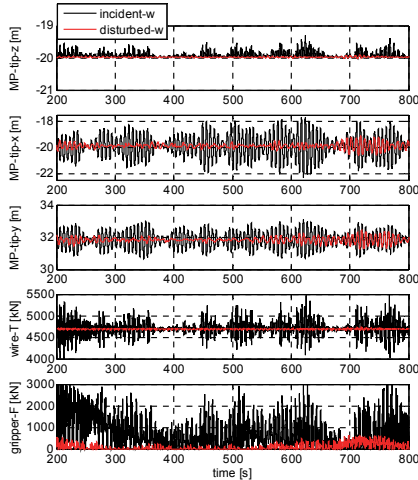


Figure 6: Time series of MP responses in incident and disturbed waves ($H_s = 2.0 \text{ m}$, $T_p = 6 \text{ sec}$, $Dir = 150 \text{ deg}$)

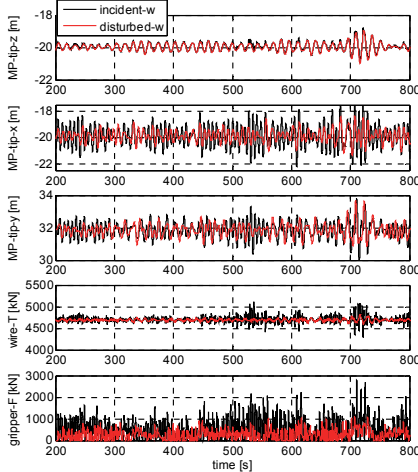


Figure 7: Time series of MP responses in incident and disturbed waves ($H_s = 2.0 \text{ m}$, $T_p = 12 \text{ sec}$, $Dir = 150 \text{ deg}$)

The response spectra were obtained using Fourier transformation of the time series. Fig. 8 shows the response spectra at $T_p = 6 \text{ sec}$ and 12 sec with direction $Dir = 150 \text{ deg}$. In short waves, the resonant motions of the monopile are excited in incident waves, which correspond to the

peak frequency of the spectrum, $\omega \approx 0.94 \text{ rad/s}$. The hydrodynamic wave loads on the monopile dominate the response of the system in this case.

In long waves, however, there are two peaks in the motion spectrum. The frequencies of the secondary peak with $\omega \approx 0.94 \text{ rad/s}$ match the natural frequencies of the monopile rotational eigen frequency, while the frequencies of the main peak with $\omega \approx 0.45 \text{ rad/s}$ are the vessel roll natural frequency. Due to the couplings of the monopile and the vessel, the increasing response of the vessel in long waves dominates the motions of the monopile. The peak frequency of the wire tension is consistently twice of the rotational peak frequency, which means that one cycle of rotational motion induces two cycles of variations in the wire tension.

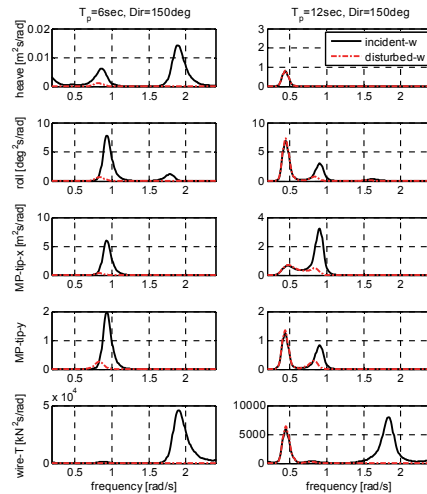


Figure 8: Spectrum density of MP responses in incident and disturbed waves ($H_s = 2.0 \text{ m}$)

For both wave conditions, the peaks at $\omega \approx 0.94 \text{ rad/s}$ in the response spectra, which is the natural frequency of the rotational motions of the monopile, are significantly reduced when the shielding effects of the vessel are considered. However, in long waves with $T_p = 12 \text{ sec}$ the response peaks corresponding to the vessel natural frequency do not decrease in disturbed waves. These results indicate the significant influence of the shielding effects on the monopile motions, particularly in short waves when the wave frequencies are close to the natural frequencies of the monopile.

Response of the jacket lifting system

Similarly, Fig. 9 shows the spectra of the responses of the jacket lifting system at a direction of 150 deg in short and long wave conditions, respectively.

In long waves with $T_p = 12 \text{ sec}$, the responses in disturbed waves are almost identical with those in incident waves. One reason is that the wave kinematics at all four legs are close to incident wave kinematics in these wave conditions as can be observed in Fig. 4 and 5. The most important reason, on the other hand, is that in the long wave condition, the vessel motions dominate the response of the whole system, which will not be affected by the shielding effects.

Comparison between the two lifting systems

The standard deviations (STD) of the responses in different wave periods and directions are obtained in disturbed and incident waves for directions from 180 deg to 135 deg, see Fig. 10 and Fig. 11 for monopile and jacket lifting systems, respectively.

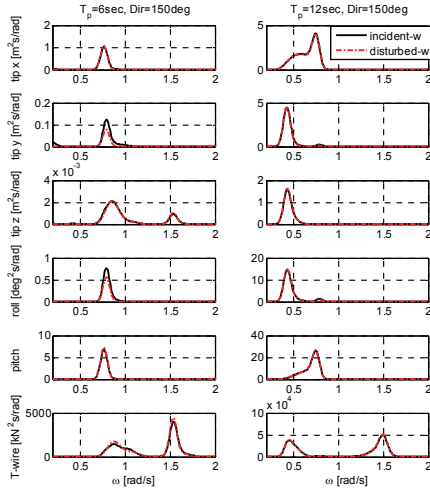


Figure 9: Spectrum density of jacket responses in incident and disturbed waves ($H_s = 2.0m$)

For the monopile lifting system, the significant decrease of the tip motion in x direction can be observed in all wave conditions when considering shielding effects, and the effects are reduced with increasing wave length. The motions in y and z directions are greatly affected by vessel roll motion which increases significantly when the wave direction moves to quartering seas in incident waves. At heading sea conditions, 3D effects from the vessel can be observed where the MP tip y motion increase dramatically when including shielding effects.

The STD for the motions reach their minimum near $Dir = 150$ to 135 deg in short waves, whereas in long waves the minimum values occur at close to head seas. Both the resonance motions of the monopile and the vessel motions affect the responses of the lifting system, and the factor that dominates the responses depends on both the wave direction and the wave length. Therefore, in order to utilize the shielding effects to increase the weather window as much as possible, the most suitable wave directions at different wave lengths should be applied for the MP lifting system.

For the jacket system, however, the STD of the jacket motions are much less influenced by the shielding effects from the vessel compared to the MP system. Although great decrease of jacket tip y motion can be observed near quartering sea in short and medium waves when considering shielding effects, the responses in x and z directions vary little. This is due to that in short waves the excitation forces on the members are very small, and the x and z motions of the jacket can be dominated by the vessel motions. The y motion is dominated by the resonance motion of the jacket in short waves. In longer waves, as the vessel motion increases rapidly, the responses from the incident waves and the disturbed waves are almost the same. Since the motions of the jacket in short waves are so small and are not critical for the operations,

the shielding effects can be ignored when estimating the critical responses of the jacket lifting system. The proper wave directions can be chosen as close to heading seas in both short and long waves.

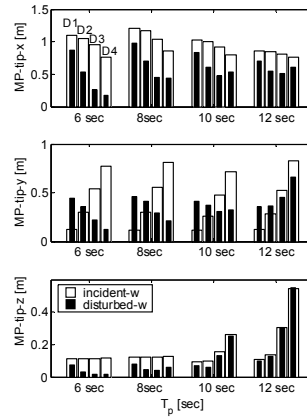


Figure 10: Standard deviation of MP motions in incident and disturbed waves ($H_s = 2.0m$, for each T_p the directions from left to right are $D_1 = 180$ deg, $D_2 = 165$ deg, $D_3 = 150$ deg, $D_4 = 135$ deg)

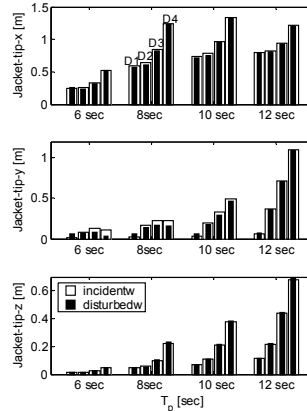


Figure 11: Standard deviation of jacket motions in incident and disturbed waves ($H_s = 2.0m$, for each T_p the directions from left to right are $D_1 = 180$ deg, $D_2 = 165$ deg, $D_3 = 150$ deg, $D_4 = 135$ deg)

In general, the jacket resonance motions are very small and the motions of the vessel can dominate the response of the jacket even in short waves. This is very different from those for the MP lifting system, where in short waves the MP resonance motion dominates. The reasons for the differences can be summarized as follows:

1. The response amplitudes at resonance are higher for the MP than the jacket due to the larger excitation force acting on the structure with larger dimension.
2. The footprint of the jacket is very large which results in the larger

distance of the legs and braces relative to the vessel hull compared to the MP. Hence, the fluid kinematics in disturbed waves on the MP are much lower than the average values on the jacket members.

3. Due to different lifting configurations and properties, the eigenvalues of the two systems are very different. For the MP system, the critical eigenperiods for the monopile are in the short wave ranges which are distinct from the vessel eigenperiods. This ensures the resonance motions of the MP in short waves can be greatly reduced by the shielding effects. The low eigenperiods are due to the application of the gripper device for the operation. While for the jacket, all the eigenperiods are coupled with the vessel and in relatively long wave range. This makes the shielding effects less important.

CONCLUSIONS

The current study investigates the shielding effects from the installation vessel on two lowering operations: the lowering of the monopile and the jacket structure.

The fluid kinematics in disturbed waves show a great dependence on the wave direction and wave periods. The RAOs of the kinematics can be reduced greatly in short waves in quartering seas. Due to different lifting configuration, the RAOs of the wave kinematics at the monopile positions are in general much smaller than the average RAOs at the four legs of the jacket.

The effects of vessel shielding on the responses of the lifting system were calculated by using an external DLL and implementing it in SIMO. The wave forces on the monopile and the jacket were calculated by interpolating fluid kinematics between pre-defined wave points near the floating vessel in the time-domain. In this paper, the steady-state responses for a given submergence were studied. The analysis on the entire lowering process of the monopile can refer to Li et al. (2014a).

The results show significant reduction of the responses of the MP lifting system in short waves and close to quartering seas when considering shielding effects, while the reduction decreases in long waves. The responses reached minimum values close to quartering seas in short waves due to the reduction of the wave excitation force by the shielding effects. In long waves the minimum were acquired at directions close to heading seas. This is because the vessel roll motion can induce large motions for the lifting system when the wave direction moves to quartering seas. However, for the jacket lifting system, the vessel motion can dominate the responses of the jacket even in short waves and the shielding effects are only observed in short waves where the responses of the system are very small. The different behavior of the two systems when considering the shielding effects are due to the differences in 1) the response amplitude at resonance; 2) the fluid kinematics at the structure positions; and 3) the eigenperiods of the system.

It is recommended to include the shielding effects from the vessel when planning the operation for the monopile and to choose the most suitable heading angles in different wave conditions. The weather window for the lowering of monopile is expected to increase by considering the shielding effect. However, the shielding effects can be ignored when evaluating critical responses of the jacket during the operation, and near heading sea conditions are suitable for the jacket lowering operation in both short and long waves.

ACKNOWLEDGEMENTS

The authors gratefully acknowledge the financial support from the

Research Council of Norway granted through the Department of Marine Technology, Centre for Ships and Ocean Structures (CeSOS) and Centre for Autonomous Marine Operations and Systems (AMOS), NTNU.

REFERENCES

- Baar, J., Pijfers, J., Santen, J., 1992. "Hydromechanically coupled motions of a crane vessel and a transport barge," *In: 24th Offshore Technology Conference*, Houston.
- Cha, J.-H., Roh, M.-I., Lee, K.-Y., 2010. "Dynamic response simulation of a heavy cargo suspended by a floating crane based on multibody system dynamics," *Ocean engineering* 37 (14), 1273–1291.
- DNV, 2008. *Wadam theory manual*, Det Norske Veritas.
- DNV, 2010. *Recommended Practice DNV-RP-C205, Environmental conditions and environmental loads*, Det Norske Veritas.
- Faltinsen, O., 1990. *Sea Loads on Ships and Ocean Structures*, Cambridge University Press.
- Hoving, J., 2013. *Bottom Founded Structures - Lecture Slides*, TU Delft.
- Junginger, M., Faaij, A., 2003. "Cost reduction prospects for the offshore wind energy sector," *In: 2003 European Wind Energy Conference and Exhibition*, pp. 16–19.
- Kaiser, M. J., Snyder, B., 2010. *Offshore wind energy installation and decommissioning cost estimation in the US outer continental shelf*, Tech. rep., U.S. Dept. of the Interior, Bureau of Ocean Energy Management, Regulation and Enforcement.
- Li, L., Gao, Z., Moan, T., 2013. "Numerical simulations for installation of offshore wind turbine monopiles using floating vessels," *In: Proceedings of the 32nd International Conference on Ocean, Offshore and Arctic Engineering*, June 9–14, Nantes, France.
- Li, L., Gao, Z., Moan, T., Ormberg, H., 2014a. "Analysis of lifting operation of a monopile for an offshore wind turbine considering vessel shielding effects," *Marine Structures* 39, 287–314.
- Li, L., Stettner, O., Gao, Z., Moan, T., 2014b. *Technical report - analysis of lifting operation of a 10 MW jacket foundation for offshore wind turbine*, Tech. rep., Statoil, Norway.
- MARINTEK, 2012. *SIMO - Theory Manual Version 4.0*.
- Moller, A., 2008. "Efficient offshore wind turbine foundations," *In: POWER EXPO 2008 - International Exhibition on Efficient and Sustainable Energy*.
- Mukerji, P., 1988. "Hydrodynamic responses of derrick vessels in waves during heavy lift operation," *In: 20th Offshore Technology Conference*, Houston.
- Park, K., Cha, J., Lee, K., 2011. "Dynamic factor analysis considering elastic boom effects in heavy lifting operations," *Ocean Engineering* 38 (10), 1100–1113.
- Sun, L., Eatock Taylor, R., Choo, Y. S., 2012. "Multi-body dynamic analysis of float-over installations," *Ocean Engineering* 51, 1–15.
- Twidell, J., Gaudiosi, G., 2009. *Offshore wind power*, Multi-Science Publishing Company.
- Van den Boom, H., Dekker, J., Dallinga, R., 1990. "Computer analysis of heavy lift operations," *In: 22nd Offshore Technology Conference*, Houston.
- Vries, W. d., 2011. *Final report WP 4.2 - support structure concepts for deep water sites (deliverable D4.2.8)*, Tech. rep., Project Upwind.
- Witz, J. A., 1995. "Parametric excitation of crane loads in moderate sea states," *Ocean engineering* 22 (4), 411–420.

A.3 Paper 3

Paper 3:

*Analysis of Lifting Operation of a Monopile Considering Vessel Shielding
Effects in Short-crested Waves.*

Authors: Lin Li, Zhen Gao, Torgeir Moan

Accepted for publication in *Proceedings of the Twenty-sixth (2016)
International Ocean and Polar Engineering Conference, Rhodes, Greece,
June 26-July 2, 2016.*

Analysis of Lifting Operation of a Monopile Considering Vessel Shielding Effects in Short-crested Waves

Lin Li¹, Zhen Gao^{1,2,3}, and Torgeir Moan^{1,2,3}

¹Centre for Ships and Ocean Structures (CeSOS), NTNU, Trondheim, Norway

²Centre for Autonomous Marine Operations and Systems (AMOS), NTNU, Trondheim, Norway

³Department of Marine Technology, NTNU, Trondheim, Norway

ABSTRACT

This paper addresses numerical simulations of the lifting operation of an offshore wind turbine monopile foundation considering both shielding effects from the vessel and the spreading of the waves. A numerical model of the coupled monopile-vessel system is established. The disturbed wave field near the vessel is investigated and observed to be affected by the diffraction and radiation of the vessel. The shielding effects of the vessel during the lifting operation are accounted for in this study by interpolating fluid kinematics between pre-defined wave points near the vessel using SIMO software and an external Dynamic Link Library (DLL). The effects of short-crested waves on the wave field and on responses of the system are investigated by implementing the directional spreading function in the wave spectrum. Based on the time-domain simulations, the critical responses of the lifting system in various conditions are studied. The results indicate that the effects of the wave spreading are considerable in both incident and disturbed waves. The shielding effects are less significant in short-crested waves than in long-crested waves.

KEY WORDS: Lifting operation; short-crested waves; shielding effect; monopile; time-domain simulation.

INTRODUCTION

Monopile (MP) substructures are the most commonly used foundations for offshore wind farms in water depths up to 40 meters. It has been estimated that more than 75% of all installations are founded on monopiles by the end of 2013 (EWEA, 2014). Monopiles can be transported to site by the installation vessel or a feeder vessel, they can be barged to the site or can be capped and wet towed (Kaiser and Snyder, 2013). An offshore crane is often employed to upend the monopile to a vertical position and lower it down through the wave zone to the seabed. During the lifting operation, the monopile and the installation vessel are coupled through the lift wire and a gripper device which limits the horizontal motions of the monopile during the lowering. The monopile is lowered at a position which is very close to the hull of the crane vessel, so the wave forces on the monopile are affected by the presence of the vessel. Furthermore, since the lifting

operation is commonly performed at a relative low sea states, the waves may spread in different directions and affect the motions of the vessel as well as the wave forces on the monopile. Therefore, it is of great interest to evaluate the effects of the wave spreading as well as the shielding effects from the vessel on the behavior of the lifting system.

Studies have been performed to investigate the heavy lifting operations in the oil and gas industry considering shielding effects, such as the lifting of a heavy load from a transport barge using a large capacity semi-submersible crane vessel (Mukerji, 1988; van den Boom et al., 1990; Baar et al., 1992). The studies found that the hydrodynamic interaction had little effect on the responses of the crane tip, but affected the responses of the transport barge and thus greatly affected the lifting operations because of the small dimension of the barge compared with that of the crane vessel (Baar et al., 1992). The sheltering effects from columns and caissons of a gravity-based substructure (GBS) on the barge during a float-over installation were studied (Sun et al., 2012). It has been shown the motions of the barge and the contact forces between the barge the GBS can be amplified due to the hydrodynamic interactions. Therefore, the hydrodynamic interaction between two floaters close to each other should be taken into consideration when estimating responses.

The approach to consider the shielding effects in those studies were to calculate the coupled hydrodynamic coefficients in frequency-domain when all the bodies are at their mean positions. This implies that the motions of all bodies in the system must be very small. However, when considering a continuous lowering operation that the positions of the lifted objects change continuously with time, the above method is not applicable. The main difficulty associated with this process lies in the large motion that the load might experience in waves during being lowered. Bai et al. (2014) introduced a 3D fully non-linear potential flow model to simulate the wave interaction with fully submerged structures either fixed or subjected to constrained motions in time-domain. The scenario of a cylindrical payload hanging from a rigid cable and subjected to wave actions was studied. However, the approach is limited to regular waves up to now and the simulation efficiency is low. The further application on more complicated operations and in irregular waves with longer duration is questionable.

In the case of lifting a monopile using a floating vessel, due to the small dimension of the monopile compared with the vessel, the hydrodynamic effects of the monopile on the vessel are minor and can be ignored. Li et al. (2014) introduced a method to account for the shielding effects from the installation vessel on a monopile during the entire lowering process. The wave forces on the monopile were calculated using Morison's equation by interpolating the disturbed wave kinematics at pre-defined wave points at each time step. It was concluded that the responses of the monopile can be significantly reduced in short waves when considering shielding effects. The study also showed it is possible to minimize the responses by choose a proper vessel heading using the shielding effects. However, only long-crested waves were considered when evaluating the shielding effects.

In the real sea condition, short-crested waves are found providing better accuracy for the wind generated seas and appear to be three-dimensional and complex (Chakrabarti, 1987; Goda, 2010; Kumar et al., 1999). The directional spreading of wave energy may give rise to forces and motions, which are different from those corresponding to long-crested waves. A large number of studies have been performed in recent years focusing on the directional wave effects on the forces and responses of various offshore structures e.g., large surface piercing circular cylinders (Isaacson and Nwogu, 1987; Nwogu, 1989; Zhu and Satravaha, 1995; Tao et al., 2007), long pipelines (Battjes, 1982; Lambrakos, 1982), TLP platforms (Teigen, 1983), box-shaped structures (Isaacson and Sinha, 1986; Nwogu, 1989), and multiple floating bodies (Inoue and Islam, 2000; Sannasiraj et al., 2001). These studies showed significant effects on the loads and responses due to the spreading of the waves. The general observations were that the directional spreading of wave leads to a reduction of the loads in the main wave direction while the loads in the direction normal to the main wave direction can be greatly amplified due to the lateral disturbance in short-crested waves. The reduction of the loads due to the wave spreading sometimes can bring saving in fabrication costs. However, the spreading may also lead to a significant increase of the estimated fatigue life of an offshore structure (Marshall, 1976). For lifting operations with multi-body coupled systems, very little work has been published with short-crested irregular waves. However, the industry has been aware of the importance of the short-crested waves for lifting operations using a floating crane by establishing relevant guidance.

DNV (2014) recommended to assess whether long crested or short crested sea is conservative for the analysis concerned. It is suggested to investigate the effect of short-crested sea when the vertical crane tip motion is dominated by the roll motion in head sea ± 15 deg. For simplicity, long-crested waves with a heading angle of ± 20 deg can be applied to account for the additional effect from short-crested sea. Nevertheless, the guidance is very general and can hardly be applied for different situations. Moreover, there is no guidance or published work regarding how to evaluate the effects of the short-crested waves when accounting the shielding effects from the installation vessel.

The focus of the paper is to study the influences of the directional waves and the shielding effects of the vessel on the responses of the monopile lifting system. Time-domain simulations are performed using multi-body code SIMO (MARINTEK, 2012) and an external Dynamic Link Library (DLL) that included the shielding effects from the installation vessel (Li et al., 2014). The results in short-crested waves are compared with those in long-crested wave fields with the same total energy. The simulation model and the methodology are presented first, followed by discussions of the results. Finally, conclusions and recommendations are given for lifting operations regarding shielding effects and the influences from short-crested waves.

DESCRIPTION OF THE LIFTING SYSTEMS

A floating installation vessel was chosen for the monopile installation. The main dimensions of the vessel are presented in Table 1. The lifting capacity and the positioning system of the floating vessel made it capable of performing the installation of monopiles in shallow-water sites. The monopile used in the model was a long slender hollow cylinder with main dimensions listed in Table 1. Fig. 1 shows a schematic layout of the arrangement of the operation. The system included two rigid bodies, i.e., the floating installation vessel and the monopile. The two bodies are coupled through the lift wire and the gripper device. The set-up of the lifting system refers to Li et al. (2014).

Table 1: Main parameters of the floating installation vessel and the monopile (Li et al., 2014)

Vessel			Monopile		
Length overall	[m]	183	Total mass	[ton]	500
Breadth	[m]	47	Length	[m]	60
Draught	[m]	12	Outer diameter	[m]	5.7
Displacement	[ton]	52000	Thickness	[m]	0.06
Lifting capacity	[ton]	5000	Draft	[m]	20

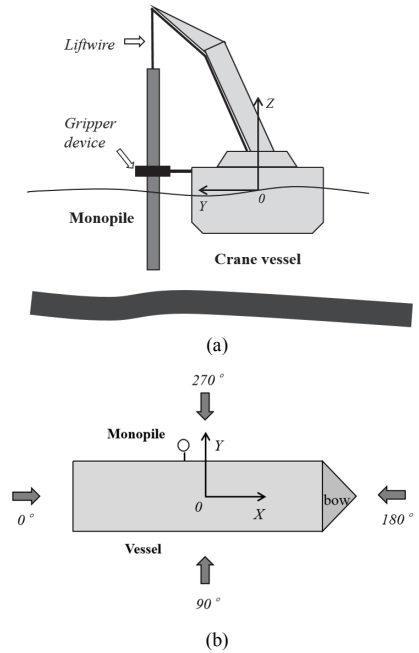


Figure 1: Monopile lifting arrangement (a) and definitions of global coordinate system (b)

The global coordinate system was a right-handed coordinate system with the following orientation: the X axis pointed towards the bow, the Y axis pointed towards the port side, and the Z axis pointed upwards. The origin was located at [mid-ship section, center line, still-water line] when the vessel was at rest. The crane tip position was chosen as [-20 m, 30 m, 80 m] in the global coordinate when the vessel was at rest. The water depth at the installation site was 25 meters, and the draft of the monopile in the time-domain simulations was constant 20 meters.

Table 2: Eigenperiods and eigenvectors of rigid body motions of coupled vessel-monopile lifting system (draft of MP = 20 m)

body	Mode		1	2	3	4	5	6	7	8	9	10	11
Vessel	Surge	[m]	0	0	-0.01	0	0.01	-0.03	-0.05	0	0	0.89	0
Vessel	Sway	[m]	0	-0.01	0	-0.01	0	0	-0.06	0.03	0.91	0	0.55
Vessel	Heave	[m]	0	0	0	0	0	-0.09	0.99	0	0.02	0	0.01
Vessel	Roll	[deg]	-0.03	0.01	0	-0.02	0	0	-0.12	0.57	0	0	-0.05
Vessel	Pitch	[deg]	0	0	0	0	-0.01	0.3	0.2	0	0	0	0.01
Vessel	Yaw	[deg]	0	0	0.01	0	-0.01	0	0	-0.01	1	0.02	-0.76
MP	Surge	[m]	0	0.02	0.45	-0.01	-0.05	-0.02	-0.06	0.01	-0.63	1	0.46
MP	Sway	[m]	0	0.56	-0.02	-0.03	0	0	-0.02	-0.12	0.59	-0.01	1
MP	Heave	[m]	1	0	0	-0.01	0	0.02	1	0.32	0.01	0	-0.02
MP	Roll	[deg]	0	-1	0.05	1	-0.02	-0.01	-0.29	1	0.05	0	0.1
MP	Pitch	[deg]	0	0.07	1	0.01	1	1	0.63	-0.01	0.08	-0.01	-0.04
Natura l period		[sec]	0.59	3.21	3.86	6.61	7.45	9.49	10.66	13.95	94.83	101.18	107.78

Two types of mechanical couplings between the vessel and the monopile were included in the numerical model: the wire coupling through the main lift wire and the coupling via the gripper device. The function of the gripper device was to control the horizontal motions of the monopile during lowering and landing as well as to support the monopile during driving operations. The gripper device was also rigidly fixed to the vessel. The detailed modelling of the mechanical couplings can refer to Li et al. (2014).

The equations of motion for the two-body coupled lifting system included 12 degrees of freedom (DOF s) and are given in Eqn. (1).

$$(\mathbf{M} + \mathbf{A}(\infty)) \cdot \ddot{\mathbf{x}} + \mathbf{D}_1 \dot{\mathbf{x}} + \mathbf{D}_2 f(\dot{\mathbf{x}}) + \mathbf{Kx} + \int_0^t \mathbf{h}(t - \tau) \dot{\mathbf{x}}(\tau) d\tau = \mathbf{q}(t, \mathbf{x}, \dot{\mathbf{x}}) \quad (1)$$

where,

\mathbf{M} the total mass matrix;
 \mathbf{x} the rigid-body motion vector;
 \mathbf{A} the frequency-dependent added mass matrix ;
 \mathbf{D}_1 the linear damping matrix;
 \mathbf{D}_2 the quadratic damping matrix;
 \mathbf{K} the coupled hydrostatic stiffness matrix, including the hydrostatic stiffness of the vessel, the stiffness from the mooring line;
 \mathbf{h} the retardation function matrix of the vessel, which is calculated from the frequency-dependent added mass or potential damping using the panel method program WADAM (DNV, 2008);
 \mathbf{q} the external force vector. In the current model only the first order wave excitation forces $\mathbf{q}^{(1)}_{WA}$ are included for the floating vessel, and no second order wave forces were included. The wind and currents were also excluded for simplicity.

The external forces on the monopile included the gravity force, the buoyancy force, as well as the hydrodynamic wave forces. The wave forces normal to the MP's central axis were calculated by applying Morison's formula (Faltinsen, 1990). The monopile was divided into strips and the forces on the whole slender elements were calculated by strip theory. The wave forces f_{ws} per unit length on each strip of a moving circular cylinder normal to the member is as follows:

$$f_{ws} = \rho_w C_M \frac{\pi D^2}{4} \cdot \ddot{\zeta}_s - \rho_w C_A \frac{\pi D^2}{4} \cdot \ddot{x}_s + \frac{1}{2} \rho_w C_d D \cdot |\dot{\zeta}_s - \dot{x}_s| \cdot (\dot{\zeta}_s - \dot{x}_s) \quad (2)$$

$\ddot{\zeta}_s$ and $\dot{\zeta}_s$ are fluid particle acceleration and velocity at the center of the strip, respectively; \ddot{x}_s and \dot{x}_s are the acceleration and velocity at the center of the strip due to the body motions; D is the outer diameter of the member; and C_M , C_A and C_d are the mass, added mass and quadratic drag force coefficients, respectively. The monopile was simulated as a slender body using strip theory, and the added mass and quadratic damping coefficients were selected according to Li et al. (2014).

The coupled eigenvectors and eigenvalues of the monopile-vessel lifting system are provided in Table 2, where the yaw motion of the monopile is excluded. The bold figures show the dominated rigid motions for each eigenvector. Modes 1-5 are dominated by monopile motions when the vessel is almost still. The vessel motions in heave, pitch and roll motions are coupled with the monopile motion and dominate modes 6-8. The other three modes are dominated by the vessel horizontal motions and corresponding to very long natural periods. It can be seen that the eigenvalues of modes 4 to 8 are in the range of 6 to 14 sec, which could be critical for the wave conditions concerned. The other modes are less critical for the responses during lifting. Moreover, in short waves with T_p less than 7.5 sec the resonant motions of the MP can be excited while in longer waves the contributions from the vessel motions may play an important role.

MODELLING OF THE SHIELDING EFFECTS

Due to the presence and the motions of the floating vessel in waves, the wave field near the vessel is different from the incident wave field. The hydrodynamic coefficients of the vessel and the fluid kinematics at any point in the wave field can be acquired in the frequency domain using potential theory. The wave fields including the effects of both radiation and diffraction of the vessel are defined as disturbed waves in this paper, which account for the vessel shielding effects. The undisturbed waves are defined as incident waves.

To calculate the wave forces on the monopile in the disturbed wave field, the fluid kinematics $\ddot{\zeta}_s$ and $\dot{\zeta}_s$ in Eqn. (2) should be consistent with the disturbed fluid kinematics. Because the position of the monopile changes in time, the fluid kinematics at each strip of the monopile are time- and position-dependent. Therefore, the approach proposed by Li et al. (2014) was applied to calculate the responses of the multi-body system in the time domain while considering the

shielding effects. However, the approach from Li et al. (2014) only considered long-crested waves and it is further developed in this paper to be able to include short-crested waves. The approach is briefly discussed here.

1. First, generate time series of disturbed fluid kinematics (fluid particle velocities and accelerations) at pre-defined wave points considering both shielding effects and wave spreading.

2. Then, at each time step of the simulation, determine the instantaneous position of each slender element based on the solutions from the previous time step. For each strip on the element, find the closest eight pre-defined wave points and apply a three-dimensional (3D) linear interpolation to obtain the fluid kinematics for this strip in disturbed waves.

3. Calculate the forces at each strip in disturbed waves using Eqn. (2) and then integrate along the submerged part of the slender element to acquire the total wave forces and moments on the structure.

4. Finally, perform the time-domain simulations of the coupled vessel-monopile system in irregular waves using the multi-body code SIMO and an external DLL that interacts with SIMO at each time step. The wave forces on the substructures in disturbed waves are calculated in DLL using the interpolation method described above. The total wave forces on the structure are returned to SIMO, and the motions of the coupled system are solved.

FLUID KINEMATICS IN SHORT-CRESTED WAVES

A short-crested sea is considered to be made up of component waves with different amplitudes, frequencies and directions. It can be characterized by a two-dimensional wave spectrum, which is often written as

$$S(\omega, \theta) = S(\omega)D(\omega, \theta) \quad (3)$$

$$\int_{-\pi}^{\pi} D(\omega, \theta) d\theta = 1 \quad (4)$$

It has been observed that the directional spreading function $D(\omega, \theta)$ is generally a function of both frequency and direction. However, for practical purposes, one usually adopts the approximation $D(\omega, \theta) = D(\theta)$; that is the frequency dependence of the directional function is neglected. One of the most widely used $D(\theta)$ is the cosine power function given by DNV (2010)

$$D(\theta) = \begin{cases} C(n) \cos^n(\theta - \theta_0) & |\theta - \theta_0| \leq \pi/2 \\ 0 & |\theta - \theta_0| > \pi/2 \end{cases} \quad (5)$$

where θ_0 is the main wave direction about which the angular distribution is centered. The parameter n is a spreading index describing the degree of wave short crestedness, with $n \rightarrow \infty$ representing a long-crested wave field. $C(n)$ is a normalizing constant ensuring that Eqn. (4) is satisfied. It is found that

$$C(n) = \frac{1}{\sqrt{\pi}} \frac{\Gamma(1+n/2)}{\Gamma(1/2+n/2)} \quad (6)$$

Where Γ denotes the Gamma function. Consideration should be taken to reflect an accurate correlation between the actual sea state and the index n . Typical values for the spreading index for wind generated sea are $n = 2$ to 4. If used for swell, $n \geq 6$ is more appropriate (DNV, 2010). Because lifting operations are usually carried out in relatively low sea states, the spreading of the waves can be significant.

The spectra of the i^{th} component of kinematics (refers to fluid particle velocities or accelerations) in disturbed waves associated with a specified incident wave spectrum may be obtained in terms of the transfer functions $H_i(\omega, \theta)$ acquired from linear potential theory for different wave frequencies ω and directions θ . The required spectra are denoted by S_{ii} . For long-crested wave, the spectra are related to the incident wave spectrum $S(\omega)$ in the main wave direction θ_0 as follows

$$S_{ii}(\omega, \theta_0) = |H_i(\omega, \theta_0)|^2 S(\omega) \quad (7)$$

For short-crested waves, the directional spreading function $D(\theta)$ should be taken into account, then

$$\begin{aligned} S_{ii}(\omega, \theta_0) &= \int_{\theta_1}^{\theta_2} |H_i(\omega, \theta)|^2 S(\omega, \theta) d\theta \\ &= \int_{\theta_1}^{\theta_2} |H_i(\omega, \theta)|^2 D(\theta) d\theta \cdot S(\omega) = |\bar{H}_i(\omega, \theta)|^2 S(\omega) \end{aligned} \quad (8)$$

To calculate the wave forces on the monopile in the disturbed wave field during lowering, the fluid kinematics $\ddot{\zeta}_s$ and $\dot{\zeta}_s$ in Eqn. (2) should be based on the disturbed fluid kinematics.

The fluid kinematics transfer functions in disturbed waves for unidirectional waves can be directly obtained from the panel method in the frequency domain, while the averaged transfer functions in short-crested waves can be calculated from Eqn (9). Thus, the realizations of the disturbed kinematics are generated. To compare the effects of the spreading on the responses of the monopile, the transfer functions of wave kinematics are first studied. The RAOs (the amplitude of the transfer function) of the kinematics in incident and disturbed waves considering long and short-crested waves with the same total energy are presented.

The RAOs of the wave elevation, fluid particle velocities in incident long-crested waves are compared with those in short-crested waves with different spreading indices, shown in Fig 2. The results at two regular wave frequencies are presented. The wave kinematics RAOs are symmetric about heading sea and beam sea directions. Compared to RAOs in long-crested waves, the RAOs of X-velocity reduce significantly in directions close to heading seas when implementing wave spreading index $n = 2$, while the RAOs close to beam seas increase. This is because the wave energy in the main wave direction reduces and the energy from the directions around the main direction contributes to the averaged RAOs. The same results can be observed for RAOs for Y-velocity. As the spreading indices increase, the wave energy is more concentrated to the main wave direction and the averaged RAOs in short-crested waves approach to those in long-crested waves. For wave elevation and particle velocity in Z direction, the RAOs in short-crested waves remain the same as those in long-crested waves since the wave spreading does not influence the quantities in the vertical direction.

When accounting for shielding effects from the vessel, the symmetry of the wave kinematics about the heading sea direction disappears. Fig. 3 to Fig. 5 provide the RAOs of wave elevation and fluid particle velocities in X and Y directions in disturbed waves with and without wave spreading, respectively. It is visible that the RAOs in disturbed waves are greatly affected by the vessel in short waves, while in long waves the RAOs are close to those in incident waves. This is due to the ability of the vessel diffraction decreases with increasing wave length. The RAOs in the leeward side of the vessel (from 0 deg to 180 deg) are significantly reduced in short waves when considering shielding

effects, while the RAOs in the windward side (from 180 *deg* to 360 *deg*) can be amplified, see $T = 7 \text{ sec}$ in Fig. 3 and $T = 5 \text{ sec}$ in Fig. 5.

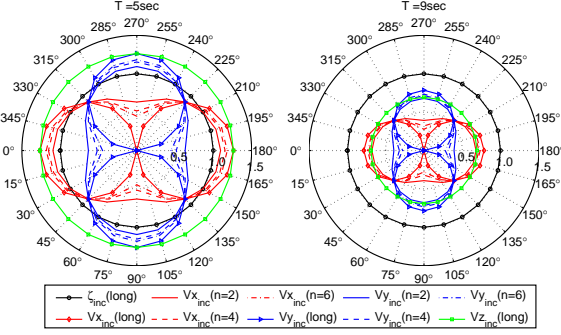


Figure 2: RAOs of fluid kinematics in incident long and short-crested ($n = 2, 4, 6$) waves ($x = -20 \text{ m}$, $y = 30 \text{ m}$, $z = 0 \text{ m}$)

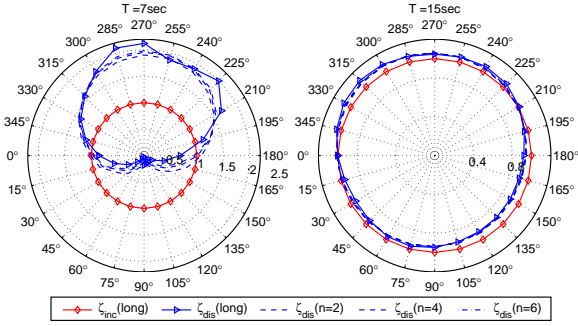


Figure 3: RAOs of wave elevations in disturbed long and short-crested waves ($n = 2, 4, 6$) waves ($x = -20 \text{ m}$, $y = 30 \text{ m}$, $z = 0 \text{ m}$)

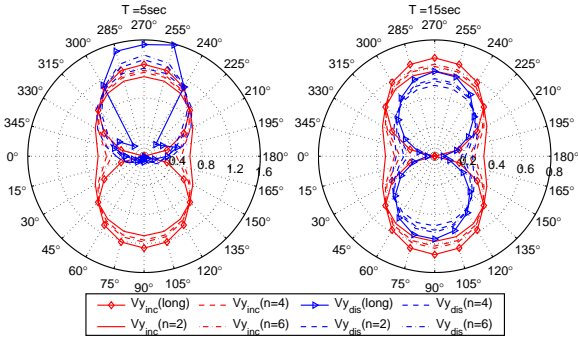


Figure 4: RAOs of Y-velocity in disturbed long and short-crested waves ($n = 2, 4, 6$) waves ($x = -20 \text{ m}$, $y = 30 \text{ m}$, $z = 0 \text{ m}$)

When only unidirectional waves are considered, the differences between the RAOs in incident and disturbed waves are significant in short wave lengths. However, these differences are reduced considerably when including the effects from the spreading waves. For

example, the averaged RAOs of X-velocity at $T = 5 \text{ sec}$ near 180 *deg* direction in disturbed waves are close to those in incident waves with spreading index $n = 2$ as shown in Fig. 5. This is because the spreading function averages the low RAOs in the leeward side and the large RAOs in the windward side of the vessel. Thus, it can be predicted that the shielding effects in short-crested waves would be less pronounced compared with the case when only long-crested waves are considered. Furthermore, similar to the results in incident waves, with increasing spreading index the disturbed RAOs in spreading waves are moving close to those in long-crested waves.

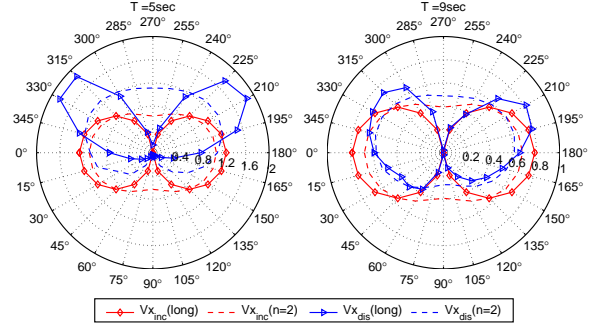


Figure 5: RAOs of fluid X-velocities in incident and disturbed waves with and without spreading ($x = -20 \text{ m}$, $y = 30 \text{ m}$, $z = 0 \text{ m}$)

TIME-DOMAIN SIMULATIONS

Step-by-step integration methods were applied to calculate the responses of the lifting system using an iterative routine with a time step of 0.02 sec . The first order wave forces of the vessel were pre-generated using Fast Fourier Transformation (*FFT*) at the mean position. The fluid kinematics used to calculate the hydrodynamic forces on the monopile were calculated in the time domain using the interpolation of the pre-generated fluid kinematics at pre-defined wave points in disturbed waves.

The environmental condition of the time-domain simulations was chosen as $H_s = 2.0 \text{ m}$. The wave spectral peak period T_p varied from 6 *sec* to 12 *sec*, thus covering a realistic range. At each combination of H_s and T_p the irregular waves were modelled by JONSWAP spectrum (DNV, 2010). In order to account for the variability of stochastic waves, 10 realizations of irregular waves were generated at each of the environmental conditions using different seeds. The duration of each realization was 20 *min*. Thus, the whole simulation corresponded to an operation with a duration of more than three hours.

RESULTS AND DISCUSSIONS

Responses in Long- and Short-crested Waves Without Shielding Effects

In the lifting operation of the monopile, the motions of the vessel affect the motions of the monopile through the lift wire and the gripper device, the motions of which in three directions are formulated in Eqn. (9):

$$\mathbf{s} = (\eta_1 + z\eta_5 - y\eta_6)\hat{i} + (\eta_2 - z\eta_4 + x\eta_6)\hat{j} + (\eta_3 + y\eta_4 - x\eta_5)\hat{k} \quad (9)$$

where η_1 to η_6 are the rigid body motions of the vessel and (x, y, z) is

the position of the crane tip or gripper relative to the fixed coordinates of the vessel body. Fig. 6 compares the standard deviations of crane tip motions ($x = -20\text{ m}$, $y = 30\text{ m}$, $z = 80\text{ m}$) in Z direction in incident waves with different spreading indices. The results are given with heading angles from 0 deg to 180 deg . The maximum Z-motions occur near beam sea due to the roll motions of the vessel. The motions increase with the wave peak period since the roll natural period of the vessel is close to 14 sec . Due to the spreading of the waves, it is clearly observed that the maximum crane tip motions close to beam sea are decreased and those close to heading and following seas are increased. The crane tip Z-motions in short-crested waves are larger than those in incident waves from 0 deg until near 60 deg with $T_p = 8\text{ sec}$ and until near 45 deg with $T_p = 12\text{ sec}$. Thus, it is non-conservative to only apply long-crested waves at these directions if crane-tip Z-motions are critical to the whole lifting system using this vessel.

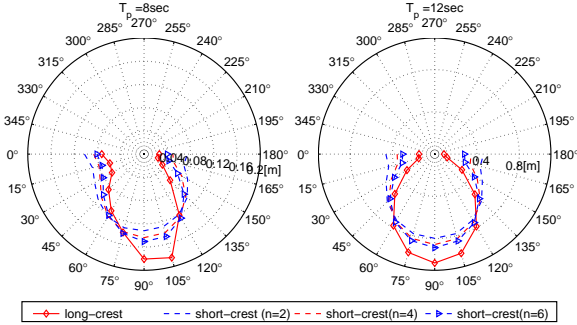


Figure 6: Crane-tip z-motions in incident waves with and without spreading ($H_s = 2.0\text{ m}$)

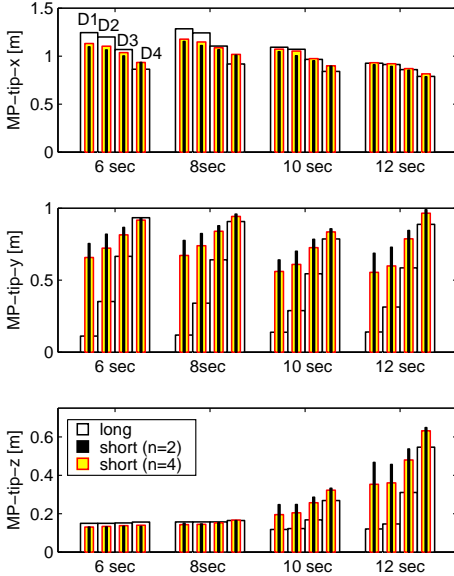


Figure 7: Standard deviation of MP tip motions in incident waves with and without spreading ($H_s = 2.0\text{ m}$, for each T_p the directions from left to right are $D_1 = 180\text{ deg}$, $D_2 = 165\text{ deg}$, $D_3 = 150\text{ deg}$, $D_4 = 135\text{ deg}$)

The motions of the lower tip of the monopile during the lifting operation in incident waves are compared with different wave spreading conditions in Fig. 7. The results at four heading angles are provided. There are two contributions for the monopile motion: one is the direct wave excitation force on the MP and the other one is the induced motion from the vessel through the mechanical couplings. In short waves and near heading seas, the wave excitation force on the MP is dominant and the vessel motion is minor. Thus, the MP tip X-motion decreases at close to heading seas when considering wave spreading, while the tip Y-motion increase considerably. The roll motion of the vessel influences the lifting system in long waves, and the MP motions in Y and Z directions in short-crested waves are much higher than those in long-crested waves at the directions considered, which are consistent with Fig. 6.

Responses in Long- and Short-crested Waves Considering Shielding Effects

Figures 8 and 9 compare the response time series (i.e., monopile tip displacements, lift wire tension and gripper device force) in disturbed long-crested and short-crested waves with spreading index $n = 2$. The response in short-crested waves are higher than those in long-crested waves when accounting for the shielding effects from the vessel. The reasons can be better explained by studying the response spectra. The spectra of the responses time series are plotted in Fig. 10. In order to compare the shielding effects, the response spectra in long-crested incident waves are also presented.

In short waves with $T_p = 6\text{ sec}$, the resonant motions of the monopile are excited, which corresponds to the peak frequency of the spectra at $\omega \approx 0.95\text{ rad/s}$. The hydrodynamic wave loads on the monopile dominate the response of the system in this case. In long waves, however, two peaks in the motion spectrum are observed. The peaks at $\omega \approx 0.95\text{ rad/s}$ match the natural frequencies of the monopile rotational motion, while the peaks at $\omega \approx 0.45\text{ rad/s}$ correspond to the vessel roll natural period. Due to the couplings of the monopile and the vessel, the increasing responses of the vessel in long wave dominate the motions of the system. The peak frequency of the wire tension and heave motion is consistently twice of the rotational peak frequency as one cycle of rotational motion induces two cycles of variations in the Z-motion and the wire tension.

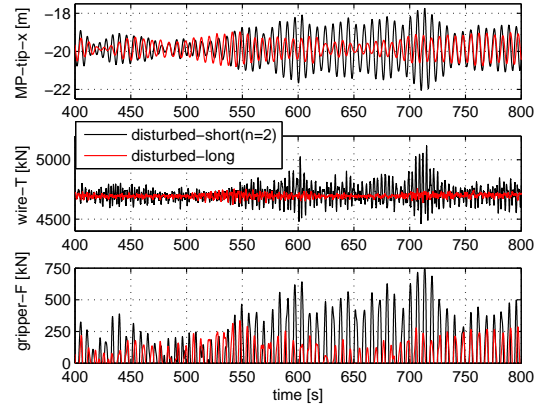


Figure 8: Time series of monopile responses in disturbed waves with and without spreading ($H_s = 2.0\text{ m}$, $T_p = 6\text{ sec}$, $Dir = 150\text{ deg}$)

For both wave conditions, the peaks at $\omega \approx 0.95 \text{ rad/s}$ in the response spectra, which correspond to the natural frequency of the rotational motions of the monopile, are significantly reduced when the shielding effects of the vessel are considered. In long waves with $T_p = 12 \text{ sec}$ the response peaks corresponding to the vessel motion do not decrease when considering shielding effects. These results indicate the significant influence of the shielding effects on the monopile motions, particularly in short waves when the wave frequencies are close to the natural frequencies of the monopile.

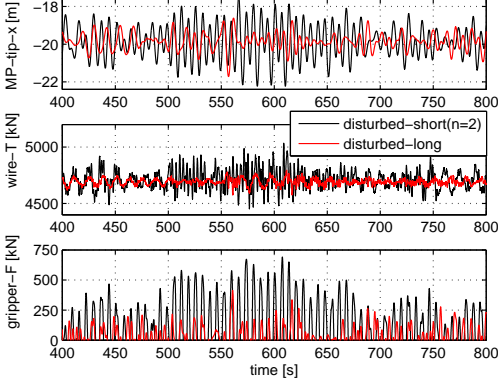


Figure 9: Time series of monopile responses in disturbed waves with and without spreading ($H_s = 2.0 \text{ m}$, $T_p = 12 \text{ sec}$, $Dir = 150 \text{ deg}$)

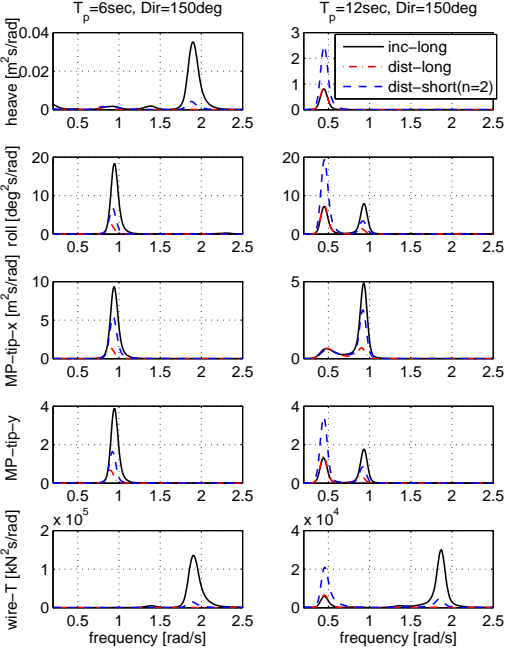


Figure 10: Response spectra in incident and disturbed waves with and without wave spreading ($H_s = 2.0 \text{ m}$, $Dir = 150 \text{ deg}$)

By comparing the results in short and long-crested waves, it can be observed the reduction of spectra peaks at $\omega \approx 0.95 \text{ rad/s}$ in long-crested waves are more pronounced than those in short-crested waves when considering shielding effects. The reason is that the averaged wave kinematic RAOs in disturbed waves with spreading index $n = 2$ are higher than those in long-crested waves (see Fig. 3 to Fig. 5). Furthermore, the spreading of waves increases the peaks with $\omega \approx 0.45 \text{ rad/s}$, which is consistent with Fig. 6 that the crane tip motion in short-crested waves are higher than those in long-crested waves with a heading angle of 150 deg .

The Influences of Wave Spreading on the Shielding Effects

Figures 11 and 12 compare the standard deviations of the monopile tip motions in incident waves with those in disturbed waves with long- and short-crested waves, respectively. For both cases, it can be seen the shielding effects reduce the responses significantly in short-waves and the reduction decreases with wave length. The shielding effects are more pronounced in long-crested waves than in short-crested waves. Thus, the reduction of extreme responses from shielding effects can be over-predicted if only considering long-crested waves.

Besides, the differences between responses at various headings in short-crested waves are much smaller than in long-crested waves. This is due to the spreading of the wave energy at neighbour directions, and the responses are averaged over directions. Moreover, from the results in disturbed waves at different wave periods and heading angles, it is possible to obtain the most suitable operational heading angle with minimum responses. In both long and short-crested cases, the most suitable angle is observed close to quartering seas in short waves and it moves towards to heading seas with increasing wave length. However, the responses at the most suitable heading angles in long-crested waves are always lower than those in short-crested waves. Thus, the wave spreading should be considered to avoid non-conservative results. The influences from the wave spreading are expected to reduce when using higher spreading index.

CONCLUSIONS

This study investigates the influences of the short-crested waves and the shielding effects from the floating installation vessel on the responses of the monopile lifting operation. The wave kinematics near the vessel were studied first in the frequency domain, followed by time-domain simulations. The shielding effects were included in the time-domain by interpolating fluid kinematics between predefined wave points near the floating vessel. The effects of the wave spreading on the responses in incident and disturbed waves were examined in detail. It is concluded that short-crested waves affect of the responses in both incident and disturbed waves significantly. The shielding effects can reduce the responses significantly, but the reduction are less in short-crested waves than in long-crested waves. Because the operational sea states are commonly short-crested, it is important to consider the effects from the directional waves to avoid non-conservative estimate of motions.

The averaged RAOs of the wave kinematics were obtained by applying the cosine spreading function and were compared with the RAOs in long-crested waves. The RAOs in incident long-crested waves can be greatly affected by the directional waves due to the spreading of the wave energy. The vessel shielding effects can result in a great decrease of the kinematics nearby and at the leeward side of the vessel, particularly in short wave lengths. However, the decrease is less considerably when accounting for the wave spreading.

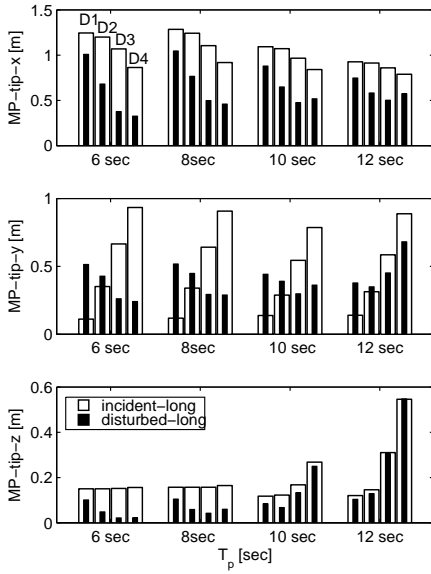


Figure 11: Standard deviation of MP tip motions in incident and disturbed waves in long-crested waves ($H_s = 2.0m$, for each T_p the directions from left to right are $D_1 = 180 \text{ deg}$, $D_2 = 165 \text{ deg}$, $D_3 = 150 \text{ deg}$, $D_4 = 135 \text{ deg}$)

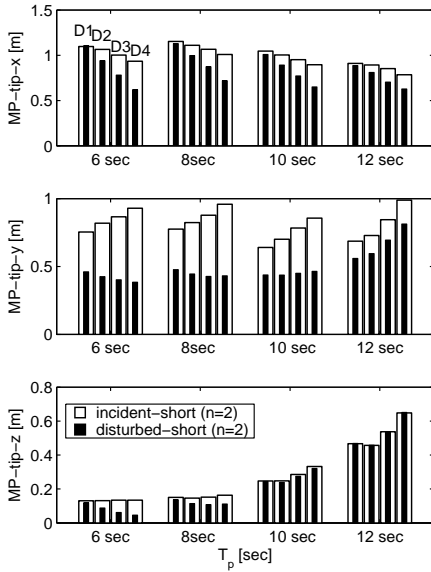


Figure 12: Standard deviation of MP tip motions in incident and disturbed waves with wave spreading ($n = 2$) ($H_s = 2.0m$, for each T_p the directions from left to right are $D_1 = 180 \text{ deg}$, $D_2 = 165 \text{ deg}$, $D_3 = 150 \text{ deg}$, $D_4 = 135 \text{ deg}$)

The shielding effects from the vessel bring pronounced reduction in the standard deviation of the monopile responses, in particular in short waves. Thus, it can be beneficial to utilize the effects to increase the operational weather window. The most suitable heading angle of the vessel are observed close to quartering seas in short waves and it moves towards to heading seas with increasing wave length. On the other hand, the responses considering shielding effects may be underestimated if only long-crested waves are applied. The spreading of wave energy narrows down the differences between the responses in incident and disturbed waves. This results in higher responses in short-crested waves than in long-crested waves at the most suitable heading angles. Therefore, short-crested waves are critical in predicting responses for the present scenario in both incident waves and disturbed waves with consideration of the shielding effects from the vessel.

ACKNOWLEDGEMENTS

The authors gratefully acknowledge the financial support from the Research Council of Norway granted through the Department of Marine Technology, Centre for Ships and Ocean Structures (CeSOS) and Centre for Autonomous Marine Operations and Systems (AMOS), NTNU. Thanks are extended to Erin Bachynski from MARINTEK for supporting the use of the software SIMO and Peter Sandvik from MARINTEK for valuable discussions.

REFERENCES

- Baar, J., Pijfers, J., Santen, J., 1992. Hydromechanically coupled motions of a crane vessel and a transport barge. In: *24th Offshore Technology Conference*, Houston.
- Bai, W., Hannan, M., Ang, K., 2014. Numerical simulation of fully nonlinear wave interaction with submerged structures: Fixed or subjected to constrained motion. *Journal of Fluids and Structures* 49, 534–553.
- Battjes, J. A., 1982. Effects of short-crestedness on wave loads on long structures. *Applied Ocean Research* 4 (3), 165–172.
- Chakrabarti, S. K., 1987. *Hydrodynamics of offshore structures*. WIT press.
- DNV, 2008. *Wadam theory manual*. Det Norske Veritas.
- DNV, October 2010. *Recommended Practice DNV-RP-C205, Environmental Conditions and Environmental Loads*. Det Norske Veritas.
- DNV, February 2014. *Recommended Practice DNV-RP-H103, Modelling and Analysis of Marine Operations*. Det Norske Veritas.
- EWEA, 2014. *The European offshore wind industry - key trends and statistics 2013*. Report, The European Wind Energy Association.
- Faltinsen, O., 1990. *Sea Loads on Ships and Ocean Structures*. Cambridge University Press.
- Goda, Y., 2010. *Random seas and design of maritime structures*. World Scientific.
- Inoue, Y., Islam, M. R., 2000. Numerical investigation of slowly varying drift forces of multiple floating bodies in short crested irregular waves. In: *The 10th International Offshore and Polar Engineering Conference*, Seattle, USA, May 28 - June 2.
- Isaacson, M., Nwogu, O., 1987. Wave loads and motions of long structures in directional seas. *Journal of Offshore Mechanics and Arctic Engineering* 109 (2), 126–132.
- Isaacson, M. d. S. Q., Sinha, S., 1986. Directional wave effects on large offshore structures. *Journal of Waterway, Port, Coastal, and Ocean Engineering* 112 (4), 482–497.
- Kaiser, M. J., Snyder, B. F., 2013. Modeling offshore wind installation costs on the US outer continental shelf. *Renewable Energy* 50, 676–691.

- Kumar, V. S., Deo, M., Anand, N., Chandramohan, P., 1999. Estimation of wave directional spreading in shallow water. *Ocean engineering* 26 (1), 83–98.
- Lambrakos, K. F., 1982. Marine pipeline dynamic response to waves from directional wave spectra. *Ocean Engineering* 9 (4), 385–405.
- Li, L., Gao, Z., Moan, T., Ormberg, H., 2014. Analysis of lifting operation of a monopile for an offshore wind turbine considering vessel shielding effects. *Marine Structures* 39, 287–314.
- MARINTEK, 2012. SIMO - Theory Manual Version 4.0.
- Marshall, P. W., 1976. Dynamic and fatigue analysis using directional spectra. In: *Offshore Technology Conference*, Houston, USA.
- Mukerji, P., 1988. Hydrodynamic responses of derrick vessels in waves during heavy lift operation. In: *20th Offshore Technology Conference*, Houston, USA.
- Nwogu, O., 1989. *Analysis of fixed and floating structures in random multi-directional waves*. PhD thesis, University of British Columbia.
- Sannasiraj, S. A., Sundaravadevelu, R., Sundar, V., 2001. Diffraction radiation of multiple floating structures in directional waves. *Ocean engineering* 28 (2), 201–234.
- Sun, L., Eatock Taylor, R., Choo, Y. S., 2012. Multi-body dynamic analysis of float-over installations. *Ocean Engineering* 51, 1–15.
- Tao, L., Song, H., Chakrabarti, S., 2007. Scaled boundary FEM solution of short-crested wave diffraction by a vertical cylinder. *Computer methods in applied mechanics and engineering* 197 (1), 232–242.
- Teigen, P. S., 1983. The response of a TLP in short-crested waves. In: *Offshore Technology Conference*, Houston, Texas, USA.
- van den Boom, H., Dekker, J., Dallinga, R., 1990. Computer analysis of heavy lift operations. In: *22nd Offshore Technology Conference*, Houston, USA.
- Zhu, S., Satravaha, P., 1995. Second-order wave diffraction forces on a vertical circular cylinder due to short-crested waves. *Ocean engineering* 22 (2), 135–189.

A.4 Paper 4

Paper 4:

Response Analysis of a Nonstationary Lowering Operation for an Offshore Wind Turbine Monopile Substructure.

Authors: Lin Li, Zhen Gao, Torgeir Moan

Published in *Journal of Offshore Mechanics and Arctic Engineering*, 2015,
Vol. 137, DOI: 10.1115/1.4030871.

Lin Li¹

Centre for Ships and Ocean Structures (CeSOS);
Centre for Autonomous Marine Operations and
Systems (AMOS);
Department of Marine Technology,
Norwegian University of Science and Technology
(NTNU),
Trondheim NO-7491, Norway
e-mail: lin.li@ntnu.no

Zhen Gao

Centre for Ships and Ocean Structures (CeSOS);
Centre for Autonomous Marine Operations and
Systems (AMOS);
Department of Marine Technology,
Norwegian University of Science and Technology
(NTNU),
Trondheim NO-7491, Norway

Torgeir Moan

Centre for Ships and Ocean Structures (CeSOS);
Centre for Autonomous Marine Operations and
Systems (AMOS);
Department of Marine Technology,
Norwegian University of Science and Technology
(NTNU),
Trondheim NO-7491, Norway

Response Analysis of a Nonstationary Lowering Operation for an Offshore Wind Turbine Monopile Substructure

This study addresses numerical modeling and time-domain simulations of the lowering operation for installation of an offshore wind turbine monopile (MP) with a diameter of 5.7 m and examines the nonstationary dynamic responses of the lifting system in irregular waves. Due to the time-varying properties of the system and the resulting nonstationary dynamic responses, numerical simulation of the entire lowering process is challenging to model. For slender structures, strip theory is usually applied to calculate the excitation forces based on Morison's formula with changing draft. However, this method neglects the potential damping of the structure and may overestimate the responses even in relatively long waves. Correct damping is particularly important for the resonance motions of the lifting system. On the other hand, although the traditional panel method takes care of the diffraction and radiation, it is based on steady-state condition and is not valid in the nonstationary situation, as in this case in which the monopile is lowered continuously. Therefore, this paper has two objectives. The first objective is to examine the importance of the diffraction and radiation of the monopile in the current lifting model. The second objective is to develop a new approach to address this behavior more accurately. Based on the strip theory and Morison's formula, the proposed method accounts for the radiation damping of the structure during the lowering process in the time-domain. Comparative studies between different methods are presented, and the differences in response using two types of installation vessel in the numerical model are also investigated.

[DOI: 10.1115/1.4030871]

Keywords: lowering operation, monopile, irregular waves, potential damping, Morison's formula, time-domain simulation

1 Introduction

Offshore operations are risky and expensive due to unstable and choppy offshore environmental conditions. For a large offshore wind farm, several tens or hundreds of wind turbine units need to be installed over a short period of time. Only a limited time window is available to install one unit before the condition becomes harsh. The most practical approach is to limit operations to a certain period of the year (e.g., from March to September) to reduce the average weather down time. Despite this practice, weather down time is still relatively high. The largest down time is observed in offshore crane operations due to wave and wind forces, but currently the crane operation remains the most important method for offshore wind farm installation. To better plan these operations and increase the weather window during the design phase, reliable and accurate numerical models for prediction of the system behavior are of great importance. This study focuses on the lowering operation of a monopile substructure for offshore wind turbines.

Offshore lifting operations have been investigated by many researchers over several decades. The study of interest in the oil and gas industry featured the lifting of substantial loads from a transport barge by means of large capacity crane vessels [1–5].

These studies have focused on building accurate numerical models for the mechanical coupling system between the load and the crane, as well as the hydrodynamic coupling between the crane vessel and the transport barge. The behavior of the lifted objects through the splash zone presents another challenge. The design loads must be predicted to increase the safety of the operation. The most critical part is selection of the correct hydrodynamic coefficients, i.e., the added mass, damping and slamming coefficients, etc. Examples of studies on the hydrodynamic coefficients can be found in Refs. [6–8]. Usually model tests or computational fluid dynamics methods are required to obtain accurate coefficients for response analysis of the lifting system.

The structures used in offshore wind farms are relatively smaller and lighter, and the installation appears to be easier compared with the installations in the oil and gas industry, which are usually one of its kinds. Nevertheless, instead of one large structure installed at a single position, repetitive installations must be performed for each unit in a wind farm. Thus, the ability to install one wind turbine unit at a higher sea state is crucial for efficient installation of the wind farm and reduction of costs.

In lifting operations with objects (e.g., monopiles, suction anchors, and subsea templates) lowered from the air into the splash zone and toward the seabed, the dynamic features of the system change continuously. A process dominated by nonlinear responses must be analyzed in a manner different from that of a stationary case. Generally, two approaches are used to simulate such cases for statistical evaluation [9]. The first approach uses steady-state simulations in irregular waves at the most critical

¹Corresponding author.

Contributed by the Ocean, Offshore, and Arctic Engineering Division of ASME for publication in the JOURNAL OF OFFSHORE MECHANICS AND ARCTIC ENGINEERING. Manuscript received April 7, 2015; final manuscript received June 16, 2015; published online July 27, 2015. Assoc. Editor: Yi-Hsiang Yu.

vertical positions, and the second approach simulates repeated lowering using different irregular wave realizations. The second method provides more realistic results because an unrealistic buildup of the oscillations that are observed in the stationary cases is avoided [9]. Therefore, to provide more accurate estimates of the operations, analyses of the entire lowering process are preferred.

However, additional challenges in analysis of the entire lowering process are due to the time-varying properties, i.e., the mass, damping, and stiffness of the lifting system. The use of traditional frequency-domain analysis to solve the problem is not applicable in this situation. The hydrodynamic properties from frequency-domain analysis express the boundary condition on the mean body surface, where the lifted structure experiences a large change of position when it moves downward toward the seabed. Therefore, time-domain solutions that consider the nonstationary processes are required. Li et al. [10] studied the entire lowering process of the monopile in the time-domain with emphasis on the shielding effects from the installation vessel. The wave forces on the monopile were calculated using Morison's formula by interpolating the disturbed wave kinematics at predefined wave points at each time step. The same installation scenario is studied further in this paper with a focus on modeling of the hydrodynamic forces on the monopile.

Because of the simple shape of a monopile with a relatively small diameter, the slender body approximation is often applied. If the diameter is less than one-fifth of the wavelength, the empirical Morison's formula is employed to calculate the forces [11]. The effects of diffraction and radiation are considered insignificant in this approach, which has been widely applied for slender cylindrical structures [10,12,13]. Based on the slender body approximation, the second-order wave loads also can be included to predict accurate responses of the structure under various conditions [14–17]. In addition, a comparison between the slender approximation and the three-dimensional (3D) potential theory has been conducted, and examples can be found in Refs. [12], [13], and [17]. The results showed favorable agreement between the two methods except for high frequencies, at which the diffraction effect became important.

The operational sea states are normally low with short waves and the wavelength can be close to five times the structure diameter. In this situation, the diffraction and radiation from the structure might be critical. This point is more relevant for installation of the offshore wind turbine monopile substructure. As mentioned previously, the accuracy of the response analysis for one single operation would affect the installation efficiency of the entire wind farm. In addition, larger support structures with larger diameters are of increasingly interest for higher capacity wind turbines in deeper water sites [18]. In this case, the assumption that ignores the diffraction and radiation from the structure is questionable. Therefore, it is of interest to evaluate this assumption and develop more accurate numerical models for the lowering operation of the monopile.

This paper investigates the lowering operation of a monopile with a diameter of 5.7 m. The purpose is to examine the importance of radiation effects of the monopile during the lowering operation. A new approach is proposed to implement the radiation effects in the time-domain numerical simulation of the lowering process. Hydrodynamic modeling of the forces on the monopile with a fixed draft is first studied and three different methods are compared. The comparisons indicate the importance of potential damping in the presented lifting system, which is absent in the slender body approximation. The proposed method thus accounts for the potential damping of the monopile during the lowering process. Linear interpolation between the retardation functions at predefined drafts is implemented in the time-domain analysis. The responses of the lifting system are compared for the proposed method and that using the slender body approximation in irregular waves. In addition, a comparative study using two types of vessel is performed applying the proposed method.

2 Description of the Lifting System

Two installation vessels are applied in this study, i.e., a fixed (jack-up) vessel and a floating installation vessel. The fixed vessel provides a stable platform for the lifting system, while the motions of the floating vessel influence the responses of the monopile during the operation. The main dimensions of the floating vessel refer to Ref. [10]. The lifting capacity and the positioning system of the floating vessel make it capable of performing the monopile installation in shallow-water sites. The monopile used in the model is a long slender hollow cylinder with an outer diameter of 5.7 m, a thickness of 6 cm, and a length of 60 m. Figure 1 shows a schematic layout arrangement of the operation with uses of the floating vessel. The system includes two rigid bodies, i.e., the floating installation vessel and the monopile. The two bodies are coupled through a lift wire. The crane is rigidly connected to the vessel in the numerical model, and a low constant flexibility of the crane is included. The position of the monopile changes continuously during the lowering process.

The global coordinate system is a right-handed coordinate system with the following orientation: the X axis points toward the bow, the Y axis points toward the port side, and the Z axis points upward. The origin is located at midship section, centerline, and still-water line when the vessel is at rest. The crane tip position was chosen as 20 m, −30 m, and 80 m in the global coordinates for both fixed and floating vessels. The water depth at the installation site is 25 m, and the monopile is lowered from air into the water during the operation.

2.1 Equations of Motion. When using a floating installation vessel, the equations of motion for the two-body coupled lifting system included 12 degrees-of-freedom (DOF). For the floating vessel, the following six equations of motion are solved in the time-domain:

$$(\mathbf{M} + \mathbf{A}(\infty)) \cdot \ddot{\mathbf{x}} + \mathbf{D}_1 \dot{\mathbf{x}} + \mathbf{D}_2 f(\dot{\mathbf{x}}) + \mathbf{K} \mathbf{x} + \int_0^t \mathbf{h}(t - \tau) \dot{\mathbf{x}}(\tau) d\tau = \mathbf{F}_{\text{ext}}(t) = \mathbf{q}_{\text{WA}}^{(1)} + \mathbf{F}_{\text{cpl}} \quad (1)$$

where \mathbf{M} is the mass matrix of the vessel; \mathbf{x} is the rigid-body motion vector of the body with 6DOF; \mathbf{A} is the frequency-dependent added mass matrix; \mathbf{D}_1 and \mathbf{D}_2 are the linear and quadratic damping matrices. The viscous effects from the vessel hull and the mooring system were simplified into linear damping terms in surge, sway, and yaw. The roll damping of the vessel was also included. Additionally, \mathbf{K} is the hydrostatic restoring matrix that includes the hydrostatic stiffness of the vessel and the stiffness from the mooring line; \mathbf{h} is the retardation function calculated

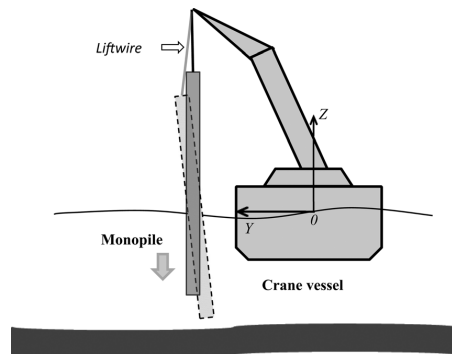


Fig. 1 Lifting arrangement of the monopile using a floating installation vessel

Table 1 Eigenperiods and eigenvectors of the vessel-monopile lifting system

Body	Mode	1	2	3	4	5	6	7	8
Vessel	Heave (m)	0	0	0	-0.2	1.0	0	0	0
Vessel	Roll (deg)	-0.03	-0.01	0	0	-0.13	0.72	0	-0.04
Vessel	Pitch (deg)	0	0	0	0.7	0.19	0	0	0
MP	Surge (m)	0	0	0.1	0.03	0	0	1.0	-0.08
MP	Sway (m)	0	-0.1	0	0	0	0.07	0.08	1.0
MP	Heave (m)	1.0	-0.01	0	0.04	1.0	0.4	0	-0.02
MP	Roll (deg)	0	1.0	0.01	0	-0.15	1.0	0.07	0.83
MP	Pitch (deg)	0	-0.01	1.0	1.0	0.23	0	-0.88	0.07
Natural period (s)		0.59	5.03	5.05	9.45	10.65	13.81	35.25	36.22

Bold figures emphasize the dominant rigid motions at each mode.

from the frequency-dependent added mass coefficient or potential damping using the panel method program WAMIT [19], and \mathbf{F}_{ext} is the external force vector, including the first-order wave excitation forces $\mathbf{q}_{\text{WA}}^{(1)}$ and the coupling force, \mathbf{F}_{cpl} of the lift wire connected with the monopile which depends on the relative motions between the vessel and the monopile. The second-order wave forces were not included in the current model, and the wind and currents were also excluded for simplicity. The equations of motion for the monopile are formulated as follows:

$$\mathbf{M} \cdot \ddot{\mathbf{x}} + \mathbf{K} \mathbf{x} = \mathbf{F}_{\text{ext}}(t) = \mathbf{F}_B + \mathbf{F}_G + \mathbf{F}_W + \mathbf{F}_{\text{cpl}} \quad (2)$$

where the matrix \mathbf{K} is the restoring matrix of the monopile including hydrostatic restoring and restoring due to the lifting arrangement. The external force on the monopile \mathbf{F}_{ext} consists of buoyancy forces, F_B , gravity forces, F_G , hydrodynamic wave forces, F_W , and the coupling force with the vessel \mathbf{F}_{cpl} . The wave forces on the monopile F_W can be calculated using different methods. The coordinate origin for Eq. (2) refers to the center of gravity of the monopile, and all of the matrices in the equation refer to this point. It should be mentioned that the mechanical coupling force \mathbf{F}_{cpl} is the internal force between the vessel and the monopile and depends on the relative motions between the two bodies. In addition to mechanical coupling, hydrodynamic couplings also exist for the coupled system. The effects from the monopile on the vessel are minor due to its small geometry compared with that of the vessel. However, the diffraction and the radiation from the vessel can significantly influence the hydrodynamic forces on the monopile, which are known as shielding effects. Li et al. [10] studied the shielding effects on the responses of the monopile lifting system in detail. In the current study, the hydrodynamic couplings are excluded. In Sec. 3, three methods are discussed and compared to calculate the wave forces on the monopile when the draft is assumed as fixed. Before focusing on the different methods for hydrodynamics, it is important to assess the natural periods of the system by assuming zero hydrodynamic forces on the two-body system in Eqs. (1) and (2).

2.2 Natural Periods of the Lifting System. The natural periods and natural modes of coupled vessel and monopile lifting system are listed in Table 1, in which the dominant rigid motions are emphasized. The draft of the monopile is chosen as 20 m in the table, and the horizontal modes of the vessel (surge, sway, and yaw) as well as the yaw of the monopile are not included in the table because they are secondary for this study. The eigenvectors shown in the table for each body refer to its own body-fixed coordinates.

Modes 1–3 and 7 and 8 are dominated by monopile motions when the vessel is nearly still, where mode 1 is heave motion of the monopile, modes 2 and 3 are dominated by rotational motion, and modes 4 and 5 are dominated by pendulum modes that correspond to a long natural period. In contrast, modes 4–6 are dominated by the vessel pitch, heave, and roll motions, respectively. Comparison of this table with the natural periods of the vessel

alone shows that the natural periods of the vessel pitch and heave motions are little affected by the monopile but the coupled roll natural period (mode 6) is slightly increased. Despite these effects, the coupling between the motions of the two bodies is visible in modes 4–6. The motions of the vessel affect the motions of the monopile through the crane tip, the motions of which in three directions are formulated in the following equation:

$$\mathbf{s} = (\eta_1 + z\eta_5 - y\eta_6)\hat{i} + (\eta_2 - z\eta_4 + x\eta_6)\hat{j} + (\eta_3 + y\eta_4 - x\eta_5)\hat{k} \quad (3)$$

where η_1 through η_6 are the rigid-body motions of the vessel and (x, y, z) is the position of the crane tip relative to the fixed coordinates of the vessel body. It is expected that the vessel motions play an important role in the response of the monopile when the wave periods are approximately $T_p = 9$ – 14 s. Moreover, due to the antisymmetry of the vessel motions, the natural periods of the two rotational modes (modes 2 and 3) and the two pendulum modes (modes 7 and 8) are slightly different.

During the installation, the position of the monopile changes with the running winch, and the increasing length of the lift wire changes the total restoring stiffness. Additionally, the added mass matrix increases due to the increasing submergence. Figure 2 shows how the natural periods of monopile dominated modes (modes 1–3 and modes 7 and 8 in Table 1) vary with the vertical position of the lower tip of the monopile. The natural period of Mode 1 (which is heave dominated) decreases slightly with increasing submergence. The other four modes all increase greatly due to changes in the restoring forces and significant contributions from the added mass. In the time-domain simulations, the rotational modes (modes 2 and 3) and pendulum modes (modes 7 and 8) are observed and might dominate the responses of the lifting system in various wave conditions.

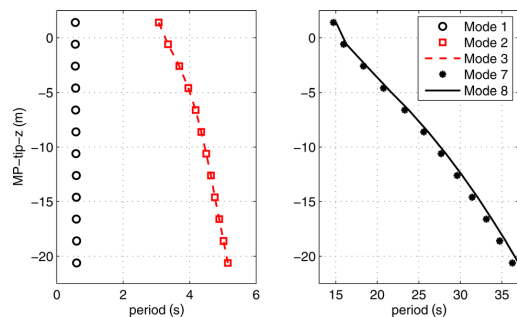


Fig. 2 Natural periods of the monopile rigid-body motions with varying positions (mode 1: heave motion dominant; mode 2 and mode 3: rotational motion dominant; and mode 4 and mode 5: pendulum motion dominant)

3 Hydrodynamic Forces on the Monopile With a Fixed Draft

In this section, three different methods used to calculate the hydrodynamic forces on the monopile (the wave force term F_W in Eq. (2)) are discussed and compared, and a new approach is proposed for further study of the lowering operation. The draft of the monopile is assumed as fixed in this section for simplicity.

3.1 Morison's Formula Approximation (ME). For slender bodies with a D/L ratio (diameter/wavelength) less than 0.20, the empirical Morison's formula [11] is often used to calculate hydrodynamic forces. The effects of diffraction and radiation are considered insignificant in the slender-body approximation of hydrodynamic forces. The wave forces acting on the bottom of the monopile are negligible due to small wall thickness. The main contributions of the wave forces are normal to the monopile's central axis and Morison's formula is applied. The monopile is divided into strips and the forces on the entire slender structure are calculated using strip theory. The wave forces $f_{w,s}$ per unit length on each strip of a moving circular cylinder normal to the member can be determined using Morison's formula as follows [20]:

$$f_{w,s} = \rho_w C_M \frac{\pi D^2}{4} \ddot{\zeta}_s - \rho_w C_A \frac{\pi D^2}{4} \ddot{x}_s + \frac{1}{2} \rho_w C_D D |\dot{\zeta}_s - \dot{x}_s| \cdot (\dot{\zeta}_s - \dot{x}_s) \quad (4)$$

where $\ddot{\zeta}_s$ and $\dot{\zeta}_s$ are fluid particle acceleration and velocity at the center of the strip, respectively; \ddot{x}_s and \dot{x}_s are the acceleration and velocity at the center of the strip due to the body motions; D is the outer diameter of the member; and C_M , C_A , and C_D are the mass, added mass, and quadratic drag force coefficients, respectively. The distributed wave forces $f_{w,s}$ are integrated along the monopile to obtain the total wave forces and moments, F_W to solve the equations of motion in Eq. (2).

The first term in the equation is the wave excitation force, including the diffraction and Froude–Krylov (FK) force. The second-term is the inertial term and the third term is the quadratic drag term. The added mass coefficient for each strip is constant and is independent of wave frequency. The wave excitation force is calculated based on the added mass coefficient. Therefore, it is important to choose proper coefficients for different strips along the monopile to provide accurate added mass and excitation force for the entire structure. The hydrodynamic coefficients of the bottomless monopile from different submergences were investigated using the panel method in WAMIT. The results were 3D hydrodynamic added mass of the entire submerged part. However, to use strip theory and Morison's formula, the two-dimensional (2D) added mass coefficients were obtained by evaluating the 3D coefficients with different submerged lengths. The following added mass coefficients are therefore applied in the Morison's formula for different strips, and the strip size was chosen as 1 m

$$C_a = \begin{cases} 1.0 & (\Delta z < 2m) \\ 1.6 & (2m \leq \Delta z < 5m) \\ 1.95 & (5m \leq \Delta z) \end{cases} \quad (5)$$

where Δz is the distance from the considered strip to the bottom of the monopile. For the strips close to the bottom of the monopile, the added mass coefficients are approximately 1.0, whereas for strips located further away from the bottom, the coefficients are close to 2.0 because the wall thickness is small compared with the diameter, and the water trapped inside the monopile follows the motions of the structure.

On the other hand, the 3D added mass at different submergences could be recalculated using the 2D added mass coefficients. Figure 3 compares the total added mass for the monopile using the 2D added mass coefficients from Eq. (5) with those directly

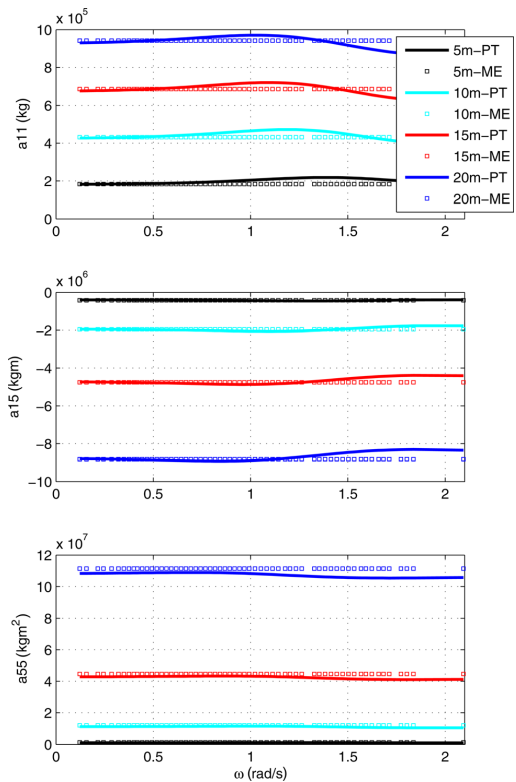


Fig. 3 Added mass of the MP at different drafts (refer to the point of MP at the mean free surface)

calculated from the panel method. Good agreement is obtained using the two methods for wave frequency smaller than 1.5 rad/s while the 2D coefficients overpredict the added mass for higher frequencies. For conditions with wave frequencies larger than 1.5 rad/s, the D/L ratio is larger than 0.2, and Morison's formula is no longer applicable.

The excitation forces calculated using the 2D added mass coefficients are also compared with those obtained directly from panel method (see Fig. 4). Good agreement is observed for wave frequencies less than 1.5 rad/s. Therefore, Morison's formula with selected 2D added mass coefficients appears to be reasonable for wave conditions with frequencies less than 1.5 rad/s. The drag coefficient C_D is a function of both the KC and Re numbers. For the monopile model, the KC number is relatively small, and the inertia force is dominant over the drag forces. Therefore, different values of C_D have limited effects on the responses except near the natural frequency. Therefore, we used the constant value, $C_D = 0.7$ for all submerged strips, which is a reasonable value for the current KC and Re range. More accurate C_D values could be obtained from full viscous-flow computation or well-designed experiments, which are beyond the scope of this paper.

3.2 Potential Theory (PT) With Viscous Damping. As pointed out, Morison's formula is based on the slender body assumption when the effects of diffraction and radiation are insignificant. However, with the increased diameter of an offshore monopile, the applicability of Morison's formula becomes questionable, especially in relatively short wave conditions in which the diameter of the structure is close to one-fifth of the wavelength. In such cases,

the diffraction and radiation of the monopile might be important. Thus, in addition to the viscous damping, it is important to examine the effects of the potential damping on the responses of the monopile. The second method uses the hydrodynamic coefficients and excitation forces from potential theory to analyze the responses of the monopile. This method can be used to check the validity of the Morison's formula approximation. However, one should bear in mind that the 3D coefficients and forces from potential theory are only applicable for a fixed draft when the motions of the monopile are small, and they fail to apply to the continuous lowering case due to the large change of position in the vertical direction. The added mass and damping as well as the excitation forces from potential theory with different drafts are shown in Figs. 3–5, respectively.

3.3 Morison's Formula Plus Potential Damping (ME + RT).

As discussed previously, Morison's formula does not account for the radiation and diffraction of the structure, and the coefficients from potential theory cannot be applied in the nonstationary case with time-varying draft of the structure. Therefore, a third method is proposed to address the limitations. The idea is to use Morison's formula to calculate the excitation forces, account for the added mass and quadratic drag coefficients using strip theory, and meanwhile include the potential damping. Because the goal is to calculate the nonstationary lowering process, time-domain simulations are required. Potential theory provides the frequency-dependent added mass and damping coefficients, and the retardation function is computed using a transform of the frequency-dependent added mass and damping to be used in the time-domain, with reference to the following equation:

$$h(\tau) = \frac{2}{\pi} \int_0^\infty c(\omega) \cos(\omega\tau) d\omega = -\frac{2}{\pi} \int_0^\infty \omega a(\omega) \sin(\omega\tau) d\omega \quad (6)$$

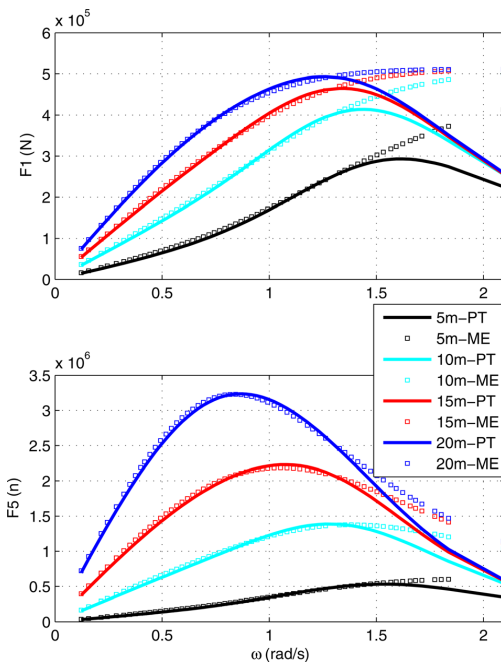


Fig. 4 Excitation force of the MP at different drafts (refer to the point of MP at the mean free surface)

The frequency-dependent added mass $a(\omega)$ and damping $c(\omega)$ also can be derived from the retardation function

$$\begin{aligned} a(\omega) &= -\frac{1}{\omega} \int_0^\infty h(\tau) \sin(\omega\tau) d\tau \\ c(\omega) &= \int_0^\infty h(\tau) \cos(\omega\tau) d\tau \end{aligned} \quad (7)$$

The relationships in Eq. (7) between the frequency-dependent added mass and damping are known as the Kramers–Kronig relationships. Either frequency-dependent added mass or frequency-dependent damping is required to calculate the retardation function. In the numerical program, frequency-dependent damping is used for calculating the retardation functions. The radiation force in the time-domain is thus formulated as a convolution integral formulation representing the memory effect [21].

The retardation forces on the monopile corresponding to a given draft in the time-domain simulations are added to the equations of motion. If we discretize the retardation function into $(N+1)$ values with a time interval $\Delta\tau$, the radiation force term in the steady-state (fixed draft) condition can be written as follows:

$$\mathbf{F}_{\text{RF}}^S(t) = \int_0^t \mathbf{h}(\tau) \dot{\mathbf{x}}_r(t-\tau) d\tau = \sum_{n=0}^N \mathbf{h}(n \cdot \Delta\tau) \cdot \dot{\mathbf{x}}_r(t - n \cdot \Delta\tau) \cdot \Delta\tau \quad (8)$$

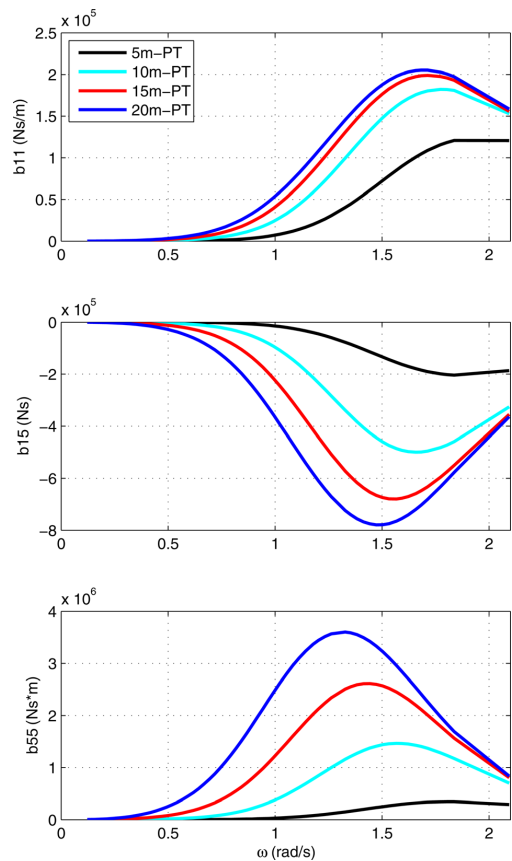


Fig. 5 Potential damping coefficients of the MP at different drafts (refer to the point of MP at the mean free surface)

Table 2 Three methods used to calculate the hydrodynamic forces on the monopile

Method	ME	PT	ME + RT
Added mass	2D C_A coefficient	Potential theory $A(\omega)$	2D C_A coefficient
Potential damping	0	Potential theory $B(\omega)$	Potential theory $B(\omega)$
Excitation force	2D C_M coefficient	Potential theory $F(\omega)$	2D C_M coefficient
Viscous damping	C_q coefficient	C_q coefficient	C_q coefficient

where $\mathbf{F}_{\text{RF}}^S(t)$ is the radiation force in the steady-state condition corresponding to a fixed draft. The retardation function \mathbf{h} depends only on the time variable τ in the steady-state condition. $\dot{\mathbf{x}}_r$ is the velocity of the structure at the reference point, which is located on the mean free surface in the numerical model.

In this paper the methods using Morison's formula and potential theory are, respectively, abbreviated as ME and PT, and the method with correction from the retardation function is referred to as ME + RT for convenience.

3.4 Comparisons Among Three Methods: ME, PT, and ME + RT. The three methods discussed above are summarized in Table 2, in which different hydrodynamic terms are listed. As mentioned, Morison's formula uses 2D coefficients tuned for different strips according to the results from the potential theory. The proposed method ME + RT is expected to be validated by the method PT in which all of the required coefficients are obtained from the potential theory. The same viscous damping coefficients were used for all three methods.

To compare the different methods and validate the proposed method, time-domain simulations were carried out. The draft of the monopile was set as a constant of 20 m such that the steady-state coefficients corresponding to 20 m draft were applied in the proposed method ME + RT. The frequency-dependent added mass and damping calculated in the frequency domain were converted into retardation functions using Eq. (6). The time-domain simulations were performed using the SIMO program [22] in which the Morison's formula force on the monopile and the wave forces on the vessel can be calculated. However, the retardation function term on the monopile was calculated separately using an external

dynamic link library (DLL). The DLL calculates the radiation forces based on the velocities from the previous time steps and returns this term to SIMO, which solves the responses of the system. The simulations in irregular waves were studied using JONSWAP spectrum [23]. To simplify the comparison, only linear forces and linear wave theory were applied. Due to the symmetry of the circular cylinder, only one wave direction of 0 deg (following sea condition) was studied.

Figures 6 and 7, respectively, compare the response spectra of surge and pitch motions of the monopile in two different irregular wave conditions. The crane tip is assumed as fixed. A significant drop in the response can be observed after adding the potential damping to Morison's formula when $T_p = 5$ s, which is close to the rotational resonance natural period. As T_p is increased to 8 s, two peaks are observed: one corresponds to the wave frequency and the other peak corresponds to the rotational natural period. The influences of potential damping on the peaks at wave frequency are less than those at the resonance period, which occurs because the diffraction and radiation from the monopile decrease with decreasing frequency. The responses using ME + RT and PT with viscous damping are generally quite similar except for the peak of the pitch motion near the rotational resonance frequency when $T_p = 5$ s. This observation is likely due to the differences between the added mass matrix and excitation forces using 2D coefficients and the 3D values from the panel method. Nevertheless, the method of ME + RT shows reasonable accuracy in the responses of the monopile.

Figures 8 and 9 again compare the response spectra from the three different methods with use of the floating installation vessel. In this case, the crane tip moves with the vessel and the motions

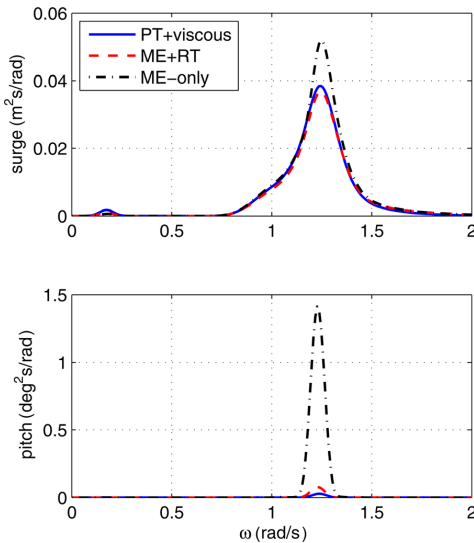


Fig. 6 Response spectra of MP in irregular waves with $H_s = 2.0$ m, $T_p = 5$ s, and $\text{Dir} = 0$ deg (fixed crane tip, FFT, up to $z = 0$)

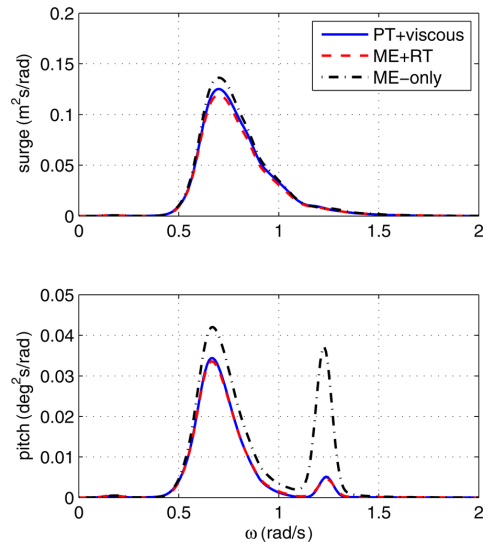


Fig. 7 Response spectra of MP in irregular waves with $H_s = 2.0$ m, $T_p = 8$ s, and $\text{Dir} = 0$ deg (fixed crane tip, FFT, up to $z = 0$)

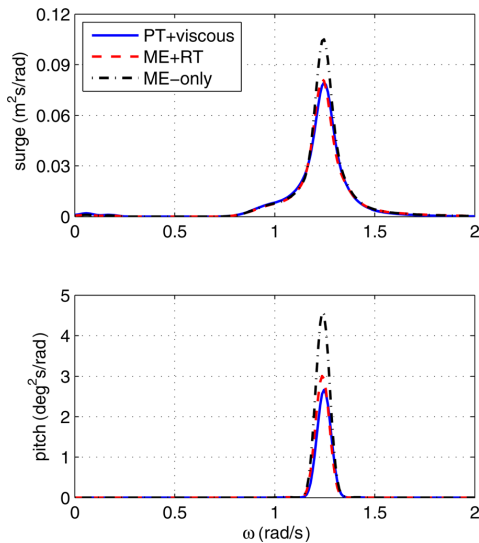


Fig. 8 Response spectra of MP in irregular waves with $H_s = 2.0$ m, $T_p = 5$ s, and $\text{Dir} = 0$ deg (floating crane vessel, FFT, up to $z = 0$)

of the monopile increase compared with those when the vessel is fixed. The decrease of the responses also can be observed after implementing the retardation functions in Morison's formula. However, the decreases of the responses are much smaller compared with those in the cases with a fixed vessel, especially if the wave period is relatively long, because the vessel-induced motions are not affected by the potential damping of the monopile. The results from ME + RT are thus validated by the potential theory method plus viscous damping.

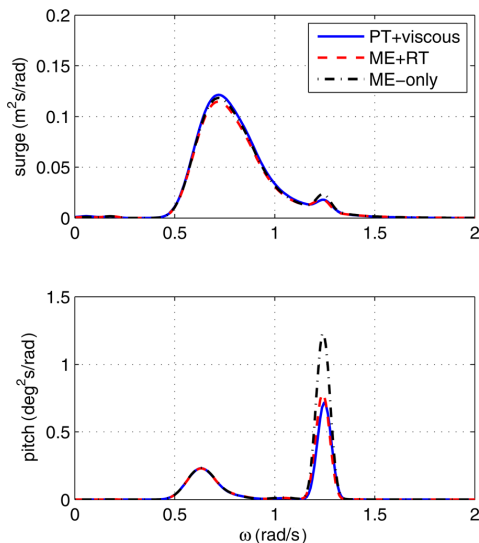


Fig. 9 Response spectra of MP in irregular waves with $H_s = 2.0$ m, $T_p = 8$ s, and $\text{Dir} = 0$ deg (floating crane vessel, FFT, up to $z = 0$)

3.5 Nonlinear Effects. The natural period of the monopile pendulum motions is rather long. As a result, the difference-frequency wave loads might provide great contributions to the low-frequency resonant responses, and hence must be included in the numerical methods for reliable dynamic analysis. Second-order wave loading has been calculated primarily via the second-order potential theory, which is computationally intensive and costly. However, for a simple slender body, the slender body approximation can be applied to consider nonlinear effects. The second-order forces on a slender body have been widely studied, i.e., in Refs. [14], [17], and [24]. The method is based on the assumptions that the structure is slender compared with the wavelength and that the water surface profile is unaffected by the presence of the structure. The current approximation is the most suitable for the case in which the inertia force is dominant compared with the drag force. In the slender-body approximation, the second-order difference-frequency inertia force is due to the axial divergence correction and fluctuation of the free surface. If the body is free to move in the waves, the instantaneous positions of the body also contribute to the second-order forces [17]. In this study, nonlinear effects due to the instantaneous free surface and the instantaneous body positions are taken into consideration, but the effects from nonlinear waves are not discussed.

For the nonlinear force and motion calculations in the time-domain, the second-order forces can be evaluated at each time step and in each strip for instantaneous body positions and integrated up to the instantaneous free surface. Next, the equation of motion can be integrated for the following time step. Figure 10 compares the results using (1) the linear ME + RT method with forces integrated up to the mean free surface $z = 0$, (2) the linear ME + RT with forces integrated up to the instantaneous free surface $z = \zeta$, and (3) the nonlinear slender-body approximation considering both instantaneous free surface and body positions. The potential damping is included in all three methods by implementing the retardation function in the time-domain. The monopile pendulum resonance motions are excited by integrating the forces up to the instantaneous free surface. The pitch motion at the rotational resonance is also greatly increased because the wave forces increase from the instantaneous free surface effects. The influences from the instantaneous positions of the structure also can be

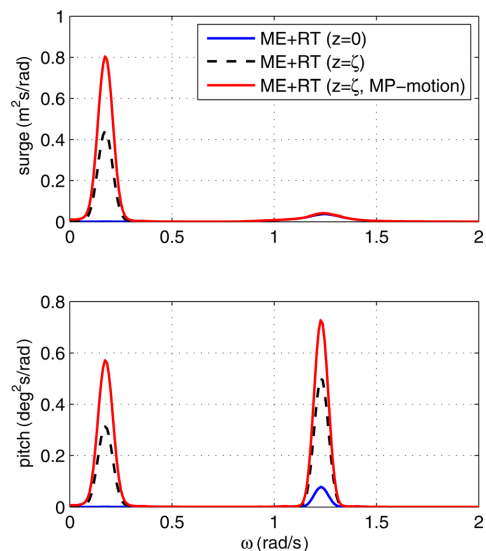


Fig. 10 Response spectra of MP in irregular waves with $H_s = 2.0$ m, $T_p = 5$ s, and $\text{Dir} = 0$ deg (fixed crane)

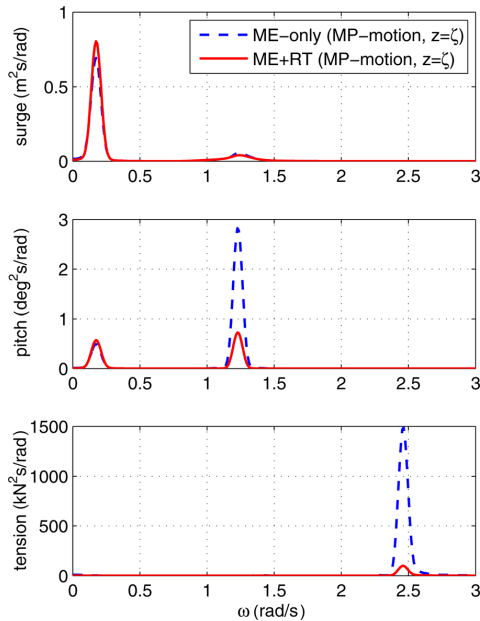


Fig. 11 Response spectra of MP in irregular waves with $H_s = 2.0$ m, $T_p = 5$ s, and $\text{Dir} = 0$ deg (fixed crane, cosine method, up to $z = \zeta$)

observed in the figure in which the motions at both resonance frequencies are amplified compared with those of the first two methods. It is therefore crucial to include the nonlinear effects in the current lifting system.

Figure 11 compares the effects from the potential damping if using the nonlinear equations to calculate the forces on the monopile. The results are consistent with those observed previously using the linear Morison's formula in which the peaks near the rotational natural frequency are significantly reduced. However, there are negligible effects on the pendulum motions due to minimal radiation from the monopile at such a low resonance frequency.

4 Hydrodynamic Modeling on the Monopile With Changing Draft

Section 3 showed that the potential damping could become important when the resonance frequency of the system is in the wave frequency range. The method used to include the potential damping at a fixed draft adds the retardation function corresponding to the given draft in the time-domain simulations. However, during the entire lowering operation, the draft of the monopile changes consistently and the steady-state condition is replaced by nonlinear effects due to the large motions in the vertical direction. The excitation and radiation forces also vary with time and correspond to the instantaneous draft. As mentioned previously, the second-order potential theory is not applicable in this situation because the quadratic transfer functions are calculated given a fixed draft and cannot be used when the structure undergoes large motions. However, Morison's formula calculates the excitation force using a 2D mass coefficient, and thus, the excitation force can be calculated based on the instantaneous draft and the second-order effects can be accounted for by considering the instantaneous free surface and instantaneous body motion effects.

Although the lowering operation is a nonstationary process, by assuming a small lowering speed, the entire lowering process can

be divided into stepwise steady-state conditions. Thus, the parameters from the steady-state conditions can be applied to the nonstationary process. The retardation function in this situation depends on both τ and the draft of the structure d . The reference point of the retardation function is always located on the mean free surface in the global coordinates, but changes in the body-fixed coordinates due to the change of draft d . Therefore, the retardation convolution term in the time-domain equation for the steady-state condition (Eq. (8)) must be modified to represent the memory effects in the nonstationary process (see the following equation):

$$\begin{aligned} \mathbf{F}_{\text{RF}}^T(t) &= \int_0^t \mathbf{h}(d, \tau) \dot{\mathbf{x}}_r(d, t - \tau) d\tau \\ &= \sum_{n=0}^N \mathbf{h}_{d(t-n\Delta\tau)}(n \cdot \Delta\tau) \cdot \dot{\mathbf{x}}_r(d(t-n\Delta\tau))(t - n \cdot \Delta\tau) \cdot \Delta\tau \quad (9) \end{aligned}$$

where $d_{(t-n\Delta\tau)}$ is the draft at time instance $(t - n \cdot \Delta\tau)$; $\mathbf{h}_{d(t-n\Delta\tau)}$ is the retardation variable at draft $d_{(t-n\Delta\tau)}$; and $\dot{\mathbf{x}}_r(d_{(t-n\Delta\tau)})$ is the velocity of the reference point when the draft is equal to $d_{(t-n\Delta\tau)}$.

In the time-domain simulation, the following approach is proposed to obtain the radiation force with time-varying draft during the lowering process. The retardation functions at several drafts along the monopile were precalculated based on the panel method. Linear interpolations are subsequently applied between retardation functions at those precalculated drafts to obtain the retardation variables in Eq. (9) at any draft during the lowering process. The interpolation of the retardation functions in the time-domain is equivalent to the interpolation of the frequency-dependent coefficients between different drafts. The proposed method is based on the following assumptions:

- (1) The lowering speed of the monopile should be small and the stepwise steady-state conditions can be used to represent the continuous lowering process.
- (2) The retardation function for the structure should decay rapidly such that the system will only "remember" the effects within a small change of the draft, in this manner the assumption is consistent with the assumption of the stepwise steady-state condition.
- (3) Linear interpolation of the retardation functions at predefined drafts can be applied to calculate the values at instantaneous drafts.

The winch speed for the lifting system is 0.05 m/s, and it takes 20 s to increase the draft by 1 m, which is equivalent to approximately four cycles with a wave period of 5 s. Thus, assumption (1) can be deemed reasonable because the change in the draft is sufficiently slow to represent the entire lowering process as stepwise steady-state conditions. The retardation functions of the monopile with different drafts are shown in Fig. 12. It can be observed that the values approach zero after 10 s. Thus, a cutoff of 10 s is sufficient to provide accurate potential damping for the dynamic system. Therefore, the system will only remember the effects within 10 s which corresponds to a draft change of 0.5 m. To validate assumption (3), as an example the interpolated retardation function at a draft of 7 m is compared with the values directly obtained from panel method (see Fig. 13). The interpolated values were calculated from drafts of 5 m and 10 m. Good agreements between the two curves can be observed. Therefore, the assumptions are reasonable for the presented lifting system and the proposed method is applied for further analysis.

5 Time-Domain Analysis of the Lowering Operation

Time-domain simulations of the entire lowering operation were performed. The winch was started at 200 s with a constant speed of 0.05 m/s and was stopped at 700 s. Thus, the total lowering length was 25 m. The environmental conditions were $H_s = 2.5$ m with T_p varying from 5 s to 12 s, thus covering a realistic range. At

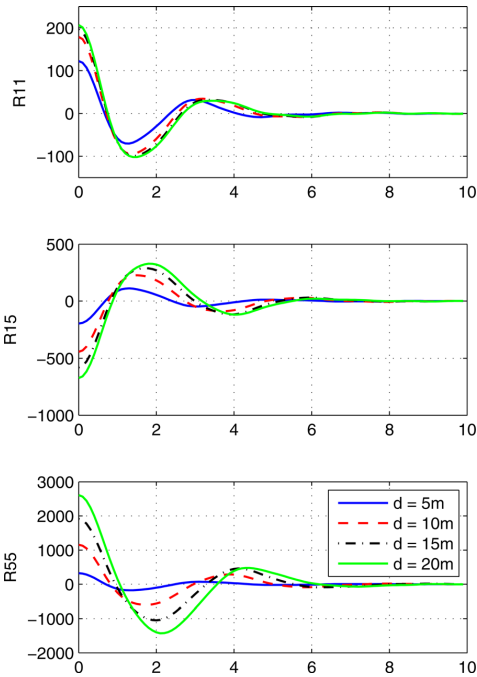


Fig. 12 Retardation functions at different drafts

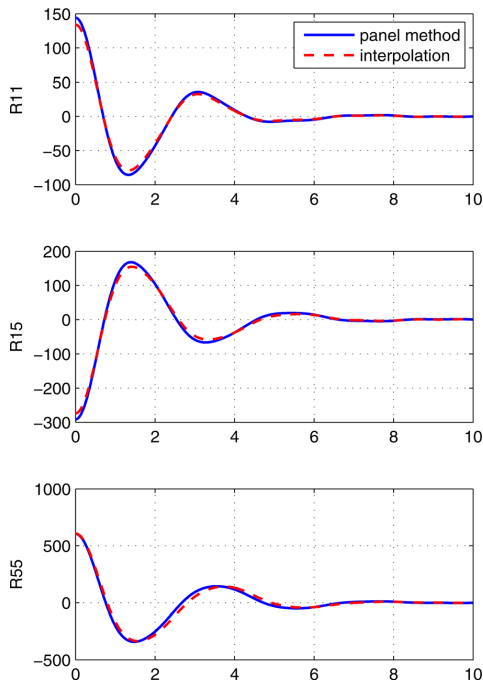


Fig. 13 Comparison of the retardation functions at a draft of 7 m

each combination of H_s and T_p , irregular waves were modeled by JONSWAP spectrum. To account for the variability of stochastic waves, 20 realizations of irregular waves were generated at each of the environmental conditions using different seeds.

Step-by-step integration methods were applied to calculate the responses of the lifting system using an iterative routine. The equations of motion were solved using Newmark-beta numerical integration ($\beta = 0.1667$ and $\alpha = 0.50$) with a time step of 0.01 s. The first-order wave forces of the floating vessel were pregenerated using the fast Fourier transformation (FFT) at the mean position. The forces on the monopile were calculated using the external DLL to account for the changing draft radiation forces. Second-order forces on the monopile were included by accounting for the effects from the instantaneous free surface and body positions. The responses of the lifting system were analyzed using both fixed and floating vessels, and the results and discussions are presented in Secs. 5.1 and 5.2.

5.1 Responses Using a Fixed Vessel. Figures 14 and 15 show the response time history of the monopile during lowering at two wave conditions. The responses in the figures include the motions of the monopile in surge, heave, and pitch as well as the tension in the lift wire. The results using Morison's formula and accounting for potential damping by adding retardation functions (ME + RT) are compared with those obtained directly from Morison's formula (ME-only).

It can be observed that the motions of the monopile decrease significantly in short waves with $T_p = 5$ s with addition of potential damping, whereas the differences of the motions in long waves with $T_p = 12$ s are much less. In short periods, the radiation of the monopile provides relatively large potential damping to the system, and the radiation is minor in long waves as observed in Fig. 5. Due to a lack of potential damping, the responses by using Morison's formula might easily overestimate the responses of the lifting system. Although the surge and pitch motions in long waves are less sensitive to potential damping, the lift-wire tension shows a great reduction with the addition of potential damping due to the tension governed by the rotational resonance motion of the monopile, which corresponds to a period of around 5 s. At this period, the potential damping is able to damp the responses considerably.

The entire time series can be divided into two phases: the lowering phase (from 250 s when the monopile end tip enters the water up to 700 s when the winch stops) and the steady-state phase

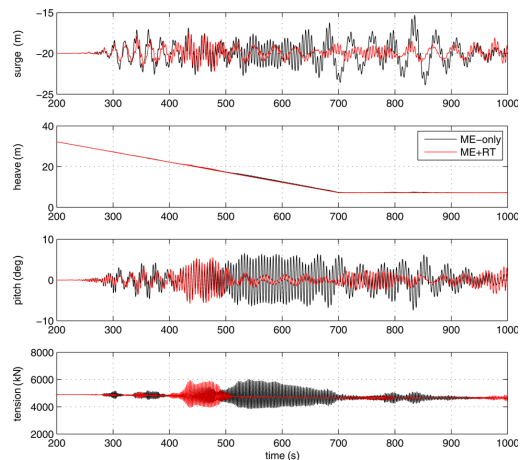


Fig. 14 Response time series of the entire lowering process (fixed vessel, $H_s = 2.5$ m, $T_p = 5$ s, and $\text{Dir} = 0$ deg)

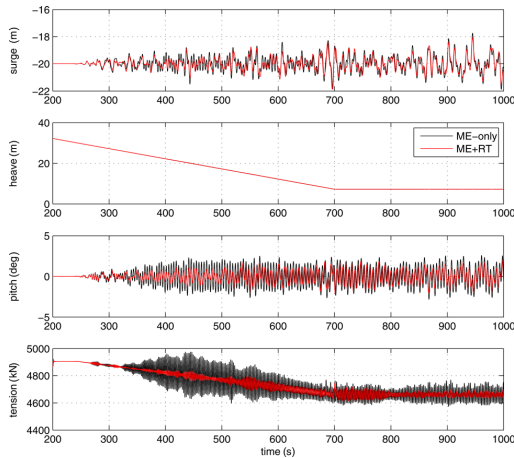


Fig. 15 Response time series of the entire lowering process (fixed vessel, $H_s = 2.5$ m, $T_p = 12$ s, and $\text{Dir} = 0$ deg)

(from 700 s until the end of the simulation). The draft of the monopile increases during the lowering phase and is stable in the second phase.

The response spectra for the lowering and steady-state phases can be obtained using a Fourier transformation of the time series. Figures 16 and 17, respectively, compare the response spectra at $T_p = 5$ s and $T_p = 12$ s for both the lowering and steady-state phases. When $T_p = 5$ s, the surge of the monopile contains two peaks at the rotational and pendulum resonance frequencies,

respectively. The pitch motion displays one main peak at the rotational resonance frequency. When $T_p = 12$ s, in addition to the peaks at the two resonance frequencies, the wave frequency peak governs the surge motion and contributes to the pitch motion of the monopile. By adding the potential damping in the time-domain simulations, the spectra peaks at the rotational resonance frequency are significantly reduced for both wave period conditions. Although little potential damping exists at the pendulum natural frequency, the responses at the pendulum resonance frequency are still affected. Because the pendulum motions are excited by the second-order forces due to the effects from instantaneous free surface and body motions, the second-order forces are therefore reduced when the first-order motions decrease with the addition of the potential damping. The reduction of the motion at the pendulum frequency can be observed in the spectra with $T_p = 5$ s, whereas little changes at this frequency are observed with $T_p = 12$ s due to smaller responses in this wave condition.

Similar trends are observed for both the lowering and steady-state phases, and the reduction of the peaks appears to be more significant in the lowering phase due to nonlinear effects. Moreover, the spectra in the lowering phase show a broader frequency range surrounding the peaks due to the variation in the natural periods of the lifting system. The peak frequency of the wire tension is observed to be twice that of rotational resonance peak, which means that one cycle of rotational motion induces two cycles of variations in the wire tension. The pendulum motion contributes little to the tension. Because the rotational resonance peaks are always reduced by adding potential damping in both short and long wave conditions, the wire tension can be reduced greatly.

The standard deviations (STDs) of the responses at various wave conditions are obtained, and Fig. 18 shows the STDs in the steady-state phases with varying irregular wave peak periods. Because the potential damping affects the responses at both

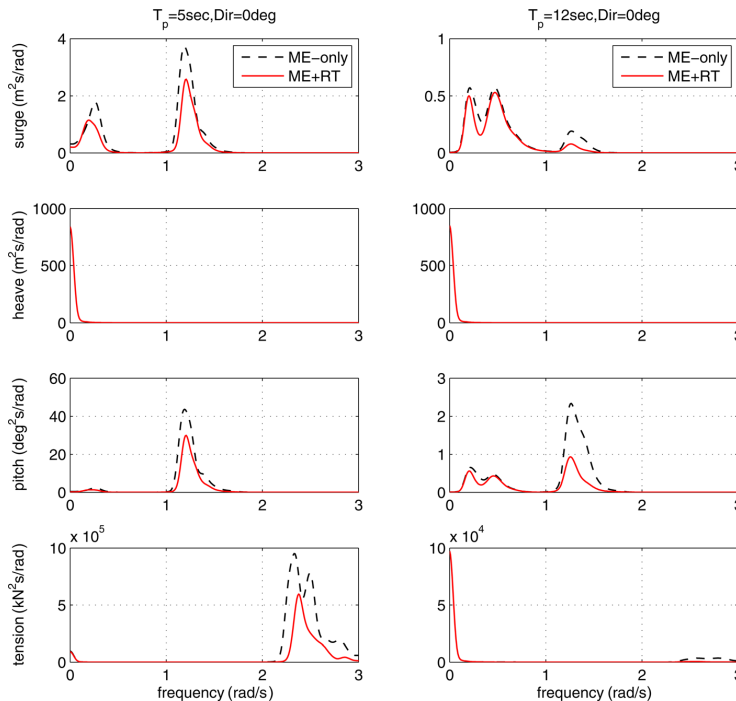


Fig. 16 Response spectra of the lowering phase (fixed vessel, $H_s = 2.5$ m)

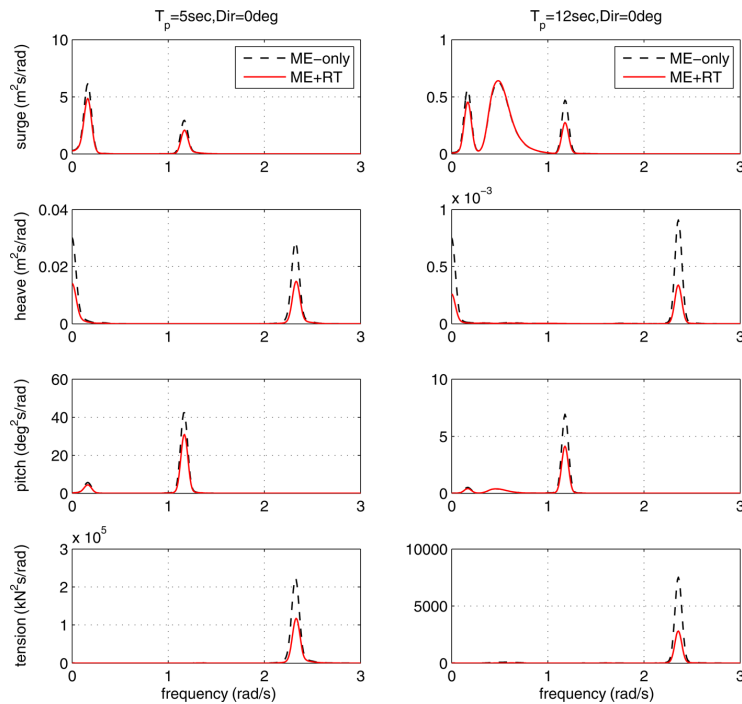


Fig. 17 Response spectra of the steady-state phase (fixed vessel, $H_s = 2.5$ m)

rotational and pendulum resonance frequencies, the STDs at two resonance frequencies are compared individually by filtering the response signals close to the resonance frequencies. The resonance motions at the rotational natural period decrease with T_p

because the wave peak period moves away from the natural period. The pendulum motions also decrease with T_p due to lesser second-order forces. The STD of motions obtained using ME-only and ME + RT is compared in the figure. The differences between

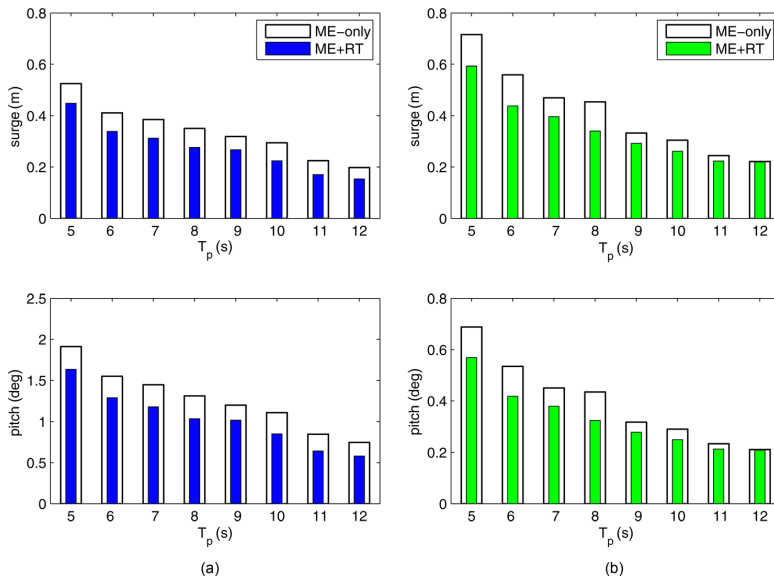


Fig. 18 STD of the responses in the steady-state phase using a fixed vessel ($H_s = 2.5$ m, Dir = 0 deg): (a) rotational resonance motion and (b) pendulum resonance motion

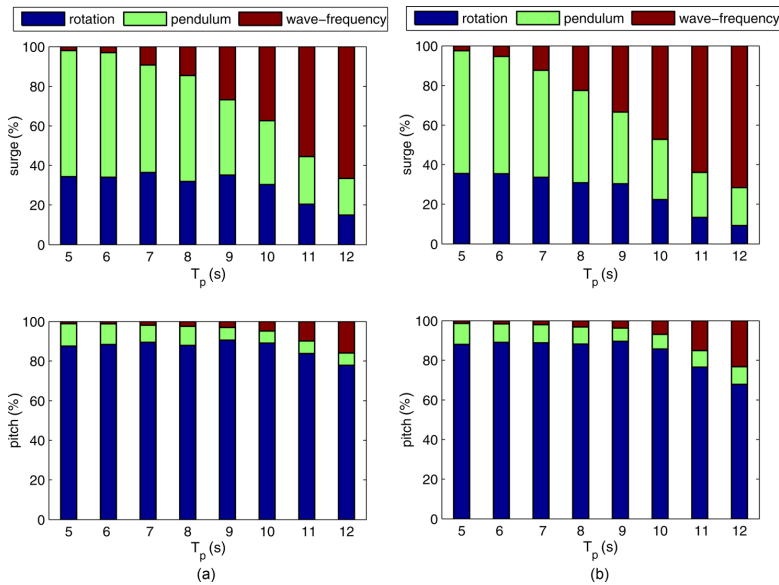


Fig. 19 Ratios of energies from different contributions using a fixed vessel ($H_s = 2.5$ m, $\text{Dir} = 0$ deg): (a) ME-only method and (b) ME + RT method

the two methods are generally smaller for the pendulum resonance motions, especially in long wave conditions. The differences decrease with T_p for both motions. Because the responses in long wave conditions using Morison's formula are already quite small, the potential damping can be ignored. However, Morison's formula can greatly overestimate the responses in short waves, especially if the wave frequency is close to the natural period of the rotational motion of the monopile. Thus, the potential damping should be taken into account in such cases to predict the responses more accurately during the operation.

In addition to the resonance motions at the two natural periods, the motions at the wave frequency also contribute to the total motions. To analyze the contributions from the three frequencies, the ratios between the variance (the square of STD) from each contribution and the total variance are calculated. This ratio represents the percentage of energy from motions at different frequencies contributed in the total energy of the motion. The ratios are shown in Fig. 19 for the fixed vessel case. It should be mentioned that the entire response time history is filtered and divided into three components: the motions at two resonance frequencies and the motions corresponding to the wave frequency, respectively. When T_p is small and close to the rotational resonance frequency, the wave loads excite the rotational resonance motion, and therefore the two contributions are mixed together. With increase in T_p , the third component separates from the resonance motions and also increases, especially for the surge motion. The rotational resonance motion always dominates the pitch motion of the monopile in all T_p conditions. The potential damping decreases the contributions from the rotational resonance motion and thus leads to the increase of contribution from the motions in the wave frequency.

5.2 Responses Using the Floating Installation Vessel.

When the floating installation vessel is applied, the responses of the monopile are affected by the motions of the vessel in irregular waves. Figure 20 shows the response spectra in the steady-state phase with wave direction $\text{Dir} = 0$ deg. Comparing Fig. 20 with

the responses using a fixed vessel in Fig. 17, the motions of the lifting system in both wave conditions increase because of the moving crane tip. The increases of the monopile response are relatively small with $T_p = 5$ s due to small vessel motions. In longer waves, the wave peak period moves closer to the natural period of the pitch, and the heave motion of the vessel and the vessel motions increase and influence the motions of the monopile in heave and pitch. The vessel motions also contribute significantly to the tension in the lift wire where the peak near the wave frequency in the spectra can be observed at $T_p = 12$ s. The vessel-induced responses are minimally affected by potential damping in long waves. The influences of potential damping on the total motions of the monopile are expected to be smaller compared with the fixed crane condition because the vessel considerably affects the monopile motions in long waves.

The STDs of the responses at various wave period conditions with use of floating vessel are shown in Fig. 21. The STDs are also given at two resonance motions to compare the effects of potential damping on different resonance motions. The effects from addition of potential damping on the monopile in the floating vessel case are observed to be similar to those of the case using a fixed vessel. The pendulum motions are nearly same in the two methods in long waves, whereas the rotational resonance motions can still be greatly reduced.

The ratios between the variance from three contributions and the variance of the total motions are shown in Fig. 22. Although only small changes occur for the ratios of the surge motion, significant differences can be observed in the pitch motions compared with those of the fixed vessel case in Fig. 18. The contribution from the motions in the wave frequency increases greatly using the floating vessel, especially in long waves due to the effects from the vessel motions. By adding potential damping, this contribution increases further because the rotational resonance motions are reduced by the potential damping, while the vessel-induced motions remain the same. The ratios of the pendulum motions appear to change little in both cases after adding potential damping.

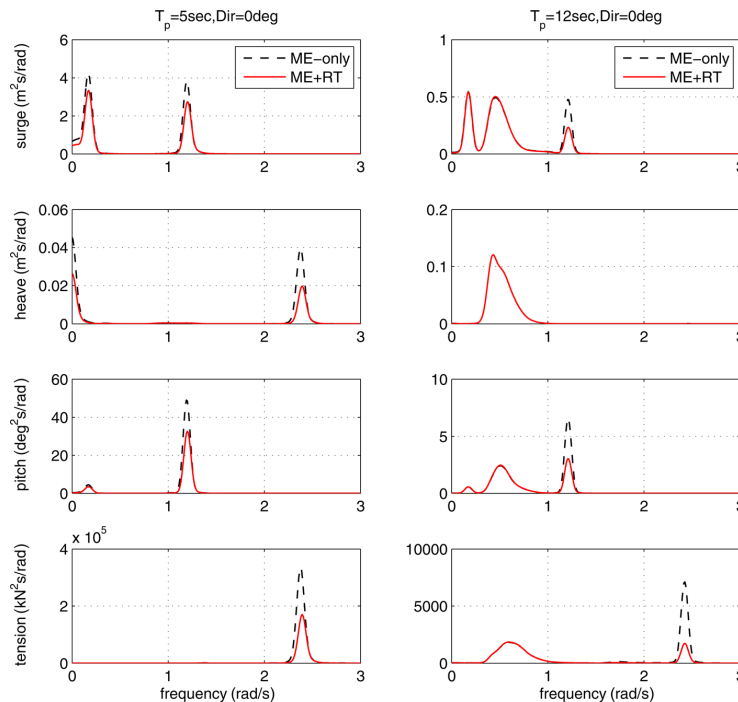


Fig. 20 Response spectra of the steady-state phase (floating vessel, $H_s = 2.5$ m)

6 Conclusions and Recommendations for Future Work

The current study examines the lowering operation of an off-shore monopile, and numerical studies are performed using different approaches. Due to the limitations of Morison's formula and the potential theory, a new approach is proposed in this paper to account for the potential damping during the lowering process of the monopile. It is concluded that the conventional pure Morison's formula could overestimate the responses of the lifting system, especially in relatively short waves, due to the exclusion of the wave potential damping. For installation of a large wind farm, the overestimation of responses might cause a great reduction in the weather window and thus a significant increase in costs. Therefore, the potential damping must be considered in the numerical model to more accurately estimate the responses.

The responses of the monopile lifting system were first studied at a fixed draft. By applying different methods to calculate the hydrodynamic forces on the monopile, it was found that Morison's formula overpredicts the responses of the lifting system due to the slender body assumption which neglects the diffraction and radiation of the structure. By including potential damping on the monopile in Morison's formula, the responses can be more accurately calculated. The importance of potential damping was validated by using conventional potential theory in the fixed draft case. Besides, the nonlinear effects were found to be considerable for resonant motions at low frequencies, and the effects from the instantaneous free surface and the instantaneous body motions should be accounted for in the time-domain simulations.

For analysis of the lowering process, a new approach was proposed based on reasonable assumptions to account for the potential damping by interpolating the retardation functions at various drafts. The retardation functions were calculated at predefined drafts assuming steady-state conditions. The numerical analysis was

performed by establishing an external DLL and implementing it in the SIMO software. The wave forces on the monopile were calculated during lowering using Morison's formula with consideration of nonlinear effects, and the radiation term was included at each time step.

The results of the time-domain simulations were analyzed using both fixed and floating installation vessels. The potential damping significantly reduced the responses at the monopile rotational natural frequency in both vessel cases and in both short and long waves. The influence on the pendulum motions was less important and can be neglected in long waves. When using the floating installation vessel, the motions of the vessel increase the responses of the monopile. The motions induced by the crane contribute greatly to the total motions of the monopile in long waves. The vessel-induced motions were found to be independent of the potential damping of the monopile. Therefore, when the crane tip motions further increase and the resonant motions are minor, the potential damping can be neglected. It should be mentioned that, the effect of potential damping was observed to be significant in this specific lifting system, and the effect may differ greatly if the natural periods of the lifting system are changed.

Although the proposed method provides more accurate results than the pure Morison's formula and implements the potential damping in the nonstationary lowering process, limitations do exist. The first limitation lies in the assumption that the lowering speed should be sufficiently low such that the entire lowering process can be divided into stepwise steady-state conditions. When increasing the lowering speed, the validity of the assumption is questionable. Therefore, validation with experiments or numerical tools that can address the nonstationary process should be applied in future work. Second, the excitation forces are calculated based on the slender body assumption using strip theory, and a more robust method should be studied for calculating the forces on a large volume structure during the lowering process. Moreover, the interactions between the monopile and the floating vessel need to

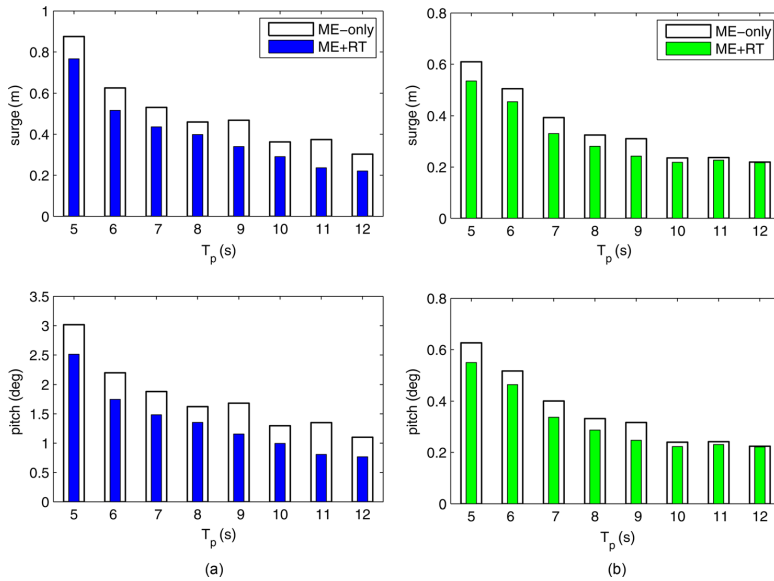


Fig. 21 STD of the responses in the steady-state phase using the floating vessel ($H_s = 2.5$ m, $\text{Dir} = 0$ deg): (a) rotational resonance motion and (b) pendulum resonance motion

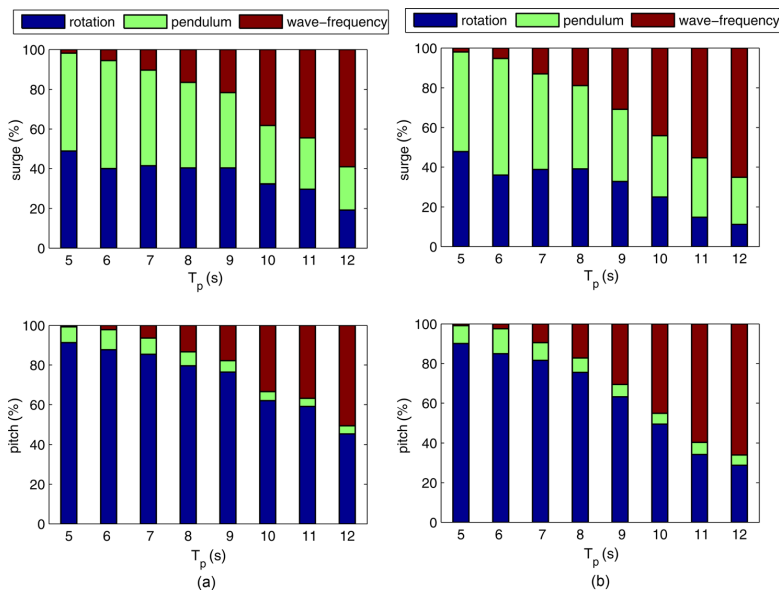


Fig. 22 Ratios of energies from different contributions using the floating vessel ($H_s = 2.5$ m, $\text{Dir} = 0$ deg): (a) ME-only method and (b) ME + RT method

be considered although they were excluded in the current model for simplicity.

Acknowledgment

Support for this work was provided by the Research Council of Norway granted through the Department of Marine Technology, Centre for Ships and Ocean Structures (CeSOS) and Centre for

Autonomous Marine Operations and Systems (AMOS), NTNU. The authors are grateful to Peter Chr. Sandvik from MARINTEK for valuable discussions.

References

- [1] Mukerji, P., 1988, "Hydrodynamic Responses of Derrick Vessels in Waves During Heavy Lift Operation," *20th Offshore Technology Conference*, Houston, TX, May 2–5.

- [2] van den Boom, H., Dekker, J., and Dallinga, R., 1988, "Computer Analysis of Heavy Lift Operations," *20th Offshore Technology Conference*, Houston, TX, May 2–5.
- [3] Baar, J., Pijfers, J., and Santen, J., 1992, "Hydromechanically Coupled Motions of a Crane Vessel and a Transport Barge," *24th Offshore Technology Conference*, Houston, TX, May 4–7.
- [4] Witz, J., 1995, "Parametric Excitation of Crane Loads in Moderate Sea States," *Ocean Eng.*, **22**(4), pp. 411–420.
- [5] Park, K., Cha, J., and Lee, K., 2011, "Dynamic Factor Analysis Considering Elastic Boom Effects in Heavy Lifting Operations," *Ocean Eng.*, **38**(10), pp. 1100–1113.
- [6] Molin, B., 2001, "On the Added Mass and Damping of Periodic Arrays of Fully or Partially Porous Disks," *J. Fluids Struct.*, **15**(2), pp. 275–290.
- [7] Sandvik, P. C., Solaas, F., and Nielsen, F. G., 2006, "Hydrodynamic Forces on Ventilated Structures," 16th International Offshore and Polar Engineering Conference, San Francisco, CA, May 28–June 2, pp. 54–58.
- [8] Næss, T., Havn, J., and Solaas, F., 2014, "On the Importance of Slamming During Installation of Structures With Large Suction Anchors," *Ocean Eng.*, **89**, pp. 99–112.
- [9] Sandvik, P., 2012, "Estimation of Extreme Response From Operations Involving Transients," 2nd Marine Operations Specialty Symposium, Singapore, Aug. 6–8.
- [10] Li, L., Gao, Z., Moan, T., and Ormberg, H., 2014, "Analysis of Lifting Operation of a Monopile for an Offshore Wind Turbine Considering Vessel Shielding Effects," *Mar. Struct.*, **39**, pp. 287–314.
- [11] Morison, J., Johnson, J., and Schaaf, S., 1950, "The Force Exerted by Surface Waves on Piles," *J. Pet. Technol.*, **2**(5), pp. 149–154.
- [12] Kim, M., and Ran, Z., 1994, "Responses of an Articulated Tower in Waves and Currents," *Int. J. Offshore Polar Eng.*, **4**(4), pp. 298–301.
- [13] Anam, I., and Røssset, J. E. M., 2004, "Slender-Body Approximations of Hydrodynamic Forces for Spar Platforms," *Int. J. Offshore Polar Eng.*, **14**(2).
- [14] Rainey, R., 1989, "A New Equation for Calculating Wave Loads on Offshore Structures," *J. Fluid Mech.*, **204**, pp. 295–324.
- [15] Kim, M.-H., and Yue, D. K., 1989, "The Complete Second-Order Diffraction Solution for an Axisymmetric Body Part I. Monochromatic Incident Waves," *J. Fluid Mech.*, **200**, pp. 235–264.
- [16] Taylor, R. E., Rainey, R., and Dai, D., 1992, "Non-Linear Hydrodynamic Analysis of TLP's in Extreme Waves: Slender Body and Diffraction Theories Compared," International Conference on the Behaviour of Offshore Structures, London, UK, July 7–10, pp. 569–584.
- [17] Kim, M., and Chen, W., 1994, "Slender-Body Approximation for Slowly-Varying Wave Loads in Multi-Directional Waves," *Appl. Ocean Res.*, **16**(3), pp. 141–163.
- [18] Golightly, C., 2014, "Tilting of Monopiles Long, Heavy and Stiff; Pushed Beyond Their Limits," Technical Note, Ground Engineering.
- [19] Lee, C., 1995, *WAMIT Theory Manual*, Massachusetts Institute of Technology, Department of Ocean Engineering, Cambridge, MA.
- [20] Faltinsen, O., 1990, *Sea Loads on Ships and Ocean Structures*, Cambridge University, Cambridge, UK.
- [21] Cummins, W., 1962, "The Impulse Response Function and Ship Motions," *Schiffstechnik*, **9**(47), pp. 101–109.
- [22] MARINTEK, 2012, *SIMO Theory Manual Version 4.0*, Trondheim, Norway.
- [23] DNV, 2010, Recommended Practice DNV-RP-C205, Environmental Conditions and Environmental Loads.
- [24] Isaacson, M. D. S. Q., 1979, "Nonlinear Inertia Forces on Bodies," *J. Waterw., Port Coastal Ocean Div.*, **105**(3), pp. 213–227.

A.5 Paper 5

Paper 5:

Operability analysis of Monopile Lowering Operation Using Different Numerical Approaches.

Authors: Lin Li, Zhen Gao, Torgeir Moan

Accepted for publication in *International Journal of Offshore and Polar Engineering*, June 2016

Operability analysis of monopile lowering operation using different numerical approaches

Lin Li

Centre for Ships and Ocean Structures (CeSOS), Norwegian University of Science and Technology, Trondheim, Norway

Zhen Gao, Torgeir Moan

Centre for Autonomous Marine Operations and Systems (AMOS), Norwegian University of Science and Technology, Trondheim, Norway

Offshore installation operations require careful planning in the design phase to minimize associated risks. This study addresses numerical modelling and time-domain simulations of the lowering operation during installation of a monopile (MP) for offshore wind turbine (OWT) using a heavy lift vessel (HLV). The purpose is to apply different numerical approaches to obtain the allowable sea states and to assess the operability. Four critical factors regarding the numerical modelling approaches for the coupled HLV-MP lowering process are studied. Those factors include wave short crestedness, shielding effects from the HLV, radiation damping from MP and the nonstationarity of the process. The influence of each factor on the allowable sea states and the operability are assessed. A large number of time-domain simulations are performed considering random waves to derive the allowable sea states. The results indicate that the radiation damping from the MP is secondary while it is essential to consider the other features. The study can be used as a reference for numerical modelling of relevant offshore operations.

KEY WORDS: MP installation, allowable sea states, heavy lift vessel, wave spreading, shielding effects, nonstationary process

INTRODUCTION

Installation of OWT components is more challenging than of land-based wind turbines. It was estimated that the installation and assembly of offshore wind turbines make up 20% of the capital costs compared with around 6% for land-based wind turbines (Moné et al., 2015). Because of the low profit margin of the offshore wind industry, it is essential to reduce the installation costs by improving the methodology during design and planning phase.

Because of the structural simplicity and low manufacturing expenses, monopiles (MPs) are the most preferable bottom-fixed foundations for offshore wind turbines in shallow water (EWEA, 2014). The installation of MP consists of several steps. After arriving the offshore site, the MPs are upended to a vertical position, then lowered through the wave zone so that it stands vertically on the seabed. A hydraulic hammer is used to drive it into the seabed to a predetermined depth. Although MPs are easy to install compared to other foundations, the installations have been carried out with various success because the challenges have not been taken seriously enough (Thomsen, 2011). Therefore, it is of great importance to evaluate and improve the allowable sea states by considering each activity during the operation. More importantly, the allowable sea states for a single operation would affect the installation efficiency of the entire wind farm. For this reason, accurate numerical models are required.

There are generally two types of vessels for installation of monopiles: the jack-ups and the floating crane vessels. A jack-up vessel provides a stable working platform for the lifting and piling operations. However, the installation and retrieval of legs of the jack-ups are time-consuming and weather sensitive. Compared to jack-ups, floating vessels have more flexibility for offshore operations and are effective in mass installations of a wind farm due to fast transit between foundations. Floating vessels have been used to install monopiles for several large offshore wind farms, e.g., Sheringham Shoal and Greater Gabbard wind farms. Hence, the potential of reducing installation costs by using floating installation vessel is huge.

Very few studies on the installation of MPs have been published. Sarkar and Gudmestad (2013) suggested a method to install MPs by isolating the installation operations from the motion of the floating vessel using a pre-installed submerged support structure. The responses of a coupled vessel-MP system during the lowering process of the MP were studied by Li et al. (2013), where sensitivity studies regarding the mechanical couplings and the vessel type were performed. Furthermore, they introduced a method to account for the shielding effects from the floating installation vessel during the entire lowering operation of the MP (Li et al., 2014). It was concluded that the shielding effects can greatly reduce the responses in short waves. This method was further studied to compare the performance of two lifting systems i.e., the lifting of a monopile and a jacket wind turbine foundation (Li et al., 2015a). Moreover, the importance of radiation damping of the MP during the nonstationary lowering operation were examined by Li et al. (2015c). A new approach was proposed to

implement the radiation damping effects into the time-domain simulation of the nonstationary lowering process.

The previous work aimed at developing more accurate numerical methods to simulate the lifting operation of the MP, with special focus on the nonstationary process. In those studies, some simplifications were made in the numerical model, e.g., the hydrodynamic forces on the vessel were simplified by only considering the first order wave excitation forces in Li et al. (2013, 2014, 2015c), and the hydrodynamic interaction between the floating installation vessel and the MP was not included when studying the influences of MP radiation damping in Li et al. (2015c). Wave short-crestedness is another factor of influence for lifting operations (DNV, 2014) which has not been considered in the mentioned references. Moreover, the previous study did not provide the allowable sea states based on their numerical approaches. The allowable sea states are essential for planning the operations.

In addition, some simplified approaches are often applied during numerical analysis of lifting operations, e.g., excluding the hydrodynamic interaction between submerged structures, and using steady-state analysis to represent nonstationary or transient operation activities. Those simplifications introduce uncertainties. However, the influences of the simplifications on the allowable sea states and the operability have not been quantified. Over-conservative results may increase the costs of the operation while non-conservative results may increase the operational risk.

This paper is an extension of the previous work on MP lowering operation focusing on numerical studies. The purpose is to use different numerical approaches to evaluate the allowable sea states and quantify their influences on the operability. The numerical approaches in this paper deal with the following issues: 1) the accuracy to use Morison's formula to calculate the hydrodynamic forces on the MP; 2) the effect from hydrodynamic interaction between the installation vessel and the MP on the lowering operation; 3) the feasibility to use simplified steady-state simulations for the nonstationary lowering process; 4) the influence of short-crestedness for such operation.

First, a general description of the operation and the numerical model is given. Second, the dynamic modelling approach including different numerical approaches are presented. Third, the operational criteria for the MP lowering operation are provided followed by discussion of the results. Finally, conclusions and recommendations regarding practical implementation are given.

MODELLING OF THE LOWERING SYSTEM

System Components

The system for MP lowering operation consists of a floating heavy lift vessel (HLV) and the MP substructure and they are coupled through the crane lift wire. A gripper device is placed on the deck of the vessel to avoid extreme motions of the MP during the operation. The gripper is normally composed of several hydraulic cylinders, and the details refer to Li et al. (2016).

During the lowering operation, there is an initial gap between the hydraulic cylinder and the wall of the MP. The initial gap is chosen based on the stroke length of the hydraulic cylinders as well as the motions of the MP during lowering operation to avoid large contact forces that could cause structural damage on the hydraulic cylinders. The system set-up for the MP lowering process is illustrated in Fig. 1.

The main particulars of the system components are shown in Table 1. After the MP being lowered down to the seabed, the gripper is then closed and the hydraulic cylinders provide compression to the MP before the hammering activity starts.

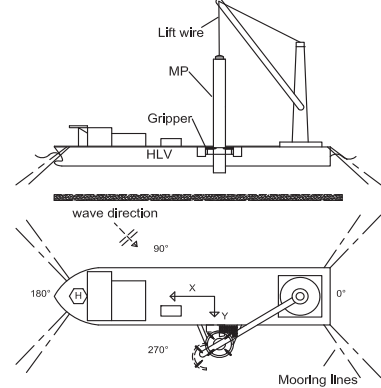


Figure 1: System set-up for the MP lowering operation using a HLV

Table 1: Structures' main particulars (Li et al., 2016)

Parameter	Notation	Value	Units
-HLV			
Displacement		5.12E+04	Ton
Length	L	183	m
Breadth	B	47	m
Draught	T	10.2	m
Vertical position of COG above keel	VCG	17.45	m
-Monopile			
Mass	M _{MP}	500	Ton
Diameter	D _{MP}	5.7	m
Thickness	t _{MP}	0.06	m
Length	L _{MP}	60	m

Modelling of the Mechanical Couplings

The coupling between the HLV crane and the MP is achieved using a lift wire. The wire coupling force is modelled as a linear spring force, and the crane flexibility is accounted for. A winch is modelled for the crane which increases the lift wire length to lower the MP towards the seabed.

The gripper device was modelled as a contact point attached to the vessel by Li et al. (2014). During the lowering of the monopile, the model was able to calculate the contact force between the HLV and the MP with changing position of the MP. During the lowering process, the hydraulic cylinder rods are normally retracted and the gap between the hydraulic cylinder and the MP allows certain relative motions between the MP and the gripper. Large axial loads and damage in the hydraulic cylinders may occur if the gaps between the hydraulic cylinders and the MP are too small. When the initial gap between the cylinder and the MP was chosen around 10 cm, it was found by Li et al. (2014) huge impact force occurred. In the present numerical model, the gripper device is excluded, but the relative motions between the MP and the HLV are calculated. The relative

motions should be kept within a limit to avoid large impact force to ensure the structural integrity of the hydraulic cylinders.

Equations of Motion for Coupled Dynamic Analysis

The HLV-MP coupled dynamic system has 12 degrees of freedom (DOF s), and for each body, the following six equations of motion are solved in the time-domain (MARINTEK, 2012).

$$(\mathbf{M} + \mathbf{A}(\infty))\ddot{\mathbf{x}} + \mathbf{D}_1\dot{\mathbf{x}} + \mathbf{D}_2f(\dot{\mathbf{x}}) + \mathbf{K}\mathbf{x} + \int_0^t \mathbf{h}(t-\tau)\dot{\mathbf{x}}(\tau)d\tau = \mathbf{F}_{ext}(t) = \mathbf{q}_{WA}^{(1)} + \mathbf{q}_{WA}^{(2)} + \mathbf{F}_{moor} + \mathbf{F}_{cpl} \quad (1)$$

where, \mathbf{M} is the total mass matrix; \mathbf{x} is the rigid-body motion vector; $\mathbf{A}(\infty)$ is the frequency-dependent added mass matrix at infinite wave frequency; \mathbf{D}_1 and \mathbf{D}_2 are the linear and quadratic damping matrices; The viscous effects from the vessel hull and the mooring system were simplified into linear damping terms in surge, sway and yaw. The roll damping of the vessel as well as the quadratic damping on the MP were also included. Additionally, \mathbf{K} is the coupled hydrostatic stiffness matrix from the HLV and the MP; \mathbf{h} is the retardation function calculated from the frequency-dependent added mass or potential damping and $\mathbf{F}_{ext}(t)$ is the external force vector that includes the first and second order wave excitation forces $\mathbf{q}_{WA}^{(1)}$ and $\mathbf{q}_{WA}^{(2)}$, the mooring line forces for the HLV, \mathbf{F}_{moor} and the coupling forces between the HLV and MP, \mathbf{F}_{cpl} . The second-order wave excitation forces on the HLV were obtained based on the Newman's approximation and only included the difference-frequency slowly varying forces (Newman, 1974). The eight catenary mooring lines for the HLV were also modelled, and both quasi-static analysis and a simplified dynamic analysis accounting for the effect of drag loading on the lines were applied.

Different approaches for the hydrodynamic modelling on the MP are explained in Sec. 3.

Natural Frequencies of the Coupled System

The natural modes of the coupled HLV-MP system include DOFs. A detailed explanation of the modes and corresponding natural periods refer to Li et al. (2015c). The gripper is excluded when calculating the natural periods because the gap between the MP and the gripper allows relative motions. Fig. 2 shows how the natural periods of the system excluding the yaw mode of MP vary with the vertical position of the MP lower tip. It should be noted that all the modes are coupled, and only the dominating DOFs are mentioned here. It is expected that in short waves the MP rotational modes (modes 02 and 03) could be excited, and in longer waves the vessel motions in the vertical plane are critical.

DIFFERENT NUMERICAL APPROACHES FOR DYNAMIC ANALYSIS

In this section, different numerical approaches are explained in detail, including the modelling of the nonstationary process, hydrodynamic forces on the MP as well as the wave spreading. Discussions on the approaches and the commonly used assumptions during numerical modelling are also presented.

Steady-state and Nonstationary Analysis Approaches

During lowering operations with structures lowered through the wave zone and towards the seabed, the dynamic features of the system change continuously. There are generally two approaches to simulate the nonstationary process (Sandvik, 2012). (1) Perform steady-state simulations in irregular waves at the most critical vertical position of the object. (2) Simulate a repeated nonstationary lowering process with different irregular wave realizations, and study the extreme response observed in each simulation. It was demonstrated that the second method provides more realistic results because an unrealistic build-up of the oscillations occurs in the stationary case (Sandvik, 2012). In principle, to provide more accurate estimates of the operations, analyses of the entire lowering process are required.

However, in order to obtain reliable statistics of the extreme responses from the nonstationary analysis, a large number of simulations is required. Furthermore, the frequency-dependence of the hydrodynamic properties based on the steady-state conditions vary with time and can not be directly applied in a nonstationary analysis. For the coupled HLV-MP model, it is challenging to include the time-varying hydrodynamic interaction between the two structures during the lowering process. Because of these issues, the simplified steady-state method is widely applied to replace the nonstationary analysis. Thus, it is useful to compare the two approaches and their influence on the allowable sea states.

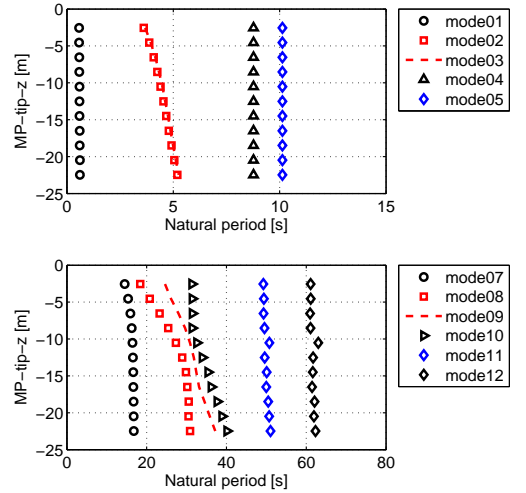


Figure 2: Natural periods for the coupled HLV-MP system with varying MP positions. Dominant motion for each mode: mode01 (MP heave); mode02 and 03 (MP roll and pitch, MP rotational motions); mode04 (HLV pitch); mode05 (HLV heave); mode07 (HLV roll); mode08 and 09 (MP pendulum motions); mode10-12 (HLV yaw, sway and surge)

Modelling of Hydrodynamic Forces on the MP

Morison's formula approximation for slender structure in incident waves

For slender bodies with a D/L ratio (diameter/wavelength) less than 0.20, the empirical Morison's formula is often used to calculate hydrodynamic forces (Morison et al., 1950). The effects of diffraction and radiation are considered insignificant in the slender-body approximation. The MP is divided into strips, and the wave forces

$f_{W,s}$ per unit length on each strip normal to the member can be determined from Morison's formula (Faltinsen, 1990):

$$f_{W,s} = \rho_w C_M \frac{\pi D^2}{4} \ddot{\zeta}_s - \rho_w C_A \frac{\pi D^2}{4} \dot{\zeta}_s + \frac{1}{2} \rho_w C_d D |\dot{\zeta}_s - \dot{x}_s| (\dot{\zeta}_s - \dot{x}_s) \quad (2)$$

where, $\ddot{\zeta}_s$ and $\dot{\zeta}_s$ are fluid particle acceleration and velocity at the center of the strip, respectively; \ddot{x}_s and \dot{x}_s are the acceleration and velocity at the center of the strip due to the body motions; D is the outer diameter of the member; and C_M , C_A and C_d are the mass, added mass and quadratic drag force coefficients, respectively. The distributed wave forces $f_{W,s}$ are integrated along the MP to obtain the total wave forces and moments, F_W . C_d for different strips along the MP are chosen according to Li et al. (2015c), where the excitation forces calculated using Morison's formula at different drafts were compared with those from panel method and good agreement was achieved.

In addition, the nonlinear effects due to the instantaneous free surface and the instantaneous body positions can be also included in the time-domain by evaluating at each time step and each strip for instantaneous body positions and integrating up to the instantaneous free surface. The Morison's formula can be applied for both steady-state and nonstationary lowering analyses. Both incident wave kinematic and the disturbed waves that include the shielding effects from the HLV can be used in the formula.

Multi-body hydrodynamics using potential theory

The hydrodynamic interaction between the HLV and the MP changes their individual hydrodynamic properties, including wave excitation forces, potential added mass and damping coefficients. The interaction should be properly included if the two structures are in close vicinity, e.g., the hydrodynamic interaction between a transport barge and a floating crane vessel during lift-off operations (Mukerji, 1988; van den Boom et al., 1990; Baar et al., 1992). These studies showed that the hydrodynamic interaction affected the responses of the transport barge because of the small dimension of the barge compared with the crane vessel (Baar et al., 1992). In this case, the hydrodynamic interaction is expected to affect the responses of the MP greatly.

According to the linear wave potential theory, the total velocity potential is expressed by (Lee, 1995):

$$\varphi = \varphi_D + \varphi_R = \varphi_I + \varphi_S + \varphi_R \quad (3)$$

where φ_D is the diffraction potential and φ_R is the radiation potential. φ_D can be further broken down into the sum of the incident velocity potential φ_I and the scattering velocity potential φ_S , which represents the disturbance to the incident wave caused by the presence of the body. The radiation potential itself is a linear combination of the components corresponding to the modes of motion such that

$$\varphi_R = i\omega \sum_{k=1}^6 \xi_k \varphi_k \quad (4)$$

Here ξ_k is the complex amplitude of the oscillatory motion in mode k of the six degrees of freedom, and φ_k is the corresponding unit-amplitude radiation potential. For multi-body case, the boundary condition for the diffraction problem has changed by adding additional body surfaces. The decomposition of the radiation potential into components, corresponding to the modes of the rigid body motion, can

be extended to multi-body interaction. This is done by defining φ_k as the velocity potential corresponding to a particular mode of one body while the other bodies are kept stationary. In this way, the total radiation potential consists of $6N$ components (N is the number of bodies).

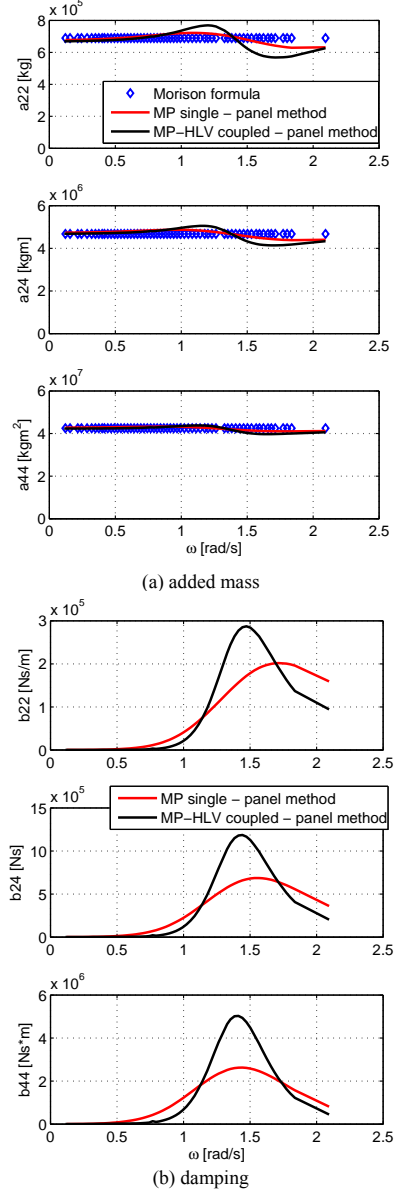


Figure 3: Comparison of added mass and damping of MP alone and when coupled with HLV using panel method(draft = 15 m)

By applying boundary conditions, the boundary value problem can be solved by numerical methods such as the panel method in the

frequency domain. In this study, the panel method program WADAM is applied (DNV, 2008). The results show that the HLV affects the properties of the MP in sway and roll more significantly compared to in surge and pitch due to the small distance in Y direction between the two structures. Fig. 3 compares the added mass and damping of MP alone and when it is coupled with HLV. The fluctuation of added mass with wave frequency increases when the MP is placed close to the HLV. A great increase of damping in the short wave range (around 1.5 rad/s) is visible. Those changes come from the scattered waves generated from HLV when the MP oscillates around its mean position. The effect of hydrodynamic interaction on the excitation force on the MP will be shown later in this section.

Simplified approach to consider shielding effects using Morison's formula for nonstationary process

In the current study, the hydrodynamic effects from the MP on the HLV are minor and can be neglected. However, the wave field near the HLV is altered from the original incident waves, and three-dimensional effects occur due to the diffraction and radiation from the vessel. Thus, the hydrodynamic interaction between HLV and MP can be simplified as "one-way" interaction by considering the shielding effects from the HLV on the MP while ignoring the effects from the MP on the HLV. Moreover, the multi-body hydrodynamic properties using potential theory are based on a steady-state condition with a fixed mean draft of all structures and can not be directly applied for the nonstationary analysis. Therefore, the approach proposed by Li et al. (2014) is applied to calculate the forces on MP.

The boundary value problem for the single body HLV in the wave field is solved by potential theory. Thus, the hydrodynamic coefficients of the vessel and the fluid kinematics at any point in the wave field in the frequency domain can be acquired. The waves affected by both radiation and diffraction of the vessel are defined as disturbed waves, which includes the vessel shielding effects, and the undisturbed waves are defined as incident waves. The following steps are followed to calculate the forces on the MP for the nonstationary process.

- 1) First, generate time series of disturbed fluid kinematics at pre-defined wave points near the MP using the fluid kinematics transfer functions from potential theory considering the radiation and diffraction of the HLV.
- 2) Then, perform time-domain simulations. At each time step, find the closest pre-defined wave points for each strip on the MP. By applying a 3D linear interpolation between those wave points, the kinematics (elevations, fluid velocities and accelerations) at the center of each strip in disturbed waves are acquired.
- 3) Calculate the forces at each strip using the disturbed wave kinematics by Eq. (2) and integrate along the submerged part of the MP to get the total wave forces. Note that the draft of the MP changes continuously during the nonstationary process. The total wave forces on the MP are then used to obtain the motions of the coupled HLV-MP system. The details of this approach can be found in Li et al. (2014).

To validate whether the slender structure assumption is reasonable to calculate MP wave forces, Fig. 4 compares the wave excitation force on the MP at a draft of 15 m for four cases: (1) MP alone using panel Method; (2) MP alone using Morison's formula in incident wave; (3) HLV-MP coupled using panel method and (4) HLV-MP coupled using Morison's formula.

It is evident that the shielding effects from the HLV (coupled HLV-MP case) reduce the excitation force on MP significantly in intermediate to short wave length. Good agreement between the Morison's formula and the panel method is observed with wave frequency less than 1.5 rad/s in incident waves. For the HLV-MP coupled case, i.e., the disturbed wave case, the slender structure assumption is suitable even for shorter wave conditions because of the great reduction from the shielding effects due to HLV. In addition, the added mass calculated from 2D coefficients used in Morison's formula are compared with the one from panel method, see Fig. 3 (a). The results show good agreement between the slender structure assumption and the multi-body potential theory in terms of hydrodynamic properties. Therefore, the simplified shielding effects approach is considered reasonable to calculate wave excitation force on the MP for the HLV-MP coupled condition during the nonstationary lowering process.

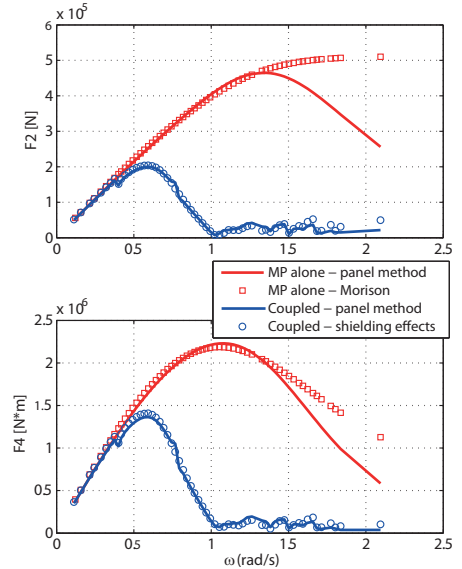


Figure 4: Comparison of excitation force on MP in incident wave and when accounting for shielding effects due to the HLV ($Dir = 90$ deg, draft = 15 m)

Morison's formula plus radiation damping for nonstationary process

As discussed previously, Morison's formula does not account for the radiation and diffraction of the structure itself, and the coefficients from potential theory cannot be directly applied in the nonstationary case with time-varying draft of the structure. Li et al. (2015c) concluded that the radiation damping on the large diameter MP is of importance especially for short wave conditions. However, the hydrodynamic interaction between the HLV and the MP was not included in Li et al. (2015c), and the influences of the radiation damping of the MP in short waves for the coupled case were unknown. This study compares the effects by implementing the radiation damping on the MP for the coupled HLV-MP case.

The approach proposed by Li et al. (2015c) is applied to implement the radiation damping effects from the MP for the nonstationary process by interpolating the retardation functions at pre-defined drafts of the MP in the time-domain. The radiation damping of the MP is

included together with the shielding effects from the HLV to include the complete hydrodynamic interaction. Fig. 3 shows the added mass and damping of the MP without and with the HLV. The retardation function is computed using a transform of the frequency-dependent added mass and damping from the coupled HLV-MP case to be used in the time-domain simulations. Limitations of this method were addressed in Li et al. (2015c) and further validations are required.

Short-crested Waves and Shielding Effects

A wave condition is classified as long-crested and short-crested based on the directions of wave propagation. Wind generated seas in real sea conditions involve short-crested waves (Chakrabarti, 1987; Goda, 2010; Kumar et al., 1999). The directional spreading of wave energy may give rise to forces and motions which are different from those corresponding to long-crested waves.

DNV (2014) recommends to check “whether long-crested or short-crested sea is conservative for the analysis concerned”. For head sea short-crested sea will give increased roll motion of the crane vessel compared to long-crested sea, while long-crested sea will give increased pitch motion. It is therefore necessary to carry out analysis to conclude on this aspect. This study evaluates the influence of the short-crestedness when including the shielding effects from the HLV on the responses of the MP lowering system.

The sea state is often represented by a wave spectrum as (DNV, 2014)

$$S(\omega, \theta) = S(\omega)D(\omega, \theta) \quad (5)$$

$$\int_{-\pi}^{\pi} D(\omega, \theta) d\theta = 1 \quad (6)$$

For practical purposes, the frequency dependence of the directional function is neglected, that is, $D(\omega, \theta) = D(\theta)$. One of the most widely used $D(\theta)$ is the cosine power function given as

$$D(\theta) = \begin{cases} C(n) \cos^n(\theta - \theta_0) & |\theta - \theta_0| \leq \pi/2 \\ 0 & |\theta - \theta_0| > \pi/2 \end{cases} \quad (7)$$

where θ_0 is the main wave direction about which the angular distribution is centered. The parameter n is a spreading index describing the degree of wave short-crestedness, with $n \rightarrow \infty$ representing a long-crested wave field. $C(n)$ is a normalizing constant ensuring that Eq. (6) is satisfied. Typical values for the spreading index for wind generated sea are $n = 2$ to 4 . Because lifting operations are usually carried out in relatively low sea states, the spreading of the waves could be significant.

For long-crested waves, knowing incident wave realization $x(t)$, the Fourier transform of the kinematics of the disturbed wave $Y(\omega, \theta_0)$ can be calculated in the frequency domain based on $X(\omega)$, the Fourier transform of $x(t)$, and the disturbed fluid kinematics transfer functions $H(\omega, \theta_0)$, see Eq. (8).

$$Y(\omega, \theta_0) = H(\omega, \theta_0) \cdot X(\omega) \quad (8)$$

For short-crested waves, the incident wave realization includes different wave direction components and is generated from the two-dimensional wave spectrum in Eq. (5). The Fourier transform of the incident wave at various directions $X(\omega, \theta)$ can be obtained. Thus, the disturbed fluid kinematics for direction θ_0 in short-crested waves are obtained as follows.

$$Y(\omega, \theta_0) = \int_{\theta_1}^{\theta_2} H(\omega, \theta) X(\omega, \theta) d\theta \quad (9)$$

where θ_1 and θ_2 are the limits for the directions. Using Eq. (2) and the disturbed wave kinematics from Eq. (9), the excitation forces on the MP accounts for both shielding effects and short-crested waves and can be applied in the nonstationary lowering analysis.

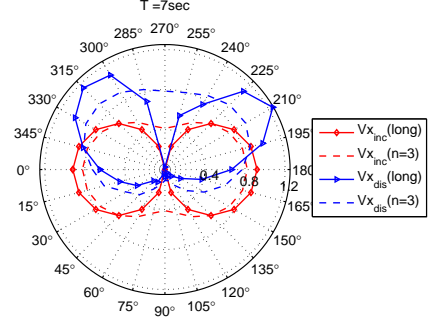


Figure 5: RAOs of fluid X -velocities in incident and disturbed waves with and without wave spreading ($T = 7$ s)

Fig. 5 gives an example of the RAOs of fluid particle X -velocity near the MP in incident and disturbed waves considering wave spreading. The shielding effects are clearly visible in that the RAOs in disturbed waves are greatly affected by the HLV. The RAOs in the leeward side of the HLV (from 0 deg to 180 deg) are significantly reduced for given wave period in disturbed waves while in the windward side (from 180 deg to 360 deg) the RAOs are amplified.

When only long-crested waves are considered, the differences between the RAOs in incident and disturbed waves are significant. However, these differences can be reduced considerably when including the wave spreading. For example, the RAOs of X -velocity at $T = 7$ s near 180 deg direction in disturbed waves are close to those in incident waves with spreading index $n = 3$. This is because the spreading function averages the low RAOs in the leeward side and the large RAO values in the windward side of the vessel. It can be predicted that the shielding effects in short-crested waves will be less pronounced compared with the case when only long-crested waves are considered.

TIME-DOMAIN SIMULATIONS AND CASE STUDIES

Case studies are performed to study the influence of different approaches on the allowable sea states. The factors used in the case studies are summarized in Table 2. Five cases are defined for the HLV-MP lowering analysis. Among those, Case 1 accounts for all the factors that might affect the response of the system and represents the most accurate numerical method, while the other cases neglect one or two factors in order to study the influence of each factor.

The spreading index $n = 3$, see Eq. (7), is used for the cases considering short-crested waves. For nonstationary lowering simulation, the winch in the crane starts from 300 s to 740 s with a speed of 0.05 m/s. The total lowering length was 22 m. Twenty repetitions of the lowering simulation are performed, corresponding to a duration of approximately two hours. The maximum relative motions between the HLV and the MP at the gripper position during the 20 simulations are used as characteristic responses to determine the allowable sea states. The most onerous draft of the MP are found

from the nonstationary lowering simulation, and 20 steady-state simulations are carried out. The same simulation length as the nonstationary simulations is applied, and the maximum relative motions are used to determine the allowable sea states for the steady-state simulation.

Step-by-step integration methods combined with an iterative routine were applied to calculate the responses of the lowering system. The

equations of motion were solved by Newmark-beta numerical integration scheme with a time step of 0.02 s. The first and second order wave forces of the HLV were pre-generated using Fast Fourier Transformation (*FFT*) at its mean position. The wave forces on the MP are calculated in an external Dynamic Link Library (DLL) and interacts with SIMO program (MARINTEK, 2012) where the motions of the coupled system are solved in the time-domain.

Table 2: Factors for case study in the time-domain simulations

Factors	A wave spreading	B shielding effects	C MP radiation	D Nonstationary
(1)	long-crested	incident wave	no radiation damping	steady-state simulation
(2)	short-crested	disturbed wave	radiation damping	lowering simulation
Simulation Cases	HLV-MP lowering system			
Case 1 (<i>A2B2C2D2</i>)	short-crested	disturbed wave	radiation damping	lowering simulation
Case 2 (<i>A1B2C2D2</i>)	long-crested	disturbed wave	radiation damping	lowering simulation
Case 3 (<i>A2B1C1D2</i>)	short-crested	incident wave	no radiation damping	lowering simulation
Case 4 (<i>A2B2C1D2</i>)	short-crested	disturbed wave	no radiation damping	lowering simulation
Case 5 (<i>A2B2C2D1</i>)	short-crested	disturbed wave	radiation damping	steady-state simulation

OPERATIONAL CRITERIA

The operational limits in terms of allowable sea states for installing a MP should be established by assessing all installation phases, including the upending, lowering and hammering operations. However, this study is limited to the lowering phase. The potential critical events that can limit the operation in this phase are as follows.

- Lift wire breakage. The tension in the lift wire should never exceed the maximum working load of the wire. A slack wire and snap forces should both be avoided.
- Large MP tip displacement before landing. The motions of the monopile, particularly its rotations and the displacements of its end tip, affect the landing process that follows the lowering process. Large excursion of the MP tip may result exceeding distance from the designed installation position.
- Failure of the hydraulic system in the gripper device. The exceedance of the allowable forces on the system will result in a hydraulic system failure. The failure will not only stop the operation but may also pollute the environment if leakage of hydraulic fluid occurs.

Because no slings are applied for the lifting arrangement, the main lift wire tension is observed to be stable and no snap loads occur under reasonable environmental conditions for this installation system. The installed position of the MP can vary from the designed position in a relatively large range (around 2 m), which exceeds the motions of the MP in the operational sea states. In addition, the inclination angle after landing can be adjusted by moving the HLV using mooring lines and thus not considered as critical (Li et al., 2016).

In this study, only the failure of the hydraulic system in the gripper device is considered as a critical event for determining the operational sea states. The corresponding limiting response parameter is the allowable gap between the MP and HLV at the gripper position. Due to large stiffness of the hydraulic cylinders, impact forces occur when the relative motion exceeds the allowable gap. Based on the dimension of the MP and the most common designs for the hydraulic cylinders used in the industry, the allowable gap is chosen as 1 m. Therefore, the

sea states which result in relative motions at the gripper position larger than this allowable limit are considered unacceptable.

RESULTS AND DISCUSSIONS

From time-domain simulations at various wave conditions, the allowable sea states are obtained by applying the above operational criteria. Different modelling approaches are applied for the corresponding cases. The results are presented with discussions in this section.

Effect of the Hydrodynamic Load Modelling Approach

Figure 6 compares the allowable H_s and T_p values for Cases 1, 3 and 4. Case 1 is the most accurate approach including all the features shown in Table 2, while Case 3 neglects the MP radiation damping and the shielding effects, e.g., the hydrodynamic couplings between the HLV and MP. Case 4 includes shielding effects but neglects the MP radiation damping. The maximum H_s values occur at wave period around 7 s for Case 1. The short waves excite the MP rotational resonant motions and the long waves excite the HLV motions in the vertical plane (see the natural periods of the system in Fig. 2), and thus the H_s values decrease for those conditions.

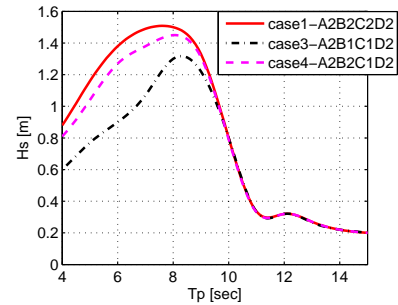


Figure 6: Comparison on allowable sea states for Cases 1, 3 and 4

Figure 7 presents the MP pitch motions in two representative sea states for the three cases. The shielding effects from the HLV are

observed critical and the resonant motions of the MP ($\omega \approx 1.2$ rad/s) are overestimated greatly for Case 3 without shielding effects, see Fig. 7 (a). The allowable sea states are thus significantly underestimated, see Fig. 6 Case 3. The effects appear more significant in short waves than in long waves due to the larger diffraction from the vessel. The shielding effects can be ignored for wave period larger than 10 s when assessing the allowable sea states. Case 3 represents the most commonly applied simplification calculating the hydrodynamic forces on slender structures using Morison's Formula in incident waves. The results here prove a great underestimation of the allowable sea states for the MP lowering operation using this simplification.

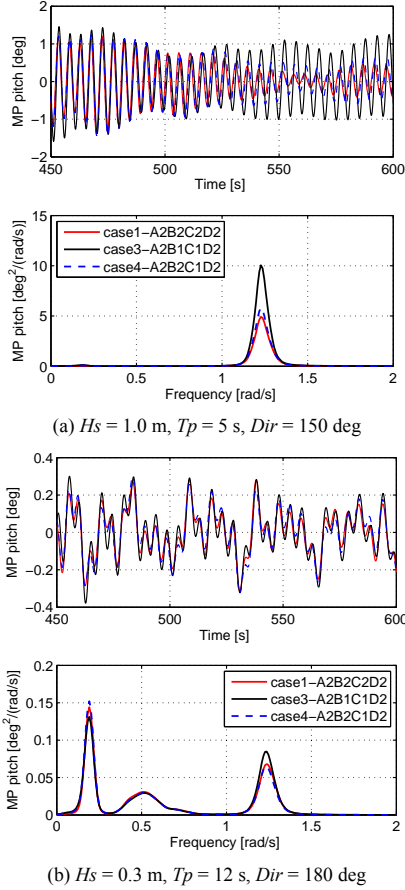


Figure 7: Response time series and spectra of MP pitch motion for Cases 1, 3 and 4

The responses in Fig. 7 also show that the MP radiation damping are secondary compared with the shielding effects. Larger peak is observed at the MP resonant frequency in short waves, and the differences are negligible in long waves. The exclusion of the radiation damping underestimates the H_s values by around 0.1 m for wave period less than 8 s, and the H_s values are almost the same as those from Case 1 for longer waves.

Effect of Wave Spreading

Another commonly applied simplification during numerical simulation is to exclude the wave spreading by using long-crested waves. Figure 8 displays the allowable sea states by using long- and short-crested waves. For T_p less than 12 s, the long-crested assumption greatly overestimates the H_s . The spectra of MP roll and pitch motions at two wave conditions for Cases 1 and 2 are presented in Fig. 9. For both sea states, one can observe large differences in the spectra. In short waves, the long-crested wave assumption provides much lower responses at the resonant frequency, see Fig. 9 (a). As mentioned, the shielding effects are significant in short waves, however, the spreading of the waves averages the low wave kinematics in the leeward side of the vessel and the high values in the windward side, see Fig. 5. Thus, the MP experiences less shielding effects from the HLV for the same heading angles in short-crested waves than in long-crested waves, which results in higher allowable sea states in short waves, as shown in Fig. 8.

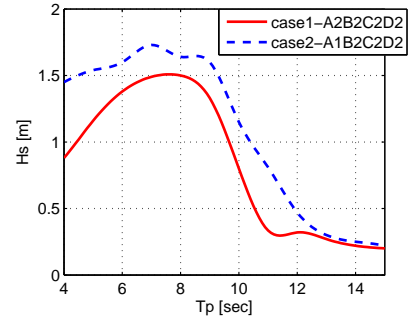


Figure 8: Comparison on allowable sea states for Cases 1 and 2

In longer waves, the shielding effects are minor. However, the spreading of the waves increases the HLV motions in the transverse direction, e.g., roll motions. Thus, MP experiences larger responses in short-crested waves in roll, see Fig. 9(b) top, where the spectra density of roll near the wave frequency for Case 1 are much higher than Case 2 with long-crested waves. The pitch motions at resonance are lower using short-crested waves in this condition due to lower wave energy presented in the longitudinal direction at heading seas. Because of the significant increase of the transverse motions in short-crested waves, and resulting allowable sea states are lower than in long-crested waves. For operational sea states with H_s less than 2 m, the waves are normally dominated by short-crested wind seas. Thus, the spreading of the waves should be taken into consideration to avoid non-conservative allowable sea states.

Comparison between Steady-state and Nonstationary Analysis

From the nonstationary lowering simulation, the most critical MP drafts are obtained for each wave peak period. It was found for most of the wave conditions, the most critical situation occurs when the MP draft is very shallow (around 2 to 3 m). With this draft, the gripper position is far from the COG of the MP and a small rotational angle of the MP gives large relative motions between the HLV and the MP. Another reason is that the MP experiences less damping at a smaller draft compared with increasing draft. Steady-state simulations at the most critical drafts were performed and the corresponding allowable sea states are compared with those from the nonstationary lowering simulations in Fig. 10.

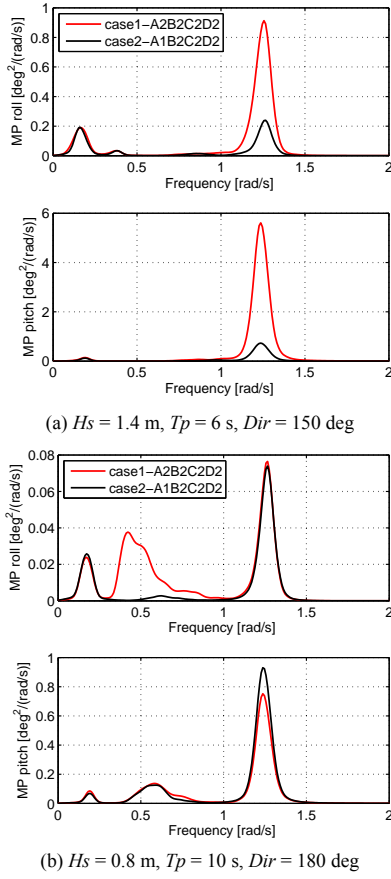


Figure 9: Response spectra of MP rotational motions for Cases 1 and 2

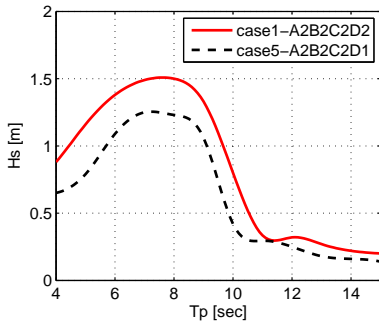


Figure 10: Comparison on allowable sea states for Cases 1 and 4

A considerable reduction of the allowable H_s value can be observed for almost all T_p conditions. The reduction appears to be more significant in shorter waves because the resonant motions are accelerated in the steady-state analysis. Although the steady-state analysis provide conservative results, it may greatly increase the

downtime and the costs for the operation.

Effect of Vessel Heading Angle on the Allowable Sea States

Because the shielding effects and the vessel motions are sensitive to the wave direction, three heading angles of the HLV are applied in the time-domain simulation, i.e., 150 deg, 165 deg and 180 deg. Fig. 11 shows the allowable sea states for Case 1 with different heading angles, and the maximum sea states for each T_p values are also shown in circles. One can observe that the system prefers 150 deg in short waves with T_p less than 7 s. The most proper heading moves to 165 deg and then to heading seas in long waves. This is because the shielding effects from the HLV are stronger close to quartering seas in short waves. In long waves, the shielding effects are minor, but the motions of the vessel increase greatly when the heading moves away from the heading seas because of the increasing transverse motions caused by short-crested waves.

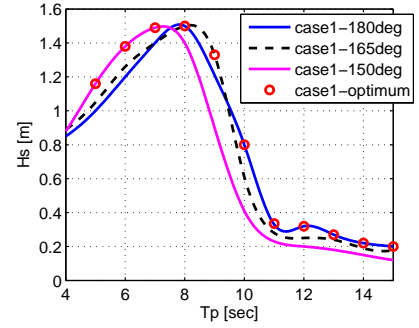


Figure 11: Comparison on allowable sea states for Case 1 with different heading angles

Figure 12 presents the most preferable heading angles which give the maximum allowable H_s values for three different cases. Case 1 and 2 show similar trend, but Case 3 results in different angles in short waves. This is because Case 3 excludes the shielding effects from the HLV and the most suitable headings are close to the heading seas to avoid large transverse motions of the vessel. Thus, the most preferable headings are affected by the approach applied in the numerical models.

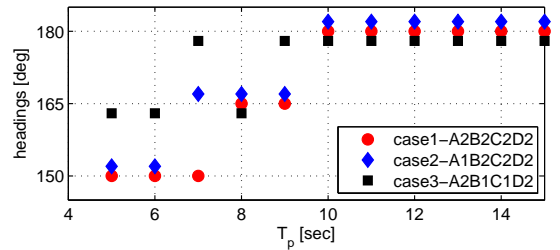


Figure 12: Comparison on the most preferable heading angles for Cases 1, 2 and 3

The allowable sea states presented in Figs. 6 and 8 correspond to the most preferable headings shown in Fig. 12. For Cases 4 and 5, the headings are the same as Case 1 since all three cases consider both shielding effects and short-crested waves which are the only two heading-dependent factors.

Operability analysis

For weather sensitive marine operations, it is useful to evaluate the probability of acceptable weather conditions. For this study, it is also important to show the influences of different factors affecting on the operational probability for a typical site. The wave data from the North Sea Center site in Li et al. (2015b) was chosen for the operability analysis. This site is suitable for MP foundations with an average water depth of 29 m, and the location is close to the Dogger Bank wind farm. The wave data were hourly sampled and generated from a hindcast model from 2001 to 2010. The wave data from April to September are used for the operability study, and the corresponding 10-year scatter diagram is shown in Table 4. The operational sea states from Cases 1, 2 and 3 are highlighted in the table.

Assuming the MP lowering process lasts for one hour, the corresponding operability for different cases are therefore calculated for this site using the derived allowable sea states. Table 3 presents the operability for different cases using the most preferable headings as well as the results from Case 1 using fixed headings. The absolute errors of the operability for different cases are also shown with respect to Case 1 which refers to the most accurate numerical model.

Table 3: Operability for MP lowering at North Sea Center in the period from April to September using different methods and heading angles

Method	Operability (%)	absolute error w.r.t Case 1 (%)
Case 1 (<i>A2B2C2D2</i>)	57.5	/
Case 2 (<i>A1B2C2D2</i>)	72.8	15.3
Case 3 (<i>A2B1C1D2</i>)	28.2	-29.3
Case 4 (<i>A2B2C1D2</i>)	50.3	-7.2
Case 5 (<i>A2B2C2D1</i>)	33.4	-24.1
Case 1 (180 deg)	49.2	-8.3
Case 1 (165 deg)	52.0	-5.5
Case 1 (150 deg)	55.1	-2.4

Using long-crested waves overestimates the operability while the other three cases provide conservative results. The table also indicates the importance of each factor in the numerical method. For the studied scenario, the shielding effects are the most critical factor, followed by the nonstationary analysis approach and the wave spreading. Although the MP radiation damping is less important than the other factors, the exclusion of the radiation damping underestimates the operability by over 7% for this site.

The comparison of the operability using three headings with the most preferable headings for Case 1 shows that it is possible to increase the operability by varying the heading of the HLV in different sea states. Because the sea states in the North Sea Center from April to September are dominated by short waves with T_p less than 8 s (see Table 4), using 150 deg gives the largest operability compared with the other two headings due to the advantage of shielding effects from the HLV. However, the system may experience strong motions in long waves with 150 deg heading in spreading waves.

CONCLUSIONS AND RECOMMENDATIONS

Obtaining the allowable sea states for offshore operations in the planning phase is important to minimize the risk and improve operation efficiency. The present work examines the allowable sea states and operability for the MP lowering operation using different

numerical approaches.

The numerical model consists of the HLV and MP with hydrodynamic interaction and mechanical couplings. The lowering process is nonstationary with time-dependent properties of the system. The factors considered in different numerical approaches include the wave spreading, the shielding effects, the MP radiation damping as well as the nonstationarity of the process. To account for the shielding effects from the HLV and the MP radiation damping during the nonstationary MP lowering process, the methods proposed by Li et al. (2014) and Li et al. (2015c) are applied. Five simulation cases are defined to study the influence of different factors. The responses obtained from time-domain simulations are evaluated with the operational criteria to acquire the allowable sea states. The main conclusions and recommendations from this study are provided as follows.

- The shielding effects from the HLV are more considerable than the radiation damping from the MP for the responses of the lowering system. Those effects are found to be critical in short waves when the diffraction of the HLV and the radiation of the MP are huge and can be neglected for waves longer than 10 s.
- Long-crested wave assumption underestimate the responses and brings pronounced increase of the allowable sea states in both short and long wave conditions. The operation may experience more risks if the allowable sea states are derived using long-crested waves.
- Using steady-state analysis at a fixed draft of the MP overestimates the responses compared with the nonstationary approach. The resulting allowable sea states are over-conservative in both short and long waves.
- The preferable heading angles for different sea states are obtained, and they change from around 150 deg in short waves to take advantage of the shielding effects to 180 deg in long waves to avoid large transverse motions of the vessel due to wave spreading.
- Operability analysis is carried out using 10-years' sea states from April to September at the North Sea Center Site. The exclusion of shielding effects, wave spreading and the nonstationarity of the process result in more than 15% absolute error in the operability analysis. The radiation damping of the MP give around 7% absolute error. It is recommended to consider the shielding effects, wave spreading in the numerical approach and use nonstationary analysis. For site conditions dominated by short waves, the radiation damping of the MP should also be included when assessing the operability.
- It is beneficial to use the most preferable headings at different sea states to increase the operability.

This study provides a basis to improve numerical analysis for nonstationary lifting operation of slender structures using a floating vessel. The considerations may be different for other types of operations. However, it is important to evaluate and quantify the influences of each factor in the numerical study to acquire reliable allowable sea states and the operability for a specific site in the design phase. For MP installation, the lowering process is only one part of the group installation activities. Future work is needed to assess the allowable sea states of other individual activities and establish the operational limits for the complete operation.

Table 4: Ten-year scatter diagram of H_s and T_p at the North Sea Center Site from April to September, with operational sea states for Cases 1, 2 and 3

T_p (s) H_s (m)	1-2	2-3	3-4	4-5	5-6	6-7	7-8	8-9	9-10	10-11	11-12	12-13	13-14	14-15	15-17	Sum
0.1	0	0	8	0	0	3	13	0	1	6	0	0	12	0	0	43
0.3	3	44	461	334	74	47	80	67	46	37	27	10	6	13	12	1261
0.5	0	86	633	1803	788	245	152	221	165	81	28	20	31	12	13	4278
0.7	0	31	707	2233	1632	686	215	242	177	180	60	26	33	14	13	6249
0.9	0	3	228	2428	2008	1201	327	270	320	263	46	24	15	11	4	7148
1.1	0	0	44	1486	1816	1151	595	265	181	235	89	36	34	7	7	5946
1.3	0	0	3	590	1677	1017	524	278	165	194	80	36	7	13	1	4585
1.5	0	0	0	175	1403	878	428	233	73	91	81	45	19	4	2	3432
1.7	0	0	0	41	930	837	381	233	36	38	45	45	10	6	2	2604
1.9	0	0	0	2	472	765	324	176	66	27	15	19	38	22	4	1930
2.1	0	0	0	1	191	818	265	165	38	20	14	14	24	2	1	1553
2.3	0	0	0	0	56	569	328	140	50	9	4	10	20	1	0	1187
2.5	0	0	0	0	14	361	269	110	38	16	2	11	17	1	0	839
2.7	0	0	0	0	1	239	267	112	34	9	2	1	12	0	0	677
2.9	0	0	0	0	0	101	218	134	45	16	3	2	22	2	0	543
3.1	0	0	0	0	0	35	170	77	65	16	3	0	7	4	0	377
3.3	0	0	0	0	0	4	133	44	42	8	6	0	2	0	0	239
3.5	0	0	0	0	0	1	117	53	51	12	3	0	0	0	0	237
3.7	0	0	0	0	0	1	59	48	41	12	4	0	0	0	0	165
3.9	0	0	0	0	0	0	44	26	43	13	5	1	0	0	0	132
4.5	0	0	0	0	0	0	35	82	112	85	16	0	0	0	0	330
5.5	0	0	0	0	0	0	0	8	31	75	25	1	0	0	0	140
6.5	0	0	0	0	0	0	0	0	0	18	7	0	0	0	0	25
Sum	3	164	2084	9093	11062	8959	4944	2984	1820	1461	565	301	309	112	59	43920
Note:	(1) Operational sea states for Case 1 are and (2) Operational sea states for Case 2 are and (3) Operational sea states for Case 3 are															

ACKNOWLEDGEMENTS

This work has been financially supported by the Research Council of Norway granted through the Department of Marine Technology, the Centre for Ships and Ocean Structures (CeSOS) and the Centre for Autonomous Marine Operations and Systems (AMOS), NTNU.

REFERENCES

- Baar, J., Pijfers, J., Santen, J., 1992. Hydromechanically coupled motions of a crane vessel and a transport barge. In: *24th Offshore Technology Conference*, Houston, USA.
- Chakrabarti, S. K., 1987. *Hydrodynamics of offshore structures*. WIT press.
- DNV, 2008. *Wadam theory manual*. Det Norske Veritas.
- DNV, 2014. *Recommended Practice DNV-RP-H103, Modelling and Analysis of Marine Operations*. Det Norske Veritas.
- EWEA, 2014. *The European offshore wind industry - key trends and statistics 2013*. Report, The European Wind Energy Association.
- Faltinsen, O., 1990. *Sea Loads on Ships and Ocean Structures*. Cambridge University Press.
- Goda, Y., 2010. *Random seas and design of maritime structures*. World Scientific.
- Kumar, V. S., Deo, M., Anand, N., Chandramohan, P., 1999. Estimation of wave directional spreading in shallow water. *Ocean engineering* 26 (1), 83–98.
- Lee, C., 1995. *WAMIT theory manual*. Department of Ocean Engineering, Massachusetts Institute of Technology, USA.
- Li, L., Gao, Z., Moan, T., 2013. Numerical simulations for installation of offshore wind turbine monopiles using floating vessels. In: *Proceedings of the 32nd International Conference on Ocean, Offshore and Arctic Engineering*, June 9-14, Nantes, France.
- Li, L., Gao, Z., Moan, T., 2015a. Comparative study of lifting operations of offshore wind turbine monopile and jacket substructures considering shielding effects. In: *The 25th International Offshore and Polar Engineering Conference*, Hawaii, USA, June 21-26.
- Li, L., Gao, Z., Moan, T., 2015b. Joint distribution of environmental condition at five European offshore sites for design of combined wind and wave energy devices. *Journal of Offshore Mechanics and Arctic Engineering* 137 (3): 031901.
- Li, L., Gao, Z., Moan, T., 2015c. Response analysis of a nonstationary lowering operation for an offshore wind turbine monopile substructure. *Journal of Offshore Mechanics and Arctic Engineering* 137 (4): 051902.
- Li, L., Gao, Z., Moan, T., Ormberg, H., 2014. Analysis of lifting operation of a monopile for an offshore wind turbine considering vessel shielding effects. *Marine Structures* 39, 287–314.
- Li, L., Guachamin Acero, W., Gao, Z., Moan, T., 2016. Assessment of allowable sea states during installation of OWT monopiles with shallow penetration in the seabed, under review in *Journal of Offshore Mechanics and Arctic Engineering*.
- MARINTEK, 2012. *SIMO - Theory Manual* Version 4.0.

- Moné, C., Simith, A., Maples, B., Hand, M., 2015. *2013 cost of wind energy review*. Technical Report NREL/TP-5000-63267, National Renewable Energy Laboratory (NREL), CO, USA.
- Morison, J., Johnson, J., Schaaf, S., 1950. The force exerted by surface waves on piles. *Journal of Petroleum Technology* 2 (05), 149–154.
- Mukerji, P., 1988. Hydrodynamic responses of derrick vessels in waves during heavy lift operation. In: *20th Offshore Technology Conference*, Houston, USA.
- Newman, J. N., 1974. Second-order slowly-varying forces on vessels in irregular waves. In: *International Symposium on the Dynamics of Marine Vehicles and Structures in Waves*, University College, London.
- Sandvik, P., 2012. Estimation of extreme response from operations involving transients. In: *Proceedings of the 2nd Marine Operations Specialty Symposium*, Singapore.
- Sarkar, A., Gudmestad, O., 2013. Study on a new method for installing a monopile and a fully integrated offshore wind turbine structure. *Marine Structures* 33, 160–187.
- Thomsen, K., 2011. Offshore wind: *A comprehensive guide to successful offshore wind farm installation*. Academic Press.
- van den Boom, H., Dekker, J., Dallinga, R., 1990. Computer analysis of heavy lift operations. In: *22nd Offshore Technology Conference*, Houston, USA.

A.6 Paper 6

Paper 6:

*Assessment of Allowable Sea States During Installation of OWT
Monopiles with Shallow Penetration in the Seabed*

Authors: Lin Li, Wilson Guachamin Acero, Zhen Gao, Torgeir Moan
Accepted for publication in *Journal of Offshore Mechanics and Arctic
Engineering*, 2016

Assessment of allowable sea states during installation of OWT monopiles with shallow penetration in the seabed

Lin Li ^{*1,2,3}, Wilson Guachamin Acero^{1,2,3}, Zhen Gao^{1,2,3} and Torgeir Moan^{1,2,3}

¹Centre for Ships and Ocean Structures (CeSOS), NTNU, Trondheim, Norway

²Department of Marine Technology, NTNU, Trondheim, Norway

³Centre for Autonomous Marine Operations and Systems (AMOS), NTNU, Trondheim, Norway

Abstract

Installation of offshore wind turbines (OWTs) requires careful planning to reduce costs and minimize associated risks. The purpose of this paper is to present a method for assessing the allowable sea states for the initial hammering process (shallow penetrations in the seabed) of a monopile (MP) using a heavy lift floating vessel (HLV) for use in the planning of the operation. This method combines the commonly used installation procedure and the time-domain simulations of the sequential installation activities. The purpose of the time-domain simulation is to quantitatively study the system dynamic responses to identify critical events that may jeopardize the installation and the corresponding limiting response parameters. Based on the allowable limits and the characteristic values of the limiting response parameters, a methodology to find the allowable sea states is proposed. Case studies are presented to show the application of the methodology. The numerical model of the dynamic HLV-MP system includes the coupling between HLV and MP via a gripper device, and soil-MP interaction at different MP penetration depths. It is found that the limiting parameters are the gripper force and the inclination of the MP. The systematic approach proposed herein is general and applies to other marine operations.

Keywords: monopile installation, heavy lift vessel, initial hammering process, critical events, limiting parameters, allowable sea states

1 Introduction

The installation of offshore wind turbines is costly due to the challenging environmental conditions and a large number of wind turbine units need to be installed. To better prepare the operations and

* Corresponding author. Email address: lin.li@ntnu.no; Tel: +47 73 55 11 12, Fax: +47 73 59 55 28

increase the weather windows during the planning phase, systematic and practical methodologies for assessing this kind of operations are needed.

Monopiles (MP) are the most commonly used foundations in water depths up to 40 *m*. It was reported that by the end of 2013 more than 75% of all installations are supported on MPs [1]. The installation of a MP wind turbine includes the erection of the MP, transition piece, tower sections and rotor and nacelle assembly. This study focuses on the installation of the MP which in general includes the following steps: upending and lowering, and driving/drilling operations. After arrival on site, the monopile is upended from a transportation barge or the crane vessel and lowered through water so that it is standing vertically on the seabed. A hydraulic hammer is placed on top of the pile and used to drive it into the seabed to a predetermined depth. In case a rocky subsurface prevents driving operations, a drilling bit is inserted into the pile to drill through the substrate [2]. The installation can be carried out using jack-ups which provide stable working platforms for the installation, but their application is limited to a maximum water depth around 45 m [3] and the lowering of the jack-up legs is time consuming and requires low sea states. Floating vessels, on the other hand, have more flexibility for offshore operations and are effective in mass installations of a wind farm due to fast transit between foundations. However, the motion of floating vessels affects the responses of the installation system and bring more challenges for load transfer operations.

There are very few publications dealing with the MP installation. Previous studies have been focused on proposing new installation methods and developing more accurate numerical methods to increase the installation weather window. Sarkar et al. suggested a method to install MP by isolating the installation operations from the motion of the floating vessel using a pre-installed submerged support structure [4]. They showed that the overturning moment on the structure during MP hammering were the limiting parameter for MP installation. The dynamic responses of a coupled HLV-MP system during the lowering process of the MP were studied in Ref. [5]. The performance using both a floating vessel and a jack-up was also compared in their study. Furthermore, Li et al. introduced a method to account for the shielding effects (crane vessel shelters the MP from the wave action) during the entire lowering operation of the MP [6]. The vessel reduces the wave kinematics at its leeward side and thus the wave forces on the MP. It was concluded that when accounting for the shielding effects, the responses obtained from the numerical analysis can be greatly reduced in short waves by selecting a proper heading of the vessel. The approach was further studied and extended to compare the performance during lifting of a MP and a jacket OWT foundation, respectively [7]. Recommendations regarding the heading angles of the vessel during the lifting operations of the two OWT substructures were given. In addition, the importance of radiation damping of the MP during the nonstationary lowering operation were examined in Ref. [8]. A new approach was proposed to account for radiation damping in the time-domain numerical simulation of the nonstationary lowering process. This study showed that accounting for the radiation damping on the large diameter MPs can reduce the responses of the lifting system and may increase the allowable sea states especially for short wave conditions.

As it is shown above, most of the previous research on the MP installation primarily focused on the numerical modelling of different installation activities and calculation of dynamic responses. However, for offshore installations it is of great importance to establish the operational limits in a pragmatic way based on installation procedures and proper identification of critical and restricting events. The procedure for the MP installation is well known by offshore installation contractors. To identify the critical events for the whole installation, numerical analysis are required to study the dynamic responses of each sequential installation activity. Each critical event has a limiting parameter and corresponding allowable limit, e.g. structural failure of hydraulic cylinders due to extreme contact forces which are limited by the allowable working loads. However, the severity of these critical events can be reduced by mitigation actions by modifying the operational procedure and by upgrading the equipments to increase the allowable limits. Thus, a systematic identification of the critical events and the corresponding parameters to describe these events (limiting parameters) is necessary to plan the operation, i.e. establish operational limits for installation, propose contingency actions and select the equipment in a cost-effective manner. Moreover, it is useful to have the operational limits in terms of environmental conditions (sea states, wind, current), and this is the main purpose of this study.

This study proposes a systematic approach for predicting allowable sea states based on installation procedures and coupled HLV-MP dynamic responses during MP installation at shallow seabed penetrations (in this paper also known as initial MP hammering process), which is a critical phase for MP installation. First, a general description of the MP's hammering procedure is given. Second, coupled HLV-MP dynamic model are established and used in steady-state time-domain simulations for incremental seabed penetration depths. Based on the numerical results, the critical events and corresponding limiting parameters are identified. Then, a systematic procedure to obtain the allowable sea states for such operations is proposed. To demonstrate the method, cases studies are conducted. Finally, conclusions are made and possible future work is presented.

2 MP hammering procedure and critical events

The system components and general MP hammering procedure are given in this section. Then, based on this procedure, a preliminary assessment of the critical events and their limiting parameters is given.

2.1 System components

The system set-up for the MP hammering process is illustrated in Fig. 1. The system is composed of HLV, MP foundation, hammer and gripper device. The common design of the gripper device includes several hydraulic cylinders. By varying the stroke length of the cylinders, the gripper is able to correct the mean inclination of the MP during the initial hammering process. The numerical modelling of the coupled system is discussed in detail in the next section. The main

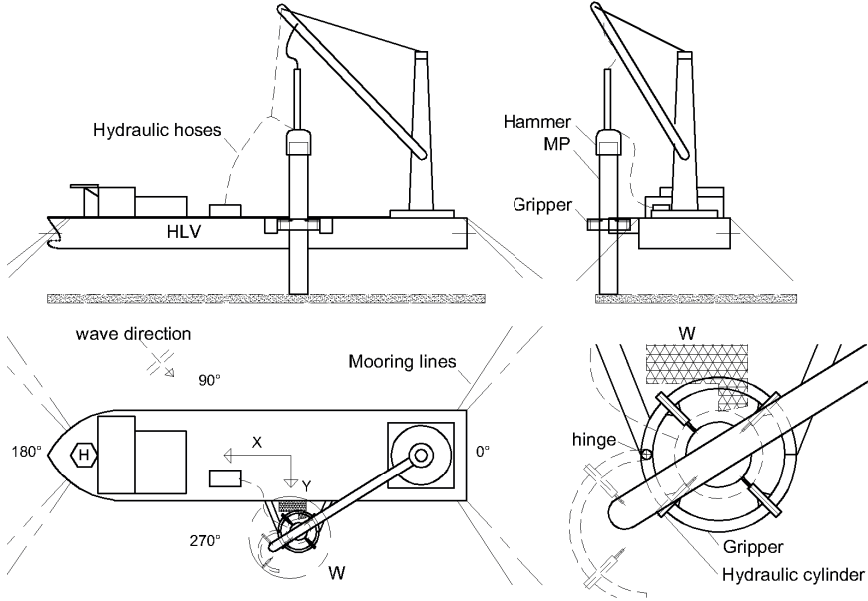


Figure 1: System set-up for the MP hammering process

particulars of the system components are shown in Table 1.

Table 1: Structures' main particulars

<i>Parameter</i>	<i>Notation</i>	<i>Value</i>	<i>Units</i>
<i>- HLV</i>			
Displacement	∇	5.12E4	Ton
Length	L	183	m
Breadth	B	47	m
Draught	T	10.2	m
Metacentric height	GM	5.24	m
Vertical position of COG above keel	VCG	17.45	m
<i>- Monopile</i>			
Mass	M_{MP}	500	Ton
Diameter	D_{MP}	5.7	m
Length	L_{MP}	60	m
<i>- Hammer</i>			
Mass	M_{Hammer}	300	Ton

2.2 General MP hammering procedure

After an initial self-penetration into the seabed, the MP is supported vertically by the soil and laterally by the gripper device. Then the main lift wire is released. The commonly applied

hammering procedure is described in the following steps.

1. Place the hammer onto the MP's top: The hydraulic lines are connected to the hammer, which is then lifted from the HLVs deck and placed onto the MP. The weight of the hammer increases the MP's self-penetration depth and moment of inertia and modifies the dynamic properties of the system.

2. Measure and correct the mean inclination of the MP: Current and wave forces normally cause an initial mean inclination of the MP which could be increased further at deeper penetrations if the hammering process starts without any correction. The conventional way to measure the verticality of the MP is using a handheld inclinometer on the outer surface of the pile. Due to the first and second-order vessel-induced motions and the irregularity of the pile surface, multiple measurements are required to ensure the accuracy. Despite this fact, the uncertainties of the measurements are relatively large. A new measurement method based on visual object recognition combined with vessel motion compensation is expected to increase the accuracy of vertically measurement and also the efficiency of the operation [9]. The corrections of MP inclination can be done using hydraulic cylinders on the gripper by varying the pressure in the cylinders to change the stroke length, see Fig. 1.

3. Pre-compress the hydraulic cylinders and hammer a few number of blows: Once the mean inclination is corrected, the hydraulic fluid supply valves are closed to keep the internal pressure, and a pre-compression force is applied to allow the cylinder rods to be in contact with the MP at all times to avoid gaps and subsequent impact loads. Corrective control of MP inclination is possible if the contact forces are not beyond the capacity of the hydraulic cylinders and the mean inclination is small. Therefore, during the initial hammering process only a few (around three) blows are given. The penetration rate of the MP depends on the soil conditions, and decreases with increasing depth. After each inclination correction, the hammer does not start immediately. There is a time interval between each correction and hammering activities, e.g, the time spent on preparation for hammering and waiting time between each blow. During this time interval, the HLV-MP system moves continuously in waves. Thus, the following hammer blows create a new MP inclination which depends on the motions of the system and the length of the time interval after the correction. This step lasts around 10 *min*.

4. Measure MP's inclination and correct it using hydraulic cylinders: After each hammering operation, correction of the mean MP inclination is required to avoid cumulative inclination angles prior to the next hammering. The hydraulic cylinders are only able to provide force to correct the inclination before the soil resistance becomes too large. An average time using inclinometers to measure the inclination will be less than 10 *min*.

5. Repeat step 3 and 4 until the hydraulic cylinders are not able to correct the MP's inclination: The previous two steps are repeated until the MP penetrates a few meters into the soil. At a certain stage, it is not possible to correct the MP's inclination by only using hydraulic cylinders.

6. Correct the inclination using thrusters and varying mooring line tension: Due to

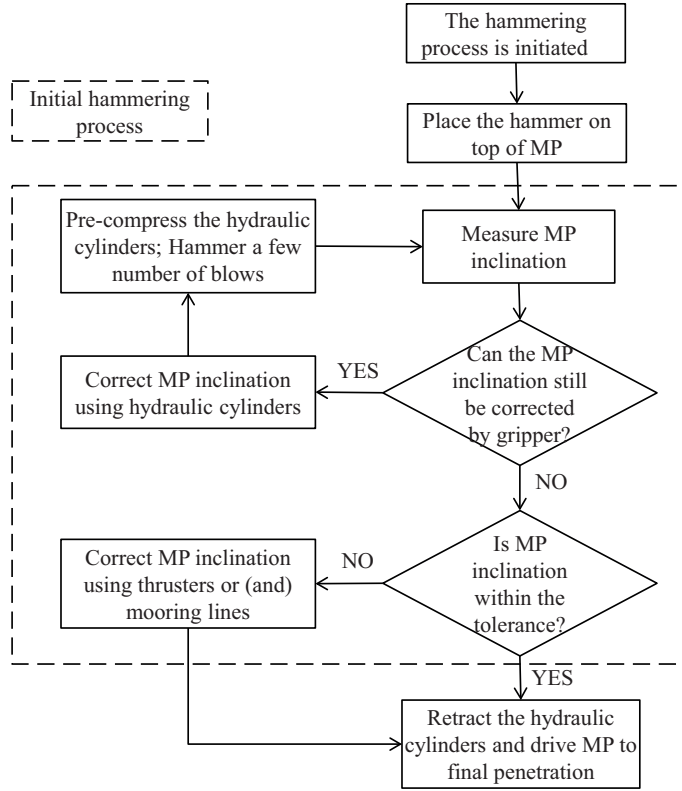


Figure 2: Flowchart of the MP hammering procedure

the high resistance from the soil, the hydraulic cylinders cannot correct the mean inclination of the MP. Therefore, it is necessary to apply the available thruster forces and change the mooring line length. These external forces will change the mean position of the vessel and they are transferred to the hydraulic cylinders which correct the mean inclination of the MP. A typical maximum combined thruster and mooring external force is around 400 kN for a HLV with characteristics used in this study.

7. Retract the hydraulic rods and drive MP to the final penetration: When the MP is stabbed deep enough into the soil, its inclination cannot be corrected due to soil resistance. The hydraulic rods are retracted. The MP is then driven to its final penetration. The inclination of the MP before retracting the rods determines the final inclination of MP since no corrections can be applied afterwards. This final piling could last less than 30 min depending on the soil properties. Note that a successful operation will require the system to be intact and the inclination to be acceptable before this activity.

The flowchart of the MP hammering procedure is shown in Fig. 2. The initial hammering process is defined in the flowchart which includes the hammering-measuring-correcting activities before retracting the rods of the hydraulic cylinders. The focus of this paper is on the initial

hammering process.

2.3 Critical events and limiting parameters

The possible critical events and limiting parameters from the initial hammering process (see Fig. 2) that may lead to an unsuccessful operation are summarized as follows.

- **Failure of the hydraulic system.** The extreme force on the hydraulic system may exceed the allowable values. These forces include the dynamic component due to HLV-MP dynamic motions and the static component which is required for the correction of the mean inclination of the MP. The exceedance of the allowable forces on the system will result in a hydraulic system failure and it is a critical event because it will not only stop the operation but also may pollute the environment if leakage of the hydraulic fluid occurs. The corresponding limiting parameters are the total force on individual hydraulic cylinder including the dynamic contact force and correction force. The probability of exceeding the allowable working forces should be kept small enough to ensure a sufficient safety margin.
- **Insufficient thruster and mooring line forces available.** The thruster and mooring lines may provide insufficient forces during the final correction of the MP's mean inclination. If the HLV is a dynamic positioning (DP) vessel, the thrusters are used to compensate the environmental forces and also to provide force to correct the mean inclination of the MP. When the penetration depth and the MP mean inclination are large, the extra static force required to correct the inclination can make the total forces exceed the thrusters' capacity. On the other hand, if only mooring lines are used to correct the MP inclination, the required tensions may not be applied. The limiting parameters for this event are the available thruster force and mooring line tension.
- **Unacceptable MP inclination.** MP inclination may exceed the allowable limit and result in an unsuccessful installation, and the typical limit is below 1° [10]. Because the hydraulic system and the thrusters are not able to correct the inclination of the MP after a certain penetration, the maximum inclination of the MP before retracting the hydraulic cylinders determines the final inclination of the MP. This event is not critical but restrictive for the installation requirement and its limiting parameter is the MP inclination due to the coupled HLV-MP motions.

The critical events and limiting response parameters differ if new procedures or equipment are employed. In this study, the thruster and mooring line capacity are assumed to be sufficient during the hammering phase and are not considered as limiting parameters in the numerical analysis. No structural damage on the MP due to gripper contact forces is assumed. In addition, the failure of the hydraulic system is driven by the extreme axial force exceeding the allowable design value, and the lateral loads are assumed secondary. A summary of the hammering process activities,

critical events, limiting parameters and allowable limits are listed in Table 2. For each activity, a preliminary estimation of the operational duration is given as reference for weather window analysis.

Table 2: Screening of MP sequential hammering activities, critical events and corresponding parameters to describe the events (limiting parameters)

No.	Activity	Duration [min]	Critical event	Limiting parameter
1	Place the hammer onto MPs top	45	/	
2	Measure and correct the inclination of the MP	20	/	
3	Pre-compress the hydraulic cylinders and hammer a few number of blows	10	/	
4	Measure MP inclination and correct it using hydraulic cylinders	10	failure of hydraulic system	individual hydraulic cylinder force
5	Repeat step 3 and 4 N times while it is possible to correct the MPs inclination	20*N	failure of hydraulic system	individual hydraulic cylinder force
6	Correct the inclination using thrusters and varying mooring line tensions	10	failure of hydraulic system, insufficient thruster capacity, mooring line failure, MP inclination not acceptable	individual hydraulic cylinder force, thruster force, mooring line tension, MP inclination
7	Retract the hydraulic rods and drive to final penetration	30	/	

3 Methodology to establish the allowable sea states

According to DNV-GL recommendations [11], the design and planning phases of marine operations shall evaluate allowable environmental conditions when the operations can be carried out and provide weather criteria for starting and interrupting the operations. In order to do this, the installation procedure and numerical models are used to identify potential restricting and critical events of the various sequentially defined installation activities. For these events, the corresponding limiting parameters are then identified. Next, characteristic responses need to be calculated from frequency- and/or time-domain analyses. By comparing the characteristic values of the limiting parameters at different environmental conditions with the allowable values, the allowable sea states can be found.

As discussed earlier, the initial hammering process finishes when the thrusters and the hydraulic cylinders cannot correct the inclination of the MP. The allowable sea states must ensure that the hydraulic system is intact and MP inclination is acceptable at this installation stage. The methodology proposed here requires the introduction of new parameters. Here let us define two “critical penetration depths”:

- d_{c1} : the penetration depth at which the MP can stand alone in the soil without any support from the vessel.
- d_{c2} : the penetration depth at which the hydraulic cylinders and thrusters are not able to correct the MP inclination;

To ensure a safe hammering operation, it is necessary to satisfy:

$$d_{c2} \geq d_{c1} \tag{1}$$

which requires the hydraulic cylinders to be able to support the MP until it can stand alone in the soil. Therefore, it is necessary to identify d_{c1} during the planning phase, and to calculate the extreme forces on the hydraulic cylinders when the penetration depth is less than d_{c1} . It will be shown later in the paper that the forces on the hydraulic cylinders increase significantly with increasing penetration depths, so it is beneficial to retract the cylinder rods upon reaching d_{c1} . In this paper, the completion of the initial hammering process is achieved when the MP’s penetration depth reaches d_{c1} . d_{c1} is calculated by evaluating the responses of the MP in relevant sea states supported only by soil at various penetration depths (MP-soil interaction model refers to subsection 4.1.3). In practice, safety factors should be included to ensure that the MP can stand alone in waves at this penetration depth.

The following procedure is then proposed to find the allowable sea states (see Fig. 3).

- For a given sea state, the first step is to calculate the “critical penetration depth” d_{c1} for which the MP (and the hammer on top) can stand in the soil for this sea states without any external supports from the HLV.

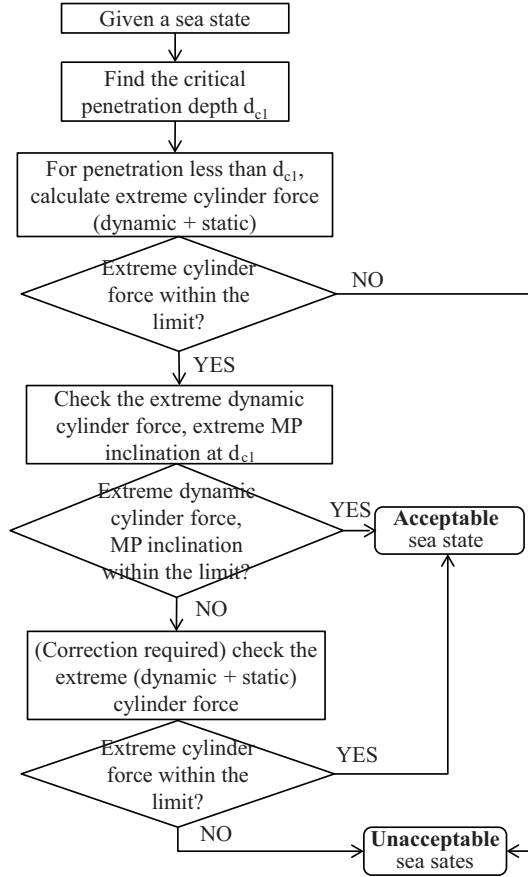


Figure 3: Methodology to find the allowable sea states for the initial hammering process

- Then, the force on the individual hydraulic cylinders which is the limiting criterion in the first several hammering actions is calculated. The extreme force should include both the dynamic force due to HLV-MP relative motions and the one required to correct the MP from a certain inclination to zero mean value. The limiting force criterion should be checked for each penetration depth less than d_{c1} to make sure the operation is acceptable for the subsequent activities. If the requirement fails at any penetration, the input sea state is considered “unacceptable”, and a lower sea state should be selected and evaluated.
- When reaching d_{c1} , the hydraulic cylinder rods are about to be retracted. If both the dynamic cylinder forces and MP’s inclination at d_{c1} are within the limits, the given sea state is acceptable without any further correction of the MP inclination. On the other hand, if the MP inclination exceeds the allowable value, further correction is required. Thus, the total correction and dynamic force on the hydraulic rods are calculated and it is acceptable if the total force is below the allowable values.

When assessing the operational limits, a probabilistic approach should be applied to take into account the uncertainties in measurements of the MP inclination, the extreme value estimates of the contact forces, soil parameters of the offshore site, numerical models and human errors. However, this study was simplified and these uncertainties were not considered. Based on the proposed procedure, the allowable sea states for a given installation site can be derived in the planning phase. In order to evaluate the responses of the system, a reliable numerical model for the hammering process is required. In addition, proper allowable values for different limiting parameters must be established. Before giving examples to find the allowable sea states, the numerical modelling of the dynamic system as well as its characteristic responses are studied in the next section.

4 Modelling and analysis of global dynamic responses of the coupled HLV-MP system

In this section, the numerical models used to investigate the responses of the coupled HLV-MP system at various seabed penetration depths are given to properly identify critical events and develop the methodology that was proposed in the previous section (see Fig. 3).

The time-domain simulations provide the dynamic global responses of the HLV-MP system in the steady-state condition at different penetration depths. Here the steady-state condition means that for each time-domain simulation, the mean draft of the vessel and the mean penetration depth of the MP do not change with time, and the wave realization follow a stationary distribution. The hammering operation itself (involving impact forces from the hammer blows) is not modelled. The hammering operation could happen at any time instance during the dynamic process when the MP moves horizontally at the gripper connection level. As a result, a new mean inclination angle of the MP is created. It is assumed that the soil force acts through the MP centre. The hammer impact does then not affect this mean inclination because the impact and the MP are perfectly aligned. The hydraulic cylinders are then used to correct the mean inclination before the next hammering operation. The correction phase is the most critical one because the forces on the hydraulic cylinders include both the dynamic component from the coupled HLV-MP motions and the actual correction force. Thus, the total contact force during the correction phase can be decomposed as the correction force from quasi-static analysis (see Sec. 5.2) and the dynamic force from the steady-state time-domain simulations in this section.

Furthermore, a sensitivity study on the effect of soil properties on the dynamic responses of the system with different soil properties are carried out in Sec. 4.3.

4.1 Theory and methodology for numerical modelling and analysis

The numerical model for this study was built using the MARINTEK SIMO program [12]. The model includes the coupled two-body HLV-MP system with mooring line positioning system on the

HLV and soil interaction forces on the MP at different penetration depths. The methodology for the modelling and the time-domain simulation are explained in detail in the following subsections.

4.1.1 Equations of motion for coupled dynamic analysis

The HLV-MP coupled dynamic system has 12 degrees of freedom (*DOFs*), and for each body, the following six equations of motion are solved in the time-domain.

$$\begin{aligned}
 (\mathbf{M} + \mathbf{A}(\infty))\ddot{\mathbf{x}} + \mathbf{D}_1\dot{\mathbf{x}} + \mathbf{D}_2f(\dot{\mathbf{x}}) + \mathbf{K}\mathbf{x} + \int_0^t \mathbf{h}(t - \tau)\dot{\mathbf{x}}(\tau)d\tau \\
 = \mathbf{F}_{ext}(t) = \mathbf{q}^{(1)}_{WA} + \mathbf{q}^{(2)}_{WA} + \mathbf{F}_{moor} + \mathbf{F}_{cpl} + \mathbf{F}_{soil}
 \end{aligned} \tag{2}$$

where, \mathbf{M} is the mass matrix; \mathbf{x} is the rigid-body motion vector of the body with 6 *DOFs*; \mathbf{A} is the frequency-dependent added mass matrix; and \mathbf{D}_1 and \mathbf{D}_2 are the linear and quadratic damping matrices. The viscous effects from the vessel hull and the mooring system were simplified into linear damping terms in surge, sway and yaw. The roll damping of the vessel as well as the quadratic damping on the MP were also included. Additionally, \mathbf{K} is the hydrostatic restoring matrix from the HLV and the MP; \mathbf{h} is the retardation function calculated from the frequency-dependent added mass or potential damping coefficients and \mathbf{F}_{ext} is the external force vector, including the first-order wave excitation forces, $\mathbf{q}^{(1)}_{WA}$, the second-order wave excitation forces, $\mathbf{q}^{(2)}_{WA}$, the mooring line forces on the HLV, \mathbf{F}_{moor} , the coupling forces between the HLV and MP, \mathbf{F}_{cpl} , and the soil reaction forces on the MP, \mathbf{F}_{soil} . The second-order wave excitation forces were obtained based on the Newman's approximation and include only the difference-frequency slowly varying forces [13]. The eight catenary mooring lines for the HLV were also modelled, and both a quasi-static analysis and a simplified dynamic analysis accounting for the effect of drag loading on the lines were applied.

It should be noted that this numerical model only accounts for wave loads on the HLV and MP. The mean wind and current speed will only create mean displacement, but the turbulence in wind may also provide dynamic loads. For this specific system with floating vessel and MP, the dynamic responses are governed by wave loads. Therefore, the effects from both wind and current are not considered.

The hydrodynamic interaction between the HLV and MP affect the wave excitation forces, the added mass and damping coefficients. In the current model, the hydrodynamic interactions mainly affect the forces on the MP due to the vessel presence, which is considered as "shielding effects" since the MP is a small structure compared with the HLV. The shielding effects from the vessel on the MP were studied during the non-stationary lowering operation when installing the MP in Ref. [6] by using interpolation of wave kinematics to calculate the wave forces on the MP. However, in the current numerical case the mean wet surface of the MP did not change during the simulation, and two panel models were built and the hydrodynamic interaction problems were solved using the panel method program WAMIT [14] in the frequency domain. In the time domain simulations, the effects on the wave excitation forces are included in the external forces on the right hand side

of Eq. (2) by applying force transfer functions from WAMIT, while effects on frequency dependent added mass and damping forces are included in the coupled retardation functions.

Step-by-step integration methods are applied to calculate the responses of the coupled HLV-MP system using an iterative routine. The equations of motion are solved using Newmark-beta numerical integration ($\beta = 0.1667, \alpha = 0.50$) with a time step of 0.01s. The first-order and second-order wave forces are pre-generated using the Fast Fourier Transformation (FFT) at the mean position of the HLV and the MP. The gripper coupling, mooring, as well as the soil-MP interaction forces are calculated in the time-domain. Short-crested waves with index $n = 3$ for the spreading function \cos^n is applied for all sea states [15].

4.1.2 Modelling of the gripper device

The gripper device is normally a ring-shaped structure with several hydraulic cylinders in a radial array which provide pressure and thus compression forces on the MP during the initial hammering process. In the numerical model, the gripper device was simplified by four fender components with chosen stiffness and damping coefficients. When the MP tends to move away from the gripper, the fenders provide compression forces and limit its horizontal motions. Fig. 1 shows the gripper model and the elastic model for the gripper contact elements are illustrated in Fig. 4. Sensitivity studies to quantify the effects of the gripper stiffness on the responses during the lowering of a MP were performed in Ref. [5]. The study showed that the contact force and the relative motion between the MP and the gripper device were very sensitive to the gripper stiffness.

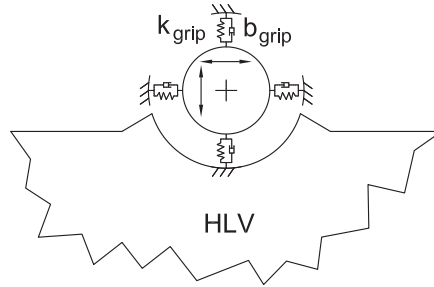


Figure 4: Elastic model of the gripper contact elements

In the present study, the parameters for the gripper are chosen based on specifications of typical hydraulic cylinders which are applied in practice for MP installation. During the hammering process, the valves of the hydraulic cylinders are normally closed. Because of the elasticity of the fluid oil, the hydraulic cylinder behaves like a mechanical spring. The stiffness of the spring was calculated according to Ref. [16] and depends on the fluid elasticity, the area of the piston and the total compression volume for the fluid. Damping is caused by friction in the actuator and the pipe system. By using technical data of hydraulic cylinders, the stiffness of the cylinder with closed

valves was found to be about $10^7 N/m$ to $10^8 N/m$, and was chosen to be $3 \cdot 10^7 N/m$ in the current model. The damping in the numerical model is taken to be 20% of critical damping which is a reasonable value for hydraulic cylinders [16].

It was also found from the numerical simulations that if an initial gap between the gripper and the MP is applied, huge impact forces will occur as compared to the case with a zero initial gap [6]. Because of the large inertia of the MP, initial gaps allow the MP to accelerate and the velocities at contact with the gripper increases. A good strategy is to provide zero gap with proper pre-compression forces to avoid gaps and consequently huge impact forces. In the current model, a pre-compression force of 150 *kN* for each hydraulic cylinder is applied.

4.1.3 Soil-MP interaction

The soil-structure interaction model is important for the global dynamic analysis of structures embedded in soil. Most of the relevant studies of the soil-MP interaction focus on installed piles, and not during the installation phase. For offshore structures, the foundation piles are normally subjected to axial, lateral and overturning loads. The method normally used to model the soil-pile interaction under these loads is based on the Winkler modelling approach with combination of $p - y$ curves, see e.g., Refs [17, 18, 19, 20, 21]. This method assumes that the pile acts as a beam supported by a series of uncoupled springs, each of which represents the local soil reaction forces. These springs are described by non-linear functions ($p - y$ curves) to define the soil reaction force, p , at a given depth, as a function of the lateral displacement, y [22, 23]. The $p - y$ curves for offshore structures are based on the results of field tests on long slender piles, with diameters around 610 *mm* and a large length to diameter ratio of 34 [24].

The conventional $p - y$ method was extended for large diameter MPs by including additional soil reaction terms [24, 25]. Four separate components of soil reaction were included in the proposed design model: the traditional distributed $p - y$ curve, the distributed moment curve due to the vertical shear (skin friction) around the pile, the base shear curve and the base moment curve [24]. Results from 3D finite element parametric studies on large piles with diameters from 5 *m* to 10 *m* indicated that $p - y$ curve features were dominant for the long piles (length to diameter ratio is 6) while the other three factors were negligible. However, for short piles (length to diameter ratio is 2), these additional terms became more significant, especially the distributed moment due to the friction between the soil and the pile [24]. For the initial hammering process with soil-MP model at shallow penetrations, the length to diameter ratio is less than 2. Therefore, both the $p - y$ curve and the distributed moment should be accounted for.

Besides the stiffness modelled by nonlinear springs, the soil damping needs to be considered to study the dynamic behaviour of the system. Soil damping comes in two main sources: radiation damping and hysteretic material damping. Radiation damping is negligible for frequencies less than 1 Hz [17]. Therefore, the main contribution for the current model is from the hysteretic material damping. The material damping can be estimated from a hysteresis loop created by loading and unloading $p - y$ curves [26].

In this study, the soil-MP interaction is modelled using the extensively applied Winkler model by means of distributed springs and the hysteretic material damping. The penetration of the MP during the initial hammering process ranges from around 2 m (self-penetration) to around 6 to 8 m (depending on soil properties) after which the gripper can not correct the MP inclination. The soil-MP interaction forces in the shallow penetration phases are three-dimensional, therefore the 2D Winkler model is extended to 3D by using non-linear springs distributed in both axial and circumferential directions along the MP. The distributed springs include the traditional lateral load-deflection $p - y$ curve, the friction $T - z$ curve which was found to be significant for large diameter piles with shallow penetrations [24], the base shear curve and the tip load-displacement $Q - z$ curve.

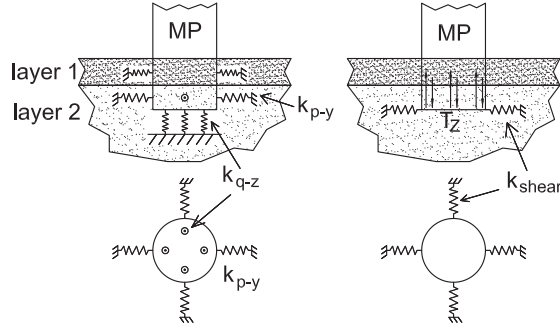


Figure 5: Numerical models for the soil-MP interactions

The configuration of springs as shown in Fig. 5 is summarized as follows: 4 vertical springs K_{q-z} to model $Q - z$ curves at the bottom of the MP; 4 springs T_z on the side of the MP to model the $T - z$ curve for the friction force from both inside and outside wall of the MP, and the vertical position of the T_z springs are calculated by considering the distribution of the friction along the whole MP penetration length. For $p - y$ curves, the whole penetration is divided into several 2m-layers, and 4 circumferential springs K_{p-y} are applied for each layer. On the bottom of the MP, 4 springs K_{shear} are used to model the shear resistance force. The number of the distributed spring is considered to be sufficient since the MP bottom tip will experience small displacement (less than 10 cm for typical sea states).

An estimate of the stiffness for all the non-linear distributed springs shown in Fig. 5 are taken from the API guideline [23]. The API approach is pertinent to the small diameter flexible piles and it underestimates the soil reaction at the top of large diameter MPs [18, 27, 28]. From Ref. [24], it was found that API and FEM methods result in different load-displacement curves. The differences are however important for site specific soil types and vary even in the same field. In this paper, the methodology is general and intended to cover typical soil parameters ranging from soft to hard soil, so that it would be applicable to any soil whose properties fall within the ranges considered here. Furthermore, from the sensitivity study on the soil properties in this paper in

Sec. 4.3, it is concluded that the dynamic system behaviour during the operation does not change with the soil properties. Therefore, representative values for the non-linear springs for the soil-MP interactions are considered to be sufficient for this study. In addition, the cyclic loading effects, such as accumulation of deformation and degradation are not considered. The soil properties used to calculate the spring stiffness are shown in Table. 3. As mentioned earlier, the soil damping is included in this model in terms of dynamic friction force. A typical soil reaction moment and MP inclination curve under cyclic loads in the current MP-soil interaction model is shown in Fig. 6.

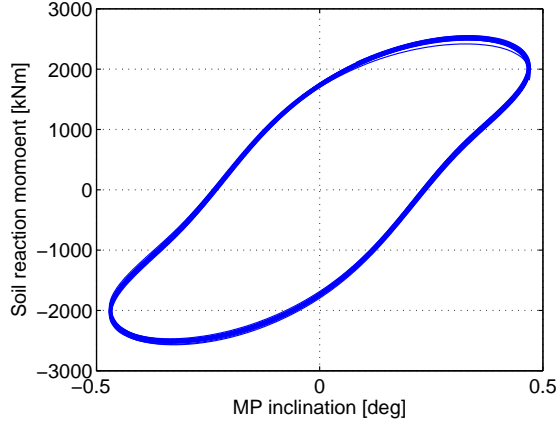


Figure 6: Typical soil reaction moment versus MP inclination due to cyclic loading with period of 6 sec.

Table 3: Soil properties applied in the numerical model (refer to Ref. [29])

layer	Type	submerged unit weight [kN/m^3]	internal friction angle [deg]	unit skin friction [kPa]	unit tip resistance [kPa]
0m-2m	sand	10	36	20	1900
2m-4m	sand	10	36	24.8	2300
4m-6m	sand	10	37	39.1	3400
6m-8m	sand	10	35	51.4	3700
8m-10m	sand	10	35	51.4	3700

4.2 Dynamic response of the HLV-MP system at different penetration depths

The purpose of the time-domain simulations is to identify the limiting parameters and critical events. The numerical model was established using MARINTEK SIMO program [12] and was verified with the one built in ANSYS AQWA [30] from where consistent results were obtained. To compare the responses of the MP in different installation stages, five penetration depths of the

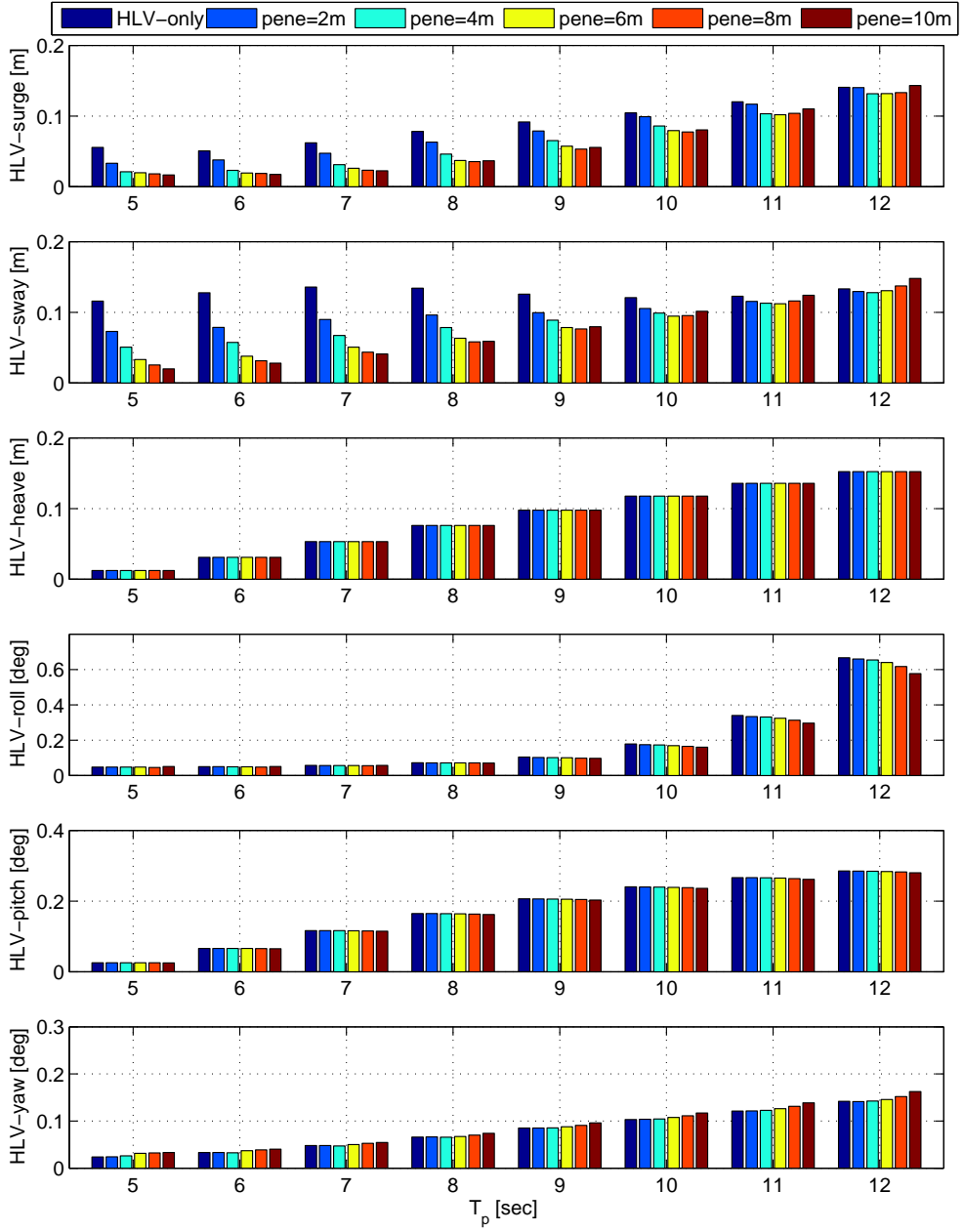


Figure 7: Standard deviations of HLV motions at different MP penetration depths ($pene$) and wave conditions from 3-hour time-domain simulations ($H_s = 1.5\text{ m}$, $Dir = 150\text{ deg}$)

MP were considered, i.e., $2m$, $4m$, $6m$, $8m$, and $10m$. The condition with HLV free floating is also included for comparison against the coupled HLV-MP dynamic responses at various loading conditions. The dynamic responses from the time-domain simulations include the motions of the HLV-MP system, and forces from the coupling in the gripper, the mooring lines of the HLV as well as the soil-MP interaction. The results presented in this section allow better understanding of the dynamic system behaviour towards identifying the limiting parameters. The characteristic values of the limiting parameters to determine the allowable sea states are evaluated later in Sec. 5.

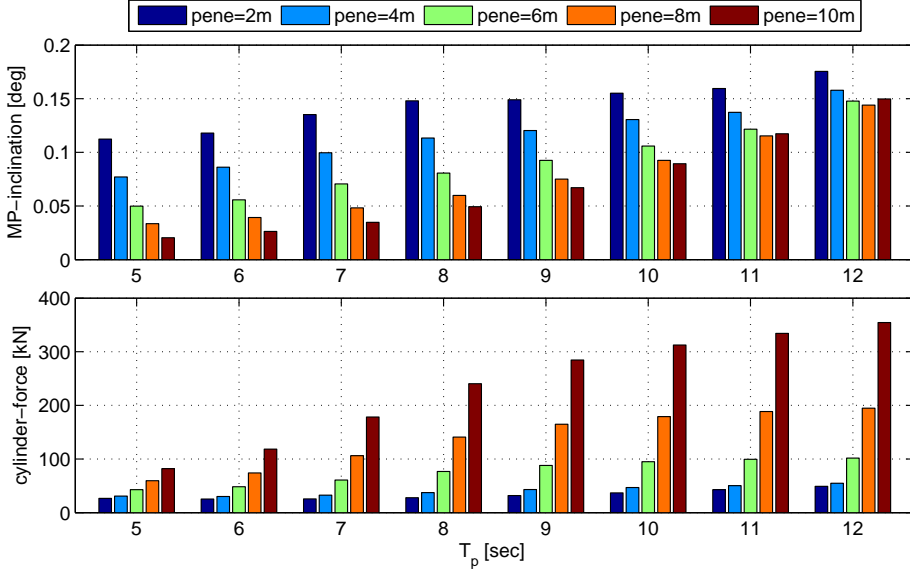


Figure 8: Standard deviations of MP inclinations and contact forces on one hydraulic cylinder at different MP penetration depths ($pene$) and wave conditions from 3-hour time-domain simulations ($H_s = 1.5\text{ m}$, $Dir = 150\text{ deg}$)

Fig. 7 compares the responses of the HLV in free floating (*HLV – only*) and the HLV coupled with the MP at different penetration depths. This figure displays the standard deviations (*STD*) of the HLV motions in 6 DOFs with respect to its COG. The responses at different wave peak periods show different trends when the penetration of the MP changes. In general, the motions of the HLV in the vertical plane (heave, roll and pitch) change little at different penetration depths. The roll motion decreases slightly with increasing MP penetrations because of the stiffness and damping contributed from the soil-MP interaction. When the wave peak period increases, the motions in the vertical plane increase due to increasing first-order resonant motions of the HLV in long waves.

On the other hand, the motions in the horizontal plane (surge, sway and yaw) show large variations for different loading conditions. In short waves, the surge and sway motions decrease rapidly with increasing penetrations. However, in long waves the motions first decrease and then

increase for larger depths (8 m and 10 m). The yaw motion of the vessel increases rapidly with the wave period.

Similarly, the responses of the MP inclination vary greatly with the MP penetration as observed in Fig. 8. The first row in Fig. 8 shows the *STD* of the MP inclination and the second row shows the *STD* of the individual hydraulic cylinder contact force. The reason why the horizontal motions of the HLV-MP system show different characteristics in short and long waves is the change of the natural modes periods of the system with the coupling between HLV and MP at different penetration depths. This can be seen from the response spectra at different conditions.

Figures 9 to 11 show the response spectra of the surge and sway motion of the gripper, the yaw motion of HLV at two wave peak period conditions. The gripper motions were calculated based on the HLV motions according to the following equation:

$$\mathbf{s} = (\eta_1 + z\eta_5 - y\eta_6)\hat{i} + (\eta_2 - z\eta_4 + x\eta_6)\hat{j} + (\eta_3 + y\eta_4 - x\eta_5)\hat{k} \quad (3)$$

where η_1 to η_6 are the 6 DOF rigid body motions of the HLV and (x, y, z) is the position of the gripper in the HLV body-fixed coordinates, which is $(x = -10m, y = 30.0m, z = 10.0m)$. Since the x and z positions of the gripper are close to the HLV COG while it is 30 m away from the HLV in y coordinate, the yaw motion of the HLV greatly affects the surge motion of the gripper.

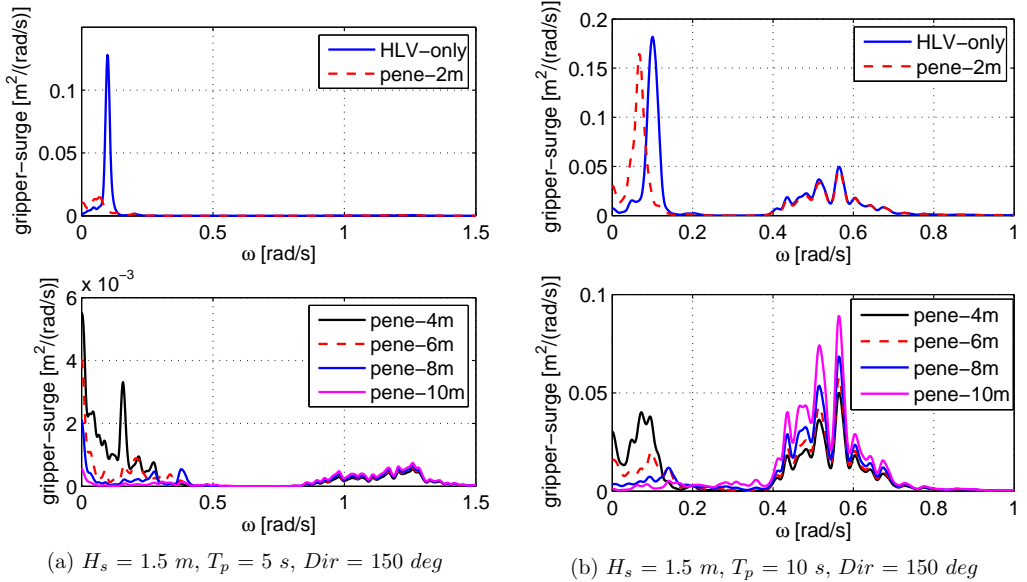


Figure 9: Response spectra of the gripper surge motion for two different wave peak periods at different MP penetration depths (*pene*)

The natural frequencies of the moored HLV alone are around 0.1 rad/s for surge and sway and around 0.2 rad/s for yaw. In contrast, for the coupled HLV-MP system, different modes are

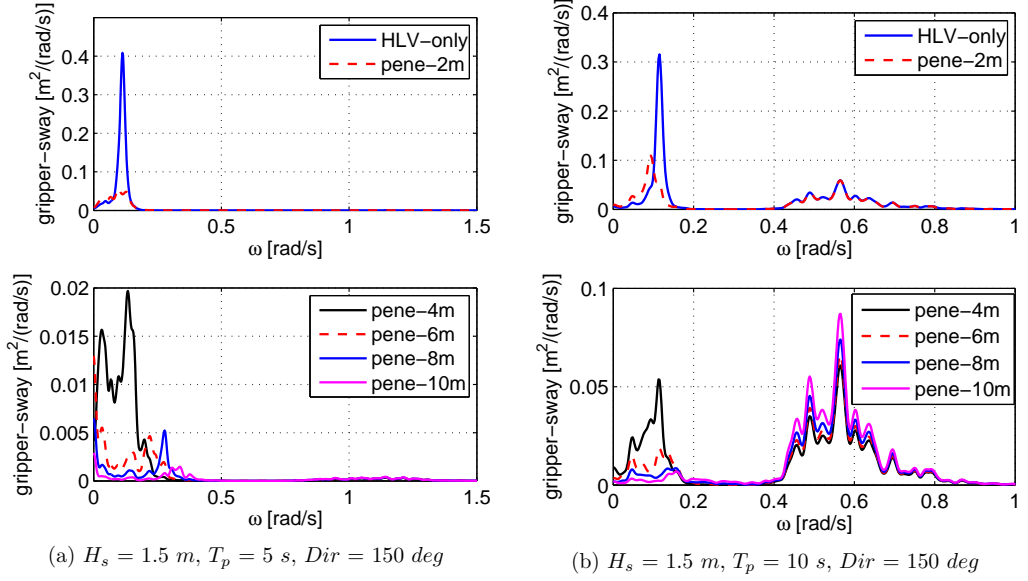


Figure 10: Response spectra of the gripper sway motion for two different wave peak periods at different MP penetration depths (*pene*)

identified. The system properties change with MP penetration depth, and the dynamic responses vary with wave conditions.

In short waves with $T_p = 5 \text{ s}$, the surge, sway and yaw motions for different MP penetrations are dominated by the second-order motions of the vessel. For sway, the peak frequencies shift to the higher values and the amplitudes decreases with increasing penetrations (see Fig. 10a). This is because of the increase on the contribution from the soil-MP interactions. For surge and yaw motions, the response modes are more complicated. The original modes for yaw and surge of the HLV change when the HLV is coupled with MP (see Fig. 9a, both surge and yaw contributes to the gripper surge motion), and the yaw rotation center is shifted from the COG of the HLV towards the MP due to large gripper and soil stiffness. As a result, the surge and yaw motions of the HLV have large coupling and two modes are observed: one mode with surge and yaw in phase and the other mode with surge and yaw out of phase. The natural frequency of the second mode increases rapidly with MP penetration and become close to the peak frequencies of long waves (see Fig. 11b).

With the increase of the wave peak period, the first-order motions of the vessel increase. For shallow penetrations, the second-order motions are still dominating, while for deeper penetrations the first-order motions dominate the total responses (see Fig. 9b). Since the natural period of the motions in deeper penetrations are closer to the wave peak periods compared to those in the shallow penetration cases, the first-order motions increase with the penetration (see Fig. 9b

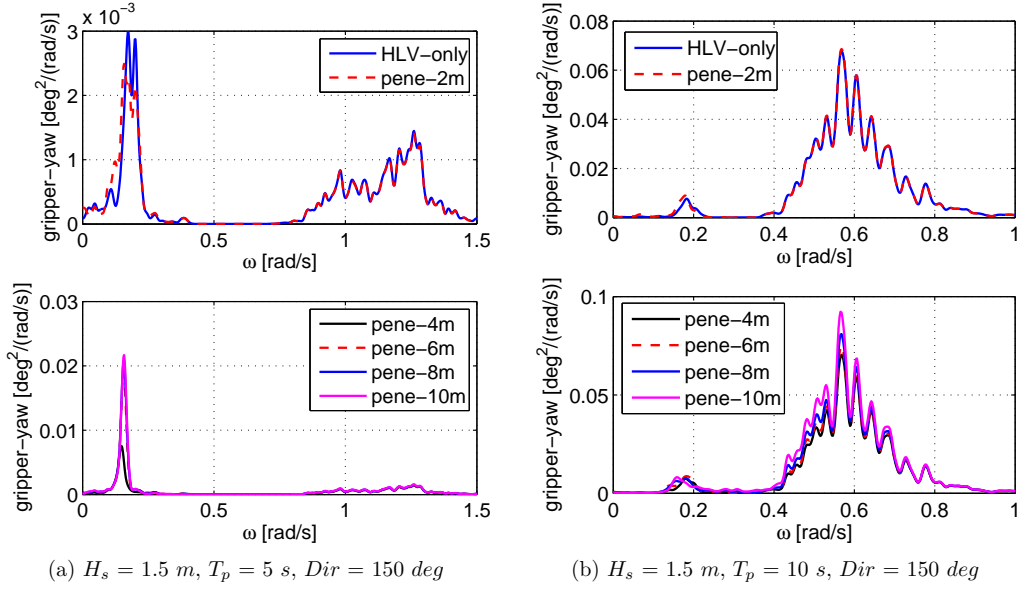


Figure 11: Response spectra of the HLV yaw motion for two different wave peak periods at different MP penetration depths (*pene*)

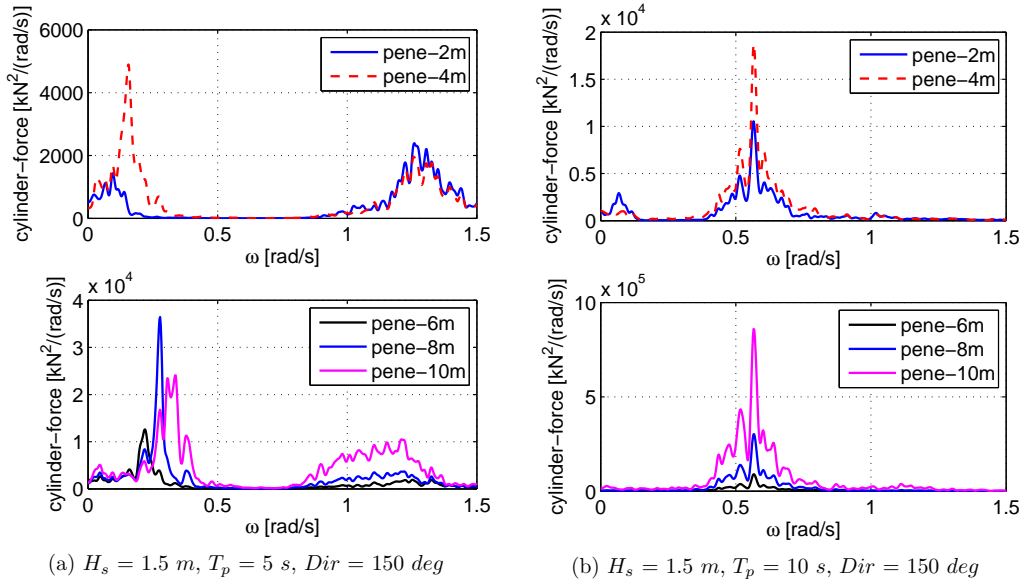


Figure 12: Response spectra of the hydraulic cylinder force for two different wave peak period conditions at different MP penetration depths (*pene*)

bottom). Therefore, the total motions begin to increase in long waves when the first-order motions dominate (e.g., Fig. 7 top). The increase of gripper surge motions are the most significant because of the contributions from both surge and yaw motions of the HLV. The cylinder contact forces keep increasing with the penetration and wave period as shown in Fig. 8. The spectra of the force on one hydraulic cylinder are shown in Fig. 12. For both short and long waves the first-order responses dominate for penetrations larger than 4 m. The second-order components contribute in short wave conditions, especially when the MP penetration is small. Due to the significant increase of the soil stiffness with penetration depth, the gripper force in general follows the same trend for different wave conditions. The cylinder contact force may exceed the design forces when the MP is deep in the soil and the wave period is large, and it is beneficial to retract the cylinder rods to avoid huge cylinder forces at larger soil penetration depths.

From the dynamic responses above, it is clear that the MP can reach unacceptable inclination angles during normal operational conditions, and the cylinder contact forces may exceed the allowable working limits. Thus, both MP inclination and cylinder contact force are considered to be “limiting parameters” of the initial hammering process.

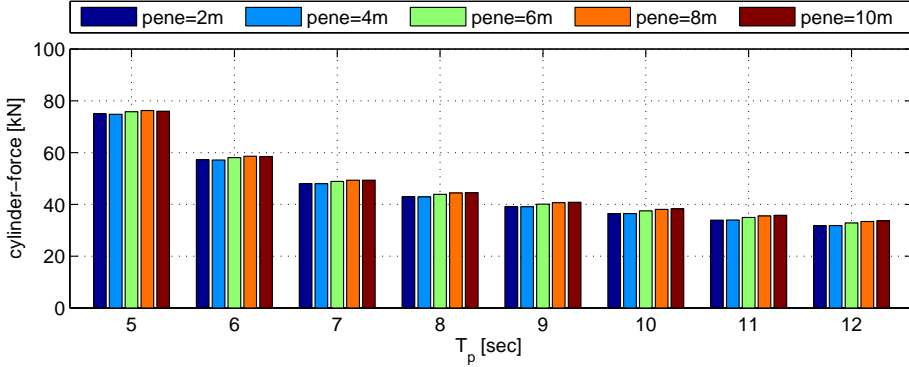


Figure 13: *STD* of hydraulic cylinder contact forces at different MP penetration depths (*pene*) when using a jack-up vessel ($H_s = 1.5$ m, $Dir = 150$ deg)

For comparison, the hydraulic cylinder forces when using a jack-up are shown in Fig. 13. Because little motion of the jack-up in waves and high stiffness of the gripper device, the inclination of the MP is negligible in all conditions, and the cylinder contact forces are in general smaller compared with using the floating vessel. The cylinder force decreases with wave periods and change little with the MP penetration depth. Since the jack-up is a fixed platform, the gripper and the soil are only required to counteract the wave excitation forces on the MP which decreases with wave periods. The increase of the penetration depth only changes the boundary condition of the MP and does not affects the wave excitation force. The cylinder contact force in short waves are observed larger when using a jack-up than using the floating vessel at shallow MP penetration. This is because the shielding effect reduces the MP excitation force when employing the floating vessel, while no shielding effect exists from the jack-up vessel [6]. The comparison shows that

the limiting parameters for floating vessel installation activities are not considered critical when using a jack-up vessel. The critical activity for a jack-up is during the installation and retrieval phases, i.e., the phases when the legs are being set down onto and lifted up from the seabed. The critical event due to the impacts from vessel motions in waves and “punch through” the soil is the consequent failure of the structural components, see e.g. Refs. [3, 31].

4.3 Sensitivity study on the soil properties and effects on the dynamic system behaviour

To generalize the methodology to different site conditions, sensitivity studies are performed using three soil properties. The chosen soil properties cover most of the sandy soils for shallow penetrations. The stiffness of the distributed springs K_{p-y} , T_z , K_{q-z} and K_{shear} as shown in Fig. 5 increase from soft soil to hard soil, and here only the representative $p - y$ curves for three soil properties at two penetrations are shown in Fig. 14. Dynamic analysis of the HLV-MP-soil system are performed in different sea states with MP at various penetrations, and the modelling parameters for the sensitivity study are shown in Table 4.

Table 4: Parameters for sensitivity study on the soil properties

	Soil identity	Type	MP penetration	Sea states
1	soft soil	sand	2m, 4m, 6m, 8m	Hs=2m, Tp=6s; Hs=1.6m, Tp=8s
2	medium soil *	sand	2m, 4m, 6m, 8m	Hs=2m, Tp=6s; Hs=1.6m, Tp=8s
3	hard soil	sand	2m, 4m, 6m	Hs=2m, Tp=6s; Hs=1.6m, Tp=8s
* the properties for medium soil refer to Table. 3				

Figure 15 displays the relation between the individual cylinder contact force versus the MP inclination, which were found to be the limiting parameters for this operation. The results using different soil properties with MP at various penetrations are included in the same figure. The axis are the maximum inclination and maximum contact forces which are used to evaluate the allowable sea states. The procedure followed for calculation of the maximum values is explained in Sec. 5.

For a given soil property, Fig. 15 shows that the contact force and the MP inclination at different MP penetrations follow a trend. It can be observed from the figure that for both sea states, the contact force increases while the MP inclination decreases in deeper seabed penetrations. For different soil types, the force-inclination relation follows the same trend as shown in Fig. 15. Although, the maximum forces for $H_s = 1.6 \text{ m}$, $T_p = 8 \text{ s}$ scatter more at higher penetrations, the results show good consistency in the force-inclination trend and therefore in the dynamic system behaviour. Thus, it is evident that the force-inclination relation is not sensitive to the soil properties. For a given allowable limit of the contact force, the MP inclination for different soils are the same, but the critical penetrations corresponding to the limiting force are different - it is deeper in soft soil than in hard soil. In other words, the allowable sea states do not depend on

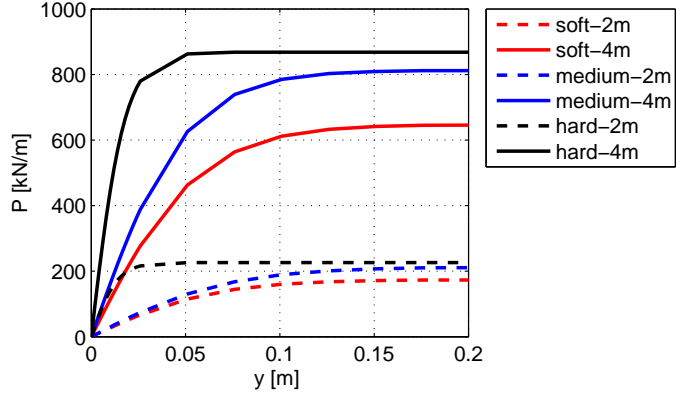


Figure 14: $p - y$ curves for different soil types

the soil types, but the critical penetration depth to retract the hydraulic cylinders d_{c1} (see Fig. 2) varies with soil properties.

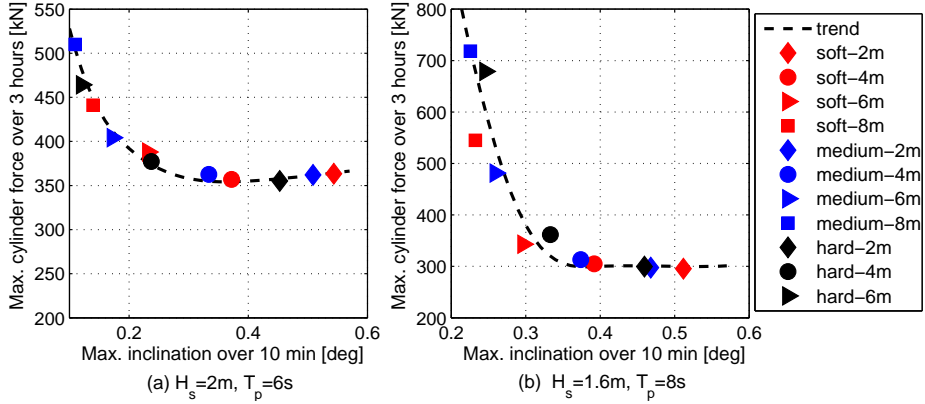


Figure 15: Extreme cylinder force in 3 hours versus MP maximum inclination in 10 *min* for different sea states and soil properties at different penetrations

Thus, the methodology proposed to assess the operational limits for this operation can be generalized for different soil conditions. In addition, this sensitivity study also proves that the soil weakening effects due to cyclic loads may change the critical penetration depth, but the maximum contact force and corresponding MP inclination are not influenced. Therefore, to identify the limiting parameters and develop methodology to establish the allowable sea states for the MP initial hammering operation, it is sufficient to use representative soil properties. In the following case studies, the “medium soil” (see Table 4) is applied for all sea states.

5 Case study on allowable sea states

The purpose of this section is to apply the proposed systematic methodology for preliminary assessment of the allowable sea states via numerical examples. The characteristic values of the limiting parameters, i.e., the cylinder contact force and the MP inclination are first obtained based on numerical simulations. The corresponding allowable limits are also presented and followed by typical case studies on allowable sea states.

5.1 Extreme dynamic forces on hydraulic cylinders

The extreme total force on the hydraulic cylinder includes the dynamic force from the steady-state conditions which is presented in this subsection and the correction force during the correcting phase which is discussed in the next subsection.

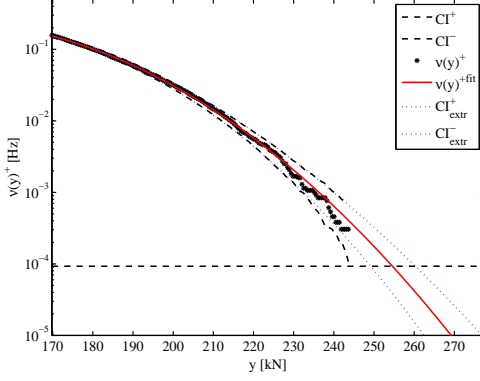
In this study, the extreme dynamic forces are calculated as the maximum value in 3 hours, corresponding to a probability of exceedance of around 10^{-4} . This value is chosen to ensure structural integrity and is commonly used for marine operation activities [11]. In practice, the equipment should be sized based on the required number of installations, and the extreme forces used for selecting the equipment should be consistent with its service life. Besides, possible sources of uncertainties (e.g., the environmental conditions) need to be included in terms of safety factors. However, it is out of the scope of this study.

The extreme dynamic force on the gripper is estimated from the steady-state time domain simulations using the empirical mean upcrossing rates. The upcrossings of high threshold limits are statistically independent events, and thus a Poisson probability distribution is assumed adequate for the extreme values [32]. The cumulative distribution function of the extreme value $M(T)$ of the response process during the time T is then given by [33]

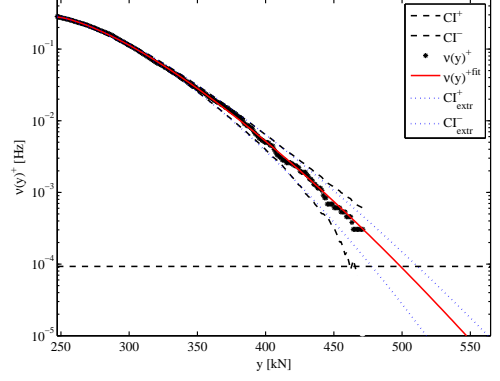
$$P(M(T) \leq y) = \exp\left(-\int_0^T \nu_y^+(t)dt\right) \quad (4)$$

where ν_y^+ denotes the positive mean upcrossing rate of the level y , which is defined as the frequency of passing the level y . ν_y^+ is found from time-domain simulations, and extrapolation is required for low upcrossing rates values. The extrapolation strategy proposed in Ref. [34] is applied.

Figure 16 shows two examples of the fitting and extrapolation of the cylinder forces with low and high extreme values, respectively. One clearly see that the present upcrossing method follows the empirical points appropriately. The confidence interval of 95% is also shown to estimate the deviation of the results. The 3-hour extreme values for different sea states are obtained using this method and presented in Fig. 17. The extreme values in this figure are obtained using 10 samples of 40-minutes simulations. As shown, the extreme dynamic forces increase significantly and non-linearly with both penetration depth and wave height.

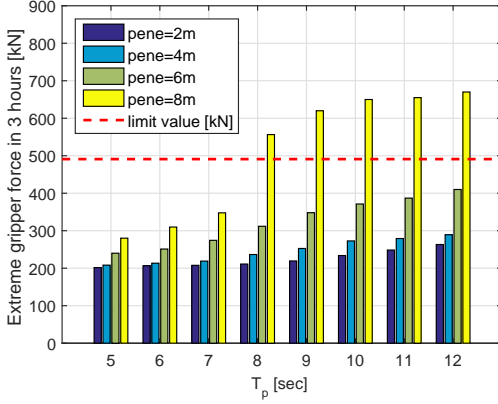


(a) $H_s = 1.5$ m, $T_p = 6$ s, $pene = 4$ m

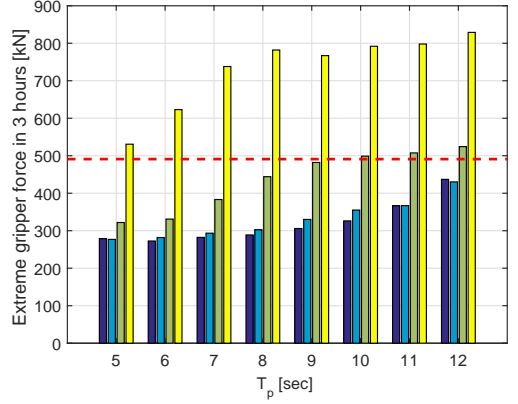


(b) $H_s = 1.5$ m, $T_p = 10$ s, $pene = 6$ m

Figure 16: Mean upcrossing rate of the hydraulic cylinder force using 20 samples. Legends: time-domain simulation (*), curve fitting (—), empirical 95% confidence band (CI^- — —), smooth confidence band (CI_{extr} ···)



(a) $H_s = 0.8$ m, $Dir = 150$ deg



(b) $H_s = 1.5$ m, $Dir = 150$ deg

Figure 17: Extreme cylinder forces in 3 hours at different penetration depths ($pene$)

5.2 MP inclinations and correction forces

As mentioned, after every hammering operation before reaching the critical depth d_{cl} at which the MP can stand alone in waves, the mean inclination of the MP should be corrected using hydraulic cylinders. This mean MP inclination is created by the hammer blows when the HLV-MP system experiences wave-induced motions. During the correction phase, the total force on the hydraulic cylinder includes the dynamic forces induced by the waves and a correction force when changing the cylinder's rod length and mooring line tensions for correction of the MP inclination. As

mentioned, in the numerical model the total correction force, F_c , is decomposed as a dynamic and a correction component. The dynamic force in waves during the correction is consistent with the one at steady-state condition with zero mean inclination and the extreme dynamic value is obtained from Fig. 17. The correction force is then calculated here by excluding the waves.

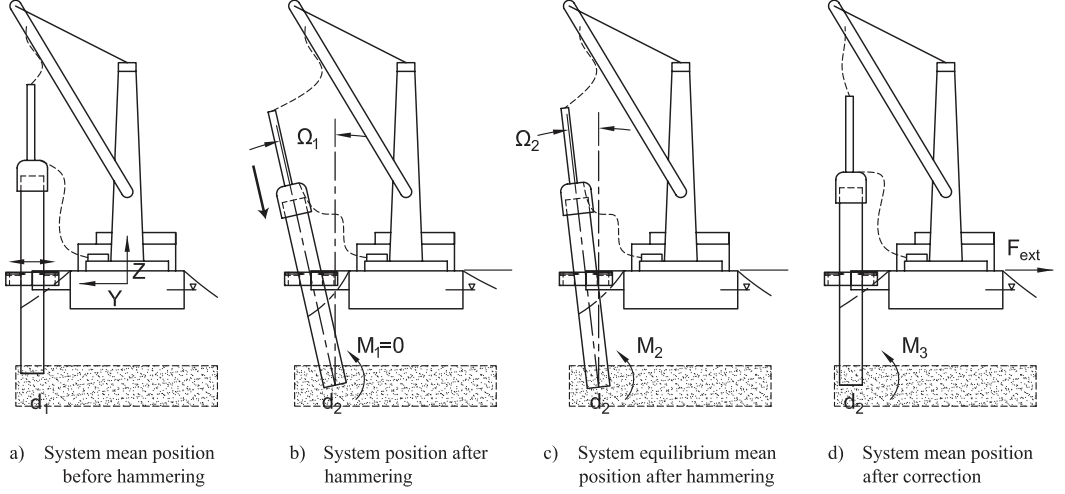


Figure 18: Illustration of the phases between hammering activities

Figure 18 illustrates the phase between each hammering activity. After each correction the mean MP inclination is zero (Fig. 18 (a)). Due to the dynamic motions of the HLV-MP system, after the hammer blows the MP has a mean inclination angle Ω_1 , and the penetration depth increases from d_1 to d_2 (Fig. 18 (b)). The hammer blows do not influence this mean inclination because it is perfect aligned with the MP. The soil is assumed to be in intact condition after each hammering activity for MP mean inclination Ω_1 , so the soil reaction moment is $M_1 = 0$. Meanwhile, the HLV has an offset from its mean position, and its mooring lines tend to restore the vessel towards its mean position and the MP inclination is reduced. The soil reaction force and the mooring line tension reach equilibrium at the MP mean inclination angle Ω_2 with soil reaction moment M_2 (Fig. 18 (c)). The phase from inclination angle Ω_1 to Ω_2 is considered to be mooring line “restoring phase”. Then, by applying external forces on the system F_{ext} , the mean inclination angle Ω_2 is corrected to a zero mean value (Fig. 18 (d)).

During the correction phase with MP mean inclination from Ω_1 to Ω_2 and further to 0, the maximum correction forces on the hydraulic cylinders are used together with the extreme dynamic forces in waves to calculate the total extreme forces on the hydraulic cylinders. The cylinder contact force at any inclination angle Ω_i between Ω_1 and 0 deg needs to overcome the soil reaction forces and the inertial moment at Ω_i . The soil reaction force is calculated using the model shown in Fig. 5, with initial intact condition at MP inclination Ω_1 . Then, the approach to estimate the correction forces here is conservative.

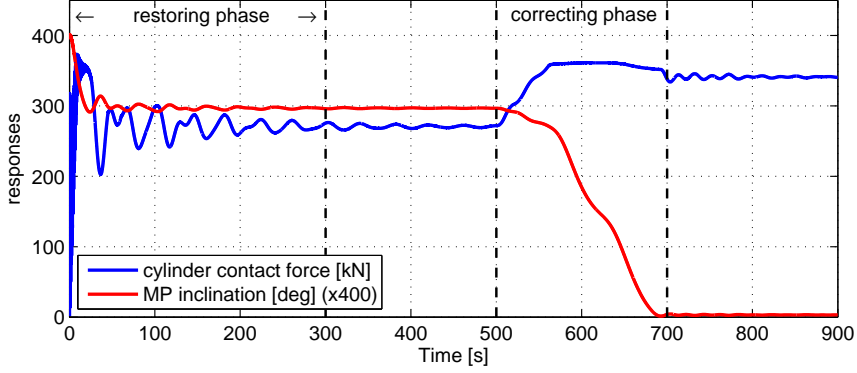


Figure 19: Responses of the HLV-MP coupled system after hammering and during the correction phase (corresponds to Fig. 18 (b) to (d))

Figure 19 shows an example on the responses of the coupled HLV-MP system during the restoring and correction phases (corresponds to Fig. 18 (b) to (d)) at MP penetration depth of $6m$ and an initial mean inclination angle from hammering $\Omega_1 = 1 \text{ deg}$. The results in Fig. 19 are for heading sea condition (while Fig. 18 illustrates the case for beam seas). During the “restoring phase”, the MP mean inclination decreases from 1 deg to around 0.75 deg and the cylinder force also decreases due to decreasing friction force from the soil. Next, by applying external forces at time instance 500 s , the cylinder contact force begins to increase to overcome the soil reaction force and the MP inclination decreases to zero. The maximum force from this process is taken as the correction force, and Fig. 20 presents the correction force for different penetration depths and initial mean inclination Ω_1 .

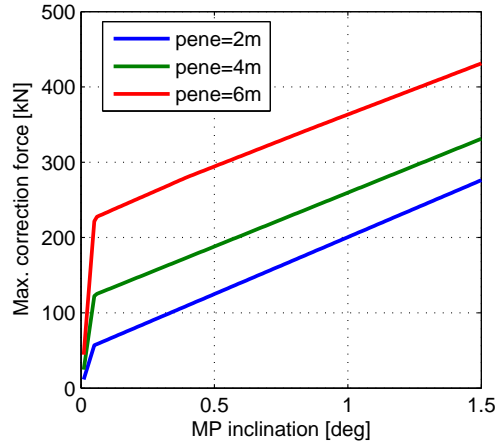


Figure 20: Correction forces at different penetration depths (*pene*) and initial mean inclinations

As shown, the correction force increases significantly with the initial inclination angle Ω_1 from

the hammer blows. As discussed earlier, Ω_1 depends on the coupled HLV-MP motion as well as the time interval between the end of the previous correction and the end of each hammering activity. This time interval is considered to be less than 10 *min* (refer to Table. 2). Therefore, the maximum inclination over 10 *min* is applied as the characteristic value for Ω_1 to obtain the correction force using Fig. 20, while the probability of exceedance of 10^{-4} (used for the characteristic cylinder forces) is not applicable because the inclination will not lead to structural failure. Similarly, the final inclination of the MP in the initial hammering process is also chosen as the maximum value over 10 *min* after the last correction. Fig. 21 shows the 10-min maximum inclinations in different conditions. The inclination increases significantly with both T_p and H_s . In lower sea states with $H_s = 0.8$ m, the inclination is below the limit value, but corrections are still required for a penetration less than the critical penetration depth to avoid cumulative inclinations.

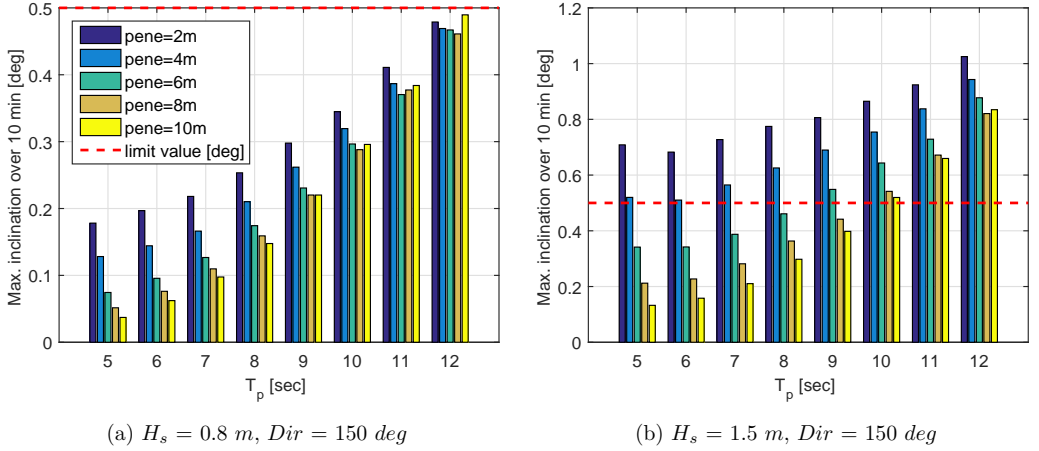


Figure 21: Maximum MP inclination over 10 *min* at different penetration depths (*pene*)

5.3 Case studies

In this study the mechanical components of the gripper and their configuration were selected based on the most common designs used in the industry. Assuming the rod diameter of the hydraulic cylinder is around 140 *mm*, according to the technical data for 100 *bar* cylinders, the limiting force is around 491 *kN* [35].

Piling tolerances are set by combining a number of aspects. The governing factor is the tolerance on the lower flange of the turbine tower. In most cases this is 0.1° . Counting back from this, combining it with the maximum correction that can be made with a transition piece or shims, the tolerance for the inclination of the piles is set. The values are normally between 0.5° and 1° for MPs [10]. In the case study, 0.5° is applied as the allowable limit for MP inclinations.

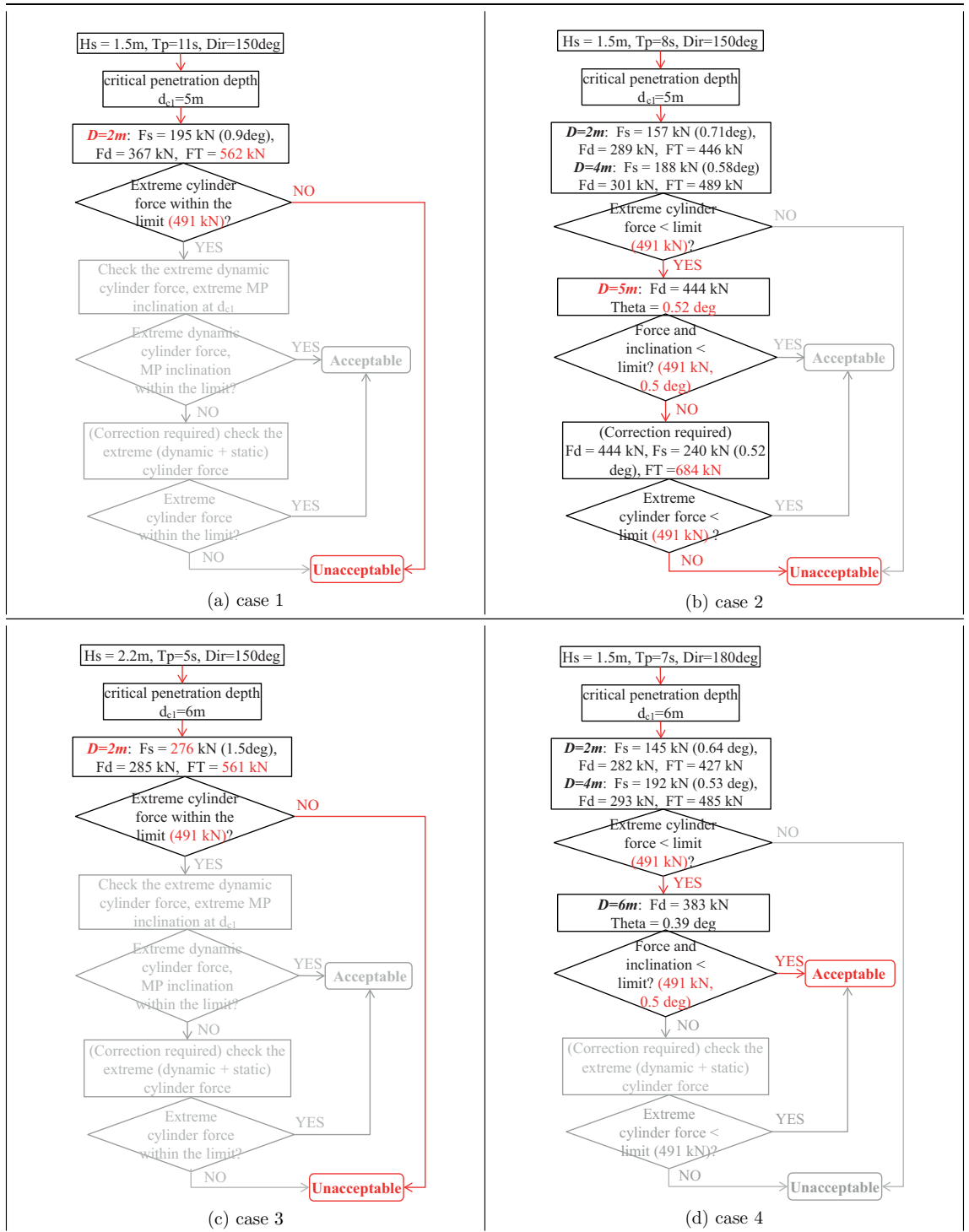


Figure 22: Case studies

Figure 22 demonstrates four typical cases when determining the limiting sea states based on the proposed methodology. These cases include three unacceptable sea states and one acceptable case. The reasons for the different cases to occur in terms of the coupled HLV-MP motions are explained as follows.

- **Case 1:** The given sea state does not satisfy the criterion at the beginning of the hammering process ($pene = 2\text{ m}$) because of large cylinder forces. Both dynamic and static correction forces are significant due to the first-order resonant motions of the HLV-MP system in long waves. The motions of the HLV in vertical plane increase in long waves as the wave peak frequencies move close to its natural frequencies.
- **Case 2:** The wave period in this case is shorter than in Case 1 and the motions are also smaller. So the operation is acceptable before reaching the critical penetration depth d_{c1} . However, the MP inclination at d_{c1} exceeds the allowable limits, and the last correction using thrusters (or mooring lines) are required. Because of large soil resistance, the total force on the gripper exceeds the limits when applying the correction at d_{c1} which makes the given sea state unacceptable.
- **Case 3:** As indicated in Section 4.2, in short wave conditions the motions of the vessel are mainly due to the second-order slow-varying motions in the horizontal plane. These motions may result in large correction forces for the MP in shallow penetrations, e.g., at 2 m . Compared to the previous cases with long wave periods, Case 3 occurs at relatively higher H_s since inclinations due to the second-order motions in short waves are less significant compared to inclinations due to first-order resonant motions in long waves with the same significant wave height as shown in Fig. 21.
- **Case 4:** With wave periods shorter than Cases 1 and 2, and lower significant wave heights than Case 3, both first and second-order motions of the coupled system are in reasonable range, so the cylinder forces and the inclination lie within the limits and thus the input sea state is acceptable.

Therefore, the different reasons for the unacceptable sea states can be identified from the case studies, and different strategies could be proposed to reduce the responses or mitigate critical events accordingly. By assessing different wave conditions, the allowable sea states can be obtained. Fig. 23 shows the results corresponding to three typical installation heading angles of the HLV based on the numerical models presented in this paper. As shown here, the allowable sea states for MP hammering operation can be predicted by applying a systematic methodology to all possible environmental conditions during the planning phase. The allowable sea states can be used to support the on board decision-making together with the weather forecast e.g., to make decisions on whether to initiate the hammering operation as shown in Fig. 2.

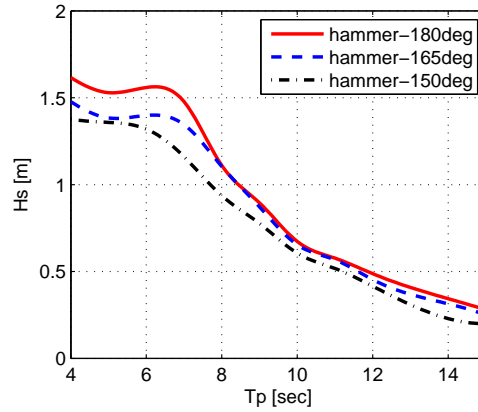


Figure 23: Allowable sea states for MP initial hammering operation for typical HLV headings

6 Conclusions and recommendations

The current work deals with the vessel-monopile coupled system during the initial hammering process. Because offshore installations require proper planning and execution of various installation activities, it is important to find the operational limits in the design phase. In practice, the installation activities are executed in sequence and the success of the following activities normally depends on the previous step. Thus, the operational limits should be evaluated for each activity and in sequential order. This study first presented the installation procedure for the MP hammering process with sequentially defined activities as commonly used by offshore installation contractors. Using a coupled HLV-MP model, numerical analysis were performed in the time-domain for various conditions, from where the critical events and corresponding limiting parameters were identified. Finally, a systematic methodology to find the allowable sea states for such operation was proposed. This study provided realistic examples to find the allowable sea states in a systematic way for a typical MP installation. The main conclusions of this study with recommendations are provided as follows.

- Numerical analysis is essential to quantify the dynamic responses for the system, and time-domain simulations are normally required for complex coupled systems including non-linearities. The time-domain simulations of the coupled HLV-MP system shows that the penetration depth of the MP and wave conditions greatly influence the dynamic responses. The slowly-varying 2nd order motions dominate the system in short waves and shallow penetration depths. The natural modes and natural periods of the HLV-MP system change significantly with the penetration depth. Because of the high gripper and soil stiffness coefficients at deeper penetrations, the natural periods of the horizontal motions of the system reduce and the first-order resonant motions are enhanced in long waves.
- The critical event for the initial hammering process is identified to be the structural failure

of the hydraulic cylinders on the gripper, while the restrictive event is the unacceptable MP inclination at the end of the process. The limiting parameters during the initial hammering process are identified as the cylinder contact force and the inclination of the MP, respectively.

- The hydraulic cylinder force increases significantly with MP penetration in all wave conditions and it is recommended to retract the hydraulic cylinder rods as soon as the MP reaches the critical penetration depth (d_{c1}) at which it can stand alone in waves. The critical depth d_{c1} can be obtained from available soil properties of the offshore site. The characteristic forces on the hydraulic cylinders can be used as design criteria. It is also recommended to monitor the forces on the hydraulic cylinders during the installation to avoid reaching the extreme forces.
- The cylinder forces and MP inclination when using a jack-up vessel were compared with the floating HLV-MP system. The observations from using a floating HLV are not applicable for the jack-up vessel. Therefore, the critical events and limiting parameters depend on the installation equipment and installation procedures.
- The sensitivity study using different soil properties shows that the system dynamic behaviour is not sensitive to the soil properties, and the critical depths for allowable cylinder contact forces occur at different penetrations.
- A methodology to obtain the allowable sea states is proposed. It can be applied in the design phase using the results from time-domain analysis and the allowable limits. The extreme hydraulic cylinder forces over 3 hours are estimated using mean upcrossing rates while the inclinations of the MP are taken as the maximum over 10 min. The allowable values are taken from the commonly used design specification for the hydraulic systems and installation requirement for MP inclination. The allowable sea states can be used on-board together with weather forecasts to support decision-making.
- From the case studies, different unacceptable conditions can be identified. The reasons for those cases to happen were given and can be useful for future improvement of the installation procedure, components design and contingency actions. It is recommended to reduce the second-order motions in short waves and to mitigate the first-order resonant motions in long waves.
- The proposed methodologies can be generalized for planning other marine operations.

7 Limitations and future work

This study describes a simplified installation procedure for MPs with a focus on the initial hammering process of the MP. Assumptions and simplifications are applied. The thruster capacity and mooring line tensions were assumed sufficient during the operation. No wind and current forces

were applied. The soil models were simplified by distributed non-linear springs. Furthermore, in practice there are many uncertainties associated with the measurements, inherent to the proposed methodology, numerical models, environmental conditions, etc. Future work can be devoted to address the above limitations.

This study provided the allowable sea states for the identified limiting parameters. It is also important to focus on improving the procedure and the system components related to those parameters to increase the allowable sea states. Possible solutions can be to upgrade the capacity of the hydraulic cylinders to increase the allowable limits or to use motion compensation system to reduce the motions of the coupled HLV-MP system for reducing the forces on the hydraulic cylinders.

In addition, the initial hammering activity is only one part of the group installation activities for MP installation. It is necessary to assess the allowable sea states of other individual activities, such as MP upending and lowering operations and combine them to establish the operational limits of the complete operation. The methodology will be generalized to other marine operations in order to establish their operational limits in a systematic way.

ACKNOWLEDGEMENTS

This work has been financially supported by the Research Council of Norway granted through the Department of Marine Technology, the Centre for Ships and Ocean Structures (CeSOS) and the Centre for Autonomous Marine Operations and Systems (AMOS), NTNU. The authors are grateful to Prof. Gudmund Eiksund from NTNU for valuable dissuasions on the modelling of the soil interaction forces, to Dr. Oleh Karpa from NTNU for providing the ACER tools to estimate extreme values using upcrssing rates, to Dr. Amir Nejad for providing insights on mechanical components, hydraulic systems and valuable discussions.

References

- [1] EWEA, 2014. The European offshore wind industry - key trends and statistics 2013. Report, The European Wind Energy Association.
- [2] Thomsen, K., 2011. *Offshore wind: A comprehensive guide to successful offshore wind farm installation*. Academic Press.
- [3] Ringsberg, J. W., Daun, V., and Olsson, F., 2015. "Analysis of impact loads on a self-elevating unit during jacking operation". In Proceedings of the 34th International Conference on Ocean, Offshore and Arctic Engineering, May 31-June 5, St. John's, Newfoundland, Canada.
- [4] Sarkar, A., and Gudmestad, O., 2013. "Study on a new method for installing a monopile and a fully integrated offshore wind turbine structure". *Marine Structures*, **33**, pp. 160–187.

- [5] Li, L., Gao, Z., and Moan, T., 2013. “Numerical simulations for installation of offshore wind turbine monopiles using floating vessels”. In Proceedings of the 32nd International Conference on Ocean, Offshore and Arctic Engineering, June 9-14, Nantes, France.
- [6] Li, L., Gao, Z., Moan, T., and Ormberg, H., 2014. “Analysis of lifting operation of a monopile for an offshore wind turbine considering vessel shielding effects”. *Marine Structures*, **39**, pp. 287–314.
- [7] Li, L., Gao, Z., and Moan, T., 2015. “Comparative study of lifting operations of offshore wind turbine monopile and jacket substructures considering shielding effects”. In The 25th International Offshore and Polar Engineering Conference, Hawaii, USA, June 21-26.
- [8] Li, L., Gao, Z., and Moan, T., 2015. “Response analysis of a nonstationary lowering operation for an offshore wind turbine monopile substructure”. *Journal of Offshore Mechanics and Arctic Engineering*, **137**(5).
- [9] Smith, C., 2014. Offshore piles on the straight and narrow. <http://www.nce.co.uk/news/geotechnical/offshore-piles-on-the-straight-and-narrow/8663331.article>. Accessed: 2015-07-16.
- [10] Strandgaard, T., and Vandenbulcke, L., 2002. “Driving mono-piles into glacial till”. *IBCs Wind Power Europe*.
- [11] DNV, 2011. *Offshore Standard DNV-OS-H101, Marine Operations, General*, October.
- [12] MARINTEK, 2012. *SIMO - Theory Manual Version 4.0*.
- [13] Newman, J. N., 1974. “Second-order, slowly-varying forces on vessels in irregular waves”. In International Symposium on the Dynamics of Marine Vehicles and Structures in Waves, University College, London.
- [14] Lee, C., 1995. *WAMIT theory manual*. Massachusetts Institute of Technology, Department of Ocean Engineering.
- [15] DNV, 2010. *Recommended Practice DNV-RP-C205, Environmental Conditions and Environmental Loads*, October.
- [16] Albers, P., 2010. *Motion control in offshore and dredging*. Springer Science & Business Media.
- [17] Carswell, W., Johansson, J., Løvholt, F., Arwade, S., Madshus, C., DeGroot, D., and Myers, A., 2015. “Foundation damping and the dynamics of offshore wind turbine monopiles”. *Renewable Energy*, **80**, pp. 724–736.
- [18] Bisoi, S., and Haldar, S., 2014. “Dynamic analysis of offshore wind turbine in clay considering soilmonopiletower interaction”. *Soil Dynamics and Earthquake Engineering*, **63**, pp. 19–35.
- [19] Andersen, L. V., Vahdatirad, M., Sichani, M. T., and Sørensen, J. D., 2012. “Natural frequencies of wind turbines on monopile foundations in clayey soils a probabilistic approach”. *Computers and Geotechnics*, **43**, pp. 1–11.

- [20] Gerolymos, N., and Gazetas, G., 2006. “Development of winkler model for static and dynamic response of caisson foundations with soil and interface nonlinearities”. *Soil Dynamics and Earthquake Engineering*, **26**(5), pp. 363–376.
- [21] Ong, M., Li, H., Leira, B. J., and Myrhaug, D., 2013. “Dynamic analysis of offshore monopile wind turbine including the effects of wind-wave loading and soil properties”. In Proceedings of the 32nd International Conference on Ocean, Offshore and Arctic Engineering, June 9-14, Nantes, France.
- [22] DNV, 2014. *Offshore Standard DNV-OS-J101, Design of offshore wind turbine structures*.
- [23] API, 2007. Recommended practice for planning, designing and constructing fixed offshore platformsworking stress design, API recommended practice 2A-WSD (RP 2A-WSD). Tech. rep., American Petroleum Institute.
- [24] Byrne, B., McAdam, R., Burd, H., Houlsby, G., Martin, C., Zdravkovi, L., Taborda, D., Potts, D., Jardine, R., and Sideri, M., 2015. “New design methods for large diameter piles under lateral loading for offshore wind applications”. In Proc 3rd International Symposium on Frontiers in Offshore Geotechnics (ISFOG 2015).
- [25] Lesny, K., and Wiemann, J., 2006. “Finite-element-modelling of large diameter monopiles for offshore wind energy converters”. In Geo Congress.
- [26] Hededal, O., and Klinkvort, R. T., 2010. “A new elasto-plastic spring element for cyclic loading of piles using the py curve concept”. *Numerical Methods in Geotechnical Engineering*, pp. 883–888.
- [27] Bekken, L., 2009. “Lateral behavior of large diameter offshore monopile foundations for wind turbines”. PhD thesis, TU Delft, Delft University of Technology.
- [28] Lombardi, D., Bhattacharya, S., and Wood, D. M., 2013. “Dynamic soil-structure interaction of monopile supported wind turbines in cohesive soil”. *Soil Dynamics and Earthquake Engineering*, **49**, pp. 165–180.
- [29] Vemula, N. K., de Vries, W., Fischer, T., Cordle, A., and Schmidt, B., 2010. Design solution for the Upwind reference offshore support structure, Deliverable D4.2.5. Tech. rep., Project Upwind, WP4: Offshore Foundations and Support Structures.
- [30] ANSYS, 2011. *The AQWA Reference manual - Version 14.0*.
- [31] Young-Kwan Kim, J.-R. S., and Yoon, D.-Y., 2012. “A design of windmill turbine installation vessel using jack-up system”. In Proceedings of the 22nd International Offshore and Polar Engineering Conference, June 17-22, Rhodes, Greece.
- [32] Naess, A., 1984. “Technical note: On a rational approach to extreme value analysis”. *Applied Ocean Research*, **6**(3), pp. 173–174.
- [33] Naess, A., 1984. “On the long-term statistics of extremes”. *Applied Ocean Research*, **6**(4), pp. 227–228.

- [34] Naess, A., Gaidai, O., and Teigen, P. S., 2007. “Extreme response prediction for nonlinear floating offshore structures by monte carlo simulation”. *Applied Ocean Research*, **29**(4), pp. 221–230.
- [35] IHC. IHC Vremac Cylinders - Cylinder Catalogue 210 bar / 300 bar. Available at <http://www.ihcvremaccylinders.com/>. Accessed: 2015-05-05.

Appendix B

List of previous PhD theses
at Dept. of Marine Tech.

**Previous PhD theses published at the Department of Marine
Technology
(earlier: Faculty of Marine Technology)
NORWEGIAN UNIVERSITY OF SCIENCE AND TECHNOLOGY**

Report No.	Author	Title
	Kavlie, Dag	Optimization of Plane Elastic Grillages, 1967
	Hansen, Hans R.	Man-Machine Communication and Data-Storage Methods in Ship Structural Design, 1971
	Gisvold, Kaare M.	A Method for non-linear mixed-integer programming and its Application to Design Problems, 1971
	Lund, Sverre	Tanker Frame Optimalization by means of SUMT-Transformation and Behaviour Models, 1971
	Vinje, Tor	On Vibration of Spherical Shells Interacting with Fluid, 1972
	Lorentz, Jan D.	Tank Arrangement for Crude Oil Carriers in Accordance with the new Anti-Pollution Regulations, 1975
	Carlsen, Carl A.	Computer-Aided Design of Tanker Structures, 1975
	Larsen, Carl M.	Static and Dynamic Analysis of Offshore Pipelines during Installation, 1976
UR-79-01	Bright Hatlestad, MK	The finite element method used in a fatigue evaluation of fixed offshore platforms. (Dr.Ing. Thesis)
UR-79-02	Erik Pettersen, MK	Analysis and design of cellular structures. (Dr.Ing. Thesis)
UR-79-03	Sverre Valsgård, MK	Finite difference and finite element methods applied to nonlinear analysis of plated structures. (Dr.Ing. Thesis)
UR-79-04	Nils T. Nordsve, MK	Finite element collapse analysis of structural members considering imperfections and stresses due to fabrication. (Dr.Ing. Thesis)
UR-79-05	Ivar J. Fylling, MK	Analysis of towline forces in ocean towing systems. (Dr.Ing. Thesis)
UR-80-06	Nils Sandmark, MM	Analysis of Stationary and Transient Heat Conduction by the Use of the Finite Element Method. (Dr.Ing. Thesis)
UR-80-09	Sverre Haver, MK	Analysis of uncertainties related to the stochastic modeling of ocean waves. (Dr.Ing. Thesis)

Report No.	Author	Title
UR-81-15	Odland, Jonas	On the Strength of welded Ring stiffened cylindrical Shells primarily subjected to axial Compression
UR-82-17	Engesvik, Knut	Analysis of Uncertainties in the fatigue Capacity of Welded Joints
UR-82-18	Rye, Henrik	Ocean wave groups
UR-83-30	Eide, Oddvar Inge	On Cumulative Fatigue Damage in Steel Welded Joints
UR-83-33	Mo, Olav	Stochastic Time Domain Analysis of Slender Offshore Structures
UR-83-34	Amdahl, Jørgen	Energy absorption in Ship-platform impacts
UR-84-37	Mørch, Morten	Motions and mooring forces of semi submersibles as determined by full-scale measurements and theoretical analysis
UR-84-38	Soares, C. Guedes	Probabilistic models for load effects in ship structures
UR-84-39	Aarsnes, Jan V.	Current forces on ships
UR-84-40	Czujko, Jerzy	Collapse Analysis of Plates subjected to Biaxial Compression and Lateral Load
UR-85-46	Alf G. Engseth, MK	Finite element collapse analysis of tubular steel offshore structures. (Dr.Ing. Thesis)
UR-86-47	Dengody Sheshappa, MP	A Computer Design Model for Optimizing Fishing Vessel Designs Based on Techno-Economic Analysis. (Dr.Ing. Thesis)
UR-86-48	Vidar Aanesland, MH	A Theoretical and Numerical Study of Ship Wave Resistance. (Dr.Ing. Thesis)
UR-86-49	Heinz-Joachim Wessel, MK	Fracture Mechanics Analysis of Crack Growth in Plate Girders. (Dr.Ing. Thesis)
UR-86-50	Jon Taby, MK	Ultimate and Post-ultimate Strength of Dented Tubular Members. (Dr.Ing. Thesis)
UR-86-51	Walter Lian, MH	A Numerical Study of Two-Dimensional Separated Flow Past Bluff Bodies at Moderate KC-Numbers. (Dr.Ing. Thesis)
UR-86-52	Bjørn Sortland, MH	Force Measurements in Oscillating Flow on Ship Sections and Circular Cylinders in a U-Tube Water Tank. (Dr.Ing. Thesis)
UR-86-53	Kurt Strand, MM	A System Dynamic Approach to One-dimensional Fluid Flow. (Dr.Ing. Thesis)
UR-86-54	Arne Edvin Løken, MH	Three Dimensional Second Order Hydrodynamic Effects on Ocean Structures in Waves. (Dr.Ing. Thesis)
UR-86-55	Sigurd Falch, MH	A Numerical Study of Slamming of Two-Dimensional Bodies. (Dr.Ing. Thesis)

Report No.	Author	Title
UR-87-56	Arne Braathen, MH	Application of a Vortex Tracking Method to the Prediction of Roll Damping of a Two-Dimension Floating Body. (Dr.Ing. Thesis)
UR-87-57	Bernt Leira, MK	Gaussian Vector Processes for Reliability Analysis involving Wave-Induced Load Effects. (Dr.Ing. Thesis)
UR-87-58	Magnus Småvik, MM	Thermal Load and Process Characteristics in a Two-Stroke Diesel Engine with Thermal Barriers (in Norwegian). (Dr.Ing. Thesis)
MTA-88-59	Bernt Arild Bremdal, MP	An Investigation of Marine Installation Processes – A Knowledge-Based Planning Approach. (Dr.Ing. Thesis)
MTA-88-60	Xu Jun, MK	Non-linear Dynamic Analysis of Space-framed Offshore Structures. (Dr.Ing. Thesis)
MTA-89-61	Gang Miao, MH	Hydrodynamic Forces and Dynamic Responses of Circular Cylinders in Wave Zones. (Dr.Ing. Thesis)
MTA-89-62	Martin Greenhow, MH	Linear and Non-Linear Studies of Waves and Floating Bodies. Part I and Part II. (Dr.Techn. Thesis)
MTA-89-63	Chang Li, MH	Force Coefficients of Spheres and Cubes in Oscillatory Flow with and without Current. (Dr.Ing. Thesis)
MTA-89-64	Hu Ying, MP	A Study of Marketing and Design in Development of Marine Transport Systems. (Dr.Ing. Thesis)
MTA-89-65	Arild Jæger, MH	Seakeeping, Dynamic Stability and Performance of a Wedge Shaped Planing Hull. (Dr.Ing. Thesis)
MTA-89-66	Chan Siu Hung, MM	The dynamic characteristics of tilting-pad bearings
MTA-89-67	Kim Wikstrøm, MP	Analysis av projekteringen for ett offshore prosjekt. (Licenciat-avhandling)
MTA-89-68	Jiao Guoyang, MK	Reliability Analysis of Crack Growth under Random Loading, considering Model Updating. (Dr.Ing. Thesis)
MTA-89-69	Arnt Olufsen, MK	Uncertainty and Reliability Analysis of Fixed Offshore Structures. (Dr.Ing. Thesis)
MTA-89-70	Wu Yu-Lin, MR	System Reliability Analyses of Offshore Structures using improved Truss and Beam Models. (Dr.Ing. Thesis)
MTA-90-71	Jan Roger Hoff, MH	Three-dimensional Green function of a vessel with forward speed in waves. (Dr.Ing. Thesis)

Report No.	Author	Title
MTA-90-72	Rong Zhao, MH	Slow-Drift Motions of a Moored Two-Dimensional Body in Irregular Waves. (Dr.Ing. Thesis)
MTA-90-73	Atle Minsaas, MP	Economical Risk Analysis. (Dr.Ing. Thesis)
MTA-90-74	Knut-Ariel Farnes, MK	Long-term Statistics of Response in Non-linear Marine Structures. (Dr.Ing. Thesis)
MTA-90-75	Torbjørn Sotberg, MK	Application of Reliability Methods for Safety Assessment of Submarine Pipelines. (Dr.Ing. Thesis)
MTA-90-76	Zeuthen, Steffen, MP	SEAMAID. A computational model of the design process in a constraint-based logic programming environment. An example from the offshore domain. (Dr.Ing. Thesis)
MTA-91-77	Haagensen, Sven, MM	Fuel Dependant Cyclic Variability in a Spark Ignition Engine – An Optical Approach. (Dr.Ing. Thesis)
MTA-91-78	Løland, Geir, MH	Current forces on and flow through fish farms. (Dr.Ing. Thesis)
MTA-91-79	Hoen, Christopher, MK	System Identification of Structures Excited by Stochastic Load Processes. (Dr.Ing. Thesis)
MTA-91-80	Haugen, Stein, MK	Probabilistic Evaluation of Frequency of Collision between Ships and Offshore Platforms. (Dr.Ing. Thesis)
MTA-91-81	Sødahl, Nils, MK	Methods for Design and Analysis of Flexible Risers. (Dr.Ing. Thesis)
MTA-91-82	Ormberg, Harald, MK	Non-linear Response Analysis of Floating Fish Farm Systems. (Dr.Ing. Thesis)
MTA-91-83	Marley, Mark J., MK	Time Variant Reliability under Fatigue Degradation. (Dr.Ing. Thesis)
MTA-91-84	Krokstad, Jørgen R., MH	Second-order Loads in Multidirectional Seas. (Dr.Ing. Thesis)
MTA-91-85	Molteberg, Gunnar A., MM	The Application of System Identification Techniques to Performance Monitoring of Four Stroke Turbocharged Diesel Engines. (Dr.Ing. Thesis)
MTA-92-86	Mørch, Hans Jørgen Bjelke, MH	Aspects of Hydrofoil Design: with Emphasis on Hydrofoil Interaction in Calm Water. (Dr.Ing. Thesis)
MTA-92-87	Chan Siu Hung, MM	Nonlinear Analysis of Rotordynamic Instabilities in Highspeed Turbomachinery. (Dr.Ing. Thesis)
MTA-92-88	Bessason, Bjarni, MK	Assessment of Earthquake Loading and Response of Seismically Isolated Bridges. (Dr.Ing. Thesis)

Report No.	Author	Title
MTA-92-89	Langli, Geir, MP	Improving Operational Safety through exploitation of Design Knowledge – an investigation of offshore platform safety. (Dr.Ing. Thesis)
MTA-92-90	Sævik, Svein, MK	On Stresses and Fatigue in Flexible Pipes. (Dr.Ing. Thesis)
MTA-92-91	Ask, Tor Ø., MM	Ignition and Flame Growth in Lean Gas-Air Mixtures. An Experimental Study with a Schlieren System. (Dr.Ing. Thesis)
MTA-86-92	Hessen, Gunnar, MK	Fracture Mechanics Analysis of Stiffened Tubular Members. (Dr.Ing. Thesis)
MTA-93-93	Steinebach, Christian, MM	Knowledge Based Systems for Diagnosis of Rotating Machinery. (Dr.Ing. Thesis)
MTA-93-94	Dalane, Jan Inge, MK	System Reliability in Design and Maintenance of Fixed Offshore Structures. (Dr.Ing. Thesis)
MTA-93-95	Steen, Sverre, MH	Cobblestone Effect on SES. (Dr.Ing. Thesis)
MTA-93-96	Karunakaran, Daniel, MK	Nonlinear Dynamic Response and Reliability Analysis of Drag-dominated Offshore Platforms. (Dr.Ing. Thesis)
MTA-93-97	Hagen, Arnulf, MP	The Framework of a Design Process Language. (Dr.Ing. Thesis)
MTA-93-98	Nordrik, Rune, MM	Investigation of Spark Ignition and Autoignition in Methane and Air Using Computational Fluid Dynamics and Chemical Reaction Kinetics. A Numerical Study of Ignition Processes in Internal Combustion Engines. (Dr.Ing. Thesis)
MTA-94-99	Passano, Elizabeth, MK	Efficient Analysis of Nonlinear Slender Marine Structures. (Dr.Ing. Thesis)
MTA-94-100	Kvålsvold, Jan, MH	Hydroelastic Modelling of Wetdeck Slamming on Multihull Vessels. (Dr.Ing. Thesis)
MTA-94-102	Bech, Sidsel M., MK	Experimental and Numerical Determination of Stiffness and Strength of GRP/PVC Sandwich Structures. (Dr.Ing. Thesis)
MTA-95-103	Paulsen, Hallvard, MM	A Study of Transient Jet and Spray using a Schlieren Method and Digital Image Processing. (Dr.Ing. Thesis)
MTA-95-104	Hovde, Geir Olav, MK	Fatigue and Overload Reliability of Offshore Structural Systems, Considering the Effect of Inspection and Repair. (Dr.Ing. Thesis)
MTA-95-105	Wang, Xiaozhi, MK	Reliability Analysis of Production Ships with Emphasis on Load Combination and Ultimate Strength. (Dr.Ing. Thesis)
MTA-95-106	Ulstein, Tore, MH	Nonlinear Effects of a Flexible Stern Seal Bag on Cobblestone Oscillations of an SES. (Dr.Ing. Thesis)

Report No.	Author	Title
MTA-95-107	Solaas, Frøydis, MH	Analytical and Numerical Studies of Sloshing in Tanks. (Dr.Ing. Thesis)
MTA-95-108	Hellan, Øyvind, MK	Nonlinear Pushover and Cyclic Analyses in Ultimate Limit State Design and Reassessment of Tubular Steel Offshore Structures. (Dr.Ing. Thesis)
MTA-95-109	Hermundstad, Ole A., MK	Theoretical and Experimental Hydroelastic Analysis of High Speed Vessels. (Dr.Ing. Thesis)
MTA-96-110	Bratland, Anne K., MH	Wave-Current Interaction Effects on Large-Volume Bodies in Water of Finite Depth. (Dr.Ing. Thesis)
MTA-96-111	Herfjord, Kjell, MH	A Study of Two-dimensional Separated Flow by a Combination of the Finite Element Method and Navier-Stokes Equations. (Dr.Ing. Thesis)
MTA-96-112	AEsøy, Vilmar, MM	Hot Surface Assisted Compression Ignition in a Direct Injection Natural Gas Engine. (Dr.Ing. Thesis)
MTA-96-113	Eknes, Monika L., MK	Escalation Scenarios Initiated by Gas Explosions on Offshore Installations. (Dr.Ing. Thesis)
MTA-96-114	Erikstad, Stein O., MP	A Decision Support Model for Preliminary Ship Design. (Dr.Ing. Thesis)
MTA-96-115	Pedersen, Egil, MH	A Nautical Study of Towed Marine Seismic Streamer Cable Configurations. (Dr.Ing. Thesis)
MTA-97-116	Moksnes, Paul O., MM	Modelling Two-Phase Thermo-Fluid Systems Using Bond Graphs. (Dr.Ing. Thesis)
MTA-97-117	Halse, Karl H., MK	On Vortex Shedding and Prediction of Vortex-Induced Vibrations of Circular Cylinders. (Dr.Ing. Thesis)
MTA-97-118	Igland, Ragnar T., MK	Reliability Analysis of Pipelines during Laying, considering Ultimate Strength under Combined Loads. (Dr.Ing. Thesis)
MTA-97-119	Pedersen, Hans-P., MP	Levendefiskteknologi for fiskefartøy. (Dr.Ing. Thesis)
MTA-98-120	Vikestad, Kyrre, MK	Multi-Frequency Response of a Cylinder Subjected to Vortex Shedding and Support Motions. (Dr.Ing. Thesis)
MTA-98-121	Azadi, Mohammad R. E., MK	Analysis of Static and Dynamic Pile-Soil-Jacket Behaviour. (Dr.Ing. Thesis)
MTA-98-122	Ulltang, Terje, MP	A Communication Model for Product Information. (Dr.Ing. Thesis)

Report No.	Author	Title
MTA-98-123	Torbergsen, Erik, MM	Impeller/Diffuser Interaction Forces in Centrifugal Pumps. (Dr.Ing. Thesis)
MTA-98-124	Hansen, Edmond, MH	A Discrete Element Model to Study Marginal Ice Zone Dynamics and the Behaviour of Vessels Moored in Broken Ice. (Dr.Ing. Thesis)
MTA-98-125	Videiro, Paulo M., MK	Reliability Based Design of Marine Structures. (Dr.Ing. Thesis)
MTA-99-126	Mainçon, Philippe, MK	Fatigue Reliability of Long Welds Application to Titanium Risers. (Dr.Ing. Thesis)
MTA-99-127	Haugen, Elin M., MH	Hydroelastic Analysis of Slamming on Stiffened Plates with Application to Catamaran Wet-decks. (Dr.Ing. Thesis)
MTA-99-128	Langhelle, Nina K., MK	Experimental Validation and Calibration of Nonlinear Finite Element Models for Use in Design of Aluminium Structures Exposed to Fire. (Dr.Ing. Thesis)
MTA-99-129	Berstad, Are J., MK	Calculation of Fatigue Damage in Ship Structures. (Dr.Ing. Thesis)
MTA-99-130	Andersen, Trond M., MM	Short Term Maintenance Planning. (Dr.Ing. Thesis)
MTA-99-131	Tveiten, Bård Wathne, MK	Fatigue Assessment of Welded Aluminium Ship Details. (Dr.Ing. Thesis)
MTA-99-132	Søreide, Fredrik, MP	Applications of underwater technology in deep water archaeology. Principles and practice. (Dr.Ing. Thesis)
MTA-99-133	Tønnessen, Rune, MH	A Finite Element Method Applied to Unsteady Viscous Flow Around 2D Blunt Bodies With Sharp Corners. (Dr.Ing. Thesis)
MTA-99-134	Elvekrok, Dag R., MP	Engineering Integration in Field Development Projects in the Norwegian Oil and Gas Industry. The Supplier Management of Norne. (Dr.Ing. Thesis)
MTA-99-135	Fagerholt, Kjetil, MP	Optimeringsbaserte Metoder for Ruteplanlegging innen skipsfart. (Dr.Ing. Thesis)
MTA-99-136	Bysveen, Marie, MM	Visualization in Two Directions on a Dynamic Combustion Rig for Studies of Fuel Quality. (Dr.Ing. Thesis)
MTA-2000-137	Storteig, Eskild, MM	Dynamic characteristics and leakage performance of liquid annular seals in centrifugal pumps. (Dr.Ing. Thesis)
MTA-2000-138	Sagli, Gro, MK	Model uncertainty and simplified estimates of long term extremes of hull girder loads in ships. (Dr.Ing. Thesis)

Report No.	Author	Title
MTA-2000-139	Tronstad, Harald, MK	Nonlinear analysis and design of cable net structures like fishing gear based on the finite element method. (Dr.Ing. Thesis)
MTA-2000-140	Kroneberg, André, MP	Innovation in shipping by using scenarios. (Dr.Ing. Thesis)
MTA-2000-141	Haslum, Herbjørn Alf, MH	Simplified methods applied to nonlinear motion of spar platforms. (Dr.Ing. Thesis)
MTA-2001-142	Samdal, Ole Johan, MM	Modelling of Degradation Mechanisms and Stressor Interaction on Static Mechanical Equipment Residual Lifetime. (Dr.Ing. Thesis)
MTA-2001-143	Baarholm, Rolf Jarle, MH	Theoretical and experimental studies of wave impact underneath decks of offshore platforms. (Dr.Ing. Thesis)
MTA-2001-144	Wang, Lihua, MK	Probabilistic Analysis of Nonlinear Wave-induced Loads on Ships. (Dr.Ing. Thesis)
MTA-2001-145	Kristensen, Odd H. Holt, MK	Ultimate Capacity of Aluminium Plates under Multiple Loads, Considering HAZ Properties. (Dr.Ing. Thesis)
MTA-2001-146	Greco, Marilena, MH	A Two-Dimensional Study of Green-Water Loading. (Dr.Ing. Thesis)
MTA-2001-147	Heggelund, Svein E., MK	Calculation of Global Design Loads and Load Effects in Large High Speed Catamarans. (Dr.Ing. Thesis)
MTA-2001-148	Babalola, Olusegun T., MK	Fatigue Strength of Titanium Risers – Defect Sensitivity. (Dr.Ing. Thesis)
MTA-2001-149	Mohammed, Abuu K., MK	Nonlinear Shell Finite Elements for Ultimate Strength and Collapse Analysis of Ship Structures. (Dr.Ing. Thesis)
MTA-2002-150	Holmedal, Lars E., MH	Wave-current interactions in the vicinity of the sea bed. (Dr.Ing. Thesis)
MTA-2002-151	Rognebakke, Olav F., MH	Sloshing in rectangular tanks and interaction with ship motions. (Dr.Ing. Thesis)
MTA-2002-152	Lader, Pål Furset, MH	Geometry and Kinematics of Breaking Waves. (Dr.Ing. Thesis)
MTA-2002-153	Yang, Qinzhen, MH	Wash and wave resistance of ships in finite water depth. (Dr.Ing. Thesis)
MTA-2002-154	Melhus, Øyvind, MM	Utilization of VOC in Diesel Engines. Ignition and combustion of VOC released by crude oil tankers. (Dr.Ing. Thesis)
MTA-2002-155	Ronæss, Marit, MH	Wave Induced Motions of Two Ships Advancing on Parallel Course. (Dr.Ing. Thesis)
MTA-2002-156	Økland, Ole D., MK	Numerical and experimental investigation of whipping in twin hull vessels exposed to severe wet deck slamming. (Dr.Ing. Thesis)

Report No.	Author	Title
MTA-2002-157	Ge, Chunhua, MK	Global Hydroelastic Response of Catamarans due to Wet Deck Slamming. (Dr.Ing. Thesis)
MTA-2002-158	Byklum, Eirik, MK	Nonlinear Shell Finite Elements for Ultimate Strength and Collapse Analysis of Ship Structures. (Dr.Ing. Thesis)
IMT-2003-1	Chen, Haibo, MK	Probabilistic Evaluation of FPSO-Tanker Collision in Tandem Offloading Operation. (Dr.Ing. Thesis)
IMT-2003-2	Skaugset, Kjetil Bjørn, MK	On the Suppression of Vortex Induced Vibrations of Circular Cylinders by Radial Water Jets. (Dr.Ing. Thesis)
IMT-2003-3	Chezian, Muthu	Three-Dimensional Analysis of Slamming. (Dr.Ing. Thesis)
IMT-2003-4	Buhaug, Øyvind	Deposit Formation on Cylinder Liner Surfaces in Medium Speed Engines. (Dr.Ing. Thesis)
IMT-2003-5	Tregde, Vidar	Aspects of Ship Design: Optimization of Aft Hull with Inverse Geometry Design. (Dr.Ing. Thesis)
IMT-2003-6	Wist, Hanne Therese	Statistical Properties of Successive Ocean Wave Parameters. (Dr.Ing. Thesis)
IMT-2004-7	Ransau, Samuel	Numerical Methods for Flows with Evolving Interfaces. (Dr.Ing. Thesis)
IMT-2004-8	Soma, Torkel	Blue-Chip or Sub-Standard. A data interrogation approach of identity safety characteristics of shipping organization. (Dr.Ing. Thesis)
IMT-2004-9	Ersdal, Svein	An experimental study of hydrodynamic forces on cylinders and cables in near axial flow. (Dr.Ing. Thesis)
IMT-2005-10	Brodtkorb, Per Andreas	The Probability of Occurrence of Dangerous Wave Situations at Sea. (Dr.Ing. Thesis)
IMT-2005-11	Yttervik, Rune	Ocean current variability in relation to offshore engineering. (Dr.Ing. Thesis)
IMT-2005-12	Fredheim, Arne	Current Forces on Net-Structures. (Dr.Ing. Thesis)
IMT-2005-13	Heggernes, Kjetil	Flow around marine structures. (Dr.Ing. Thesis)
IMT-2005-14	Fouques, Sebastien	Lagrangian Modelling of Ocean Surface Waves and Synthetic Aperture Radar Wave Measurements. (Dr.Ing. Thesis)
IMT-2006-15	Holm, Håvard	Numerical calculation of viscous free surface flow around marine structures. (Dr.Ing. Thesis)
IMT-2006-16	Bjørheim, Lars G.	Failure Assessment of Long Through Thickness Fatigue Cracks in Ship Hulls. (Dr.Ing. Thesis)

Report No.	Author	Title
IMT-2006-17	Hansson, Lisbeth	Safety Management for Prevention of Occupational Accidents. (Dr.Ing. Thesis)
IMT-2006-18	Zhu, Xinying	Application of the CIP Method to Strongly Nonlinear Wave-Body Interaction Problems. (Dr.Ing. Thesis)
IMT-2006-19	Reite, Karl Johan	Modelling and Control of Trawl Systems. (Dr.Ing. Thesis)
IMT-2006-20	Smogeli, Øyvind Notland	Control of Marine Propellers. From Normal to Extreme Conditions. (Dr.Ing. Thesis)
IMT-2007-21	Storhaug, Gaute	Experimental Investigation of Wave Induced Vibrations and Their Effect on the Fatigue Loading of Ships. (Dr.Ing. Thesis)
IMT-2007-22	Sun, Hui	A Boundary Element Method Applied to Strongly Nonlinear Wave-Body Interaction Problems. (PhD Thesis, CeSOS)
IMT-2007-23	Rustad, Anne Marthine	Modelling and Control of Top Tensioned Risers. (PhD Thesis, CeSOS)
IMT-2007-24	Johansen, Vegar	Modelling flexible slender system for real-time simulations and control applications
IMT-2007-25	Wroldsen, Anders Sunde	Modelling and control of tensegrity structures. (PhD Thesis, CeSOS)
IMT-2007-26	Aronsen, Kristoffer Høye	An experimental investigation of in-line and combined inline and cross flow vortex induced vibrations. (Dr. avhandling, IMT)
IMT-2007-27	Gao, Zhen	Stochastic Response Analysis of Mooring Systems with Emphasis on Frequency-domain Analysis of Fatigue due to Wide-band Response Processes (PhD Thesis, CeSOS)
IMT-2007-28	Thorstensen, Tom Anders	Lifetime Profit Modelling of Ageing Systems Utilizing Information about Technical Condition. (Dr.ing. thesis, IMT)
IMT-2008-29	Berntsen, Per Ivar B.	Structural Reliability Based Position Mooring. (PhD-Thesis, IMT)
IMT-2008-30	Ye, Naiquan	Fatigue Assessment of Aluminium Welded Box-stiffener Joints in Ships (Dr.ing. thesis, IMT)
IMT-2008-31	Radan, Damir	Integrated Control of Marine Electrical Power Systems. (PhD-Thesis, IMT)
IMT-2008-32	Thomassen, Paul	Methods for Dynamic Response Analysis and Fatigue Life Estimation of Floating Fish Cages. (Dr.ing. thesis, IMT)
IMT-2008-33	Pákozdi, Csaba	A Smoothed Particle Hydrodynamics Study of Two-dimensional Nonlinear Sloshing in Rectangular Tanks. (Dr.ing.thesis, IMT/ CeSOS)

Report No.	Author	Title
IMT-2008-34	Grytøyr, Guttorm	A Higher-Order Boundary Element Method and Applications to Marine Hydrodynamics. (Dr.ing.thesis, IMT)
IMT-2008-35	Drummen, Ingo	Experimental and Numerical Investigation of Nonlinear Wave-Induced Load Effects in Containerships considering Hydroelasticity. (PhD thesis, CeSOS)
IMT-2008-36	Skejic, Renato	Maneuvering and Seakeeping of a Singel Ship and of Two Ships in Interaction. (PhD-Thesis, CeSOS)
IMT-2008-37	Harlem, Alf	An Age-Based Replacement Model for Repairable Systems with Attention to High-Speed Marine Diesel Engines. (PhD-Thesis, IMT)
IMT-2008-38	Alsos, Hagbart S.	Ship Grounding. Analysis of Ductile Fracture, Bottom Damage and Hull Girder Response. (PhD-thesis, IMT)
IMT-2008-39	Graczyk, Mateusz	Experimental Investigation of Sloshing Loading and Load Effects in Membrane LNG Tanks Subjected to Random Excitation. (PhD-thesis, CeSOS)
IMT-2008-40	Taghipour, Reza	Efficient Prediction of Dynamic Response for Flexible amd Multi-body Marine Structures. (PhD-thesis, CeSOS)
IMT-2008-41	Ruth, Eivind	Propulsion control and thrust allocation on marine vessels. (PhD thesis, CeSOS)
IMT-2008-42	Nystad, Bent Helge	Technical Condition Indexes and Remaining Useful Life of Aggregated Systems. PhD thesis, IMT
IMT-2008-43	Soni, Prashant Kumar	Hydrodynamic Coefficients for Vortex Induced Vibrations of Flexible Beams. PhD thesis, CeSOS
IMT-2009-43	Amlashi, Hadi K.K.	Ultimate Strength and Reliability-based Design of Ship Hulls with Emphasis on Combined Global and Local Loads. PhD Thesis, IMT
IMT-2009-44	Pedersen, Tom Arne	Bond Graph Modelling of Marine Power Systems. PhD Thesis, IMT
IMT-2009-45	Kristiansen, Trygve	Two-Dimensional Numerical and Experimental Studies of Piston-Mode Resonance. PhD thesis, CeSOS
IMT-2009-46	Ong, Muk Chen	Applications of a Standard High Reynolds Number Model and a Stochastic Scour Prediction Model for Marine Structures. PhD-thesis, IMT

Report No.	Author	Title
IMT-2009-47	Hong, Lin	Simplified Analysis and Design of Ships subjected to Collision and Grounding. PhD-thesis, IMT
IMT-2009-48	Koushan, Kamran	Vortex Induced Vibrations of Free Span Pipelines, PhD thesis, IMT
IMT-2009-49	Korsvik, Jarl Eirik	Heuristic Methods for Ship Routing and Scheduling. PhD-thesis, IMT
IMT-2009-50	Lee, Jihoon	Experimental Investigation and Numerical in Analyzing the Ocean Current Displacement of Longlines. Ph.d.-Thesis, IMT.
IMT-2009-51	Vestbøstad, Tone Gran	A Numerical Study of Wave-in-Deck Impact usin a Two-Dimensional Constrained Interpolation Profile Method, Ph.d.thesis, CeSOS.
IMT-2009-52	Bruun, Kristine	Bond Graph Modelling of Fuel Cells for Marine Power Plants. Ph.d.-thesis, IMT
IMT-2009-53	Holstad, Anders	Numerical Investigation of Turbulence in a Sekwed Three-Dimensional Channel Flow, Ph.d.-thesis, IMT.
IMT-2009-54	Ayala-Uraga, Efren	Reliability-Based Assessment of Deteriorating Ship-shaped Offshore Structures, Ph.d.-thesis, IMT
IMT-2009-55	Kong, Xiangjun	A Numerical Study of a Damaged Ship in Beam Sea Waves. Ph.d.-thesis, IMT/CeSOS.
IMT-2010-56	Kristiansen, David	Wave Induced Effects on Floaters of Aquaculture Plants, Ph.d.-thesis, CeSOS.
IMT-2010-57	Ludvigsen, Martin	An ROV-Toolbox for Optical and Acoustic Scientific Seabed Investigation. Ph.d.-thesis IMT.
IMT-2010-58	Hals, Jørgen	Modelling and Phase Control of Wave-Energy Converters. Ph.d.thesis, CeSOS.
IMT-2010-59	Shu, Zhi	Uncertainty Assessment of Wave Loads and Ultimate Strength of Tankers and Bulk Carriers in a Reliability Framework. Ph.d. Thesis, IMT/CeSOS
IMT-2010-60	Shao, Yanlin	Numerical Potential-Flow Studies on Weakly-Nonlinear Wave-Body Interactions with/without Small Forward Speed, Ph.d.thesis, CeSOS.
IMT-2010-61	Califano, Andrea	Dynamic Loads on Marine Propellers due to Intermittent Ventilation. Ph.d.thesis, IMT.
IMT-2010-62	El Khoury, George	Numerical Simulations of Massively Separated Turbulent Flows, Ph.d.-thesis, IMT
IMT-2010-63	Seim, Knut Sponheim	Mixing Process in Dense Overflows with Emphasis on the Faroe Bank Channel Overflow. Ph.d.thesis, IMT

Report No.	Author	Title
IMT-2010-64	Jia, Huirong	Structural Analysis of Intact and Damaged Ships in a Collision Risk Analysis Perspective. Ph.d.thesis CeSoS.
IMT-2010-65	Jiao, Linlin	Wave-Induced Effects on a Pontoon-type Very Large Floating Structures (VLFS). Ph.D.-thesis, CeSOS.
IMT-2010-66	Abrahamsen, Bjørn Christian	Sloshing Induced Tank Roof with Entrapped Air Pocket. Ph.d.thesis, CeSOS.
IMT-2011-67	Karimirad, Madjid	Stochastic Dynamic Response Analysis of Spar-Type Wind Turbines with Catenary or Taut Mooring Systems. Ph.d.-thesis, CeSOS.
IMT-2011-68	Erlend Meland	Condition Monitoring of Safety Critical Valves. Ph.d.-thesis, IMT.
IMT-2011-69	Yang, Limin	Stochastic Dynamic System Analysis of Wave Energy Converter with Hydraulic Power Take-Off, with Particular Reference to Wear Damage Analysis, Ph.d. Thesis, CeSOS.
IMT-2011-70	Visscher, Jan	Application of Particle Image Velocimetry on Turbulent Marine Flows, Ph.d.Thesis, IMT.
IMT-2011-71	Su, Biao	Numerical Predictions of Global and Local Ice Loads on Ships. Ph.d.Thesis, CeSOS.
IMT-2011-72	Liu, Zhenhui	Analytical and Numerical Analysis of Iceberg Collision with Ship Structures. Ph.d.Thesis, IMT.
IMT-2011-73	Aarsæther, Karl Gunnar	Modeling and Analysis of Ship Traffic by Observation and Numerical Simulation. Ph.d.Thesis, IMT.
IMT-2011-74	Wu, Jie	Hydrodynamic Force Identification from Stochastic Vortex Induced Vibration Experiments with Slender Beams. Ph.d.Thesis, IMT.
IMT-2011-75	Amini, Hamid	Azimuth Propulsors in Off-design Conditions. Ph.d.Thesis, IMT.
IMT-2011-76	Nguyen, Tan-Hoi	Toward a System of Real-Time Prediction and Monitoring of Bottom Damage Conditions During Ship Grounding. Ph.d.thesis, IMT.
IMT-2011-77	Tavakoli, Mohammad T.	Assessment of Oil Spill in Ship Collision and Grounding, Ph.d.thesis, IMT.
IMT-2011-78	Guo, Bingjie	Numerical and Experimental Investigation of Added Resistance in Waves. Ph.d.Thesis, IMT.
IMT-2011-79	Chen, Qiaofeng	Ultimate Strength of Aluminium Panels, considering HAZ Effects, IMT
IMT-2012-80	Kota, Ravikiran S.	Wave Loads on Decks of Offshore Structures in Random Seas, CeSOS.

Report No.	Author	Title
IMT-2012-81	Sten, Ronny	Dynamic Simulation of Deep Water Drilling Risers with Heave Compensating System, IMT.
IMT-2012-82	Berle, Øyvind	Risk and resilience in global maritime supply chains, IMT.
IMT-2012-83	Fang, Shaoji	Fault Tolerant Position Mooring Control Based on Structural Reliability, CeSOS.
IMT-2012-84	You, Jikun	Numerical studies on wave forces and moored ship motions in intermediate and shallow water, CeSOS.
IMT-2012-85	Xiang, Xu	Maneuvering of two interacting ships in waves, CeSOS
IMT-2012-86	Dong, Wenbin	Time-domain fatigue response and reliability analysis of offshore wind turbines with emphasis on welded tubular joints and gear components, CeSOS
IMT-2012-87	Zhu, Suji	Investigation of Wave-Induced Nonlinear Load Effects in Open Ships considering Hull Girder Vibrations in Bending and Torsion, CeSOS
IMT-2012-88	Zhou, Li	Numerical and Experimental Investigation of Station-keeping in Level Ice, CeSOS
IMT-2012-90	Ushakov, Sergey	Particulate matter emission characteristics from diesel engines operating on conventional and alternative marine fuels, IMT
IMT-2013-1	Yin, Decao	Experimental and Numerical Analysis of Combined In-line and Cross-flow Vortex Induced Vibrations, CeSOS
IMT-2013-2	Kurniawan, Adi	Modelling and geometry optimisation of wave energy converters, CeSOS
IMT-2013-3	Al Ryati, Nabil	Technical condition indexes doe auxiliary marine diesel engines, IMT
IMT-2013-4	Firoozkoobi, Reza	Experimental, numerical and analytical investigation of the effect of screens on sloshing, CeSOS
IMT-2013-5	Ommani, Babak	Potential-Flow Predictions of a Semi-Displacement Vessel Including Applications to Calm Water Broaching, CeSOS
IMT-2013-6	Xing, Yihan	Modelling and analysis of the gearbox in a floating spar-type wind turbine, CeSOS
IMT-7-2013	Balland, Océane	Optimization models for reducing air emissions from ships, IMT
IMT-8-2013	Yang, Dan	Transitional wake flow behind an inclined flat plate – Computation and analysis, IMT
IMT-9-2013	Abdillah, Suyuthi	Prediction of Extreme Loads and Fatigue Damage for a Ship Hull due to Ice Action, IMT

Report No.	Author	Title
IMT-10-2013	Ramírez, Pedro Agustín Pérez	Ageing management and life extension of technical systems. Concepts and methods applied to oil and gas facilities, IMT
IMT-11-2013	Chuang, Zhenju	Experimental and Numerical Investigation of Speed Loss due to Seakeeping and Maneuvering. IMT
IMT-12-2013	Etemaddar, Mahmoud	Load and Response Analysis of Wind Turbines under Atmospheric Icing and Controller System Faults with Emphasis on Spar Type Floating Wind Turbines, IMT
IMT-13-2013	Lindstad, Haakon	Strategies and measures for reducing maritime CO2 emissions, IMT
IMT-14-2013	Haris, Sabril	Damage interaction analysis of ship collisions, IMT
IMT-15-2013	Shainee, Mohamed	Conceptual Design, Numerical and Experimental Investigation of a SPM Cage Concept for Offshore Mariculture, IMT
IMT-16-2013	Gansel, Lars	Flow past porous cylinders and effects of bio-fouling and fish behavior on the flow in and around Atlantic salmon net cages, IMT
IMT-17-2013	Gaspar, Henrique	Handling Aspects of Complexity in Conceptual Ship Design, IMT
IMT-18-2013	Thys, Maxime	Theoretical and Experimental Investigation of a Free Running Fishing Vessel at Small Frequency of Encounter, CeSOS
IMT-19-2013	Aglen, Ida	VIV in Free Spanning Pipelines, CeSOS
IMT-1-2014	Song, An	Theoretical and experimental studies of wave diffraction and radiation loads on a horizontally submerged perforated plate, CeSOS
IMT-2-2014	Rogne, Øyvind Ygre	Numerical and Experimental Investigation of a Hinged 5-body Wave Energy Converter, CeSOS
IMT-3-2014	Dai, Lijuan	Safe and efficient operation and maintenance of offshore wind farms, IMT
IMT-4-2014	Bachynski, Erin Elizabeth	Design and Dynamic Analysis of Tension Leg Platform Wind Turbines, CeSOS
IMT-5-2014	Wang, Jingbo	Water Entry of Freefall Wedged – Wedge motions and Cavity Dynamics, CeSOS
IMT-6-2014	Kim, Ekaterina	Experimental and numerical studies related to the coupled behavior of ice mass and steel structures during accidental collisions, IMT
IMT-7-2014	Tan, Xiang	Numerical investigation of ship's continuous-mode icebreaking in level ice, CeSOS

Report No.	Author	Title
IMT-8-2014	Muliawan, Made Jaya	Design and Analysis of Combined Floating Wave and Wind Power Facilities, with Emphasis on Extreme Load Effects of the Mooring System, CeSOS
IMT-9-2014	Jiang, Zhiyu	Long-term response analysis of wind turbines with an emphasis on fault and shutdown conditions, IMT
IMT-10-2014	Dukan, Fredrik	ROV Motion Control Systems, IMT
IMT-11-2014	Grimsmo, Nils I.	Dynamic simulations of hydraulic cylinder for heave compensation of deep water drilling risers, IMT
IMT-12-2014	Kvittem, Marit I.	Modelling and response analysis for fatigue design of a semisubmersible wind turbine, CeSOS
IMT-13-2014	Akhtar, Juned	The Effects of Human Fatigue on Risk at Sea, IMT
IMT-14-2014	Syahroni, Nur	Fatigue Assessment of Welded Joints Taking into Account Effects of Residual Stress, IMT
IMT-1-2015	Bøckmann, Eirik	Wave Propulsion of ships, IMT
IMT-2-2015	Wang, Kai	Modelling and dynamic analysis of a semi-submersible floating vertical axis wind turbine, CeSOS
IMT-3-2015	Fredriksen, Arnt Gunvald	A numerical and experimental study of a two-dimensional body with moonpool in waves and current, CeSOS
IMT-4-2015	Jose Patricio Gallardo Canabes	Numerical studies of viscous flow around bluff bodies, IMT
IMT-5-2015	Vegard Longva	Formulation and application of finite element techniques for slender marine structures subjected to contact interactions, IMT
IMT-6-2015	Jacobus De Vaal	Aerodynamic modelling of floating wind turbines, CeSOS
IMT-7-2015	Fachri Nasution	Fatigue Performance of Copper Power Conductors, IMT
IMT-8-2015	Oleh Karpa	Development of bivariate extreme value distributions for applications in marine technology, CeSOS
IMT-9-2015	Daniel de Almeida Fernandes	An output feedback motion control system for ROVs, CeSOS/AMOS
IMT-10-2015	Bo Zhao	Particle Filter for Fault Diagnosis: Application to Dynamic Positioning Vessel and Underwater Robotics, CeSOS
IMT-11-2015	Wenting Zhu	Impact of emission allocation in maritime transportation, IMT

Report No.	Author	Title
IMT-12-2015	Amir Rasekhi Nejad	Dynamic Analysis and Design of Gearboxes in Offshore Wind Turbines in a Structural Reliability Perspective, CeSOS
IMT-13-2015	Arturo Jesùs Ortega Malca	Dynamic Response of Flexibles Risers due to Unsteady Slug Flow, CeSOS
IMT-14-2015	Dagfinn Husjord	Guidance and decision-support system for safe navigation of ships operating in close proximity, IMT
IMT-15-2015	Anirban Bhattacharyya	Ducted Propellers: Behaviour in Waves and Scale Effects, IMT
IMT-16-2015	Qin Zhang	Image Processing for Ice Parameter Identification in Ice Management, IMT
IMT-1-2016	Vincentius Rumawas	Human Factors in Ship Design and Operation: An Experiential Learning, IMT
IMT-2-2016	Martin Storheim	Structural response in ship-platform and ship-ice collisions, IMT
IMT-3-2016	Mia Abrahamsen Prsic	Numerical Simulations of the Flow around Single and Tandem Circular Cylinders Close to a Plane Wall, IMT
IMT-4-2016	Tufan Arslan	Large-eddy simulations of cross-flow around ship sections, IMT
IMT-5-2016	Pierre Yves-Henry	Parametrisation of aquatic vegetation in hydraulic and coastal research, IMT
IMT-6-2016	Lin Li	Dynamic Analysis of the Installation of Monopiles for Offshore Wind Turbines, CeSOS

